# Interactions between the plant Golgi apparatus and the cytoskeleton

**Alessandra Rocchetti**

A thesis submitted in partial fulfilment of the requirements of
Oxford Brookes University for the degree of Doctor of Philosophy

September 2016

# ACKNOWLEDGMENTS

This work would have not been possible with the support and help of so many people.
First of all, I would like to express my gratitude to Prof Chris Hawes for the possibility to work together and scientific conversation that helped me to do grow as a scientist. A thank you also goes to my second supervisor Dr Anne Osterrieder for opening the doors to the science communication and outreach world. I am also grateful to all the member of the lab for being collaborative and providing feedbacks, and especially to Dr Verena Kriechbaumer for the constant support and being always available. Prof. Stanley W. Botchway and Dr Andy Ward for their essential help with the optical tweezers.
A big thank you to all the present and past inhabitants of the PhD offices, and particularly Frances, Vanessa, Vidya, Maria and Michela for being amazing colleagues and our chats (scientific and not) over lunch.

There is also a very long list of people out of the work environment to whom I would like to express my sincere love and gratefulness. All my flatmates and particularly Stav for the food&sofa sessions and epic parties. All my Oxford crew: Antonella, Andrea and Barbara, Raffaele, Francesca and Marco (plus two), Carl, Alessandro, Sara, Andy, Eileen and Eman and Jess for kind words, fun and most of all making me feel home. Thank you Brit for bringing 'Merica' to me and being an dream friend. All my friends back home, thank you for making me feel loved and sharing amazing moments together. I will always grateful to Manu, for our secret escapes; to Pietro and Cristina for listening, encouraging and believing in me; to Ilaria for the statistical conversations accompanied by home-made nocino. During my years in Oxford I was lucky to meet my yoga teacher and friend Mariella, thank you for being such an inspiring and strong woman and giving me so much.

Finally, I would like to express my gratitude to my family for their support and for being understanding (despite the fact that they have no idea of what have been doing during my PhD).

This thesis is dedicated to all of you.

# ABSTRACT

In animal cells, the relationship between the Golgi apparatus and cytoskeleton has been well characterised but not much is known in plants.

The functions of the Golgi apparatus are conserved amongst eukaryotes. It is one of the main stations in the secretory pathway and is involved in protein processing and sorting to different destinations. In plants, it is also involved in trafficking and positioning of cell wall components.

In tobacco epidermal cells, fluorescent labelling with Golgi marker proteins has shown that the Golgi apparatus is made of hundreds of individual units scattered in the cortical cytoplasm and moving on the actin cytoskeleton. The contribution of actin filaments to Golgi body motility in plant has been extensively described, but this actin-centric view has recently been challenged.

Emerging evidence suggests that microtubules may contribute to short distance movement and 'fine tuning' of Golgi body displacement. Moreover, proteomic studies linking the actin-cytoskeleton to microtubules have demonstrated that these two components of the cytoskeleton are closely related and a role of the microtubules in Golgi movement cannot be excluded.

In this thesis, automated tracking of Golgi bodies was used to understand and quantify the contribution of actin filaments and microtubules to the organelle dynamics. The tracking technique is also used to assess how the labelling of the cytoskeleton, with a novel fluorescent nanoprobe, affects the dynamics and stability of the actin filaments and the movement of Golgi bodies; FRAP analysis (fluorescent recovery after photo-bleaching) was also used to investigate the binding properties of the fluorescent nanoprobe to the actin filaments. The nanoprobe was compared

with another cytoskeletal marker, Lifeact-GFP, to evaluate their suitability for studying the organelle's motility in relation to the actin-cytoskeleton.

Micromanipulation of Golgi bodies with optical tweezers was used to test if there are physical links between the organelles and the cytoskeleton.

The widely accepted model is that organelles move on actin filaments and movement is powered by myosins. The hypothesis that actin filaments slide one of top of the other, and drag the organelles along, was tested using the FRAP technique.

Kinesin-13a is the only microtubule motor protein localized on Golgi bodies by immunochemical studies. Its localization was investigated *in vivo* to evaluate if it is involved in linking Golgi bodies to microtubules.

# LIST OF FIGURES

# LIST OF TABLES

# LIST OF ABBREVIATIONS

| | |
|---|---|
| ADF | Actin depolymerization factors |
| Arf1 | ADP-ribosylation factor 1 |
| At | *Arabodopsis thaliana* |
| ABP | Actin binding protein |
| ATM | *Arabidopsis thaliana* myosin |
| BFA | Brefeldin A |
| Cb | Chromobody |
| CDF | Cumulative distribution of frequencies |
| COP | Coat protein |
| DMSO | Dimethyl sulfoxide |
| ER | Endoplasmic reticulum |
| ERES | Endoplasmic reticulum export sites |
| FABD2 | Fimbrin actin binding domain-2 |
| FH4 | Fimibrin homologue 4 |
| FIM1 | Fimbrin-1 |
| FRAP | Fluorescent recovery after photobleaching |
| GA | Golgi apparatus |
| GAP | GTPase activating protein |
| GEF | Guanine exchange factor |
| GFP | Green fluorescent protein |
| GTP | Guanosine triphosphate |
| KCBP | Kinesin-like calmodulin binding protein |
| KCH | Kinesin calponin homologue |
| LatB | Latrunculin B |

LIM Lin-11 in *C.elegans* , Isl1 in rat , and Mec-3 in *C.elegans*.

MDD1 Microtubule depletion domain-1

MFIR Mean fluorescence intensity recovery

MI Meandering index

mRFP Monomeric red fluorescent protein

MTOC Microtubule organizing centers

NET Networked superfamily of actin binding proteins

OD Optical density

Ory Oryzalin

PM Plasma membrane

R Fluorescence recovery per second

Rab Ras-related proteins in brain

Rep Replicate

RTNLB Reticulon like protein subfamily B

SD Standard deviation

SNARE Soluble *N*-ethylmaleimide-sensitive factor protein attachment protein receptor

ST Sialyl transferase

SW Shapiro-Wilk

VAP VAMP-associated proteins

YFP yellow fluorescent protein

# 1 INTRODUCTION

## 1.1 The endomembrane system

The endomembrane system consists of membrane-bounded compartments that are functionally and morphologically distinct. In plant cells, it comprises the nuclear envelope and the endoplasmic reticulum (ER), the Golgi bodies (GB), various endosomal post-Golgi compartments, the vacuole(s), the plasma membrane (PM) and all the vesicles shuttling between these compartments (Sparkes and Brandizzi 2012).The system is essential for the correct processing and flow of proteins and other molecules, such as lipids, glycans and polysaccharides, from the compartment where they are synthesized to the final destinations (Drakakaki and Dandekar 2013).

The biosynthetic, anterograde or secretory pathway starts at the endoplasmic reticulum (ER) where secretory proteins and most phospholipids are synthesised. The Golgi bodies then process the proteins received from the ER and mediate the traffic to the final destinations (vacuoles, plasma membrane or apoplast).

### *1.1.1 Endoplasmic reticulum*

The endoplasmic reticulum (ER) is the largest organelle in cells; it is connected to the nuclear envelope membrane and it is located under the plasma membrane spread through the cytosol (Staehelin 1997). The morphology of ER and its function are conserved across animals and plants; it is a continuous membrane system of sheets interlinked by tubules; the sheets can be further

classified in nodes or punctae (with an area between 0.1 and 0.3 $\mu m^2$) or cisternae (area more than 0.3 $\mu m^2$) (Sparkes *et al*. 2009a). The structural domains also represent functional domains. ER sheets can be associated with ribosomes and these are the sites of the synthesis of proteins destined to follow the secretory pathway; proteins are inserted in the ER lumen co-transitionally or post-translationally and in the ER undergo to N-glycosylation, folding and quality control (Chen *et al*. 2012, Galili *et al*. 1998). In animal cells, ribosomes contribute to maintain the structure of the cisternae (Puhka *et al*. 2007). In plants, the ER has specific and additional functions such as cell-to-cell communication via plasmodesmata, storage of lipids and proteins (Galili *et al*. 1998).

Transitions between sheets and tubules are observed during the development of Arabidopsis cells; ER sheets are predominant in developing cells while more tubules are found in mature cells. The conversion between the two structures is also induced by pathogen infection (Takemoto *et al*. 2003). The ER structural elements maintain their transient nature also in non-dividing cells. The analysis of persistency of ER sheets and tubules in tobacco leaf mature cell, demonstrated that certain areas of the reticulum remain stable over the time and form the framework on which the remodelling occurs (Sparkes *et al*. 2009a).

The ER membrane is shaped by a class of proteins called reticulons (Chen *et al*. 2013). Reticulons are integral transmembrane proteins containing four transmembrane domains; the topology of such domains is wedge-like and is responsible for curving the ER membrane and induce ER tubulation (Tolley *et al*. 2010). In plant, reticulon RTNLB (reticulon like protein subfamily B) belonging to the subfamily 1,2,4 and 13 are the most abundantly expressed of the reticulon family and their ability to curve the membrane depends on interactions between reticulons (Sparkes *et al*. 2010). RTNLB3

and RTNLB6 constrict the endoplasmic reticulum to plasmodesmata tubules and might have a role in linking the ER to the plasma membrane (Kriechbaumer *et al*. 2015).
The rearrangements of the ER are also dependent on intact actin-cytoskeleton and on the functional actin motor protein myosin XIK ( Sparkes *et al*. 2009a).

The ER represents the entry point for proteins destined to follow the secretory pathway to either intracellular compartments or exocytosis (Stefano *et al*. 2014). Once the proteins are glycosylated, folded and passed the quality control in the ER, they can follow a conventional route through the Golgi apparatus or an unconventional route by-passing the Golgi apparatus stacks (Drakakaki and Dandekar 2013).The mechanism regulating the exchange of cargo proteins between the ER and Golgi apparatus (GA) is matter of debate in the plant field. In eukaryotes, the anterograde transport (proteins leaving the ER towards the GA) and retrograde transport (from GA to ER) is mediated by COPII and COPI coated vesicles respectively (Barlowe and Miller 2013). In plants however, the existence of COPII vesicles and their role in the anterograde transport is matter of debate (Robinson *et al*. 2015). Electron microscope and live-cell images combined with fluorescent labelling and laser manipulation (optical trapping) shows that there is a physical link between the Golgi apparatus and ER (Sparkes *et al*. 2009b); these evidences lead to an alternative model where proteins move from the ER to the Golgi via tubules connecting the two compartments (Hawes 2012) (Figure 1).

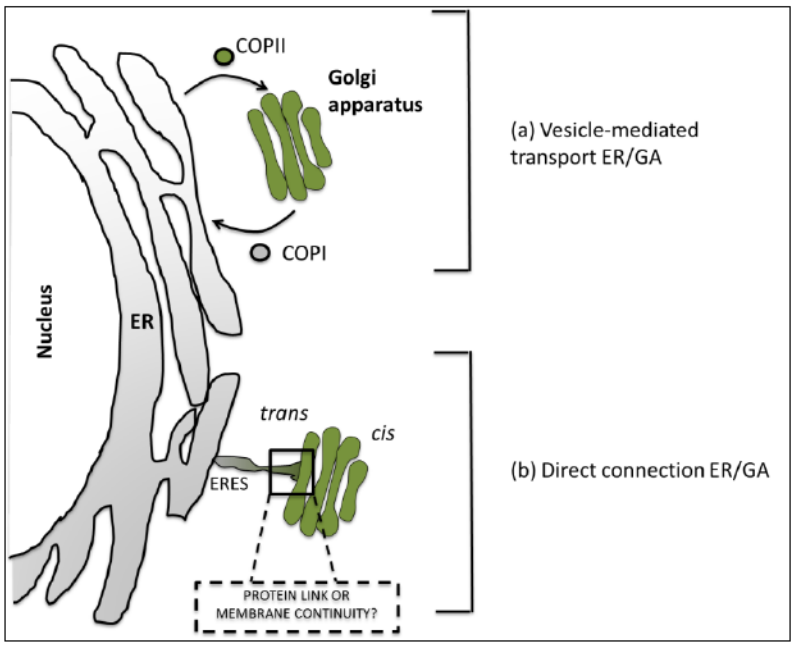


**Figure 1. Overview of the traffic between Endoplasmic reticulum (ER) and Golgi apparatus (GA).**
Transport between ER and GA is performed by the Coat protein I (COPI, retrograde transport) and Coat protein II (COPII, anterograde transport) vesicles (a).
According to second possible model (b), the ER and GA are linked through ER exit Sites (ERES), but it is not known whether there is membrane continuity or proteins bridging between the two compartments.

## *1.1.2 The Golgi apparatus*

The first observation of Golgi apparatus was reported in 1898 by Camillo Golgi while working on nerve cells. In the minutes published in the Medical-Surgical society of Pavia, he communicated the discovery of the novel organelle as "internal reticular apparatus" in the cytoplasm of nerve cell body. Initially considered an artefact of the fixation process, only in the 50s with the development of electron microscopy it was confirmed to be a unique organelle (Mazzarello *et al.* 2009, Dröscher 1998).

The Golgi apparatus is a ubiquitous organelle in eukaryotes and the main architecture is conserved, with few structural differences between mammalian and plant cells. The Golgi apparatus consists

of a pile of flattened membrane bounded cisternae with dilated rims, surrounded by small vesicles. In animal cells, the single Golgi stacks are connected by tubules to form the Golgi ribbon (Klumperman 2011).

The plant Golgi are dispersed in the cytoplasm and are structurally and functionally independent units; Golgi bodies are composed of five to eight cisternae with *cis*-*trans* polarity (Staehelin and Moore 1995). The number of Golgi bodies per cell and of cisternae depends on the plant physical conditions, developmental stage and cellular specificity (Andreeva *et al*. 1998). Live cell imaging combined with targeted fluorescent protein techniques provided the evidence that Golgi bodies are motile in the cytoplasm (Boevink *et al*. 1998).

Within Golgi body stacks, cisternae are morphologically and enzymatically different: protein cargo from the ER enters the *cis*-side cisternae and exits the *trans*-side of the organelle (Nebenführ and Staehelin 2001, Day *et al*. 2013). The function of the Golgi apparatus is conserved in animal and plant cells. Across the Golgi stacks, enzymes such as glycosyltransferases, glycosidases and nucleotide sugar transporters are dispersed to progressively modify proteins (Stanley 2011). Plant Golgi bodies are the sites where CSC (cellulose synthases complexes) assemble into hexameric rosette structures (Haigler and Jr 1986, Olek *et al*. 2014) and then are transported to the plasma membrane; Golgi bodies pause on microtubules to insert the CSC into the plasma membrane where the complex becomes active and synthetizes the cellulose (Crowell *et al*. 2009).

Plant Golgi bodies are dynamic organelles, unlike their mammalian counterpart which is stationary. Fluorescent protein technology made it possible to image the plant Golgi bodies in living cells and revealed that they are dispersed and move on the ER/cytoskeleton interface in the cortical cytoplasm (Boevink *et al*.

1998). Preliminary studies demonstrated that these organelles are in close association with the actin-cytoskeleton and move on the underlying ER network: treatment with the actin depolymerising agent cytochalasin D caused the Golgi bodies to stop moving and cluster in groups. The model proposed was that Golgi stacks might act as "vacuum cleaner" collecting cargo from the ER as they pass over the endoplasmic reticulum export sites (ERES) (Boevink *et al*. 1998).

A further study on Golgi dynamics characterised in more detail the nature of the movement. Golgi bodies alternate between rapid linear motions and pauses, in which the organelles are wiggling around a position for a variable period of time. A model for Golgi dynamics, named "stop and go" was postulated: Golgi bodies travel associated with the actin filaments and arrest on activated ER exit sites (ERES), increasing the efficiency of the traffic between the two compartments (Nebenführ *et al*. 1999). ERES are sites through which the secretory proteins exit the endoplasmic reticulum (Langhans *et al*. 2012, Lerich *et al*. 2012) and in plant are associated and move together with the Golgi bodies to form a secretory unit (daSilva *et al*. 2004).

The protein trafficking between the endoplasmic reticulum and Golgi bodies is mediated by vesicles covered by COP proteins (coat proteins). COP proteins form complexes that assemble on a membrane surface, where they select cargo proteins and polymerize into spherical cages to deform the membrane into a bud, which subsequently separates as a vesicle (Bonifacino and Glick 2004). COPII proteins (coat protein II) cover the vesicle trafficking proteins from the ER to the Golgi apparatus (anterograde transport). The transport from the Golgi apparatus to the ER (retrograde transport) is instead mediated by COPI (coat protein I) coated vesicles.

Once the vesicle has been separated from the original organelle, it is transported on the cytoskeleton and once it recognizes its target membrane, it releases its coat proteins (Hwang and Robinson 2009) and eventually fuses with the target through the formation of the SNARE (soluble *N*-ethylmaleimide-sensitive factor protein attachment protein receptor) complex. The SNAREs present at the vesicle membrane (v-SNAREs) specifically interact with the SNARE present at the target membrane (t-SNARE); the formation of this complex drives the fusion between the two membranes (Grefen and Blatt 2008). The docking and fusion of the vesicles with the target membrane is regulated by Rab GTPases, which are part of the Small GTPase family (Woollard and Moore 2008). Rab GTPases cycle between active GTP- and inactive GDP-bound state. This cycle is accomplished thanks to guanine exchange factors (GEFs) which convert the GTPases into their active state and the GTPase-activating proteins (GAPs) which stimulate the GTPase activity and GTP hydrolysis. The active GTP-bound form is attached to the membrane through two 20 prenyl groups. After GTP hydrolysis and inactivation, Rab proteins are removed from the membrane by RabGDI (GDP-displacement inhibitor) which masks the prenyl groups and retains the Rab proteins in the cytosol. To return into the membrane, Rab protein must be recruited by RabGDI-displacement factor, which allows GTP-bound conversion by GEFs. GTP-bound Rab proteins offer interaction surfaces for tethering factors, enzymes of phosphatidyl-inositol metabolism, myosins, kinesins and regulators of SNARE protein assembly. (Woollard and Moore, 2008)

The components of these machineries were originally identified in animal and yeast cells (Rothman 1996) and were identified in plants by homology (Robinson *et al*. 2007) however the existence

of such machinery in plant is matter of debate (Robinson *et al*. 2015).

In plants, the formation of COPI vesicles has been confirmed *in vivo* (Pimpl *et al*. 2000), in cryofixed immunolabelled samples (Donohoe *et al*. 2007) and fluorescent proteins technique combined with live cell imaging (Stefano *et al*. 2006). Fluorescent COPII proteins localize on the secretory unit components such as Golgi bodies (Hanton *et al*. 2009) or the interface between the cis-side of the Golgi and ER exit sites (Langhans *et al*. 2009). Although it is accepted that the COPII machinery contributes to ER-to-Golgi transport in plants (Foresti and Denecke 2008), the existence of COPII vesicle is still hypothetical. COPII coated vesicles have never been isolated and only in a few publications, using high pressure freezing fixation technique and electron tomography, is their presence reported (Kang and Staehelin 2008, Robinson *et al*. 2007).

Studies with Brefeldin A (BFA) gave additional information about the anterograde transport. BFA treatment stop the secretion of proteins from the ER to the Golgi apparatus by inhibiting with Arf1 (ADP-ribosylation factor 1), a small GTPase localised on Golgi apparatus that assists the assembly of COPI (Donaldson *et al*. 1992, Klausner *et al*. 1992). Golgi resident proteins redistribute to the ER and this results into the re-absorption of the Golgi into ER; upon BFA washout, the Golgi system reforms as Golgi proteins are exported from the ER (Ward *et al*. 2001).

The absorption of the Golgi bodies into the ER, upon BFA treatment, and the reformation of such organelles, following the BFA washout, does not depend on actin-cytoskeleton (Saint-Jore *et al*. 2002). Additionally, after BFA washout, it was expected to detect numerous COPII vesicles sustaining the Golgi re-constitution, however no COPII proteins are detected on pre-Golgi tubular-vesicular cluster (Langhans *et al*. 2007). This evidence

together with imaging techniques suggested that an alternative mechanism to the retrograde transport could exist. In Brandizzi *et al*. (2002) tubular direct connections between the ER and the *cis*-side of the Golgi are observed in electron micrographs of cells stained with zinc iodide and osmium tetroxide, which selectively stain the ER and Golgi.

Optical trapping and *in vivo* imaging allowed trapping of individual Golgi bodies and they were pulled across the cytosol. As a consequence, growth of attached ER tubules following Golgi body movements was observed. However, there was an apparent small 'gap' of fluorescence between the ER tubule and the Golgi body; this could either represent the exclusion of the ER soluble marker from the ERES or indicate that the Golgi is separated from the ER and tethered through protein bridges rather than membrane continuity (Sparkes *et al*. 2009b)(Figure 1).

An alternative model postulates the existence of transient tubular connections between the ER and the Golgi stacks, subjected to regulation by the COPII machinery (Hanton *et al*. 2009).

As the Golgi apparatus is a multi-cisternal and polarized structure, it needs to be held together in a correct structural order while moving. The protein family of golgins have been suggested to hold together the scaffold of cisternae and act as tethers, directing the vesicles to their destination. Components of the Golgin family share the localization in different parts Golgi apparatus (*cis*- and *trans*-face and cisternal rims) and they all share a common structure: a C-terminal domain anchored to the Golgi apparatus via transmembrane domain or binding of small GTPases, and at the N-terminal the presence of a long coiled-coil domains which wrap around each other as a rod-like structure protruding from Golgi stacks (Munro 2011). The N-terminal domain can interact with other Golgins, with components of the Rab family and also SNAREs (Burkhard *et al*. 2001, Short *et al*. 2005, Sztul and

Lupashin 2006). The model of "tentacular" Golgi body is proposed, where coiled coil domains of golgins stretch out the Golgi apparatus and capture Rab proteins associate to vesicles and guide them to the correct destination in the stack (Sinka *et al*. 2008).

In plants, golgins were identified via homology to the animal counterparts and according to their position in the Golgi stacks, and it is suggested they have different roles: golgins present at the *trans*-side might guide the protein cargo towards the next intracellular destination, whereas golgins localized on the *cis*-face might be involved in the Golgi biogenesis and maintain the close association between the ER and Golgi bodies (Osterrieder 2012).

## 1.2 The cytoskeleton

Eukaryotes share a conserved filamentous three-dimensional structure that spans across the cytoplasm and is called the cytoskeleton. The cytoskeleton frame is made up of three types of protein filaments: actin filaments, intermediate filaments and microtubule (Chang and Goldman 2004).

The cytoskeleton has three main functions: it provides structure, spatially organizes the contents of the cell and transmits stress signals (Fletcher and Mullins 2010). It also provides the lines of transport for intracellular trafficking. In plants both actin and microtubules are involved in cell compartmentalization, vesicle transport and organelle movement (de Forges *et al*. 2011). While the role of actin filaments in Golgi body dynamics is clear (Akkerman *et al*. 2011, Boevink *et al*. 1998), not much is known about the function of microtubules in plant membrane trafficking (Brandizzi and Wasteneys 2013).

### 1.2.1 The actomyosin system in plant and animal cells

Actin filaments (filamentous F-actin) are polymers of globular actin monomers (globular G actin). Each actin monomer is rotated 167° to the adjacent one to form a tight helix of 7 nm in diameter (Dominguez and Holmes 2011). Actin filaments are polar polymers with a fast-growing plus end, termed the "barbed end", and a slow-growing minus end. The definition barbed end comes from the observation of early EM micrographs of synthetic myosin filaments: myosins heads bind the filament laterally, to a tilted angle off the filament axis and the rod domain protrude outwards creating an indented growing end (Koretz 1979).

Actin filaments can occur either isolated or cross-linked into a very dynamic higher order structure. The actin cytoskeleton is continuously rearranging and its dynamics have been described according to a stochastic model: filaments rapidly elongate at the barbed end, change shape, slide one along the other to bundle and finally break down (Staiger *et al*. 2009). Actin filaments provide arrays on which the motor proteins myosins slide. The principles of myosin biochemistry and functional domains are conserved across eukaryotes; they are ATPases that use the energy released from the hydrolysis of ATPs to power the movement of cargo on actin filaments. Their movement is unidirectional either towards the plus end or minus end. A myosin molecule is generally organized in structural and functional domains: N-terminal motor domain with ATP-hydrolysis and actin-binding sites, a neck domain which contains IQ motifs and is responsible for binding calmodulin, and a C-terminal tail region (also referred as globular domain) defining the function and with class-specific properties (Foth *et al*. 2006, Li and Nebenführ 2008).

Phylogenetic analysis of the motor domain, divides myosins into 15 distinct classes. No class of myosin is present across the eukaryotes; animal cells contains at least one component of the group II and multiple members of group I (Sellers 2000) and some groups of myosins are specific for plants such as VIII, XI and XIII (Reddy 2001). The group XIII is found only in the green alga *Acetabularia cliftonii* and includes only two members myo1 and myo2 (Vugrek *et al*. 2003). The combination of actin filaments and myosin is referred as the actomyosin system (Betapudi 2014). The actomyosin system carries out different functions in animal and plant cells. In animal cells, actin filaments are involved in numerous processes such as the interaction between signalling receptors and protein partners (Mattila *et al*. 2016) and triggering the cell migration and shaping (Sackmann 2015). Unlike animal cells, plant cells are unable to migrate and are caged into a rigid cell wall; the actin and myosin system sustains the rapid bulk flow of the cytoplasm (cytoplasmic streaming) (Tominaga and Ito 2015) and intracellular transport cell components (Shimmen and Yokota 2004).

The actin-cytoskeleton in non-muscle animal cells mediates the cellular mechanics such as cell shaping, polarity and motility. This is achieved through the assembly/disassembly of the actin-cytoskeleton and the sliding of actin filament (Sens and Plastino 2015). The assembly and disassembly of actin cytoskeleton occurs in proximity of the cell membrane. The cell membrane contains assembly factors which work as sensors and transmit signals (Sens and Plastino 2015).

The sliding of actin filaments is mediated by the motor proteins myosins; myosins belonging to class II are expressed in all animal cells and were used as model for actin motor proteins being the first to be characterized (Sellers 2000). Myosins II form homo-

dimers and interact with the actin filaments through the head domain, which hydrolyses ATP; the hydrolysis of ATP molecules regulates the association/dissociation from the actin filaments and powers unidirectional walk. Myosins II also associate with each other through the tail domain and this allows a sliding of the actin filaments towards opposite directions that overall results in a contraction effect (Beach and Hammer 2015). Moreover, myosins of class two exist as complexes formed by myosin II heavy chain dimers which are not-covalently associated to four other light chain polypeptides and the activity of the complex is regulated by phosphorylation. Mutations or co-expression of myosins II showed that they are essential to survival and to maintain normal growth, development, and disease resistance (Betapudi 2014).

Mammalian and yeast class V myosins have domain architecture similar to plant myosins of class XI and are required for organelle/vesicle movement as well. The mechanical and enzymatic activity of the animal homologs is regulated by conformational changes: myosin V is active when unfolded, and it is inhibited when the head domain folds and interacts with the tail domain (Sellers and Knight 2007). The residues involved in the head-tail interactions are conserved in the plant XIK and essential for its activity. It is not excluded that plant homologs might undergo conformational changes and regulation (Avisar *et al*. 2011). Studies of myosin V functions demonstrate that it is involved in the intracellular distribution of melanosome, endosome recycling, secretory vesicles and mRNA (Desnos *et al*. 2007).

In the plant cortical array, the F-actin can be divided into two populations: individual thin actin filaments, which are highly dynamic, and actin cables, which are larger and stiffer. Individual

actin filaments are not ordered and have a short life-time: they appear, elongate and disappear very rapidly. Larger actin cables are arranged in longitudinal bundles or cables and are less dynamic than the single filaments (Henty-Ridilla *et al*. 2013). The actin bundles are formed according to a "catch and zipper" mechanism, a process mediated by four families of actin-binding proteins fimbrins, formins, LIMs and villins (Blanchoin *et al*. 2010).

The actin-cytoskeleton interacts with all the compartments of the endomembrane system and plants have developed a set of specific proteins acting at the interface between cytoskeleton and membranes; among cytoskeleton-endomembrane mediators (Introduction 2.3) there are the actin motor protein myosins (Wang and Hussey 2015). The Arabidopsis genome contains 17 genes encoding myosins, which are classified into two subfamilies: class VIII and XI (Lee and Liu 2004). Some roles of myosin are specific in plants; they are involved in triggering the motility of Golgi bodies, peroxisomes and mitochondria in non-dividing tobacco leaves, pollen tubes and Arabidopsis roots hair (Avisar *et al*. 2008, Madison *et al*. 2015, Prokhnevsky *et al*. 2008), regulating movement and remodelling of the endoplasmic reticulum (Griffing *et al*. 2014, Sparkes *et al*. 2009), organizing the actin cytoskeleton (Staiger *et al*. 2009, Ueda *et al*. 2010), cell and plant growth (Peremyslov *et al*. 2010, Sparkes 2011a), intracellular movement of plant viruses in host cells (Amari *et al*. 2014, Harries *et al*. 2009), regulating the nuclear shape and movement (Tamura *et al*.. 2013).

Phylogenetic analysis indicates class VIII and XI diverged prior to the division of green algae from land plants from a common ancestor (Avisar *et al*. 2008). In Arabidopsis class VIII comprises proteins four proteins (ATM1, ATM2, myosin VIIIA, and myosin VIIIB) and are poorly characterized in plants. Myosin ATM1 is

more similar to VIIIA, while myosin ATM2 is related to VIIIB both in sequence and expression pattern (Golomb *et al*. 2008). Enzymatic analysis of ATM1 myosin show that it has a low sliding velocity, low ATPase activity and high affinity for actin. Their localization is reported on plasmodesmata, plastids, newly formed cell walls, and mainly in the cell cortex throughout the life cycle of the plant. Truncated versions of ATM1 localize to the plasma membrane (Avisar *et al*. 2009) and ER in *N. benthamiana* leaves, and in Arabidopsis roots the localization changes in different root cells (Golomb *et al*. 2008). ATM2 and VIIIB are highly expressed in Arabidopsis pollen and truncated proteins localized to the nucleolus and/or plasma membrane (Avisar *et al*. 2009).

The effect of the myosin VIII on Golgi body movement was evaluated in Avisar *et al*. (2009); truncated mutants of ATM1 and ATM2 reduce the motility of Golgi bodies in *N.tabacum* and *N. bethamiana* respectively, to a lesser extent compared to myosins of class XI.

The members of the class XI are 13 (XI-A, -B, -C, -D, -E, -F, -G, -H, -I, -J, and -K, MYA1, and MYA2) and move exclusively towards the barbed end of actin filaments. The molecular morphology analysis revealed that XI myosins have a coiled-coil domain, localized between the neck region and tail, for dimerization; the interaction between coiled-coil domains is stabilized by the organelle targeting (Li and Nebenführ 2008). Phylogenetic analysis of myosin XI members revealed that duplication events and functional specialization occurred during the evolution of this gene family resulting in pairs of myosin paralogs; this is supported by single and double gene knock-out experiments where single mutants lack a phenotype while double knock-out of XIK (involved in organelle motility) and XI2 (required for root development) show redundant and additive roles in the transport of intracellular organelles (Peremyslov *et al*. 2008, Peremyslov *et*

*al*. 2011, Prokhnevsky *et al*. 2008). This might indicate that that the organelle trafficking is coordinated with other processes.

In Sparkes *et al*. (2008) and Avisar *et al*. (2009) a non-functional version of *A. thaliana* XIK was created by truncating the motor domain and fusing it to fluorescent markers. Both works reported that the transient expression in tobacco of the truncated XIK gives a weak cytoplasmic signal and occasionally motile punctae, which do not co-localize with Golgi bodies. The non-functional XIK inhibits the movement of Golgi bodies and mitochondria; other myosins (XIE, XIC, XII,MYA1) also reduce the motility of these two organelles indicating that they might have redundant functions or work together to power the movement. Moreover, arabidopsis T-DNA insertion lines of myosin XIK have reduced cytoskeleton dynamics. Despite the fact that the control and mutated lines have similar arrangement of the actin-cytoskeleton, the lack of functional XIK reduced the lateral displacement of the actin filaments. The complementation of the mutant line with YFP-XIK showed that this myosin accumulates at the tip of growing root hair and that its localization is dependent on the actin-cytoskeleton; when the cells were treated with latrunculin B, YFP-XIK appeared in large aggregates dispersed in the cytosol (Park and Nebenführ 2013).

### *1.2.2 Microtubules and kinesins in plant and animal cells*

The structure of microtubules is conserved across eukaryotes: they are hollow cables of 25 nm diameter consisting of 13 protofilaments. The protofilaments are composed of heterodimers of α-tubulin monomers and β-tubulin monomers of 55 KDa (Ohta *et al*. 1987) that join together laterally and longitudinally to each other to form cylindrical polar cables (Ledbetter and Porter

1964). Beta subunit are exposed to the plus, or growing end, while alpha subunit the minus end (Nogales *et al*. 1999). A third type of microtubule subunit, γ-tubulin, is associated to microtubule organizing centers (MTOC) in animal and most algal cells; in plants, γ-tubulin is associated with microtubule nucleation sites and is involved in the assembly of new filaments from existing microtubules (Kollman *et al*. 2011, Schmit 2002).

Microtubules have an intrinsic structural polarity: the rapidly growing plus ends extend out into the cytoplasm and the minus end loses subunits if not stabilized. An individual microtubule goes through cycles of growth and shortening at the plus end, a behaviour known as "dynamic instability" (Desai and Mitchison 1997, Mimori-Kiyosue 2011). Microtubule organization undergoes a continuous rearrangement: repeated collapse and reassembly determines the formation of new patterns in the cell (Vassileva *et al*. 2005). The network reorganization is triggered by external stimuli, which activate the tubulin/microtubule modulators such as MAPs (Microtubule Associated Proteins)(Mimori-Kiyosue 2011).

The movement of cargo on microtubules is mediated by ATP-dependent motor proteins. In eukaryotic cells two conserved motor protein superfamilies have been identified: the kinesin superfamily (KIFs) and dynein. The first drives a plus-end directed movement, while the second determines the movement towards the minus-end (Horgan and McCaffrey 2011). Kinesins have a motor domain hydrolizing ATP and binding microtubules, followed by a short α-helical domain of 50 amino acids called the neck and C-terminal end binding adaptors, which interact with specific cargos. The position of the motor domain can vary, and according to this kinesins are classified in N-type (motor domain at the N-terminus), M-type (internal motor domain) and C-type

(motor domain present at the C-terminus). N-type and M-type kinesins move towards the plus end of microtubules, while C-type towards the minus end (Seog *et al*. 2004). The widely accepted classification and nomenclature is based on phylogenetic analysis, which group them into 14 families (kinesin-1 to kinesin-14) (Lawrence *et al*. 2004). Microtubule motor proteins can form dimers through the neck domain or work as monomers (Seog *et al*. 2004) and, across eukaryotes, they are involved in different processes such as transport of vesicles and organelles, spindle formation and elongation, chromosome segregation, microtubule dynamics and morphogenesis (Reddy and Day 2001).

Other than microtubule motor functions, kinesins can also have microtubule depolymerizing activity like kinesins of the group 13, which remove tubulin subunits from the plus end of microtubules (Walczak *et al*. 2013)

Dyneins are required for intraflagellar transport, organisation of the Golgi apparatus and spindle poles, are also involved in moving nuclei, vesicles, pigment granules, and chromosomes (King 2000). The analysis of eukaryote genomes revealed that land plants lost dynein before the divergence land plant and algae; plants compensated the loss of dynein developing the functionally homologous minus-end kinesins (Wickstead and Gull 2007).

In non-dividing plant cells, the microtubule array spreads in a two-dimensional plane at the cell cortex, under and parallel to the plasma membrane and they lack microtubule organizing centres (Hashimoto 2015). The filaments originate from scattered nucleation sites, are dispersed and get self-organised at the cell cortex and successively form bundles via polymer treadmilling (Kollman *et al*. 2011, Murata and Hasebe 2007). Microtubules contribute to cellular organization in that they play a major role in vesicle targeting, organelle positioning and shaping (Collings and

Nick 2008), and plus-end orientation of cellulose fibrils (Lloyd 2011). Microtubules align perpendicular to the axis of cell expansion and direct the insertion of cellulose microfibrils in an ordered manner. The insertion of the cellulose is coordinated to the regulation of Golgi body positioning; Golgi bodies, carrying the assembled and inactive CESA complex (Cellulose Synthase Complex), pause on cortical microtubules allowing CesA to insert into the plasma membrane where they become active and synthetize cellulose microfibrils (Crowell *et al*. 2009). Cellulose microfibrils provide the major mechanical resistance to the cell and constrain radial expansion (Hashimoto 2015). As the cell expansion terminates, irrespective of why, the microtubules lose their aligned disposition and this process seems to be regulated by a signalling cascade initiated by the cell wall (Panteris *et al*. 2013). Microtubules may also be involved in the transport or positioning of other plant compartments such as mitochondria, chloroplast and endoplasmic reticulum (Cai and Cresti 2012).

In tobacco cells, the movement of mitochondria depends on actin filaments and the depolymerisation of microtubules affects the positioning of mitochondria in parallel arrays, suggesting that microtubules regulate the positioning of mitochondria (Van Gestel *et al*. 2002). *In vitro* studies demonstrated that mitochondria isolated from tobacco pollen tubes could move on microtubules but at a slower speed compared to the movement on actin filaments, supporting the hypothesis that microtubules might have a role in the regulation of short-range transport (Romagnoli *et al*. 2003). The kinesin AtKP1 (kinesin-like protein 1) is tightly associated to mitochondria via its C-terminal tail domain and its interaction with microtubules is regulated by the mitochondria outer membrane voltage-dependent anionic channel VDAC3, that is involved in the respiratory activity of the organelle. The interaction between these two proteins would coordinate the

positioning of the mitochondria on microtubules and the respiration process in a specific position at low temperature (Yang *et al*. 2011)

The movement of chloroplasts is directed by light intensity: chloroplasts accumulate in the area of the cells exposed to low light, and are scattered from the area exposed to high intensity of light (Kong and Wada 2014). This mechanism defined as photorelocation is dependent mainly on actin filaments, but microtubules may be involved. In moss, when microtubules are disrupted, short distance movement of chloroplasts is inhibited and the parallel orientation to the cell axis is disturbed (Sato *et al*. 2001).

During the progression of the cell cycle, microtubules change their disposition and organization. At prophase, microtubules cluster and form a spindle at the cell cortex, while the nuclear envelope starts to disintegrate, and in the metaphase the microtubules direct the alignment of chromosomes along the equatorial plane of the cell. In anaphase, the newly formed daughter chromosomes are pulled in opposite directions and the phragmoplast starts to form. Golgi-derived vesicles are transported along microtubules to the phragmoplast, where they deposit their enclosed cell wall contents and build the cell plate until the cytokinesis is complete. In the two daughter cells, microtubules start to reform under the plasma membrane and disperse in the cytoplasm (Hashimoto 2015). The involvement of microtubules in long distance transport is also documented in non-dividing cells. In Arabidopsis leaf cells, the kinesin FRA-1 belongs to the subfamily 4 (Lee and Liu 2004). It mediates the plus-end transport of Golgi derived vesicles to the plasma membrane and the export of matrix polysaccharides, but does not affect the motility of CESA complex. Knockout mutants of FRA-1 show that Golgi bodies have less cisternae surrounded by enlarged vesicles, and drastic reduction

of the cell wall thickening indicating a defect in post-Golgi trafficking and secretion (Zhu *et al*. 2015).

In Arabidopsis 61 kinesins have been identified (Lee and Liu 2004) and this model plant contains the largest known number of kinesins among eukaryotes. Some Arabidopsis kinesins do not fall into any of the 14 defined groups and are unique to plants (Reddy and Day 2001). The high number of kinesins in plants can be in part correlated to processes that are specific in plant cells such as the lack of microtubule organizational centre, the transport of cargo through plasmodesmata, the formation of phragmoplast during the cell division (Reddy and Day 2001).

In non-dividing animal cells the microtubule minus end is stabilised by an organizing structure, from which the microtubules grow, referred to as microtubule organising centre (MTOC) and located adjacent to the nucleus. Microtubules also nucleate from the Golgi apparatus and Golgi-derived microtubules are involved in post-Golgi trafficking, maintenance of Golgi architecture, cell polarity and motility (Sanders and Kaverina 2015). The centrosomal protein Cep192 regulates the balance between microtubule nucleation at centrosome and Golgi apparatus (O'Rourke *et al*. 2014). Microtubules radiate from these organising centres into the cytoplasm (Erhardt *et al*. 2002) and drive the intracellular trafficking and cell motility (Olmsted and Borisy 1973). During cell division, microtubules play a fundamental role in aligning the chromosomes at the equatorial plane of the cell and subsequently pulling them towards the opposite spindle poles (Pavin and Tolić 2016). Additionally, just before the abscission, the two daughter cells are connected through a thin cytoplasmic bridge filled with microtubules that direct the movement of vesicles carrying protein essential for the cell separation (Neto *et al*. 2011).

Kinesins have three major functions: organize the chromosomal and mitotic spindle movement, direct the various cargo, such as lysosomes, vesicles, endosomes along microtubules (Hirokawa and Noda 2008, Seog *et al*. 2004) and control microtubule dynamics via depolymerisation (Vicente and Wordeman 2015). In animal cells, the Golgi apparatus is positioned in close proximity to the nucleus and is a stationary organelle. Kinesins play a role in directing the perinuclear positioning of Golgi apparatus and maintaining its architecture; the overexpression of Rabkinesin-6 (Kinesin-6 bound to GDP bound form of Rab-6) induces the loss of the perinuclear position of Golgi apparatus and its dispersion in the cytoplasm (Wei and Seemann 2010). A similar observation is made when the gene coding for C-motor kinesin KIFC3 and cytoplasmic dynein are suppressed, demonstrating also that these two motor proteins have a complementary role (Wei and Seemann 2010).

In the animal kingdom, kinesins belonging to the group 13 share a high sequence similarity in the motor domain, and remove tubulin subunits from the plus end similarly to plant kinesin-13, but also have additional functions such as mitotic spindle assembly and the attachment of the microtubules to kinetochores in mitosis (Ems-McClung and Walczak 2010, Lu *et al*. 2005). Animal kinesin-13 is not located on the Golgi apparatus and is involved in the mitotic spindle formation; kinesin-13 members are also present in the flagellum of eukaryotes and regulates the length of this structure (Vicente and Wordeman 2015)

# 1.3 Cytoskeleton, motor proteins and endomembrane system

## *1.3.1 Endoplasmic reticulum dynamics*

Various lines of evidence demonstrate that the endoplasmic reticulum (ER) is structurally and functionally connected to the cytoskeleton in the plant kingdom (Brandizzi and Wasteneys 2013a).

A first study demonstrating the correlation between ER organization and actin-cytoskeleton was performed in epidermal cells of onion. Cold treatment causes the disappearance of ER cisternae and reorganization in short tubules. When the sample is transferred to room-temperature, the ER re-forms and this process is dependent on the actin-cytoskeleton but not cortical microtubules (Quader *et al*. 1989).

The labelling of actin filaments and endoplasmic reticulum in tobacco epidermal cells showed that the organization of the ER matches that of the actin filaments suggesting that the actin-cytoskeleton can provide the template for the endoplasmic reticulum organization (Boevink *et al*. 1998).

Actin- motor proteins also participate in connecting the ER to the actin cytoskeleton. A study regarding the morphological organization of the ER, in which truncated version of myosins XI were used, demonstrated that remodelling of the ER is dependent on actomyosin system and that more persistent tubules are present (Sparkes *et al*. 2009b). Lack of myosin XIK results in a reduction of the ER streaming, changes the ER structure and induces a prevalence of ER sheets, and actin filaments lose their organization (Ueda *et al*. 2010). Fluorescent versions of myosin

XIK localize on motile endomembrane vesicles that partially correspond to Golgi, *trans* Golgi, secretory vesicles and ER microsomal fractions indicating that this myosin is broadly associated with the endomembrane system (Peremyslov *et al*. 2012). A member of vesicle associate proteins family (VAP27) localizes to the ER network as well as ER anchor sites to the plasma membrane, which are also associated with microtubules and the actin binding protein NET3 suggesting that the ER and cytoskeleton might be connected through a proteic linker at the plasma membrane (Wang *et al*. 2014).

Microtubules may also participate in the remodelling of the ER. In Hamada *et al*. (2014) it was suggested that endoplasmic reticulum elongates along microtubules and the force may be generated by protein dependent-sliding mechanism but the evidence for this is weak.

### *1.3.2 Golgi apparatus dynamics*

The directional and fast movement of the Golgi body depends on the actin-cytoskeleton and the depolymerisation of actin arrays stop the movement of Golgi bodies (Boevink *et al*. 1998, Akkerman *et al*. 2011).

Evidence shows that myosins have a role in Golgi body motility. Two myosins, XIK and XIE, are mainly involved in Golgi body movement and over expression of mutants stops the streaming of this organelle (Avisar *et al*. 2009). The predicted expression of myosins in Arabidopsis revealed that XIE is expressed exclusively in pollen while XIK is ubiquitously expressed in vegetative organs (Sparkes 2011a). As mentioned before, the myosin XI gene family gene underwent to duplication events so the functional redundancy of XIK was also investigated. RNA-silencing

demonstrated that XIK has a major role in the movement of Golgi bodies, peroxisomes and mitochondria in tobacco leaf cells and that XI2 and XI1 contribute to a lesser extent (Avisar *et al*. 2011).

Despite the quantity of evidence demonstrating that myosins are involved as motors in the endomembrane system, some aspects of the mechanism of action are not clear yet. For instance, it is unknown if myosins directly interact with the cargo organelles or adaptor proteins (Buchnik *et al*. 2015). The fact that the expression XIK tail domain inhibits the movement of Golgi bodies and that such myosin mutant does not co-localize with either actin filament or Golgi bodies markers (Avisar at al 2011) and the evidence that myosin XIK can mediate the movement of the actin filaments (Reddy 2001) lead us to hypothesises that either myosin XIK works as bridge between Golgi bodies and the actin cytoskeleton or it bridges between actin filaments, and its ATPases activity powers the sliding of actin filaments one on top of the other thus a linker between Golgi bodies and actin would be necessary (Figure 2).

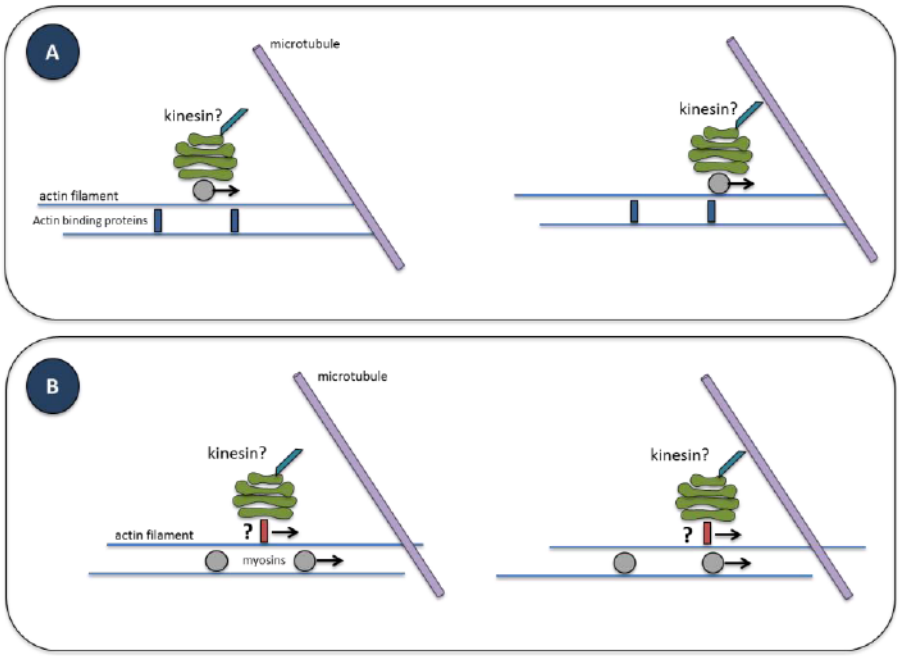


**Figure 2. Models of the Golgi body movement regulation by cytoskeleton motor proteins.**

The most accepted model is shown in panel A. Actin filaments are connected by actin binding proteins such as fimbrins, formins, LIM and villins (Blanchoin *et al.* 2010) and they act as track on which myosin slide and power the movement of their cargo, such as Golgi bodies. When the organelle comes to the proximity of a microtubule, kinesins would mediate the interaction.

A second possibility is that myosins mediate sliding of actin filaments one on top of the other. Golgi bodies are anchored to the filaments via a linker and would be drag along as the filaments are sliding. When Golgi bodies encounter microtubules, microtubule motor proteins would interact with the microtubules to pause the movement.

Unlike when actin filaments are disrupted, the depolymerisation of microtubules does not stop the movement of Golgi bodies (Brandizzi *et al.* 2002, Crowell *et al.* 2009, Nebenführ *et al.* 1999). Microtubule alignment is correlated with cellulose microfibril deposition in the cell wall; the work by Crowell *et al.* (2009) demonstrated that in Arabidopsis the insertion of the cellulose synthase complex (CSC) in the plasma membrane aligns with microtubules and is concomitant with Golgi pausing on microtubules. In another work by Hamada *et al.* (2012) it was hypothesized that microtubules are not required for pausing;

instead microtubules would facilitate the interaction with the underlying ER.

Microtubule motor proteins may be involved in mediating the interaction between microtubules and Golgi bodies. Among the Arabidopsis microtubule motor proteins, kinesin-13a is the only one has been shown to localize on Golgi bodies in Arabidopsis cells by immunocytochemistry techniques (Lu *et al*. 2005). Mammalian Kinesin 13a is has an internal motor domain and it is not able to move along microtubules; mammalian kinesin 13a does have a depolymerizing activity and its motor domain has a high sequence similarity to the animal counterpart (Fujikura *et al*. 2014, Oda and Fukuda 2013). The analysis of the sequence flanking the motor domain demonstrates that the rest of the protein differs from the homolog in animals and it is lacking the functional motif that is essential for the depolymerizing activity of the animal homologue (Lu *et al*. 2005).

Knock-out mutants of Kinesin-13a shows a different morphology of Golgi stacks in root-cap peripheral cells (Wei *et al*. 2009), four branched trichomes and aggregation of Golgi bodies (Lu *et al*. 2005) and smaller secondary cell wall pits (Oda and Fokuda 2013). The overexpression of kinesin-13a results in the disruption of cortical microtubules in root epidermal cells and the formation of large secondary cell wall pits in root metaxylem vessel (Oda and Fokuda 2013). The depolymerizing activity of kinesin-13a is regulated by the interaction with MDD1 (Microtubule depletion domain 1). Mutants of kinesin-13a lacking the motor domain but maintaining the coiled-coil domain localize to the cytoplasm, and upon the co-expression of MDD1, are re-located to the cortical microtubules, indicating that MDD1 is essential for the localization on microtubules. Additionally microtubules remain intact, confirming the depolymerizing activity of the motor domain (Oda and Fokuda 2013). Another microtubule motor

protein associated with the Golgi bodies is AtPAKRP2, a member of kinesin-10 subfamily. This is a phragmoplast associated kinesin and is involved in transporting Golgi associated vesicles towards the plus end of phragoplast microtubules to assemble the cell plate (Lee *et al*. 2001). In addition to Golgi stacks and vesicles, kinesins interact with mitochondria and chloroplasts probably assisting their positioning (Cai and Cresti 2012).

Proteins other than kinesin, are also involved in linking Golgi and microtubules. TGN/early endosome interact with microtubules through the protein tether CLASP (Ambrose and Wasteneys 2008). Similarly, a class of matrix protein detected on Golgi bodies, and named Golgins, could mediate the interaction with microtubules (Osterrieder 2012).

### *1.3.3 Actin and microtubule interactions*

For a long time, actin and microtubule networks have been viewed as separate and with different functions. Recent results demonstrate that instead these two components can cross-talk and a physical dynamic interaction exists both in animal and in plant cells (Akhshi *et al*. 2014, Petrasek and Schwarzerova 2009, Wang *et al*. 2014).

Live imaging in Arabidopsis cells revealed that cortical microtubules and actin filaments transiently co-align. Treatment with the actin filament depolymerising compound latrunculin B showed that the different filament types were associated, and microtubule depolymerisation led to a partial loss of actin filament organization. A washout of the drug showed that the actin filament pattern recovered on microtubule arrays, indicating that microtubules could work as a scaffold for actin network formation (Sampathkumar *et al*. 2011). The actin binding protein NET3C interacts with VAP27, localised at the attachment sites of

the ER to PM and is found associated to the microtubules, to form a complex with actin and microtubules (Wang *et al*. 2014).

The interaction and cross-talk between actin filaments and microtubules is also mediated by cross-linking proteins and cytoskeletal motor proteins. The formins are actin-organising proteins which are conserved across eukaryotes and can act as linking proteins between microtubule and actin arrays (Cvrčková 2013). The plant formin FH4 is a transmembrane protein localized at the plasma membrane and in Arabidopsis binds directly to microtubules (Deeks *et al*. 2010). Recent evidence suggests that both actin filaments and microtubules are involved together in moving and positioning organelles, such as plastids and mitochondria. According to these results, in plants actin-F generates organelle motility and microtubules stabilize the position (Petrasek and Schwarzerova 2009). In Arabidopsis, kinesins containing a calponin homology domain (KCHs) constitute a subgroup of Kinesin family; KCHs bind to both actin filaments and microtubules (Dixit 2012, Schneider and Persson 2015).

KCBP (kinesin-like calmodulin-binding protein), a class of kinesin unique to the plant kingdom, binds to both microtubules and actin filaments. It contains a C-terminal motor domain and a myosin tail homology region 4 (MyTH4) at the N-terminus, which interact with actin arrays (Tian *et al*. 2015). Additionally, two members of the kinesin family 14 contain a CH domain and participates in the movement of chloroplast on actin filaments (Frey *et al*. 2009). In dividing tobacco cells, myosin VIII is detected at ends of peripheral phragmoplast microtubules and it is proposed that myosin VIII coordinates the cytoskeletal components during the directional expansion of the phragmoplast (Wu and Bezanilla 2014).

Several aspects of the myosin-kinesin cooperation are not clear yet. Rab-GTPases could be involved in the simultaneous regulation of myosin and kinesin activity (Batoko *et al*. 2000, Horgan and McCaffrey 2011, Seabra and Coudrier 2004). The cytoskeletal motor proteins could either directly bind the surface of the organelle and Rabs modulate their activity or Rabs could recruit the motor proteins to the cargo (Cai and Cresti 2012).
It has been proposed that kinesins are involved in short distance movement while myosins in long distance movement; microtubule motor proteins slow down and tune the fast movement powered by actin motor proteins guiding a fast and precise intracellular delivery of the cargo (Cai and Cresti 2012).

### *1.3.4 In vivo labelling of the actin-cytoskeleton*

The cytoskeleton is a continuously rearranging network and different labelling strategies have been developed to study its organization in plants.
Phalloidin is a toxin extracted from the death cap fungus *Amanita phalloides*, which binds and stabilizes F-actin. Phalloidin conjugated to the fluorescent dye rhodamine selectively stains actin filaments in permeabilized and fixed plant cells. Phalloidin-rhodamine staining is also effective in unfixed cells, but favours the formation of bundles (Sonobe and Shibaoka, 1989).
In plants, fluorescent fusion proteins have been tested to label the cytoskeleton. Expression of fluorescent G-actin monomers itself in Dictyostelium cells did not prove to be efficient because most of it remained in monomeric form diffused in the cytoplasm, resulting in a strong fluorescent cytoplasmic background (Lemieux *et al*. 2013).

Actin binding proteins (ABPs) are involved in regulating the assembly of actin filaments and therefore are good marker candidates (Higaki *et al*. 2007). The actin binding domains of different ABPs have been fused to fluorescent proteins and expressed in plants. Lifeact is a 17 amino acid peptide from the yeast protein Abp140 and decorates F-actin (Riedl *et al*. 2008). In *A. thaliana*, Lifeact fused to the fluorescent protein Venus reduced the rearrangement of the actin cytoskeleton in a concentration-dependent manner (van der Honing *et al*. 2010). The mouse ABP mTalin can be used to image actin filaments, but has severe effects on the actin cytoskeleton and its depolymerisation (Ketelaar *et al*. 2004). One of the two actin-binding domains of the *A. thaliana* fimbrin1 protein (AtFIM1) fused to GFP (GFP-fABD2) labels the fine actin dynamic scaffold in different species and cell types. Stable expression in *A. thaliana* did not show adverse effects on general morphology or development (Sheahan *et al*. 2004).

All of the fluorescent reporters available so far depict differing organizations of the actin network. This may be due to a preferential binding to fine actin filaments rather than bundles, or because the marker is derived from an actin-bundling protein, therefore causing the aggregation of actin filaments. Considering that the actin-cytoskeleton is a continuously re-arranging scaffold that provides tracks for movement and positioning of diverse organelles such as Golgi bodies (Akkerman *et al*. 2011), a more reliable and less interfering fluorescent marker would be good for *in vivo* imaging.

Nanobodies have been proven to be advantageous in detecting intracellular structures. They consist of the smallest functional domain of single heavy chain antibody isolated from alpaca blood serum (De Meyer *et al*. 2014). Because of their small size, solubility and stability it is possible to use them in heterologous systems. They also can be fused to fluorescent proteins to detect

and label cell structures *in vivo* (Olichon and Surrey, 2007). When the nanobody is conjugated to a fluorescent protein, it becomes a "chromobody". The Actin-Chromobody® (ChromoTek, Martinsried, Germany) allows detection of dynamic changes in actin cytoskeleton (Rocchetti *et al.* 2014, Rothbauer *et al.* 2006) (Figure 3).

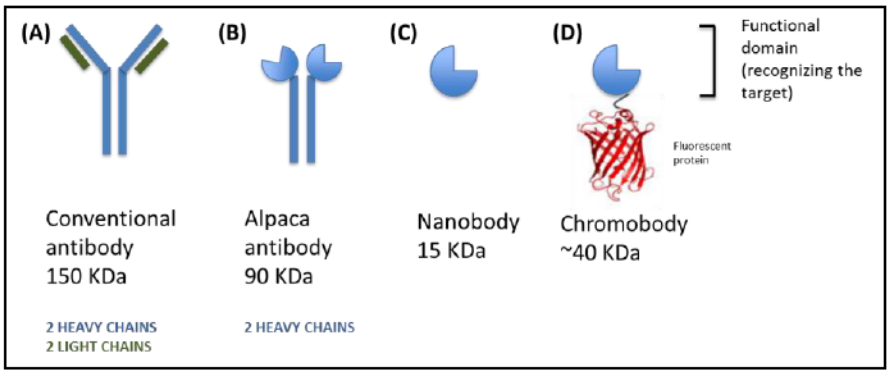


**Figure 3. Conventional antibody, alpaca antibody and nanobody.**
A conventional antibody (A) is composed of 2 heavy chains and 2 light chains, which recognize and bind the epitope (target). Alpaca produce antibody made of 2 heavy chains only and the functional domain resides on the heavy chains (B). A nanobody is the smallest functional fragment of the alpaca antibody (C). A nanobody fused to fluorescent protein takes the commercial name chromobody (D).

This chromobody was previously used to transfect HeLa cells to show the recovery of the actin filaments after Cytochalasin D treatment (ChromoTek homepage), where it was shown that the nanobody binding does not influence cell viability or motility. The actin chromobody proved to be efficient in labelling and studying the dynamics of the actin cytoskeleton in living animal cells (Rothbauer *et al.* 2006) but until now it had never been used in living plant cells. To use the actin chromobody in plant, the sequence coding for the nanobody sequence was cloned in a vector suitable for the expression in plant and fused to a fluorescent reporter (Rocchetti *et al.* 2014). As actin monomers

have conserved sequence in eukaryotes and the structure of actin filaments is highly conserved (Dominguez and Holmes 2011) expression of the actin chromobody in plant living tissue was expected to decorate the actin cytoskeleton (See Chapter 4).

This research focusses on exploring the relation between the actin/microtubule cytoskeleton and cortical Golgi bodies and how the cytoskeleton components regulate the movement of the organelles. The role of cytoskeletal motor proteins is also studied and a new model of actin-filaments dynamics is tested.

# Aims

**The aims of this thesis are:**

- Quantify the contribution of microtubules and actin filaments to the regulation Golgi body dynamics (Chapter 3).

- Develop a new probe for the fluorescent *in vivo* labelling of the actin cytoskeleton that is not interfering with the actin organization and suitable for the study of organelles movement (Chapter 4).

- Understand if there is a physical connection between Golgi bodies and the cytoskeleton (Chapter 5).

- Test a new model of mechanism of actin/myosin/Golgi body interaction (Chapter 6).

- Confirm *in vivo* the localization of only the microtubule motor protein associated with Golgi bodies (Chapter 7).

# 2 Materials and methods

## 2.1 Bacterial strains

Bacterial cloning was done in *Escherichia coli* (*E.coli*) chemical competent high efficiency strain DHα (NEB).

The chemical competent *Agrobacterium tumefaciens* (*A. tumefaciens*) strain GV3101, containing the gene for the resistance to Rifampicin and the Gentamycin resistant helper plasmid pMP90, was used for subcloning the plant expression vectors and transforming tobacco plants (Koncz and Schell 1986).

## 2.2 Bacterial growth and media

*E.coli* strains were grown in liquid LB medium (Lysogeny broth: 10 g/L Bacto-trypton, 5 g/L yeast extract, 10 g/L NaCl in distilled water at pH 7.5 ± 1%) in shaking cultures over night at 220 rpm or as solid agar plates (LB 1% w/v agar) at 37°C for 24 hrs.

*A. tumefaciens* were grown in YEB medium (5g/L tryptone, 1g/ yeast extract, 5g/l nutrient broth, 5 g/l sucrose, 0.49 g/l $MgSO_4$ $7H_20$ in distilled water) as liquid culture shaken over night at 180 rpm or on solid agar plates (YEB 1% w/v agar) for 48 hrs at 28°C. The antibiotic concentrations were used as Table 1.

**Table 1: List of antibiotic concentrations used in bacterial media.**

| Antibiotics | Concentration (μg/ml) |
|---|---|
| Gentamycin | 10 |
| Rifampicin | 25 |
| Kanamycin | 100 |
| Spectinomycin | 50 |

Glycerol stocks of *E.coli* and *A. tumefaciens* colonies were prepared mixing 800 μl of cell culture with 200 μl of autoclaved 100% glycerol for long term storage at -80°C.

## 2.3 Bacterial transformation

A 50 μl or 25 μl aliquot of chemical competent *E. coli* DHα was thawed on ice for 10 minutes, 1-5 μl of plasmid DNA (50-100 ng) were added to the cells and left on ice for 30 minutes. Cells were heat shocked in a water bath at 42°C for 1 minute and straight after placed on ice for 5 minutes. Cells were then suspended in 1000 μl of LB medium and placed in a shaking incubator at 37°C for 1 hour. Cells were centrifuged at low speed for one minute, and 600 μl of the supernatant were discarded. The cell pellet was re-suspended in the 400 μl remaining by flicking the tube and the cell suspension spread on to two separate plates (200 μl each). The plates were left to dry and allowed to grow over night in the incubator at 37°C. Isolated colonies were picked and the presence of the cloned construct was confirmed with colony PCR (See section 2.6.1). The positive colonies were grown over night in liquid culture and used to make a glycerol stock (800 μl and 200 μl 100% autoclaved glycerol) and stored at -80°C. Plasmid DNA was isolated from the positive colonies (See section 2.6.3) and used to transform *A. tumefaciens*.

To transform *A. tumefaciens*, 1-5µl of plasmidic DNA (50-100ng) were added to 25 µl of the chemical competent strain GV3101 and kept on ice for 5 mins. After that, the cells were stored at -80 °C for 5 minutes and heat-shocked at 37 °C in a water bath for 5 mins. Cells were then transferred in 1 ml of liquid YEB medium and placed in a 27 °C incubator shaking at 180 rpm for 2 hours. Aliquots of the cell suspension were plated on YEB agar medium containing selection antibiotics and allowed to grow for 2 days at 28 °C. Colonies were randomly picked and inoculated in 5 ml of liquid YEB with selection antibiotics and infiltrated into *N. tobacco* plants to check for the expression (Sparkes *et al*. 2006). Positive colonies were used to make glycerol stocks for long-term storage.

## 2.4 Plant transformation

*Nicotiana tabacum* plants were grown in the greenhouse and moved to the incubator two days prior to infiltration and used when 4-8 weeks old.

Tobacco leaves were infiltrated with transgenic *A. tumefaciens* bacteria containing the plasmid for transient transformation according to the protocol in Sparkes at al (2006). Five ml of agrobacterium in liquid selection medium were grown over night; 1 ml was centrifuged for 5 minutes at 8000 rpm and the pellet suspended in 1 ml of infiltration buffer (50mM MES hydrate, 2 mM sodium orthophosphate, 5% D-glucose, 0.1 M acetosyringone in distilled water). This step was repeated another time to wash the pellet and the pellet was re-suspended in 1 ml of infiltration buffer. The optical density (OD) of the cell suspension was measured with the nanodrop spectrophotometer (Thermoscientific, Basingstoke, UK) at a wavelength of 600 nm.

The cell culture was then diluted in the infiltration buffer to the optimal infiltration OD as shown in Table 2.

**Table 2: List of agrobacterium strains, infiltration and expression setting in *N.tabacum*.**

| Agrobacterium | $OD_{600}$ | Expression days (After transformation) | |
|---|---|---|---|
| ST-GFP | 0.05 | 2 | (Boevink *et al*. 1998) |
| Lifeact-GFP | 0.01 | 3 | (Riedl *et al*. 2008) |
| FABD2-GFP | 0.03 | 3 | (Voigt *et al*. 2005) |
| Talin-GFP | 0.03 | 3 | (Kost *et al*. 1998) |
| GFP-TUA | 0.03 | 3 | (K. Ueda *et al*. 1999) |
| ST-GFP<br>Lifeact-GFP | 0.05<br>0.01 | 3 | |
| ST-GFP<br>FABD2-GFP | 0.05<br>0.01 | 3 | |
| ST-RFP<br>GFP-TUA | 0.05<br>0.03 | 2 | |
| GFP-actin-Cb | 0.01 | 2 | (Rocchetti *et al*. 2014) |
| YFP-actin-Cb | 0.05 | 2 | (Rocchetti *et al*. 2014) |
| RFP-XIK-tail | 0.05 | 2 | (Avisar *et al*. 2009) |

The agrobacterium suspension was gently injected into the tobacco leaf using a syringe without needle. The lower side of the leaf was lightly scratched with the tip of the syringe in order to facilitate the passage of the agrobacterium suspension into the leaf tissue and only the space between the main veins become infiltrated, avoiding the leaf margin and apex.

For each experimental set, at least two plants were used, and after the infiltration event they were incubated in the growth chamber under controlled conditions for 2-3 days. The expression was checked using confocal microscopy (See section 2.7).

## 2.5 Seed stocks, germination and growth conditions

Wild type *N. tabacum* plants were used for agrobacterium-mediated infiltration and transient expression. Plants were potted

on compost (Levington F2 Seed and Modular Compost Scotts Miracle-Gro, Ohio, USA) mixed with perlite for aeration, pre-treated with 0.2 g/L Intercept 70WG (Everris, Ispwich. UK) and grown in the greenhouse with 16 hours of light and 8 hours dark. Plants 5-8 weeks old were infiltrated according to Sparkes *at al.* (2006) and observed after 2-3 days from the infiltration event.

*A.thaliana* stably expressing ST-GFP line was made by Sant-Jore (2001). *Arabidopsis* seeds were placed in 1.5 ml Eppendorf tubes and 500 μl of 80% v/v ethanol added. The seeds were then rinsed 3 times in deionised and autoclaved water and left to dry on autoclaved Millipore filter paper in the flow hood. Sterile seeds were sown on ½ Murashige and Skoog medium and (MS, MP Biomedicals, USA) and 1% w/v (BD Bacto™ Agar), and grown for 7-10 days in the incubator with 16 hours light and 8 hours dark at 28°C.

# 2.6 Polymerase Chain Reaction (PCR)

PCR reactions were performed for colony screening or gene cloning and different protocols and polymerase enzymes, Crimson Taq polymerase or Q5 High fidelity DNA polymerase respectively, were used as described in the following sections.

All the PCR reactions were performed in a T100™ Thermal Cycler (BioRad, Hemel Hempstead, UK) and the products detected on an agarose gel (See section 2.6.4).

## *2.6.1 PCR colony screening*

Colony PCR was used to check the positive colonies transformed with the product of the BR reaction (pDONOR containing either kinesin-13a or truncated kinesin-13aD). The colonies were picked up from the plate with a sterile micropipette tip and dipped into the tube containing the PCR reaction solution (Table 5). Crimson Taq polymerase was used (Table 6).

**Table 3: PCR reaction assembly for colony PCR screening using Crimson Taq polymerase.**

| Solution | Volume (µl) | Final concentration |
|---|---|---|
| Template DNA | variable (colony) | |
| 5X reaction buffer | 10 | 1X |
| 10 mM dNTPs (NEB) | 1 | 200 µM |
| 10 µM Forward Primer | 1 (of 1:10 dil) | 0.2 µM |
| 10 µM Reverse Primer | 1 (of 1:10 dil) | 0.2 µM |
| Crimson Taq polymerase | 0.25 | 1.25 units/50µl PCR |
| Autoclaved water | 41.5 | |
| Final volume | 50 µl | |

**Table 4: Thermocycling conditions for Crimson Taq polymerase**

| Step | Temperature (°C) | Time |
|---|---|---|
| Initial denaturation | 98 | 30 sec |
| Step -1 | 98 | 30 sec |
| 15 cycles | 48 | 30 sec |

| | | |
|---|---|---|
| | 68 | 1 min |
| Step -2<br>15 cycles | 98 | 30 sec |
| | 52 | 30 sec |
| | 68 | 1 min |
| Final extension | 68 | 1 min |
| Hold | 4 | |

Colonies positive to the PCR screening were grown in liquid LB over night containing the selective antibiotic and the DNA was extracted following the protocol. The extracted DNA was quantified using a Nanodrop spectrophotometer (Spectrophotometer ND-1000) and used for the LR reaction.

### *2.6.2 PCR gene cloning*

The DNA sequence of kinesin-13a was kindly provided by Prof Yoshihisa Oda (Oda and Fukuda 2013) as *E.coli* colonies containing the plasmid pGWB501 coding pkinesin-13a:GFP-kinesin-13a.

*E. coli* was grown in liquid LB over night with the selective antibiotic spectinomycin (See section 2.2) and the DNA was extracted via plasmid DNA extraction (See section 2.6.3).The extracted plasmid was then quantified with a Nanodrop spectrophotometer (See section 2.7), diluted to 1ng/μl and used as template for the PCR reaction (Table 7). Q5 high-fidelity DNA polymerase (New England Biolabs, Herts, UK) was used (Table 8).

**Table 5: PCR reaction for PCR gene cloning using Q5 High-Fidelity PCR.**

| Solution | Volume (μl) | Final concentration |
|---|---|---|
| Template DNA | 2 | |
| 5X reaction buffer | 10 | 1X |
| 10 mM dNTPs (NEB) | 1 | 200 μM |
| 10 μM Forward Primer | 1 | 0.2 μM |
| 10 μM Reverse Primer | 1 | 0.2 μM |
| Q5 High-Fidelity | 0.5 | |
| Enhancer | 10 | 1X |
| Autoclaved water | 24.5 | |
| Final volume | 50μl | |
| | | |

**Table 6: Themocycling conditions for Q5 High-Fidelity PCR**

| Step | Temperature | Time |
|---|---|---|
| Initial denaturation | 98 | 30 sec |
| 30 cycles | 98 | 30 sec |
| | 61 | 30 sec |
| | 72 | 1 min |
| Final extension | 72 | 1 min |
| Hold | 4 | |

The PCR reaction was performed in a T100 Therma Cycler (BioRad, Hemel Hempstead, UK) and 10 μl PCR products detected on agarose gel (See section 2.6.4) and successively purified from gel (gel purification). The purified PCR product was successively cleaned up following the procedure detailed in section 2.6.5.

The purified and cleaned PCR products were used for the BP Gateway reaction, where the PCR full length kinesin or truncated version was inserted into pDONR vector (See section 2.6.7).

### *2.6.3 Primer design for Atkinesin13a cloning*

The coding DNA sequence (CDS) of the protein *At*kinesin-13a, corresponding to the gene At3g16630, was obtained from Gene Bank (accession number AY056129).

The forward primers were designed to pair at the start codon ATG or from nucleotide 1601 and the reverse primers at the stop codon to generate the full length construct or truncated version of the protein, respectively. A flanking sequence was also added for the Gateway cloning. The primers are listed Table 3. The part of the primer sequence in bold is pairing with the CDS, while the rest is the flanking sequence inserting the attB recombination sites for Gateway cloning.

**Table 7: List of primers used for the cloning of *At*kinesin-13a.**

| No. | Primers | Sequence |
|---|---|---|
| 1 | Forward full length | GGGGACAAGTTTGTACAAAAAAGCAGGCTTCCCGCCA**ATGGGCGGCCAAAT** |
| 2 | Forward truncated | GGGGACAAGTTTGTACAAAAAAGCAGGCTTCCCGCCA**ATGAAGGATCCTTTGTTGGG** |
| 3 | Reverse + stop codon | GGGGACCACTTTGTACAAGAAAGCTGGGTC**CTACCGAGGAACTCTCTTAC** |
| 4 | Reverse – stop codon | GGGGACCACTTTGTACAAGAAAGCTGGGTC**CCGAGGAACTCTCTTACG** |

The melting temperature was the same for all the primers (Tm: 61 °C) and calculated using the NEB website https://www.neb.com/tools-and-resources/interactive-tools/tm-calculator. Primers were ordered from Eurofins MWG Operon (Ebersberg, Germany).

The primers were used in different combinations (Table 4 and Figure 1) to obtain full length kinesin-13a or a truncation of the motor domain (Kinesin-13aD), which were successively fused at either N- or C- termini with fluorescent markers via Gateway cloning (table 9). The construct were sequenced and the sequence alignments are shown in Appendix IV.

**Table 8: Combination of primers used for cloning of kinesin-13a.**

| Combination of primers | Construct obtained | Gateway cloning |
|---|---|---|
| 1 - 3 | kinesin-13a (+ stop codon C-term) | RFP/GFP-kinesin-13a |
| 1 - 4 | Kinesin-13a (- stop codon) | Kinesin-13a-RFP/GFP |
| 2 - 3 | kinesin-13aD (+ stop codon C-term) | RFP/GFP-kinesin-13a-D |
| 2 - 4 | Kinesin-13a-D-RFP/GFP (- stop codon) | Kienesin-13a-D-RFP/GFP |

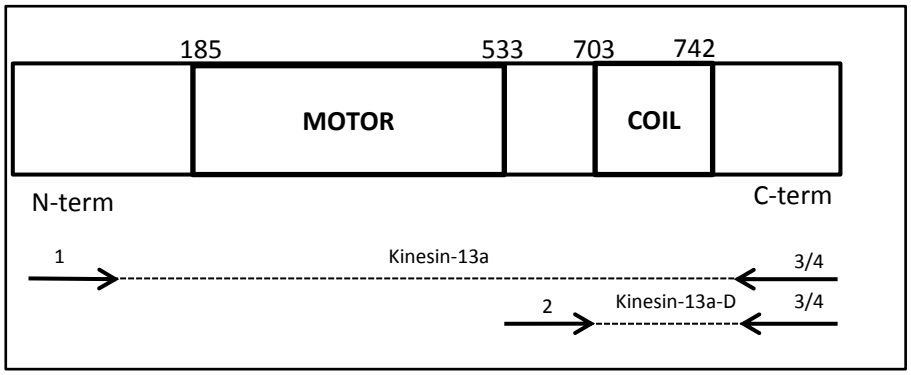


**Figure 4. Representation of the cloning strategy to obtain kinesin-13a full sequence and the mutant deleted of the motor domain (kinesin-13aD).**
Different primers combinations are used to clone the entire sequence of the kinesin gene of the mutant lacking the motor domain.

### *2.6.4 Plasmid DNA extraction*

Plasmid DNA was extracted using the Wizard Plus SV Miniprep DNA Purification System (Promega). A volume of 5-10 ml of over night *E.coli* culture was centrifuged at 5000 rpm for 5 mins. Pellets were re-suspended in 250 µl of re-suspension solution at room-temperature; 250 µl of lysis solution was added and mixed inverting 4 times followed by the addition of 10 µl of a protease solution. The mix was incubated for 5 minutes at room temperature and 350 µl of neutralization buffer was added and

mixed by inverting. The cell lysate was centrifuged at 13000 rpm for 10 minutes to pellet the cell debris. The clear supernatant was decanted into a miniprep spin column, placed into a collection tube and centrifuged 1 min at 13000 rpm. The flow through was discarded and the column was washed by adding 250 μl wash solution and centrifuging for 1 minute at 13000 rpm; the column was washed again repeating this step. The column was left to dry at room temperature for 10 mins and the DNA eluted by adding 50 μl of deionised autoclaved water and spinning for 1 minute at 13000 rpm. The concentration of the plasmid DNA is measured using the Nanodrop spectrophotometer (wavelength 260 nm). Where necessary, the plasmid DNA was diluted in autoclaved deionised water and stored at -20°C.

### *2.6.5 Agarose gels*

PCR products were run on 1% agarose gels in 1 X Tris Acetate EDTA buffer (TAE: 40 mM Tris, 20 mM acetic acid and 1 mM EDTA). The agarose solution was heated by microwave until the agarose dissolved in solution and was allowed to cool to 40-50°C before adding 0.5 μg/ml of ethidium bromide (Thermoscientific). The gel solution was poured into a gel cast and allowed to polymerise, and the gel was covered with 1X TAE buffer. PCR products were prepared as follow: 10 μl of gel loading dye (NEB) was added to the PCR reaction (50μl) and 10μl of the mix was loaded into the gel wells. Alongside to samples, 10 μl of DNA ladder (Quick load 1 kbp DNA ladder, NEB) was also loaded. The gel was run at 80V until the dye front reached 2 cm from the front of the gel. DNA bands were imaged using an UV transilluminator (Ultra-Violet Products Ltd., Cambridge, UK) and Uvisave gel documentation camera (UVlec Ltd, Cambridge, UK).

### 2.6.6 DNA extraction from agarose gel and PCR clean-up

PCR products were extracted from agarose gels using the Wizard SV Gel (Promega). The band was cut out of the gel using a razor, placed in a 1.5ml Eppendorf and dissolved adding 10 μl of membrane binding solution per 10 mg of gel mg and incubated at 50°C.

The dissolved gel or the solution containing the PCR product, was transferred into a purification mini-column, inserted into a collection tube and incubated for 1 minute at room temperature. The column assembly was centrifuged for 1 minute at 13000 rpm, the flow through discarded, and the column was washed by the addition of 500 μl of wash solution and centrifuged at 13000 for 1 minute. The wash step was repeated adding the same volume of washing solution and centrifuged. The flow through was discarded and the column centrifuged for 1 minute at 13000 to eliminate any residue of ethanol. The DNA was eluted from the column by adding 25-50 μl of autoclaved water, incubated 1 minute at room temperature and centrifuged at 13000 for 1 minute. The purified PCR products were quantified using the Nanodrop spectrophotometer and stored at -20°C.

### 2.6.7 Gateway cloning

PCR products were cloned into the Gateway entry vector pDONR207 (Invitrogen) through a BP reaction to produce the entry clone. The BP reaction is composed as listed and had a final volume of 5 μl:

- 3μl of PCR product (approximately 100 ng) purified from gel;
- 1μl pDONR (100 ng approximately);

- 1µl BP enzyme

The reaction was incubated over night at 25°C then deactivated adding 0.5 µl of proteinase K for 10 min at 37°C.

Highly competent *E.coli* cells DHα were transformed (See section 2.3) using 1µl of BP reaction mix and plated on LB agar plates containing gentamycin, the selection antibiotic for pDONR. A transformation was performed using 5 µl of empty pDONR (corresponding to 20ng) as a control. Positive colonies resistant to the selection antibiotic were picked for colony PCR. Four clones resulting positive from the colony PCR reaction were grown in LB culture, and the plasmid DNA was extracted for the LR reaction

In the LR reaction, the PCR product was fused to a fluorescent reporter at either end and inserted into an expression vector suitable for expression in plant via agrobacterium infection (Table 9).

**Table 9: List of expression vectors and their use to obtain the fusion proteins.**

| Vector | Fluorescent tag | Final construct |
|---|---|---|
| pB7FWG2 | C- term GFP | kinesin-13a-GFP<br>kinesin-13a-D-GFP<br>Cb-actin-GFP |
| pB7RWG2 | C-term RFP | kinesin-13a-RFP<br>kinesin-13a-D-RFP |
| pB7YWG2 | C –term YFP | Cb-actin-YFP |
| pB7WGF2 | N-term GFP | GFP-kinesin-13a<br>GFP-kinesin-13a-D<br>GFP-Cb-actin |
| pB7WGR2 | N-term RFP | RFP-kinesin-13a<br>RFP-kinesin-13a-D |
| pB7WGY2 | N-term YFP | Cb-actin-YFP |

The LR reaction components are:

- 25-75ng of pDONR containing PCR product
- 1µl expression vector (75 1µg/1µl approximately )

- 1µl LR enzyme

The reaction was incubated over night at 25°C then deactivated adding 0.5 µl of proteinase K for 10 min at 37°C.

At this stage, the desired plasmid DNA was sent to Source Bioscience (Oxford, UK) for Sanger sequencing and the results aligned with the CDS using the blast suite (http://blast.ncbi.nlm.nih.gov). 1µl of DNA of the positive clones was used to transform 25µl of *E.coli* high efficiency DHα cells according to the standard protocol and selected for the antibiotic resistance. Plasmid DNA was extracted from positive colonies and used to transform agrobacterium.

### *2.6.7.1 Gateway cloning of the actin nanobody*

Constructs fusing the antibody sequence with both N- and C-terminal fluorescent protein tags (YFP or GFP) respectively, were prepared by Dr Verena Kriechbaumer to optimize the construct for the expression in plants; this was part of a collaboration to produce better fluorescent markers for the plant cytoskeleton. In the original construct provided by Chromotek, a short peptide of ~20 amino acids (AGGTGGAGGAGGTTCTGGA) is present at the C-terminus of the nanobody sequence, linking the antibody to the fluorophore (Figure 2A). Such a linker was maintained, as suggested by the provider, when the sequence of the nanobody was cloned into a vector suitable for the expression in the plant and tagged with eYFP or GFP at the C-terminus or N-terminus (Figure 2B and 2C).

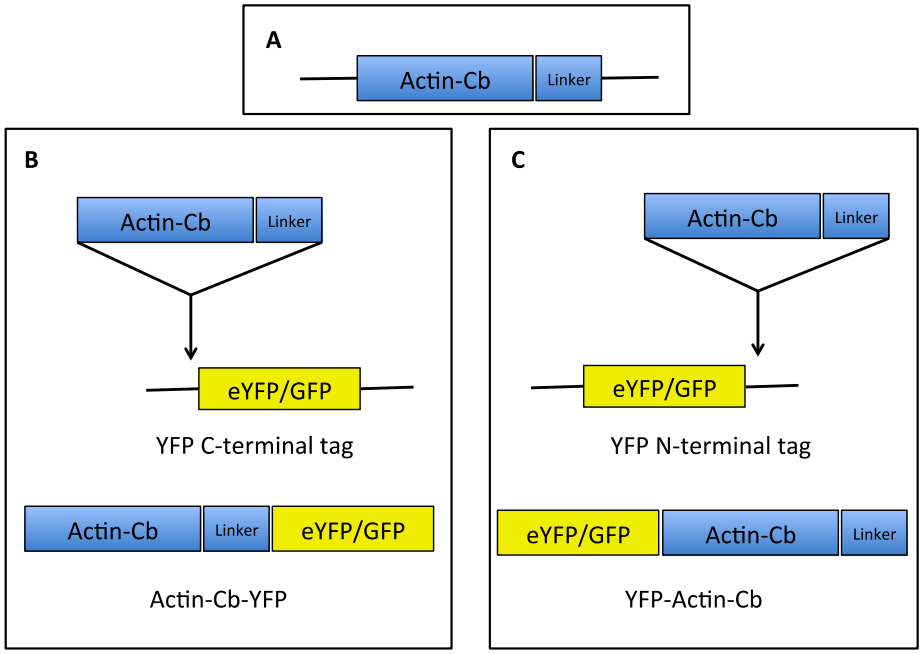


**Figure 5. Fusions of the actin nanobody to fluorescent markers.**
(A) Sequence of the nanobody as provided by Chromoteck company, with linker of ~20 aa at C-terminal end; (B) YFP fused to C-terminal end of actin-Cb (actin-Cb-YFP); (C) YFP fused to N-terminal end of actin-Cb (YFP-actin-Cb).

# 2.7 Confocal Microscopy

## *2.7.1 Image acquisition*

Confocal laser scanning microscopes (Zeiss UK, Welwyn Garden City, UK - LSM 510 META uprights and an LSM 510 inverted) equipped with 63X and 100X oil immersion objectives (Numerical aperture 1.4) were used for image and movie acquisition.

A segment of approximately 0.5 $cm^2$ was cut out of tobacco leaves expressing the protein of interest and mounted on a microscope slide with the lower epidermis facing upward. About 20 µl of water was added before mounting the cover slip to keep the sample moisturized. A drop of oil was deposited on the coverslip to allow the imaging with oil-immersion objectives. Specific settings were used to image different fluorophores (Table 10).

**Table 10: Imaging settings for the different fluorophores.**

| Fluorophore | Excitation laser (nm) | Emission spectra (nm) | Beam splitter |
|---|---|---|---|
| GFP | 488 | BP 505-530 | HFT 458/514<br>NFT 595<br>NFT 515 |
| RFP | 543 | BP 560-615 | HFT 488/543<br>NFT 545 |
| YFP | 514 | BP 470-500 | HFT 405/488/543/633<br>NFT 515 |
| Pinhole 250 μm | | | |

### *2.7.2 Drug treatments*

To depolymerize the actin/microtubules cytoskeleton, leaf sections were soaked in a solution containing depolymerizing agents. The depolymerising drugs are solvents in DMSO (dimethyl sulfoxide).

DMSO is an industrial compound which finds a wide use in clinical applications (Wood and Wood 1975). Due to its chemical properties, DMSO is a good solvent for a wide range of drugs and increases cell permeability, thus enhancing the cellular uptake (MacGregor 1967, Rammler and Zaffaroni 1967, Sciuchetti 1967).

Actin filaments were disrupted by treating the samples with 25 μM latrunculin B (Calbiochem, Nottingham, UK; dissolved in DMSO and successively diluted in water to obtain the final concentration of 25 μM) for 30 minutes. For latrunculin B treatment, the DMSO control is 1 μl/ml.

LatranculinB is an actin depolymerizing compound isolated from the Red Sea sponge *Latrunculia magnifica* known to bind actin monomers and form 1:1 complexes, thereby preventing the polymerization of monomeric actin into actin filaments (Wakatsuki *et al*. 2001).

Microtubules were depolymerized by treating the sample with 10μM oryzalin (Oryzalin Technical Min 95%, DowElanco; dissolved in DMSO to make stock solution 10mM and further diluted in water to the final concentration 10μM) for 45 mins. The DMSO control is 10 μl/ml (Hugdahl and Morejohn 1993).

### *2.7.3 Time-lapse image series acquisition*

One or two leaves of at least 2 tobacco plants expressing the fluorescent markers were infiltrated and one movie taken per cell. The laser settings for time-lapse image acquisition was the same as for images acquisition. The 63X oil-immersion objective was used, the zoom was set at 3.7 and a square ROI of size 244 X 244 was selected. The rate of acquisition was 0.4 sec per frame, and a total of 50 frames per movie was recorded. Each leaf sample was used for no longer than 20 minutes and at least 20 time-lapse image series per condition were taken.

## 2.8 Tracking

Time-lapse series of fluorescent cortical Golgi bodies were acquired as above and their movement was tracked using the tracking module of Volocity 6.3 (Improvision, Perkin Elmer). The software can detect and track objects (fluorescent Golgi bodies) over all time-lapse images (movie 1). The tracking algorithm works by calculating the centroid position of the object and generates tracks by connecting the centroids. Objects are detected on the basis of specified parameters (Intensity of the fluorescence (50-100%), object size (0.04 $\mu m^2$) and the tracking model can be chosen as well (shortest path model, minimum distance 2.6 $\mu m$). The software is able to detect most of the objects and the tracks were manually checked one by one to make sure that the organelles were accurately tracked and that a same organelle was not tracked multiple times; additionally, clusters of Golgi bodies and tracks combining less than 5 sequential images were excluded because it was necessary to analyse the movement of single objects and over a significant amount of time.

For each track, velocity, displacement rate and meandering index were chosen to describe Golgi body movement. The velocity (V) is the track length divided by the time; the displacement rate (DR) is the linear distance between the starting point and the end point divided by the time; the meandering index (MI) is the ratio between displacement rate the velocity (Figure 3).

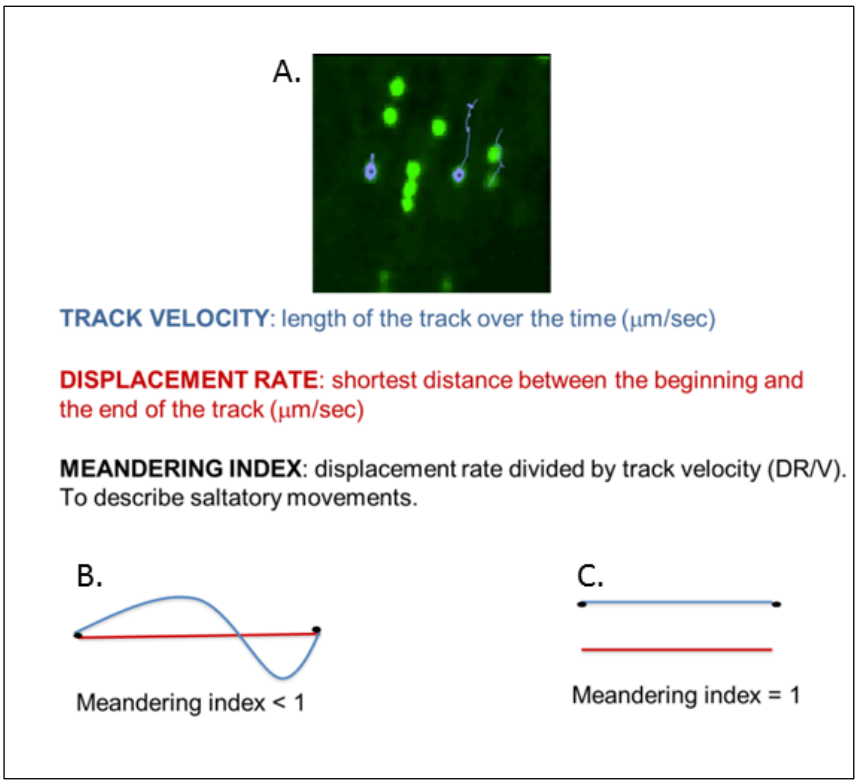


**Figure 6. Screenshot of tracking and the parameters calculated by the software.**
The software recognizes and generates tracks for most of the Golgi bodies (A) and can calculate the track velocity (μm/sec)(blue line), the displacement rate (μm/sec) (red line) and the meandering index, which is the ratio between the velocity and displacement rate. If the organelle has a salutatory movement, the track is more curved and the meandering index would be less than one (B); if the movement of the object is linear, the shape of the track approximately a straight line then the meandering index would be close to one (C).

Tracking measurements were performed on samples under different conditions (untreated sample, DMSO control and treatment with depolymerizing agents) and a variable number of between 65 and 238 Golgi bodies were tracked per condition. One or two leaves of at least 2 tobacco plants expressing the fluorescent markers were used. The untreated sample consisted of tobacco plants expressing the Golgi marker ST-GFP solely; different approaches were used to recognize cells that were effectively treated with the depolymerizing agents. In cells treated

with latrunculin B, Golgi bodies were not motile and only these cells are chosen for the analysis because the lack of motility of Golgi bodies indicates that the treatment was effective. In the case of treatment with oryzalin, the Golgi marker ST-GFP was co-expressed with the microtubule marker GFP-TUA and the treatment performed. The depolymerisation of microtubules was determined by the loss of fluorescent filaments and the appearance of cytoplasmic fluorescence, which are units of fluorescent tubulin dispersed in the cytoplasm. Only cells showing this fluorescent pattern were used for tracking. The DMSO control was performed at either concentration of 10 µl/ml for oryzalin or 1 µl/ml for latrunculin B (See section 2.7.2). In this case, the cells were chosen randomly for time-series acquisition.

To estimate the differences between the samples and experimental conditions, a statistical analysis was carried out as described in section 2.14.1.

### *2.8.1 Statistical analysis of tracking data*

The data were processed using the software SPSS 22 (IBM). The datasets of the velocity, displacement rate and meandering index were analysed in two phases.

Initially, a descriptive statistic was carried out to characterise the sample; information such as sample size, mean, median, range, standard deviation and skewness were obtained. The skewness provides a measurement about the symmetry of the dataset distribution. Normally distributed datasets are bell shaped, symmetrical around the median and mean and the skewness value is 0; positive values of skewness indicates that the peak of the curve is shifted toward left, and has the long tail of low values on the right; negative values of skewness indicates that the peak

of the curve is shifted right, with the long tail of low values on the left (Figure 4) (Freund and Wilson 2003).

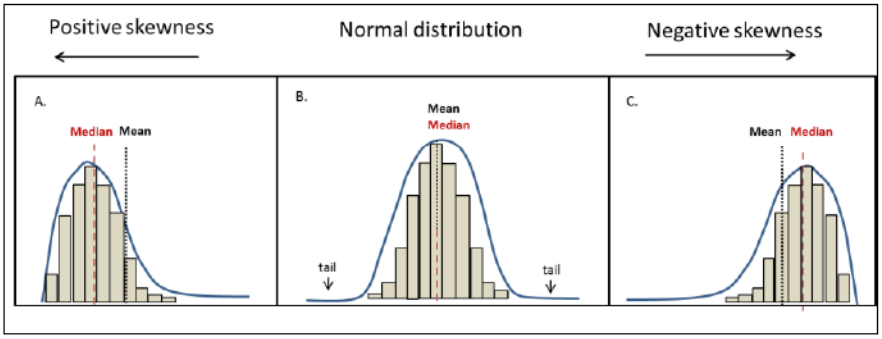


**Figure 7. Histograms display sample distribution.**
Normally distributed datasets are bell-shaped and symmetrical around the mean and median (B). Positive skewed dataset have the tail of high values longer than the tail of low values and the mean is bigger than the median (A). Negative skewed distributions have the tail of higher values longer than the tail of smaller values (C).

Whisker boxplots (Figure 5) and histograms of frequency were also generated to show the distribution of the datasets. The former, are useful tools to detect and classify outliers and extreme outliers which can correspond to errors (See Appendix I).

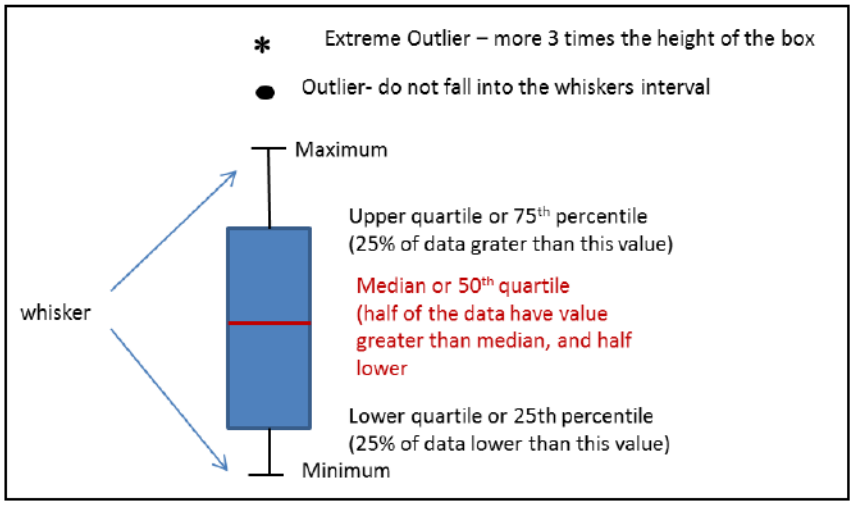


**Figure 8. Reading whisker boxplots.**

Whisker boxplot are diagrams made of three parts: the rectangular box defining the upper quartile and the lower quartile, with the median dividing the box; the whiskers (or fences) indicating the minimum and the maximum; outliers (•)are values beyond the end of the whiskers which are 1.5 times the interquartile range; extreme outliers (*) are values 3 times bigger the interquartile range. Adapted from: Landau and Everitt (2004).

The normality of the distributions was also tested with the Shapiro-Wilk test which is used for samples smaller than 2000 datapoints and starts from the hypothesis that the dataset is normally distributed. The significance level (p.value) is set as a default (0.05); for p.values results below 0.05, the null hypothesis is accepted and the dataset is normally distributed; for p.values above 0.05, the null hypothesis is rejected and the dataset is not normally distributed.

All tracking datasets were not statistically distributed; alternative tests for non-normally distributed datasets (which are named non-parametric tests) are chosen to assess the differences between them. The non-parametric Kolmogorov-Smirnov (KS) test for independent samples and the Mann-Witney (MW) were chosen (See Appendix I).

The Mann-Whitney test was performed to detect differences in the median, being the statistical measurement closest to the central tendency of the distribution. The test assumes that the median is the same across the samples (null hypothesis) and the significance level is set at 0.05; results lower than 0.05 indicate that the median is statistically different while results bigger than the significance level indicate that the median is close and not different (Figure 6).

The Kolmogorov-Smirnov test (KS) was also selected to detect differences in the shape of the cumulative distribution function (CDF) plot (See Appendix II) and to compare the results with published data (Avisar *et al.* 2009). The null hypothesis is that the tested samples have the same distribution and the significance level is set at 0.05; the null hypothesis is retained for values below the significance level and is rejected for values above the significance level, indicating that the distribution of the two samples is different. To build the CDF plots, the frequencies of the values were first calculated and the plots successively generated (See Appendix II).

SPSS provides a detailed analysis of the datasets; the outputs of the analysis were re-tabled to extrapolate only the most significant data (example of original SPSS outputs in Appendix I) (Freund and Wilson 2003).

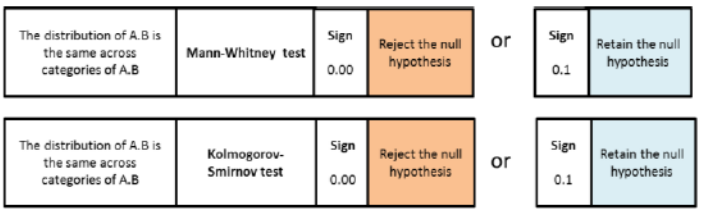


**Figure 9. How to read the results of non-parametric tests.**
Any statistical tests start from the assumption that there are no differences between the datasets (null hypothesis). In the figure the datasets are indicated as A and B. If the result of the test is lower than the significance level 0.05, the null hypothesis is rejected, meaning that

there are differences between the datasets; if the result of the test is bigger than the significance level 0.05, the null hypothesis is retained, meaning that the two datasets are not statistically different.
Non-parametric tests were run for the datasets of velocity and displacement rate. The Kolonogorov-Smirnov test (KS) compares the sample distribution function; The Mann-Whitney (MW) test compares the mean. For both, the significance level is set to 0.05

Relative median of the meandering index and displacement rate was calculated to quantify the variation in the sample treated with the depolymerizing agents compared to the control. Excel was used and the following formula (1) to estimate the relative mean:

(1) $100 : MI_{depoly}(\%) = MI_{control} : MI_{depolym}$

Where $MI_{control}$ is the meandering index of the DMSO control, $MI_{depoly}$ is the meandering index of the sample treated with either latrunculin B or oryzalin and $MI_{depoly}(\%)$ is the meandering index of the sample treated with depolymerizing agents and expressed as percentage of the control. The meandering indices as percentages are represented as boxplots. The differences between the meandering indeces were assessed using t-test.

# 2.9 Optical trapping

The imaging and trapping of Golgi bodies was performed on a TIRF microscope (total internal reflection fluorescence) equipped with a far-red laser optical trap (Central Laser Facility, Rutherford Appleton laboratory, Harwell).
To image the fluorescent organelles, a 490 nm excitation laser was used with a maximum output power of 5 mW. Emitted fluorescence was filtered using a long pass filter 500 nm, plus a band pass filter 520 ± 12.5 and an ND8 filter.

The optical trap consisted of a highly focused infrared beam generated by 1990nm laser and was focused using a 100X oil immersion TIRF objective lens (Nikon). The laser power at the source was set at 3.5V corresponding to 380mW when it enters in the TIRF system and corresponding to approximately 64mW at the stage, after it passed through the objective. For moving the trap, the laser was maintained in a fixed position while the microscope stage was moved; the positioning of the stage and velocity (10 μm/sec) was controlled through the custom programmed LabVIEW software (National Instruments), which also controlled the EMCCD camera (Andor Ixon, exposure time: 0.1 sec, gain: 2600-2800) and a shutter across the trapping laser beam.

Before starting each experiment, the laser was calibrated and the power measured at the source, through the system and at the microscope stage.

A leaf sample (untreated, treated with DMSO control or depolymerizing agents) was mounted on the microscope slide (cover slip size 22X50 mm #0, Menzel-Glaser) (See section 2.12.1). Tape was used to seal the sample and avoid coverslip movement and drying of the sample. Each sample was imaged for a maximum of 20 minutes.

To check if the settings of the laser were similar to previous experiments, a total of 50 Golgi bodies are trapped and the number of organelles that fall into the trap was compared to the figures obtained in the previous experiments.

### *2.9.1 Data collection and analysis of optical trapping data.*

In *N. tabacum* a maximum of 100 Golgi bodies per sample per condition were trapped (100 Golgi body test) and classified according to two categories: 'trapped' (if the object is held by the

trap and can be displaced from the original position) or 'not trapped' (if the object could not be trapped and displaced from the original position). Due to plant material availability, in *A. thaliana* a maximum of 50 Golgi bodies were trapped per sample, per condition (untreated, DMSO, oryzalin or latrunculin B treatment), and the data extrapolated to the count of 100 and presented as percentage. Five Golgi bodies were trapped per cell (non-contiguous cells were chosen. The totals reported and analysed represent the data collected from between four and ten repetitions, where each repetition is from one leaf sample taken from independent plants. The trapping data were analysed using Exel or Staplus (equivalent of Excel for Mac OSX).

Initially, the homogeneity of variance was assessed using an F-test, which is whether the variances of two populations are equal at the significance. The null hypothesis is that the variances of the sample are equal. The null hypothesis is retained if the F-value (the ratio between the variances) is smaller than the F-critical one tail (that is the critical value to accept or reject the null hypothesis) that is the two samples have homogeneous variances. The null hypothesis is rejected if F-value > F-Critical one-tail, that is the two samples have heterogeneous variances (Figure 6).

| | DMSO | Latrunculin B |
|---|---|---|
| Mean | 58.00 | 74.56 |
| Variance | 601.71 | 324.53 |
| Observations | 15.00 | 16.00 |
| df | 14.00 | 15.00 |
| F | 1.85 | |
| P(F<=f) one-tail | 0.12 | |
| F Critical one-tail | 2.42 | |

**Figure 10. Example of F-test output.**
The F-test is used to assess if the two samples have equal or unequal variances. In the output table different statistical parameters are listed (Mean, Variance, observations, df or degree of freedom).

F is the ratio between the variances. If F > F critical one-tail, the null hypothesis is rejected that is the samples have heterogeneous variances; if F < F critical one-tail, the null hypothesis is retained and the samples have homogeneous variances.

According to this result, the appropriate paired t-test (equal variance or unequal variance) was performed to assess the differences between the means (alpha: 0.05). A t-test result (indicated as p) smaller than 0.05 indicates that the mean values of the samples are statistically different, and a t-test result bigger than 0.05 indicates that the mean values of the samples are not statistically different. The mean values are represented as percentage of the mean of the control and plotted as a boxplot where the significance of the differences is represented as (*) $p \leq 0.05$, (**) $p \leq 0.01$, (***) $p \leq 0.001$, , (****) $p \leq 0.0005$.

## 2.10 FRAP acquisition

For FRAP (fluorescent recovery after photobleaching) experiments the, fluorescent fusion constructs (Lifeact-GFP, GFP-actin-Cb, RFP XIK-tail) were transiently expressed in *N. tabacum* plants (Sparkes *et al*. 2006). The concentration of agrobacterium (OD) for each combination of constructs were: Lifeact-GFP $OD_{600}$: 0.01; GFP-actin-Cb $OD_{600}$: 0.03; Lifeact-GFP $OD_{600}$: 0.01 and RFP-XIK-tail $OD_{600}$: 0.05; GFP-actin-Cb $OD_{600}$: 0.01 and RFP-XIK-tail $OD_{600}$: 0.05.

The FRAP experiments were performed with both the Inverse Zeiss/LSM and the 510 META confocal microscopes. The FRAP parameters were maintained the same in all the experiments to obtain comparable results.

A 63X oil immersion objective with digital zoom of x0.7 was used. The photobleaching area was defined as a ROI circle of 25 $\mu m^2$. To

image the GFP fusions, an argon laser excitation wavelength at 488 nm at 50% of the output power was used and the GFP emission was detected with a 505-530nm band-pass filter.
Five scans at a laser power of 15% were performed to assess the level of fluorescence for the bleaching. For the bleaching, the laser beam was increased to 100% for 70 iterations. The recovery of the fluorescence was followed over a period of 30-40 seconds with a lower transmission laser (15%). During the whole experiment, an additional ROI of the same size and shape as the bleached one, was drawn to monitor that the bleaching effect was restricted to the ROI and to compensate for any bleaching due to the laser scanning during the recovery period. One ROI per cell was bleached, and at least 20 cells were analysed per combination of fluorescent markers.

### *2.10.1 Normalisation and fitting of FRAP data*

Analysis was restricted to the recovery of the fluorescence after the photobleaching. The data of recovery of the fluorescence were analysed using Microsoft Exel: the recovery was normalised against the pre-bleaching fluorescent conditions and expressed as percentage using the equation (2)

$$(2)\quad In = [(I_t - I_{min})/(I_{max} - I_{min})] \times 100$$

where In is the normalized intensity, $I_t$ is the intensity at time t, $I_{min}$ is the minimum intensity in the data set and $I_{max}$ is the maximum intensity in the data set (Runions *et al*. 2005).

Statistical curve fitting was carried out using Prism 4 (GraphPad , San Diego, CA U.S.A.) and data was fit to an exponential one-phase association curve having the equation (3):

(3) $I = I_0 + (I_{max}-I_0)*(1-exp^{-K*t})$

Where $I_0$ is the fluorescence intensity after the bleaching event, $I_{max}$ the maximum intensity of the fluorescence recovery and K a rate constant, t the time. The half-time ($t^{1/2}$) of recovery is the time taken to obtain the recovery of half of the fluorescence and is calculated as ½ ln(K).

Considering that the initial section of the curve is approximating to a linear function, the slope of this linear segment would correspond to the percentage of fluorescence that recovers over the time span of one second.
To extrapolate the rate of fluorescence per second (R), the following equation (4) was used:

(4) $I_{t1/2}$ (%)= R x t½ (sec)

From which R = I t1/2 (%) / t½ (sec)

Where $I_{t1/2}$ is half of the max fluorescence, t½ (sec) is the half-time and R is the rate of fluorescence per second.

### *2.10.2 Statistical analysis of FRAP results*

The $t_{1/2}$ values and I max were statistically analysed and compared per condition.
The statistical analysis was carried out with Excel or Statplus Mac. Initially the equality of variances was assessed using an F-test and

followed by t-test for equal or unequal variances were performed, with the significance level at 0.05.

# 3 Tracking the movement of Golgi bodies.

## 3.1 Introduction

Live cell imaging and fluorescent markers for Golgi bodies showed for the first time that these organelles move on the ER surface in plant cells. Treatment with the actin-cytoskeleton depolymerizing agent latrunculin B caused the cessation of the translational movement and aggregation of Golgi bodies in small clusters (Boevink *et al*. 1998) (movie 2) indicating that there was a correlation between actin arrays and Golgi body motility. Mutants of the actin-motors myosins belonging to the class XI, reduce the motility of Golgi bodies and other organelles when expressed in Arabidopsis pollen tubes and tobacco leaf epidermal cells (Avisar *et al*. 2009, Avisar *et al*. 2008, Griffing *et al*. 2014, Madison *et al*. 2015).

Interestingly, the depolymerisation of microtubules does not stop the movement of Golgi bodies but a role in regulating the movement cannot be excluded. In Nebenführ *et al*. (1999) Golgi stacks were tracked and the movement numerically described as 'streaming level'. Leaf epidermal cells treated with various microtubule-disrupting agents showed an increase of the number of active cells and increase of streaming activity. Such change in the streaming activity was not quantified and a small sample was used, so a conclusion cannot be drawn.

A successive study in hypocotyls by Crowell *et al*. (2009), suggested that Golgi stacks pause on microtubules and this is concomitant to the insertion of the cellulose synthase complex

(CSC) into the plasma membrane. When microtubules are absent, following treatment with a depolymerizing agent, the CSCs are distributed uniformly whereas when the microtubules are present and stabilized with taxol the cellulose complexes are aligned (Crowell *et al*. 2009). This led to the hypothesis that microtubules are participating to the fine tuning of the fast translational movement of Golgi stacks on actin filaments (Brandizzi and Wasteneys 2013). So far, the only microtubule-related protein localized on Golgi bodies, is the non-motor *At*kinesin-13a but its role in the organelle's motility regulation has not been shown (Wei *et al*. 2009).

Considering the whole cytoskeleton network, it is still unclear if the two classes of filaments are physically connected and which protein bridges are involved (Schneider and Persson 2015, Wang *et al*. 2014, Wang and Hussey 2015). Some evidence shows that actin and microtubules cross–talk (Collings 2008), and that the recovery of microtubules requires the presence of actin filaments and *vice versa* (Sampathkumar *et al*. 2011), so a role of the microtubules in directly or indirectly regulating the Golgi motility, cannot be excluded.

In this chapter, the contribution of the single cytoskeleton components was measured in order to understand how each type of filament regulates the movement of Golgi bodies in the cortical region of leaf cells. This is achieved by combining live cell imaging time-series, which were taken with the confocal laser scanning microscope, and the software 'Volocity' to analyse the time series. The software Volocity is able to automatically detect fluorescent Golgi bodies and quantify parameters that can describe their movement. Of all the parameters that the software gives as output, velocity, displacement rate and meandering index are taken into consideration and compared in different conditions to dissect the mechanism underlying Golgi body dynamics.

# 3.2 Results

## *3.2.1 Setting the statistical approach: analysis of velocity values and comparison between repetitions*

In all the experiments, movies of *N. tabacum* leaf epidermal cells transiently expressing ST-GFP labelled Golgi bodies were collected at 48 and 72 hours after the infiltration event and following the treatment of samples with cytoskeleton depolymerisation drugs or DMSO as control. For each expression day, the experiment was performed two times, and at least 20 movies per condition (untreated, depolymerizing drugs, DMSO) were recorded. The movies were analysed with the software Volocity to calculate the velocity (V), displacement rate (DR) and meandering index (MI) (Figure 11A). Each movie represented a biological replicate and each Golgi body is a datapoint; the size of the dataset was between 65 and 215 entries (n). The datasets of V, DR and MI were statistically analysed using the software SPSS. The analysis was carried in two steps: a descriptive statistical analysis to characterize the datasets and a subsequent analysis to evaluate the differences between repetitions for a same expression day and ultimately differences between untreated and treated samples (with DMSO, latrunculin B or oryzalin).

Initially, the datasets of repetitions for a same expression day were analysed in order to assess the variability within the sample and repetitions. For a same expression day (48 hrs from the infiltration event), the descriptive statistics of the velocity showed that the first replicate (rep 1) had 129 datapoints, where a

datapoint is a Golgi body, and the second replicate (rep 2) had 215 datapoints (Figure 11B).

To further characterize the dataset, the mean and the standard deviation (SD), which represents how much the values are spread about the mean, were considered. In replicate 1, the velocity has a mean of 0.61 μm/sec and SD of 0.49 μm/sec; replicate 2 has a mean value of 0.75 μm/sec and SD of 0.57 μm/sec (Figure 11B). It could be observed that the mean values of the replicates were close and that in both cases the standard deviation was quite large. The same trend of the mean and SD of the sample excludes the possibility that the high variability is due to a technical error while collecting data. The large SD might suggest that in the dataset there are outlier points (Figure 11C) and that the datasets might assume a distribution different from a normal one. The skewness values give information about the distribution of the datasets. The skewness defines the symmetry of a distribution (See Figure 7).

As figure 11B shows, the skewness value for replicate 1 was 2.30 and for replicate 2 was 1.89, meaning that the data are not symmetrically distributed but shifted towards the left. The normality test (Shapiro-Wilk) was run to confirm the distribution of the datasets (See section 2.8.1). Both Shapiro-Wilk test (Figure 11B) and histograms (Figure 11D and 11E) showed that the distribution of the data was positively skewed. The black dashed line represents the mean while the red dot line represents the median. For large datasets normally distributed, mean and median were close to each other and represent the central tendency of the data (Figure 7). As demonstrated in the histograms in figure 11D and 11E, the mean and median were shifted. The median was closer to the peak of the distribution, meaning that the median was more representative of the central

tendency of the data. The median was used instead of the mean for further analysis.

Non-normally distributed datasets with a skewed distribution, can be transformed into normally distributed datasets by applying a function (e.g. logarithm) and a t-test or ANOVA can be used to assess differences (Figure 19); this possibility will be discussed later in this chapter.

For non-normally distributed datsets, the non-parametric Kolmogorov-Smirnov (KS) test for independent samples and the Mann-Witney (MW) were chosen (See section 2.8.1).

Both tests show that there were significant differences between the replicates of Golgi measurement at 48hrs from the infiltration day for the significance level of 0.05 (See Appendix III).

Because of the high variability in the samples, the option of pooling together the repetitions to constitute one dataset of velocity values collected at 48 hrs from the infiltration day was considered. The dataset (n= 344) had a median velocity of 0.56 μm/sec. It was positively skewed, non-normally distributed (Figure 12A) and maintained the left skewed distribution with the central tendency close to the median (Figure 12B). There was an increase in the number of values in the tail fraction of the distribution as was more clear in the whisker boxplot graph (Figure 12C). The sum of two positive skewed distributions increases the number of values at the tail of the distribution, which are far from the central tendency. The whisker boxplot graph (Figure 12C) better represents what is happening to the dataset when the replicates are pooled: the circles and stars in the graphs indicate the data which the statistical programme classifies as outliers and possible errors, respectively. The sum of

replicate 1 and replicate 2 determines an increase of the number of data that lie outside the whisker fences (Figure 12C).
To assess if the same pattern of distribution of data was observed when the velocity values were collected after 72 hrs of expression, the procedure described above was repeated.

The number of datapoints for replicate 1 (n= 127) and for replicate 2 (n= 198) (Figure 13A); the mean value of replicate 1 was 0.8 μm\sec and SD 0.44 μm/sec; the mean value of replicate 2 was 0.5 μm\sec and SD is 0.47 μm/sec (Figure 13A). In this case, the mean values of the velocity in replicate 1 and replicate 2 were largely different and, similarly to what observed for the velocity values recorded at 48 hrs, the SD values were quite high compared to the means. A third replicate of smaller size (10 movies) was conducted to assess if the source of variability in this case was generated by a technical error, such as non-consistent tracking settings. The velocity mean value of replicate 3 was 1.23 μm/sec and SD 1.04 μm/sec (Figure 13A).
The normality test Shapiro-Wilk, confirmed that the datasets were non-normally distributed (Figure 13A). The distribution of the data (Figure 13B, 13C and 13D) proved to be non-normal and positively skewed, as also was observed for the first dataset collected at 48hrs from the infiltration event (Figure 11D and 11E).
This was confirmed in the boxplot analysis (Figure 13E), which clearly showed that the median of replicate 1 was far from the median of replicate 2 and replicate 3 and that the pattern of the outlier data was different. The KS test and MW test (See Appendix III) confirmed that the replicates were statistically different.

## 3.2.2 The effect of depolymerisation of actin filaments on Golgi dynamics

### 3.2.2.1 Velocity

Differences in the velocity between untreated samples and samples treated with the actin depolymerizing agent latrunculin B and the chemical compound DMSO were assessed. The effect of DMSO, commonly used as a solvent in experiments such these, on organelle motility had not been assessed before. DMSO is a polar aprotic molecule that has amphiphilic properties, that is, miscible in water and organic compounds (MacGregor 1967). It interacts with lipid bilayers and its effect on the organization of the membrane is dose dependent (Gurtovenko and Anwar 2007, Hughes *et al*. 2012). The interaction of DMSO with the plant cell wall and its dose-dependent effects have not been analysed in plant tissues. In plant cell cultures it is used to permeabilize cell membrane in the concentration range of 2-20 % (Parr *et al*. 1984). It has been also used to enhance *in vitro* polymerization and stability of microtubules isolated from both plants and animal cells (Mitchison *et al*. 2013, Mizuno 1985).

Initially the velocity values recorded for the untreated sample were compared to those collected after the treatment with DMSO 10 μl/ml (See sections 2.8 and 2.7.2).

The dataset of DMSO (n=198, Figure 14A), had a median Golgi velocity of 0.37 μm/sec very close to the one of the untreated sample (0.44 μm/sec), was positively skewed as can be appreciated from the table 14A and in the histogram 14B, and non-normally distributed as the normality test Shapiro-Wilk demonstrated (Figure 14A).

The KS and MW tests were performed to assess differences between the untreated sample and the treatment with 10 μl/ml of DMSO. Both tests proved that there was no significant difference between them (See Appendix III). The same result was obtained from the same analysis performed on the second replicate (data not shown).

The sample size of the latrunculin B sample was n= 88, the median value of the velocity was 0.28 μm/sec, 1.3 times less than the velocity of the sample treated with DMSO (Figure 15A). The standard deviation remained large and was of 0.25 μm/sec and the skewness was positive (Figure 15A), as also the normality test (Figure 15A) and histogram showed (Figure 15B). The dataset was non-normally distributed and its centre was shifted towards the left. The boxplot permitted a better appreciation of how the range of velocity values was also reduced compared to the treatment with DMSO (Figure 15C). The differences observed in the median were significant as the MW test showed and also the differences in the distribution were significantly different as assessed by the KS test (See Appendix III). The same results are reported for the second repeat of the experiment (data not shown).

The KS test detects differences in the location and shape of the cumulative distributions of frequency. Cumulative distribution of frequencies plots of the velocity (CDF %) were used to provide a visual representation of the distribution of the whole dataset and make it possible to appreciate any change in the distribution (Figure 15E). The treatment with the actin depolymerizing agent determined a reduction of the size of the range of values that Golgi bodies can acquire.

When the sample was treated with DMSO, the range of the velocity values was 3.13 μm/sec whilst when treated with

latrunculin B it was reduced to 1.76 μm/sec (Figure 15A). The lower limit of the range (minimum) is comparable for DMSO and latrunculin B; the upper limit (maximum) for DMSO was 3.65 μm /sec while for latrunculin B was 1.89 μm /sec (Figure 15A). Indeed, CDF curves show that the curve of latrunculin B was shifted towards lower values of velocity, confirming that the treatment resulted in a reduction of the distance travelled over the time (Figure 15E).

All these data together indicated that upon the treatment with latrunculin B, the Golgi bodies acquired a narrower range of velocity values and that they were slower, being the maximum velocity being 1.89 μm/sec.

To provide a quantification of the reduction in the velocity, treated samples were standardized against the control DMSO and represented as relative percentage of the control (relative median %). The velocity reduced by 25% compared to the control (Figure 15E).

### *3.2.2.2 Displacement rate*

The effect of 10 μl/ml DMSO on displacement rate was considered and compared to the untreated sample.

The dataset of the untreated sample had a median of 0.23 μm/sec, SD of 0.54 μm/sec and was positively skewed; the dataset of the sample treated with DMSO 10 μl /ml had median of 0.22 μm/sec, SD of 0.58 μm/sec and was positively skewed; as the normality tests confirmed, both datasets were non-normally distributed (Figure 16A). The shape of the distribution for the untreated sample and sample treated with DMSO 10 μl/ml was similar and is logarithmic (Figure 16B and 16C, respectively).

The boxplot 16D shows that the median values were very close and the MW test confirms that they were not significantly different (See Appendix III). The CFD curves (Figure 16E) had similar shape and the KS test confirmed that were not significantly different (See Appendix III). Taken altogether, these results were indicating that DMSO at concentration of 10 μl /ml had no effect on the displacement rate; the displacement rate values of 10 μl/ml DMSO were taken as control and compared to the depolymerisation of actin filaments with latrunculin B.

The dataset of the sample treated with latrunculin B 25 μM had a median displacement rate of 0.016 μm/sec, a SD of 0.21 μm/sec and was positively skewed (Figure 17A). The range of displacement rate values was also taken into consideration to have an estimate of the variation of this measurement. Upon latrunculin B treatment the range was 2.68 μm/sec, similar to the range of the control (2.73 μm/sec) (Figure 17A). From histogram 7B and boxplot 7C it could be observed that most of the data fell in the range 0.5 μm/sec when the sample was treated with latrunculin B, except an entry that had value between 2.50 μm/sec and 3 μm/sec (as highlighted by the red arrow in histogram 17B); the boxplot representation 17C (asterix in the red box) classified this entry as an outlier and this might explain the value of the range reported in the table 17A.

The presence of this outlier data might affect the accuracy of the estimation of the median, standard deviation and range so this entry was further investigated. From screening of all the values of the dataset, it resulted that it was an error, probably due to the joining of two distinct tracks or tracking of a Golgi bodies in a cell non affected by the treatment, and was eliminated from the dataset. The edited dataset of the displacement rates acquired after latrunculin B treatment was analysed. The dataset had

median of 0.016 μm/sec, standard deviation 0.05 μm/sec, range of 0.33 μm/sec and was positively skewed (Figure 18A). The histogram of displacement rates upon latrunculin B treatment was generated similarly to the other histograms. The depolymerizing treatment showed a drastic reduction of the displacement rates with maximum value of 0.33 μm/sec and plotting the data as done as for the other histograms did not allow an appreciation of the distribution of the dataset within such a narrow range (Figure 18B, panel above); for this reason another histogram was generated with the x-axis covering the range 0.35 μm/sec (Figure 18B, panel below). The enlarged representation permitted to appreciate that upon latrunculin B treatment the dataset maintained a logarithmic distribution and the most frequent values were slightly above the zero (Figure 18B, panel below). Boxplot (Figure 8C) and CDF graph (Figure 8D) show the differences in the median, spread and shape of the distribution of data that were all significantly different (See Appendix III).

To better understand how much the displacement rate was reduced, the median relative to the control was calculated. The depolymerisation of actin filaments results in a reduction of the displacement rate of almost 90% of the DMSO control (Figure 18E). Comparable results were obtained from the second replicate of this experiment (not shown).

A transformation of the dataset is applied to check if the non-normally distributed dataset can be transformed into a normally distributed dataset (Figure 19).

### *3.2.2.3 Meandering index*

The meandering index (MI) is a numerical value representing the complexity of the movement; values closer to one indicate that the

organelle moves on a more linear track (Sparkes *et al*. 2008)(See Figure 6).

The MI values for untreated sample was 0.47, for the DMSO control was 0.49 and for the treatment with latrunculin B of 0.11. The unpaired t-test unequal variances ($p<0.05$) indicated that there is not a significant difference between the untreated sample and the control, while there is significant difference between the control and actin depolymerisation (Figure 20).

The relative mean compared to the control was calculated to give an indication of how much the meandering index is reduced when actin arrays are not present. The latrunculin B treatment determines a reduction of the meandering index of almost 80% (Figure 21).

A snapshot of the Golgi bodies tracks in absence of actin filaments is represented in Figure 22.

## *3.2.3 The effect of microtubule disruption on Golgi movement*

### *3.2.3.1 Velocity*

To investigate the role of microtubules in the motility of Golgi bodies, tobacco leaves transiently expressing ST-GFP, were treated with 10 μM solution of the microtubule depolymerizing agent oryzalin (movie 3). As control 1 μl/ml of DMSO was used. Similarly to data collection described above, movies of fluorescent Golgi bodies untreated, treated with DMSO or oryzalin were recorded and analysed.

At first the differences between the velocity of the untreated sample and DMSO were analysed. In the untreated sample of replicate one (n= 126) the Golgi bodies had a velocity median of

0.7 μm/sec (SD 0.44 μm/sec) and the distribution was skewed to the left (Figure 23A); the DMSO control of replicate one (n=229), had median velocity 0.56 μm/sec (SD 0.66 μm/sec) and is positively skewed. As can be observed in the boxplot 13B, the distribution of the DMSO treatment has a longer tail, as indicated by the outliers points above the upper edge of the whisker. To assess if the differences in the median and in the distribution are significant, the MW and KS tests were performed and results show that there are no significant differences between the untreated sample and the control (See Appendix III). On treatment with oryzalin (n=238) the sample had a median velocity of 0.4 μm/sec (SD 0.63 μm/sec) and was skewed to the left (Figure 23A and 23B). The MW test and KS tests comparing the DMSO control to the oryzalin treatment indicated that the differences in the median and distribution were statistically different (See Appendix III). The same type of analysis was performed on a second replicate. The untreated (n=198), had median velocity 0.34 μm/sec (SD 0.49 μm/sec) and is skewed to the left (Figure 23C). The velocity of the untreated sample was compared to the one treated with DMSO. The DMSO sample (n=142), had median velocity 0.45 μm/sec, (SD 0.36 μm/sec) and was skewed to the left (Figure 13C). Further information about the distribution of the untreated and DMSO sample can be obtained from the boxplot in figure 23D, where it can be seen there is a different pattern in the distribution and in the median between the untreated sample and DMSO control. KS and MW tests confirm that the two distributions are statistically different (See Appendix III). The sample treated with oryzalin (n=173) had median velocity 0.46 μm/sec (SD 0.45 μm/sec) and skewness 1.9 (Figure 23C). KS and MW tests, comparing the control DMSO to the treatment with oryzalin, revealed that the differences observed are not significant

(See Appendix III). A further repetition of the experiment was carried out. The third replicate had a smaller sample size (n=66) had median 0.92 μm/sec (SD 1.04 μm/sec) and is skewed to the right (Figure 23E). In the control DMSO (n=42) the median velocity was 0.65 μm/sec (SD is 0.8 μm/sec) and the skewness was 2 (Figure 23E). In the oryzalin treatment (n=74), the median velocity was 0.66 μm/sec (SD 0.72 μm/sec) and the distribution was skewed to the right (Figure 23E). The boxplot representation in figure 23F shows the untreated, DMSO and oryzalin treated samples behave similarly. The MW and KS test assess that the three distributions (untreated, DMSO and oryzalin) and that the median were not statistically different (See Appendix III).

The velocities of single Golgi bodies were plotted for each movie, to evaluate if the data acquisition was a source of variability. Between movies there was a high variability in either the untreated (Figure 24A), DMSO sample (Figure 14B) or sample treated with oryzalin (Figure 24C). The second and the third replicate show the same pattern (results not shown).

To understand if there is a trend in the dynamic behaviour of Golgi bodies, the three conditions were plotted together (Figure 25). No trend or population could be seen in any of the conditions, and this reflects the high variability in Golgi dynamics, as the values of instant velocities shows in Figure 26.

### *3.2.3.2 Meandering index*

The meandering indices (MI) of the untreated sample, the DMSO control and specimen treated with the microtubule depolymerizing chemical were calculated for each replicate. The plots in figure 27A, 27B and 27C show the mean values of the meandering index in each condition for the first second and third

replicate, respectively. An un-paired t-test unequal variances was performed to assess any significant differences. In the first replicate (Figure 27A), the MI of untreated sample was 0.76, the DMSO control was 0.77 and oryzalin treatment was 0.11. The statistical t-test showed that the difference between the untreated sample and DMSO is not significant, and the treatment with the depolymerizing drug causes a significant reduction of the MI mean value compared to the control. In the second replicate (Figure 27B), the MI of the untreated sample was 0.40, of the DMSO sample was 0.47 and oryzalin was 0.50. The differences recorded between the untreated sample and DMSO are statistically different according to the t-test, but not the treatment with the depolymerizing chemical. In replicate 3 (Figure 27C), the mean MI of the untreated sample was 0.57, of the DMSO was 0.54 and of the sample where the microtubules are disrupted was 0.64. None of the differences observed are statistically significant.

# 3.3. Discussion

## *3.3.1 Tracking of fluorescent Golgi bodies using the software Volocity.*

The fluorescent marking of Golgi stacks combined with time-series acquisition and object tracking are useful tools to quantify and understand the mechanisms guiding and modulating organelle movement (Chen *et al*. 2012).

A variety of approaches have been used to track organelles. In Madison *et al*. (2015) the program ImageJ was used for automated tracking; some errors can occur in the organelle identification and linking between frames and this affected the following analysis of the velocity.

The Volocity software (Improvision, Image Processing and Vision Company; http://www.improvision.com/products/volocity/) proved to be an accurate and established tool in tracking the fluorescent Golgi bodies (Avisar *et al*. 2008, Runions *et al*. 2006). The editing of the tracks is possible and necessary to eliminate errors arising from repetitions of tracking the same organelle. A great advantage of Volocity is that the single tracks are easy to see and check at the same time, and the data output contains all the parameters of interest (velocity, displacement rate and meandering index).

The characterization of the movement of an object can be done in different ways. In Nebenführ *et al*. (1999) the 'streaming level' was used, which is calculated as the net velocity multiplied by directional factor, average velocity and instantaneous velocity. This measurement does not provide information about the complexity of the movement; indeed it has been demonstrated that Golgi bodies undergo saltatory movement, where rapid directional shifts alternate to a reduced motility, a model known as stop and go (Nebenführ *et al*. 1999). Therefore more appropriate numerical tools to define the motility profile of the organelles have been chosen according to Avisar *et al*. (2008).

The settings used in the acquisition of the time series are critical especially for the calculation of velocity values (Avisar *et al*. 2009); consistency in the protocol analysis and software version are also essential to obtain comparable results.

### 3.3.2 The statistical analysis: considerations about the method and use of velocity values of the replicates to validate the approach.

The data were first analysed calculating the descriptive statistics such as mean, median and standard deviation and by graphical representations, such as histograms and whisker boxplots.

Initially the mean and standard deviation were considered to assess differences between the technical replicates of velocity of Golgi bodies recorded at 48 hrs from the infiltration day. In both replicates, the standard deviation was quite large, indicating that the values were spread far from the mean. The whisker boxplots (such as Figure 11C) showed that there was quite a large number of datapoints classified as outliers. It can be observed that both replicates had a similar spread of the data, in terms of SD and outliers (Figure 11C). This led to the conclusion that is not a technical error but indicated a high variability in the sample and also that the datasets might be non-normally distributed. To further investigate this aspect, a graphical display of the datasets was created. Histograms show the frequencies with which each value occurs in certain ranges (or bin) within the sample. SPSS chooses the ranges widths automatically and the length of x/y axis according to the dataset. The ranges width were left as calculated by the programme to show which categories were more frequent under each condition, and the length of the axis was instead customised (x axis: 0-4 μm\sec; y axis: 0-100%) so that the histograms were comparable (Landay and Everitt 2004). It can be observed that the shape of the distributions was similar, that the datasets were non-normally distributed and positively skewed (Figure 11D and 11E), as also indicated by the skewness values in

11B. For comparison, a normally distributed dataset is bell-shaped and symmetrical around the mean and median and the skewness is 0. If the distribution of variables is not symmetrical about the mean, it is said to be skewed and the statistical parameter closer to the central tendency is the median (See section 2.8.1 and Figure 7). Therefore, the mean is not an appropriate tool to describe Golgi motility. Moreover the median is more robust than the mean to outliers (Upton and Cook, 2002). This type of distribution also explains why the standard deviation was large and led to the consideration that the data classified as outliers in the whisker boxplot display (Figure 11C) were actually valid data. Extreme outliers in the whisker boxplot are values three times bigger than the interquartile range and can represent errors (See section 2.8.1 and Figure 8). The extreme outliers of the whisker boxplot 11C were compared to the histograms 11D and 11E. The data classified as outliers in the whisker boxplot are located at the tail of the distribution therefore they are not errors and are part of the distribution.

Other methods of analysis include a general linear model analysis followed by Scheffé multiple comparison test (Avisar 2012). The general linear model is the combination of the regression, which explores the relation between variables in such a way that one variable can be used to predict the other, and analysis of variance; the post hoc Scheffé test is performed for comparing the mean values (Freund and Wilson 2003). A quantification of the differences is represented as bar chart of the mean (Avisar *et al*. 2008) or relative mean (Avisar *et al*. 2009). All these types of analysis assumes that the distribution of the sample is normal and is based on the comparison of the mean, therefore is not appropriate for a skewed dataset.

Another approach found in the literature to determine whether differences were statistically significant, is the Kolmogorov–Smirnov (KS) test executed via FORTRAN (Sparkes at al 2009). FORTRAN is a programming language used to automate the analysis and translate it in more user-friendly language (IBM-FORTRAN 2011). The statistical test used in this paper is appropriate to explore a non-normally distributed dataset as will be explained later in this chapter. Access to this programme was not available so an alternative source to run the statistical analysis was used. SPSS is a statistics software package used for complex analysis; with this program it was possible to perform and further implement the analysis of the dataset.

Non-normally distributed datasets can be compared using non-parametric tests (Kitchen 2009). Based on a literature review (Avisar *et al*. 2009, Sparkes *et al*. 2008), the KS test was chosen. The Kolmogorov-Smirnov two sample test compares the cumulative frequency distributions of two uneven and non-normally distributed datasets per time. It also detects any difference in dispersion and skewness, furthermore it detects differences in the shape of the distribution so it is a suitable statistical tool to analyse the distributions like that of the velocity.

As discussed previously, the distribution of replicates for the velocity values have the same shape and the central tendency is close to the median. Mann-Whitney (MW) was additionally used to assess differences between distributions with the same shape and differences between the median (Anon 2016) and confirm the results obtained with KS test. Both tests start from the hypothesis that there are no differences (null hypothesis) between the two datasets and the significant value is set $p= 0.05$. If the significance value lower is than the p-value ($p<0.05$) the two distributions are statistically different and the null hypothesis is rejected; if the significance value is bigger than p-value ($p>0.05$), the null

hypothesis is retained meaning that there are no differences between the two distributions.

An additional approach was tested in analysing the data. The repetitions were pooled together with the aim to increase the sample size and possibly decrease the standard deviation. When the analysis of the dataset constituted by the two replicate was performed, the data remained highly spread around the mean and the distribution positively skewed. As can be seen in the graphical representation of the dataset (Figure 12B), the shape of the distribution remains the same and the long tails becomes heavier; this can be more appreciated in the whisker boxplot 12C where more values are present beyond the whisker fences. This suggests that the sum of two distribution of this shape determines the increase of extreme and less frequent values, therefore not giving any additional information about the main core of the data. As can be observed from any of the frequency histograms (e.g. Figure 11D) the distribution of the sample was not symmetrical around the median but was skewed towards the left, where the most frequent values were recurring in the range of velocity < 2 μm/sec. The long tail at the right contains the least frequent values of the sample, which are far from the central core of the distribution. The distribution was similar across all the samples indicating that is a feature of the dynamics of Golgi bodies. These histograms of frequencies are indicating that Golgi bodies tend to acquire a restricted range of velocity values, and within this range there is distinct peak that falls between 0 μm/sec and 0.05 μm/sec.

This led to the conclusion that, despite the highly dynamic nature of the organelle, there is a trend in the most frequent velocity that they can have.

A further observation about the distribution needs to be made. According to the stop-and-go model, Golgi bodies alternate between rapid directional movement with periods of pausing or limited movement (Nebenführ at al 1999). These two classes of movement were expected to be observed in the pattern of the distribution of the velocity as a bimodal distribution, where two peaks are present, one representing the rapid movement and one the pausing. All the frequency histograms show that the distribution is unimodal, that is has only one peak. This might be explained by the fact that the population of Golgi bodies in a cell shifts from directional movement to wiggling movement not at the same time. Golgi bodies are involved in different processes and this may reflect the dynamic nature of the organelle. It can be also commented that the velocity values calculated by the software Volocity are mean values and this might leverage the variations in the velocity along a track. This can be appreciated looking at the instantaneous velocity, which is the velocity that the Golgi stacks at a certain time. The values of velocity largely vary within the track (Figure 26).

The statistical analysis carried out represents a novel approach to the analysis of the movement of Golgi bodies. The representation of the datasets should include histograms, boxplot and CDF curves since they all convey a different piece of information and taken altogether provide a complete representation of the processes involved. Histograms provide a visual representation of the distribution and show any shift or change in the distribution shape and the position of the median and most frequent values categories. Moreover, they permit the highlighting of errors in the dataset, such as in Figure 17B. CDF graphs are useful understand the differences between the control and treatment curves and support the result of KS test.

Box plots are valid tools to compare the position of the median and the dispersion of the values, and to identify errors as shown in figure 17C. Additionally, boxplots allow one to appreciate differences in the medians and visually confirm the Mann-Whitney test results. The combination of the software Volocity and these two tests constitutes a more complete approach to the analysis of organelle dynamics.

The statistical analysis of the velocity measurements in untreated samples
demonstrated that the biological system is highly variable and this can be due to growing conditions is the greenhouse and biological variability between seeds and plant stages; a larger number of samples and more repetitions of the experiments could provide more consistent data.
The tracking approach revealed a high variability in Golgi dynamics: these organelles alternate between rapid linear motions and pauses, in which they are wiggling around a position for a variable period of time (Nebenfuhr *et al*. 1999). The directional motion of Golgi bodies is mainly dependent on an intact actin cytoskeleton (Akkerman *et al*. 2011). It has been suggested that Golgi body movement is correlated with the insertion of the cellulose complex CesA into the plasma membrane (Crowell *et al*. 2009); it has also been suggested that Golgi bodies stop in contact with ER exit sites, increasing the efficiency of the traffic between the two compartments (Nebenfuhr *et al*. 1999, Hamada *et al*. 2012) but with no evidence shown in the paper. However, micromanipulation of Golgi bodies in Arabidopsis leaf epidermial cells has shown that the Golgi bodies are physically associated with the endoplasmic reticulum (Sparkes *et al*. 2009), almost certainly at the ER exit sites thus the stop and go model of

Golgi stopping at the exit sites is unlikely to be correct (Robinson *et al*. 2015). These evidences suggest that different factors are regulating the movement of Golgi bodies.

## *3.3.3 Absence of actin filaments*

### *3.3.3.1 Velocity*

From the disruption of actin filaments, the main guides for Golgi bodies, a change in the shape of the velocity distribution would be expected. The comparison between the DMSO control (Figure 14B) and the treated sample (Figure 15B) showed that the distributions are comparable and this might indicate that there are other forces acting on the Golgi bodies.

A decrease in the number of the histograms bars and increase of their width indicate that the categories of values are reduced, as well as the whole range of the data. The same is shown by the CDF graphs (Figure 18D) where the latrunculin B curve is shifted towards smaller values of velocity and the curve is extending in a smaller range. These results confirm what have been already reported by Akkerman *et al*. (2011), that actin filaments represent the fast lane on which the organelles move. When disrupted, the organelles keep moving, but slower, and acquire a limited range of velocity values.

The movement of Golgi bodies on actin filaments is also regulated by the molecular motor protein myosin XIK (Avisar *et al*. 2008). The expression of the truncated non-functional version of this protein results in a reduction of the velocity of Golgi bodies but the effect is less severe than the treatment with latrunculin B. In the presence of the mutated myosin XIK and intact actin filaments,

the organelles keep on moving but more slowly; this suggests that the displacement of the organelles in the cytoplasmic space is guided by several cooperating factors. It cannot be excluded that the movement is dependent on native myosins present in the cells, which can form dimers of native motor proteins or dimers composed of the native myosin and the mutated versions; the remaining movement could be also due to myosins with redundant function (Sparkes 2010b).

### *3.3.3.2 Displacement rate*

The frequency histograms of the displacement rate have a logarithmic distribution. In plant physiology, the log-normal distribution fits the permeability and solute motility in plant cuticles (Baur 1997). Log-normal distributions are generated by processes that involve more than one dimensional measurement, like for example volume and surfaces areas (Limpert *et al*. 2001) and, similarly is observed for Golgi displacement rate and velocity. Previously, velocity and displacement rates have been described using the means (Avisar *et al*. 2008), which is an appropriate statistical tool to describe a dataset normally distributed; in Limpert *et al*. (2001) it is suggested that dataset with a Log-normal distribution should be "back-transformed" applying the exponential function. The back-transformation of the displacement rate and velocity datasets was attempted. As in Figure 19 demonstrates, applying the transformation to the displacement rate dataset was effective in rendering the logarithmic distribution into a normal one. Normally distributed datasets can be analysed using conventional analysis such as t-test (for a pair of samples) or ANOVA (for multiple comparison) The major limitation to the use of these tests is that they can be

performed only on equal size samples, while the datasets that were recorded have unequal sample size due to different number of Golgi bodies in each movie. Additionally, the analysis carried on velocity values so far was on the original un-transformed datasets (Avisar *et al*. 2009) and a consistent approach needs to be maintained.

Initially, the untreated sample was compared to the sample treated with DMSO at 10 μm/ml to understand if the solvent had an effect on the displacement rate of the Golgi bodies. Statistical analysis demonstrated that the DMSO data can be comparable to the untreated conditions; therefore the treatment with the DMSO was used as control in further experiments. The depolymerizing agent latrunculin B resulted in a severe reduction of the range of movement of Golgi bodies (Figure 18B, 18C and 18D); the range of displacement rate in depolymerizing conditions was 8 times less than the untreated sample (Figure 18A). The estimate of the relative median indicates that, when actin filaments were disrupted, the linear distance travelled was less than one tenth of the linear distance calculated when actin filaments were intact (Figure 18F). This confirmed that the actin arrays provide the main tracks for the long distance directional movement, and when actin filaments are depolymerised, the organelles do not have directional and short distance residual movement (Figure 11A and 22A) which has been already observed and defined as wiggling or saltatory (Boevink *et al*. 1998b, Nebenführ *et al*. 1999). The residual movement had a logarithmic distribution (Figure 18B), which is similar to that obtained from the control (Figure 16C), and this might indicate that Golgi bodies are involved in multiple processes and that actin filaments might not the only mechanism to regulate Golgi dynamics. This is accordance with what was obtained from the analysis of the

velocity (See section 3.3.3.1). It could be hypothised that the wiggling or saltatory movement is dependent on microtubules or residual stubs of depolymerised actin. There is also the possibility that the residual movement is random Brownian motion (Nebenführ *et al*. 1999).
These results are in line with Avisar *et al*. (2009) where it was shown that the disruption of actin filaments significantly perturb the dynamics of Golgi bodies. In this work the effect of latrunculin B was compared to the effect of the expression of a non-functional myosin XIK, an actin motor protein participating in the movement of Golgi bodies (Avisar *et al*. 2008)

In *N. tabacum*, the expression of a non-functional tail domain of XIK cause a significant reduction of the displacement rate, but less severe than the treatment with latrunculin B (Sparkes *et al*. 2008) as the relative mean also indicates ( Avisar *et al*. 2008).
This result led to the conclusion that the directional translocation of Golgi bodies is regulated by proteic motors and actin filaments play a major role.

### *3.3.3.3 Meandering Index*

The analysis of velocity and displacement rate required the use of CDFs to provide a visual representation of the distribution of the dataset and make it possible to appreciate any change in the shape of the distribution. A different graphical representation is used for meandering index because the values vary in the range of <1. Indeed, the resulting CDF curve would approximate linear function and CDF plots would not provide any additional information to the relative mean. The datasets are normally distributed, therefore an unpaired t-test unequal variances was used to assess the differences between the conditions.

The bar chart in figure 20 shows that DMSO has no effect on the meandering index, as proved also for the velocity and displacement rate, and the treatment with the actin depolymerising agent gives a drastic reduction of the relative meandering index (Figure 21) suggesting that the residual movement is more saltatory. From movie frames in figure 22 it can be confirmed that Golgi bodies oscillate around a position when the actin filaments are absent (movie 2).

Golgi bodies in cells expressing XIK-tail have lower meandering index than the control cells. Thus the effect on the meandering index is not as severe as the depolymerisation of actin (Sparkes *et al*. 2009).

### *3.3.3.4 Final considerations about the effect of actin filaments on the whole dynamic of Golgi bodies*

The study of the depolymerisation of actin filaments on Golgi body dynamics gives an insight into the mechanisms propelling and regulating the movement.

In cells deprived of the actin framework, the velocity relative mean of the organelle drops by 25% compared to DMSO (Figure 15E) and the categories of velocity values are restricted.

This indicates that Golgi bodies are still moving but slower than in presence of actin arrays; it can be suggested that actin filaments have a major role in supporting the active flow of Golgi bodies but are not the only components to be involved. A comparison with the mutants expressing the actin motor proteins myosin XIK shows that they are also involved in sustaining the velocity of

these organelles but lo less extent compared to actin network (Sparkes *et al*. 2008).

The displacement rate analysis shows that the relative mean of the displacement rate drops by 85% compared to DMSO (Figure 18E) and, as observed for the velocity, the categories of possible values are less (Figure 18B). The residual movement is only on a short distance, meaning that the actin arrays have a key role on maintaining the long distance translocation and that this last is an active process rather than a passive flow. To support this last, the expression of non-functional truncated motor proteins XIK causes a reduction of the displacement rate as well ( Sparkes *et al*. 2008).

The meandering index allows a better analysis of the type of movement of Golgi bodies. The absence of actin filaments results in a reduction by 80% of in the meandering index, meaning that movement is less unidirectional and more saltatory (Figure 11). A similar pattern was observed when the truncated myosin XIK is expressed, but they determined a minor reduction of the meandering index rates compared to the absence of actin filaments (Sparkes *et al*. 2008) suggesting that the movement is not totally depending on myosins motors. Taken altogether, the data indicate that actin filaments provide the main network on which Golgi bodies move rapidly and directionally. Indeed the lack of the actin network determines the loss of the long distance translational movement and an increase of a slower saltatory dynamics; myosin motor proteins are also involved in sustaining the intracellular trafficking on the intact actin filaments.

When the actin filaments are depolymerized, Golgi bodies do not stop completely but a residual mobility is left. This could depend on stubs of actin filaments that remain intact after the treatment. The depolymerisation of actin filaments labelled with either FABD2-GFP or Lifeact-GFP (Figure 32 and Figure 34, respectively) revealed that even after a long incubation with the

depolymerizing drugs, small parts of actin filaments are present. As described in Chapter 4, the effect of labelling of actin filaments perturbs the structure of the cytoskeleton and has an impact on Golgi body dynamics (Figure 30). It can not be excluded that the labelling has a stabilizing effect on actin filaments, which explains why parts of the arrays are still present after a prolonged treatment.
However, another possibility is that the residual movement of the organelles is driven by microtubules. The involvement of microtubules in the Golgi bodies dynamics discussed in the next sections.

## 3.3.4 Absence of microtubules

### *3.3.4.1 Velocity*

To understand the role of the microtubules in the regulation of the motility of Golgi bodies, an analysis of the velocity measurements was performed after microtubule depolymerisation and compared to the untreated condition, when microtubules were intact.
Results from the first replicate showed that the DMSO had no effect and the depolymerisation of microtubules resulted in a small but significant reduction of the velocity of Golgi bodies (Figure 23B). However, the outcomes of the second replicate were not in accordance to the first. The DMSO had an effect and it was not different from the sample treated with oryzalin (Figure 23D). A third replicate was carried out to investigate further these results and neither of the treatments showed a significant effect (See Appendix III). Based on the results from previous experiments, the DMSO treatment at a concentration of 10 µl/ml

had no effect on the velocity and displacement rates of Golgi bodies (See Appendix III); the concentration used in the experiment to study the absence of microtubules was 10 times lower so an effect was not expected.
If we take into consideration the differences between the DMSO control and the treatment with oryzalin, a clear conclusion about the effect of the microtubules depolymerisation on Golgi body dynamics cannot be drawn.

The velocities of single Golgi bodies were plotted for each movie, to evaluate if the movies acquisition is a source of variability and the three experimental conditions (untreated, control and treated with depolymerizing chemicals) were plotted together to understand if is there is a trend in the dynamic behaviour of Golgi bodies. No trend or population can be highlighted in any of the conditions, and this reflects the high variability in Golgi dynamics.
The outcomes from the depolymerisation of microtubules give an indication that the measurements performed by the software Volocity are not sensitive enough to pick up small changes in the fast movement of the organelles. The velocity estimated as average of the velocity of the organelles over the whole track; this means that any change in the velocity would be levelled in the calculation of the average. This might explain why no differences are recorded between the controls and the treatment with the depolymerizing chemical. Instant velocities (Figure 26) related to positions of labelled microtubules could provide a more accurate and useful estimate of any modulation of the velocity in proximity of the microtubules.

### 3.4.2 Meandering index

The procedure to statistically analyse the displacement rate is the same as the analysis of the velocity values. The averaging of the track velocity results in a loss of information and it becomes clear that, to understand the role played by the microtubules in regulating the Golgi body movement, the track velocity is not an accurate tool. The same reasoning can be applied to the displacement rates, and for this reason the analysis of this parameter is not performed since would give not accurate and relevant results.

To understand if there is a variation in the complexity of the movement and if the variability pattern of the results is conserved throughout all the parameters, the meandering index measurements were analysed. Similarly to the results obtained from the analysis of the velocity, a conclusion about the participation of the microtubules to the dynamics of Golgi bodies cannot be drawn.

## 3.5 Actin filaments and microtubules: an overall discussion

Live cell imaging of Golgi bodies with the use of software Volocity and statistical analysis are promising tools to understand the mechanisms underlying the movement regulation.

When actin filaments are disrupted, the whole dynamics of the organelle drastically change. The velocity and displacement rates are reducedwhile meandering index increases, indicating that actin filaments are the main arrays on which Golgi bodies travel at high speeds and directionally.

Unfortunately, conclusions could not be drawn when microtubules are absent. The Volocity software computes the average values of velocity, displacement rates and meandering index of the entire track; this means that information about changes of dynamics over a short time (like pausing or slowing down) are lost in the averaging calculation. A possible solution is to obtain the parameters values for each time frame, to get closer to instant changes in the behaviour of the organelle.

The components of the cytoskeleton are connected and cross-talk (Schneider and Persson, 2015) and several proteins are involved. For instance the protein family of formins (FH) is composed of transmembrane proteins that nucleate and modify actin and are localized in the plasma membrane. AtFH1 was found to bridge between the cell wall and the actin cytoskeleton (Martinière *et al*. 2011) and AtFH4 proved to interact with both microtubules and actin filaments (Deeks *et al*. 2005) and these perhaps should also be assessed when analysing Golgi dynamics. The microtubule motor kinesin-14 can interact with both actin and microtubules, acting as a bridge between them (Schneider and Persson, 2015).

This evidence indicates that, when one component of the cytoskeleton is disrupted, the remaining filaments might be affected. The tracking results should be reinterpreted as providing information about the remaining intact filaments.

Tracking techniques could be combined to the study of non-functional mutants of cytoskeletal molecular motors and proteins bridging the microtubules and actin filaments (e.g. Formins) to give a more accurate description of the regulation of the organelles trafficking. Additionally, the values of the Golgi body velocity in correspondence of microtubules can provide key data about how microtubules regulate the organelle motility.

**Figure 11.**
**Velocity data of fluorescent Golgi bodies, in untreated samples, recorded at 48 hrs from the infiltration of ST-GFP.**

Tobacco plants were transiently transformed with the Golgi marker ST-GFP and the movement of the fluorescent organelles was studied after 48hrs from the infiltration event. The velocities values of the repetitions were compared.

**A**: Tracks of fluorescent Golgi bodies. Scale bar 3 μm. See also movie 1.
**B**: Descriptive statistics of the untreated sample.
**C**: Whisker boxplot comparing two replicates. The red line indicates that there are significant differences between the distributions. (*) Outliers; (•) extreme outliers.
**D and E**: Histogram showing the distribution of the frequency of the velocity values (dotted red line is representing the median, dashed black line mean) of the replicates.

**Figure 11.**

A.

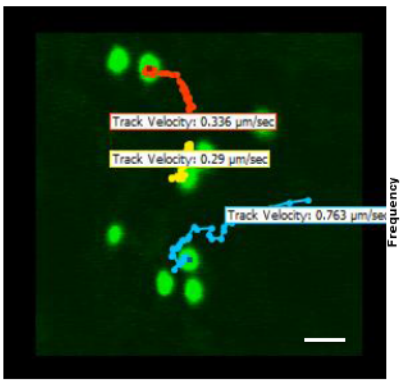


B.

| Velocity comparison replicates 48h | | |
|---|---|---|
| | Rep 1 | Rep 2 |
| Count | 129 | 215 |
| Mean | 0.61 µm/sec | 0.75 µm/sec |
| Median | 0.44 µm/sec | 0.62 µm/sec |
| St.Deviation | 0.49 µm/sec | 0.57 µm/sec |
| Minimum | 0.12 µm/sec | 0.07 µm/sec |
| Maximum | 3.17 µm/sec | 3.42 µm/sec |
| Range | 3.05 µm/sec | 3.35 µm/sec |
| Skewness | 2.3 | 1.89 |
| Sign. Normality test (SW) | 0.000 | 0.000 |

C.

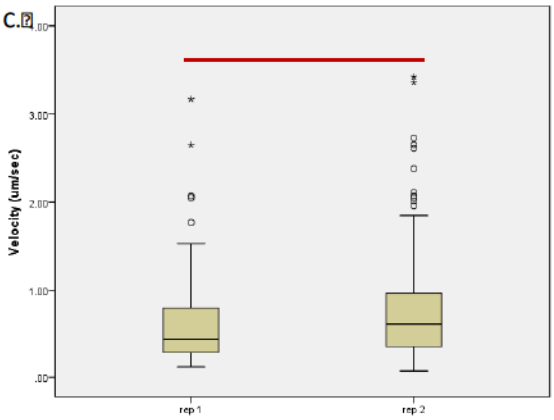


D.

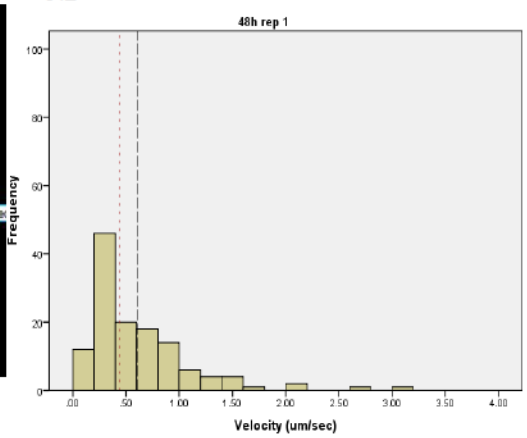


E.

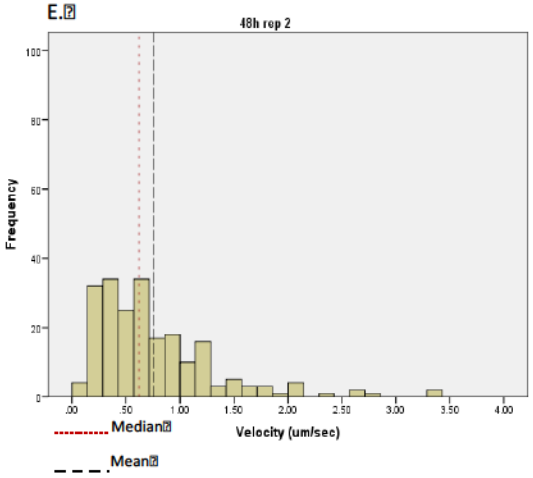

**Figure 12.**
**Statistical analysis of the sum of replicates (untreated sample) of Golgi bodies velocity data recorded at 48 hrs from the infiltration of ST-GFP.**

Tobacco plants were transiently transformed with the Golgi marker ST-GFP and the movement of the fluorescent organelles was studied after 48hrs from the infiltration event; the velocities values of the repetitions were summed and a statistic analysis performed.

**A**: Descriptive statistics of the sample.
**B**: Histogram showing the distribution of the frequency of the velocity values (dotted red line representing the median).
**C**: Whisker boxplot of replicate 1, replicate 2 and sum of the replicates. (*) Outliers and (•) extreme outliers.

## Figure 12.

A.

| Velocity replicate 1 + replicate 2 48hrs | |
|---|---|
| Count | 344 |
| Mean | 0.7 m/sec |
| Median | 0.56 m/sec |
| St.Deviation | 0.54 m/sec |
| Minimum | 0.07 m/sec |
| Maximum | 3.42 m/sec |
| Range | 3.35 m/sec |
| Skewness | 2.02 |
| Sign. Normality test (SW) | 0.000 |

C.

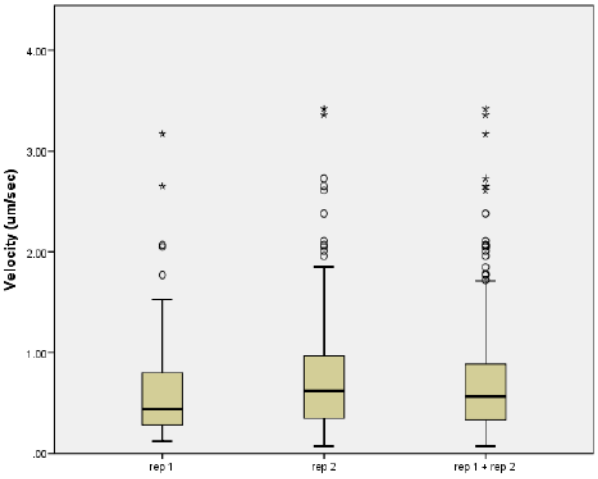


B.

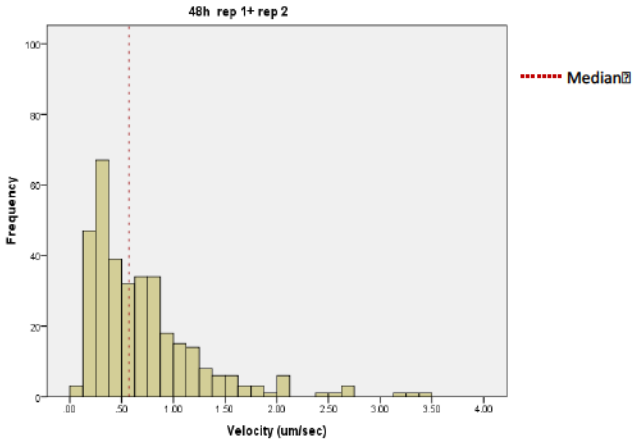

**Figure 13.**
**Statistical analysis of the velocities of Golgi bodies, in untreated samples, recorded at 72 hrs from the infiltration of ST-GFP.**

The Golgi fluorescent marker ST-GFP was transiently expressed in tobacco plants and the movent of the organelles was recorded after 72 hrs from the infiltration event. Three replicates are compared.

**A**: Descriptive statistics of replicate 1, replicate 2 and replicate 3.
**B, C, D**: Histogram showing the distribution of the frequency of the velocity values (dotted red line is the median) of replicate 1, 2 and 3.
**E**: Whisker boxplot comparing replica 1, replica 2 and replica 3. The red line indicates that there are significant differences between replicates.
(*) Outliers and (•) extreme outliers .

**Figure 13.**

A.

**Velocity untreated sample**

| | Rep 1 | Rep 2 | Rep 3 |
|---|---|---|---|
| Count | 127 | 198 | 65 |
| Mean | 0.8 m/sec | 0.5 m/sec | 1.23 m/sec |
| Median | 0.7 m/sec | 0.3 m/sec | 0.92 m/sec |
| St.Deviation | 0.44 m/sec | 0.47 m/sec | 1.04 m/sec |
| Minimum | 0.16 m/sec | 0.11 m/sec | 0.3 m/sec |
| Maximum | 2.14 m/sec | 3.65 m/sec | 5.41 m/sec |
| Range | 1.98 m/sec | 3.54 m/sec | 5.11 m/sec |
| Skewness | 0.9 | 3 | 2.4 |
| Significance Normality test (SW) | 0.000 | 0.000 | 0.000 |

C.

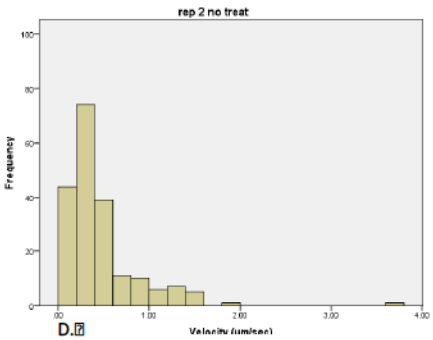


D.

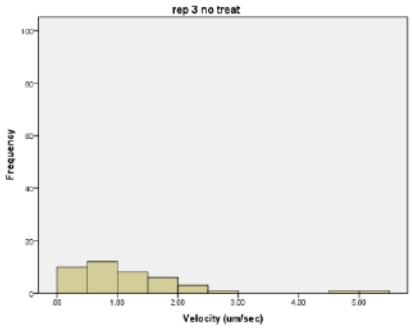


B.

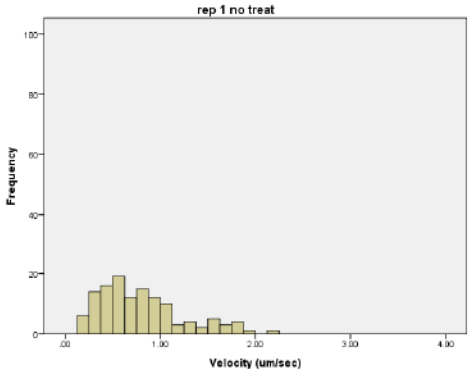


E.

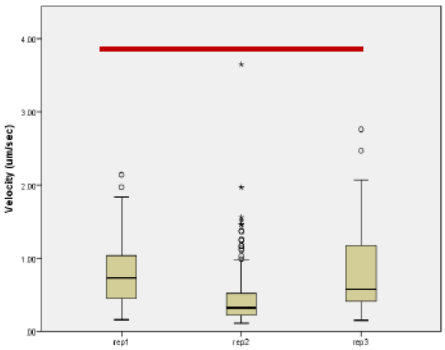

**Figure 14.**
**Comparison between the velocity dataset of fluorescent Golgi bodies in untreated sample and treatment with DMSO (10 μl/ml).**

**A:** Descriptive statistics.
**B:** Histogram representing the distribution of the frequency of velocity values after treatment with DMSO.

**Figure 14.**

A.

| Velocity untreated vs DMSO | | |
|---|---|---|
| | untreated | DMSO 10 µl/ml |
| Count | 129 | 198 |
| Mean | 0.61 µm/sec | 0.53 µm/sec |
| Median | 0.44 µm/sec | 0.37 µm/sec |
| St.Deviation | 0.49 µm/sec | 0.47 µm/sec |
| Minimum | 0.12 µm/sec | 0.07 µm/sec |
| Maximum | 3.17 µm/sec | 3.65 µm/sec |
| Range | 3.05 µm/sec | 3.13 µm/sec |
| Skewness | 2.33 | 1.89 |
| Sign. Normality test (SW) | 0.000 | 0.000 |

B.

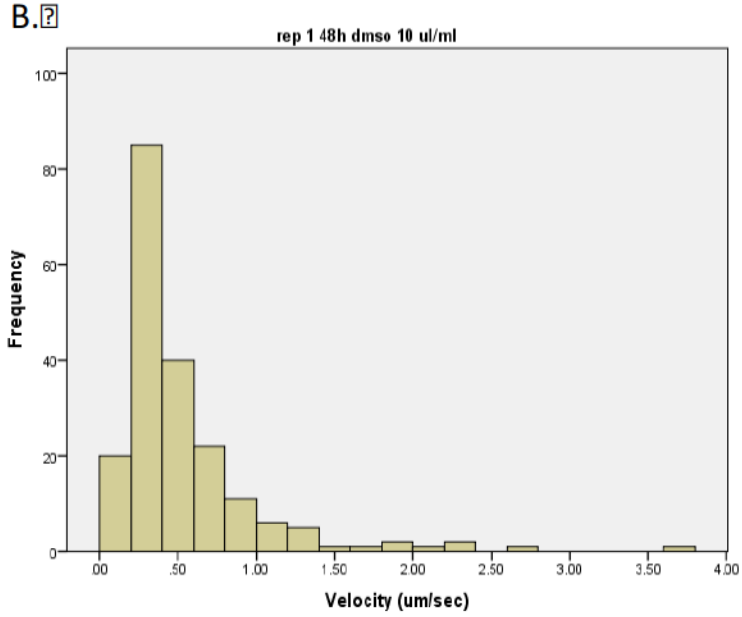

**Figure 15.**
**Comparison of Golgi bodies velocity dataset following the treatment with 10 μl/ml DMSO and 25 μM latrunculin B.**

The velocity values of Golgi bodies treated with the control compound and the cytoskeleton disrupting agent are statistically analysed and compared.

**A**: Descriptive statistics of the DMSO control and sample treated with latrunculin B.
**B**: Histogram representing the distribution of the velocity frequency values after treatment with latrunculin B.
**5C**: Whisker boxplot comparing DMSO to latrunculin B. The differences are statistically different as indicated by the red line. (*) Outliers and (•) extreme outliers.
**D**: CDF of velocity values comparing the DMSO (green line) and latrunculin B treatment (blu line). The distributions are significantly different as results from KS test (See Appendix III) and indicated by the asterix.
**E:** Bar-chart of velocity relative median. The treatment with latrunculin B is expressed as percentage of the DMSO control. The differences are significant as results from MW test and indicated with the asterix (See Appendix III).

## Figure 15.

A.

| Velocity DMSO vs latB | | |
|---|---|---|
| | DMSO 10µl/ml | latB 25 µM |
| Count | 198 | 88 |
| Mean | 0.53 µm/sec | 0.35 µm/sec |
| Median | 0.37 µm/sec | 0.28 µm/sec |
| St.Deviation | 0.47 µm/sec | 0.25 µm/sec |
| Minimum | 0.07 µm/sec | 0.13 µm/sec |
| Maximum | 3.65 µm/sec | 1.89 µm/sec |
| Range | 3.13 µm/sec | 1.76 µm/sec |
| Skewness | 1.89 | 3.28 |
| Sign. Normality test (SW) | 0.000 | 0.000 |

B.

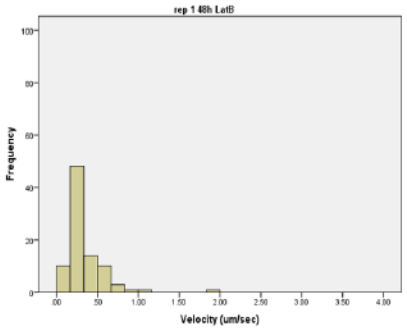


C.

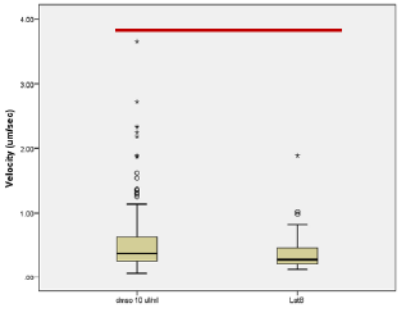


D.

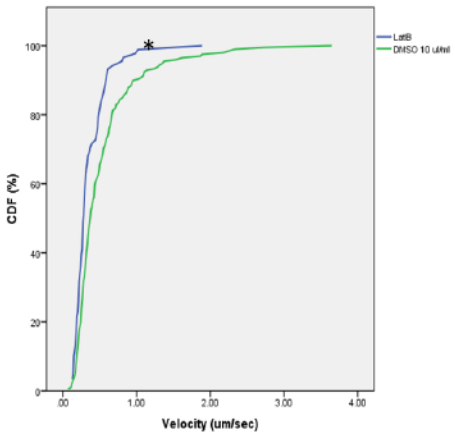


E.

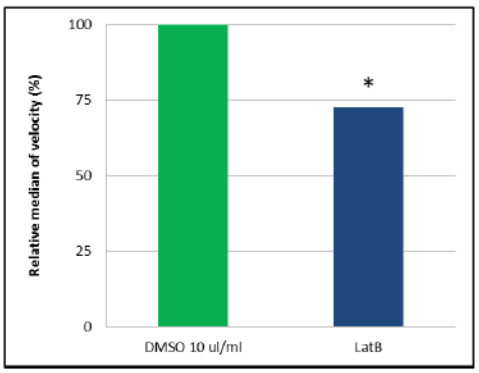

**Figure 16.**
**Statistical analysis of the displacement rates of Golgi bodies. Comparison between the untreated sample and treatment with 10 µl/ml DMSO.**

**A**: Descriptive statistics of the displacement rates of the untreated sample and DMSO.
**B**: Histogram showing the distribution of the displacement rates in the untreated sample. The median (red dotted line) and mean (black dashed line) are represented.
**C**: Histogram showing the distribution of the displacement rate in DMSO sample.
**D**: Boxplot comparing the displacement rates of the untreated sample and DMSO. (*) outliers and (•) extreme outliers. The median values are not statistically different as assessed by MW (See Appendix III).
**E**: CDF graph displaying the curve of the untreated sample (black line) and DMSO (green line). The two distributions have similar shape and are not statistically different as assessed by the KS test (See Appendix III).

**Figure 16.**

A.

| Displacement rate untreated vs DMSO | | |
|---|---|---|
| | untreated | DMSO 10 µl/ml |
| Mean | 0.46 µm/sec | 0.46 µm/sec |
| Median | 0.23 µm/sec | 0.22 µm/sec |
| St.Deviation | 0.54 µm/sec | 0.58 µm/sec |
| Minimum | 0.01 µm/sec | 0.00 µm/sec |
| Maximum | 3.36 µm/sec | 2.73 µm/sec |
| Range | 3.35 µm/sec | 2.72 µm/sec |
| Skewness | 2.06 | 1.9 |
| Sign. Normality test (Shapiro-Wilk) | 0.000 | 0.000 |

B.

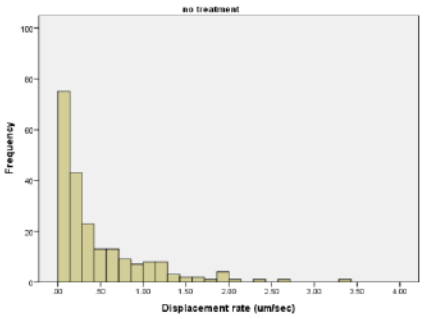


C.

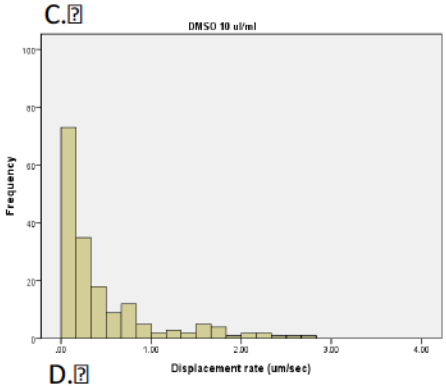


D.

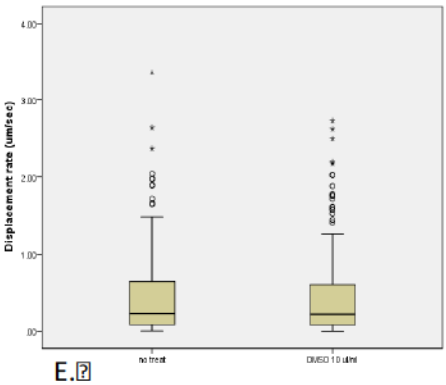


E.

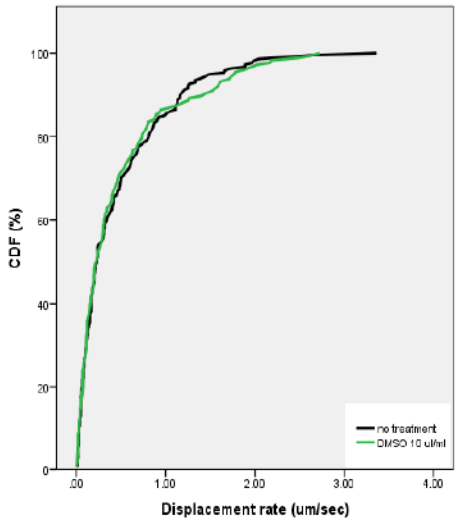

**Figure 17.**
**Statistical analysis of the displacement rates of fluorescent Golgi bodies. Comparison between treatment with latrunculin B and the DMSO control (10 μl/ml).**

**A**: Descriptive statistics of the sample treated with latrunculin B and the control DMSO.
**B**: Histogram representing the distribution of the displacement rates in the actin-depolymerised sample. The red arrow highlights the out-layer point excluded from the dataset.
**C**: Boxplot comparing the latrunculin B treated to the DMSO control sample. The red box is highlighting the outlier point excluded from the dataset.

**Figure 17.**

A.

| Displacement rate DMSO vs latB | | |
|---|---|---|
| | DMSO 10 µl/ml | latB |
| Mean | 0.46 µm/sec | 0.05 µm/sec |
| Median | 0.22 µm/sec | 0.016 µm/sec |
| St.Deviation | 0.58 µm/sec | 0.21 µm/sec |
| Minimum | 0.00 µm/sec | 0.00 µm/sec |
| Maximum | 2.73 µm/sec | 2.69 µm/sec |
| Range | 2.72 µm/sec | 2.68 µm/sec |
| Skewness | 1.9 | 11.9 |
| Sign. Normality test (SW) | 0.000 | 0.000 |

C.

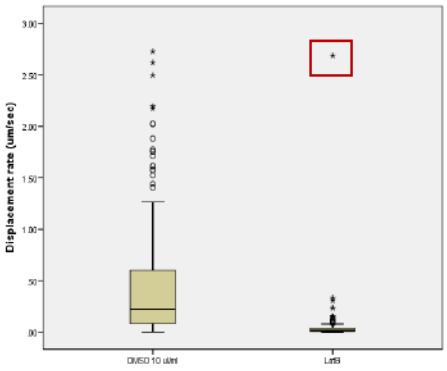


B.

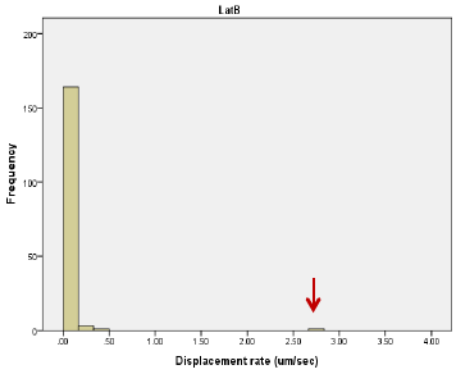

**Figure 18.**
**Statistical analysis of the displacement rates of Golgi bodies. Comparison between the DMSO control (10 μl/ml) and treatment with latrunculin B (edited dataset).**

**A**: Descriptive statistics of the displacement rate of samples treated with latrunculin B (an extreme outlier excluded from the analysis) and DMSO control.
**B**: Histogram representing the distribution of the displacement rate values of the sample treated with the actin-depolymerising agent. An enlarged graph was generated (below) to better appreciate the distribution of the data.
**C**: Whisker box-plot of the displacement rate of DMSO and latrunculin B treatment.
**D**: CDF curves of DMSO (green line) and latrunculin B (blue line). The differences in the distribution are significant as results from the KS test (See Appendix III).
**E**: Relative median of the displacement rate of latrunculin B treated sample compared to DMSO control. As the MW test results (See Appendix III), the differences are significant.

**Figure 18.**

A.

| Displacement rate DMSO vs latB | | |
|---|---|---|
| | DMSO 10 µl/ml | latB |
| Mean | 0.46 µm/sec | 0.035 µm/sec |
| Median | 0.22 µm/sec | 0.016 µm/sec |
| St.Deviation | 0.58 µm/sec | 0.05 µm/sec |
| Minimum | 0.00 µm/sec | 0.00 µm/sec |
| Maximum | 2.73 µm/sec | 0.33 µm/sec |
| Range | 2.72 µm/sec | 0.33 µm/sec |
| Skewness | 1.9 | 1.9 |
| Sign. Normality test (SW) | 0.000 | 0.000 |

C.

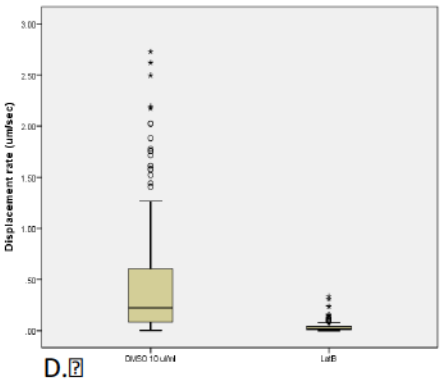


D.

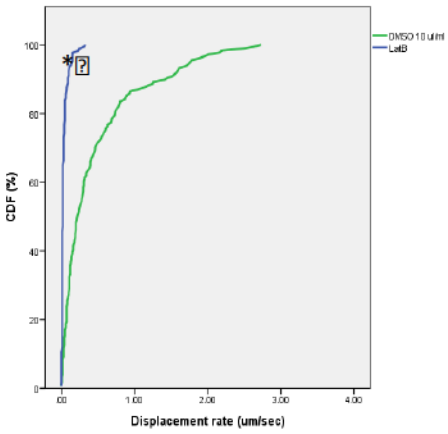


B.

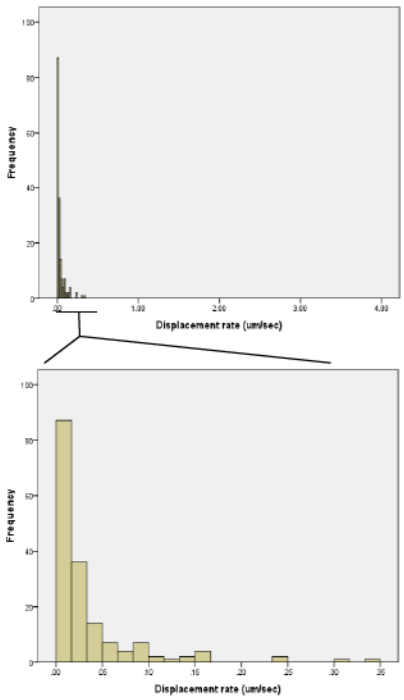


E.

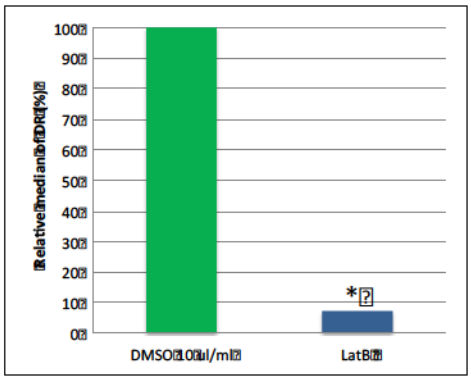

**Figure 19.**

**Transformation of the non-normally distributed displacement rate dataset into a normally distributed dataset.**

A logarithmic function is applied to the displacement rate dataset to transform the non-normally distributed dataset into a normally distributed one.

**Figure 19.**

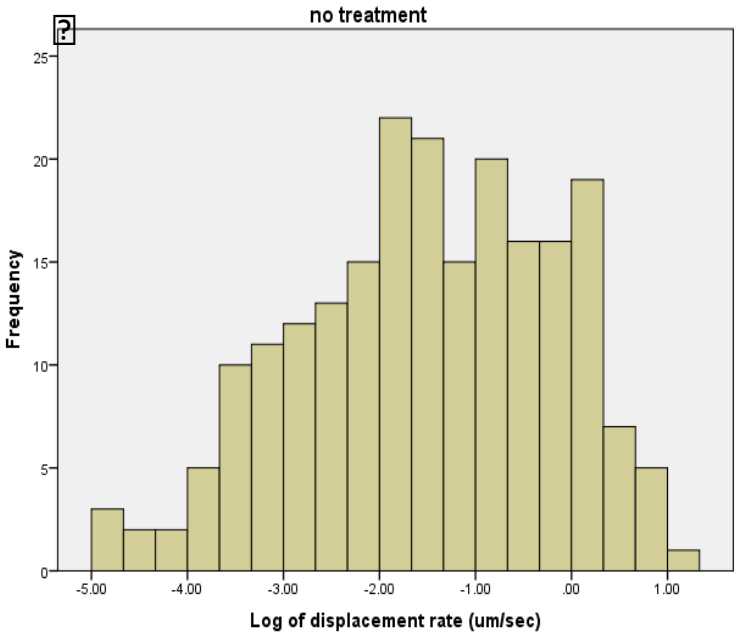
no treatment
Frequency
25
20
15
10
5
0
-5.00
-4.00
-3.00
-2.00
-1.00
.00
1.00
Log of displacement rate (um/sec)

**Figure 20.**
**Bar-chart of meandering indexes mean values.**

The meandering index mean value of the untreated sample is 0.47 (purple bar) and is similar to the mean of DMSO 0.49 (green bar). The difference between the untreated sample and the control is not significant. Instead there is a significant difference between the mean of DMSO and the mean of the sample treated with the depolymerizing chemical latrunculin B (blue bar). Differences assessed with t-test, significance level set at $p<0.05$.

**Figure 21.**
**Bar-chart of the relative meandering index values.**

The meandering indexes of the sample treated with latrunculin B is expressed as percentage of the DMSO control. Treatment with the depolymerizing chemical determines a drop of the MI by 80%. As assessed by the unpaired t-test for unequal variances ($p<0.05$) the variation in the MI is significant.

**Figure 20.**

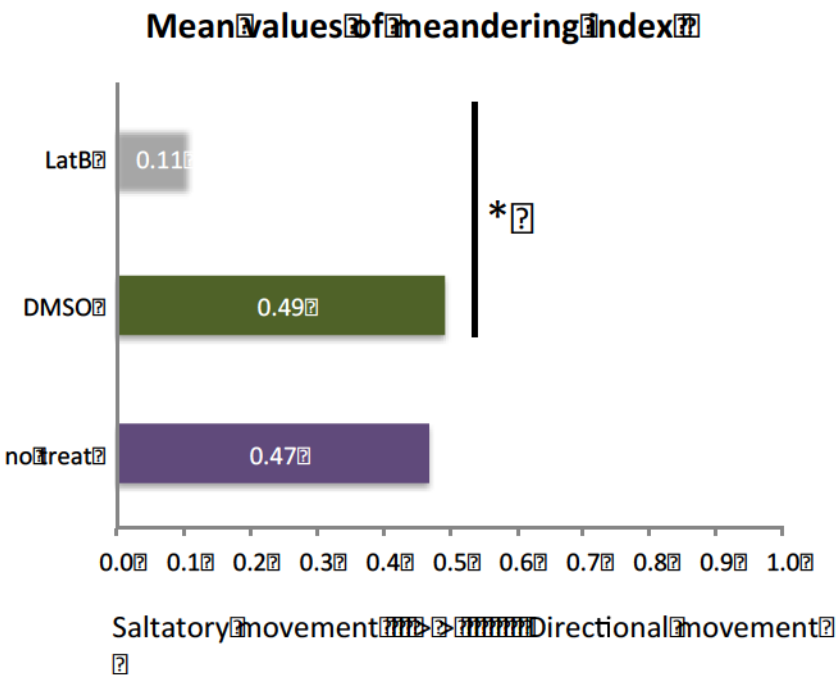


**Figure 21.**

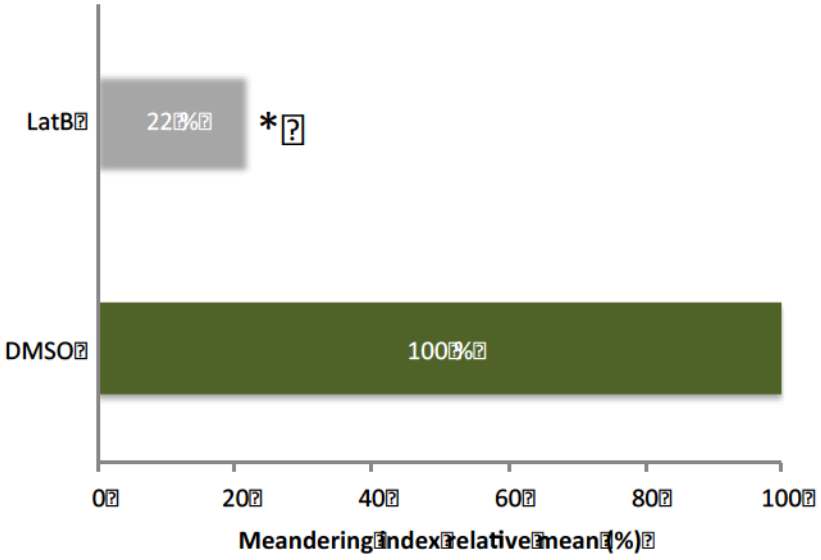

**Figure 22.**
**Snapshot of tracks generated by the software Volocity.**

Image showing the tracks of fluorescent Golgi bodies when the actin filaments are disrupted. The organelles lose their directional movement and their tracks are short, and develop around the initial position. Scale bar 3 μm.

**Figure 22.**

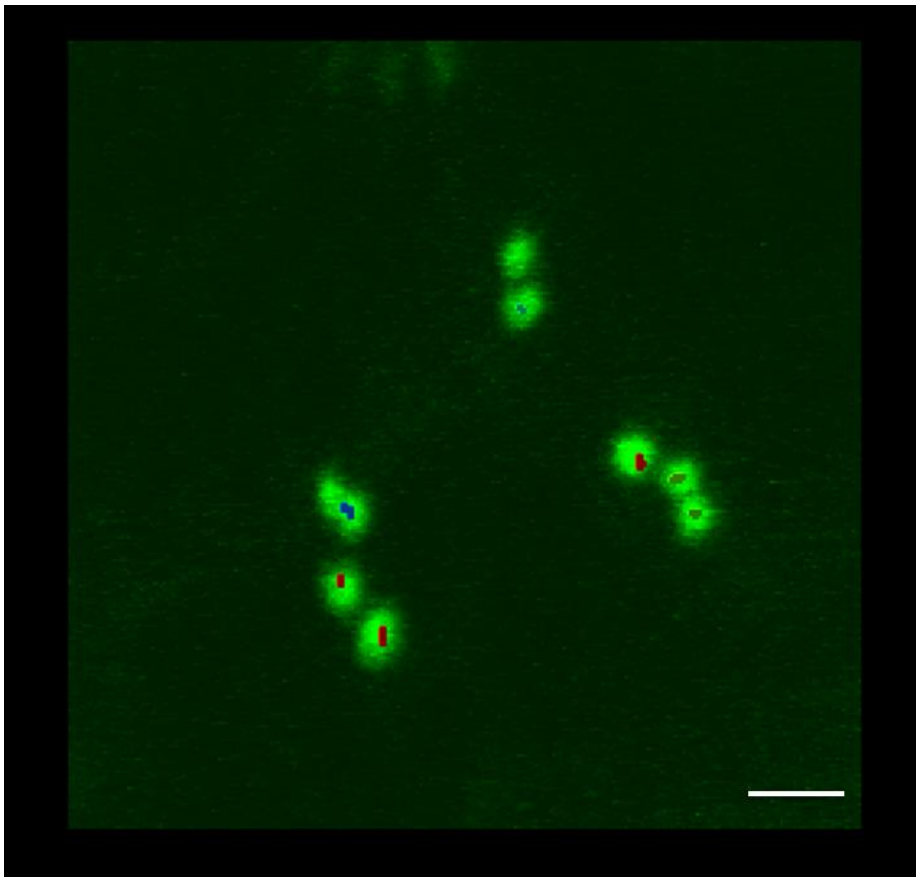

**Figure 23.**
**Statistical analysis of the velocity values of fluorescent Golgi bodies recorded at 72hrs from the infiltration of organelle marker. Comparison between untreated sample, treatment with oryzalin and the DMSO control (1 μl/ml) of two replicates.**

**A**: Descriptive statistics of the velocity of the untreated samples, and samples treated with oryzalin and DMSO control of the first replicate.
**B:** Whisker-boxplot of the velocity values of replicate 1. The red line indicates that the control and the treatment with oryzalin are significantly different according to MW and KS test (See Appendix III).
**C**: Descriptive statistics of the velocity of untreated samples and treated with oryzalin or DMSO of the second replicate.
**D:** Whisker-boxplot of the velocity values of the second replicate. The red line indicates that the control and the treatment with oryzalin are significantly different according to MW and KS test (See Appendix III).

**Figure 23.**

A.

| Velocity rep1 72hrs untreated vs DMSO vs bryzalin | | | |
|---|---|---|---|
| | Untreated | DMSO (1 /ml) | Oryzalin |
| Count | 126 | 229 | 238 |
| Mean | 0.8 m/sec | 0.81 m/sec | 0.6 m/sec |
| Median | 0.7 m/sec | 0.56 m/sec | 0.4 m/sec |
| St.Deviation | 0.44 m/ sec | 0.66 m/sec | 0.63 m/sec |
| Minimum | 0.16 m/ sec | 0.12 m/sec | 0.10 m/sec |
| Maximum | 2.14 m/ sec | 3.07 m/sec | 3 m/sec |
| Range | 1.98 m/ sec | 2.95 m/sec | 2.9 m/sec |
| Skewness | 2.9 | 1.47 | 2.1 m/sec |
| Significance Normality test (SW) | 0.000 | 0.000 | 0.000 |

C.

| Velocity rep2 72hrs untreated vs DMSO vs bryzalin | | | |
|---|---|---|---|
| | Untreated | DMSO (1 /ml) | Oryzalin |
| Count | 198 | 142 | 173 |
| Mean | 0.5 m/sec | 0.56 m/ sec | 0.61 m/ sec |
| Median | 0.34 m/sec | 0.45 m/ sec | 0.46 m/ sec |
| St.Deviation | 0.49 m/sec | 0.36 m/ sec | 0.45 m/ sec |
| Minimum | 0.11 m/sec | 0.12 m/ sec | 0.13 m/ sec |
| Maximum | 3.65 m/sec | 2.22 m/ sec | 2.53 m/ sec |
| Range | 3.54 m/sec | 2.10 m/ sec | 2.40 m/ sec |
| Skewness | 2.9 | 2.02 | 1.9 |
| Significance Normality test (SW) | 0.000 | 0.000 | 0.000 |

B.

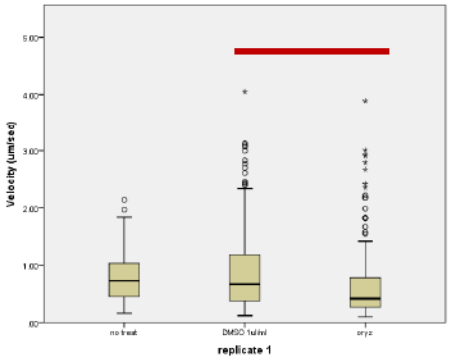


D.

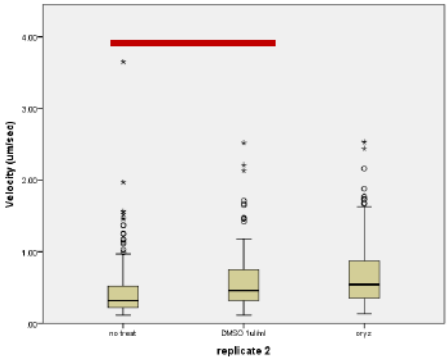

**Figure 23**
**Statistical analysis of the velocity values of fluorescent Golgi bodies recorded at 72hrs from the infiltration event. Comparison between untreated sample, treatment with oryzalin and the control 1 μl/ml DMSO of the third replicate.**

The analysis of the first two replicates of this experiment showed that results are not consistent. A third replicate is performed and analysed.

**E:** Descriptive statistics of the velocity values of the third replicate.
**F:** Boxplot comparing the dataset of the untreated sample, DMSO control and treatment with oryzalin**.** None of the treatments are significantly different from the untreated sample.

**Figure 23.**

E.

| Velocity rep3 72hrs untreated vs DMSO vs oryzalin | | | |
|---|---|---|---|
| | Untreated | DMSO (1 l/ml) | Oryzalin |
| Count | 66 | 42 | 74 |
| Mean | 1.2 m/sec | 0.95 m/sec | 0.95 m/sec |
| Median | 0.92 m/sec | 0.65 m/sec | 0.66 m/sec |
| St.Deviation | 1.04 m/sec | 0.8 m/sec | 0.7 m/sec |
| Minimum | 0.3 m/sec | 0.25 m/sec | 0.17 m/sec |
| Maximum | 5.14 m/sec | 3.75 m/sec | 2.8 m/sec |
| Range | 5.11 m/sec | 3.50 m/sec | 2.63 m/sec |
| Skewness | 2.3 | 2 | 1 m/sec |
| Significance Normality test (SW) | 0.000 | 0.000 | 0.000 |

F.

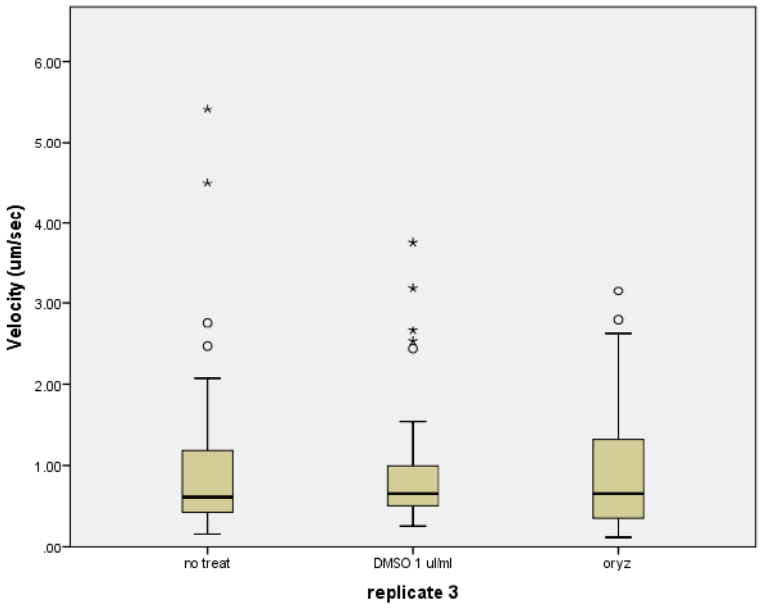

**Figure 24.**

**Scatter plots of the velocity values of Golgi bodies divided by movies.**

To understand if the source of variability of Golgi bodies movement is due to an error in the acquisition of the movies, the velocity values were plotted separately for each movie. (**A**) untreated sample, (**B**) DMSO control and (**C**) oryzalin treatment.

**Figure 24.**

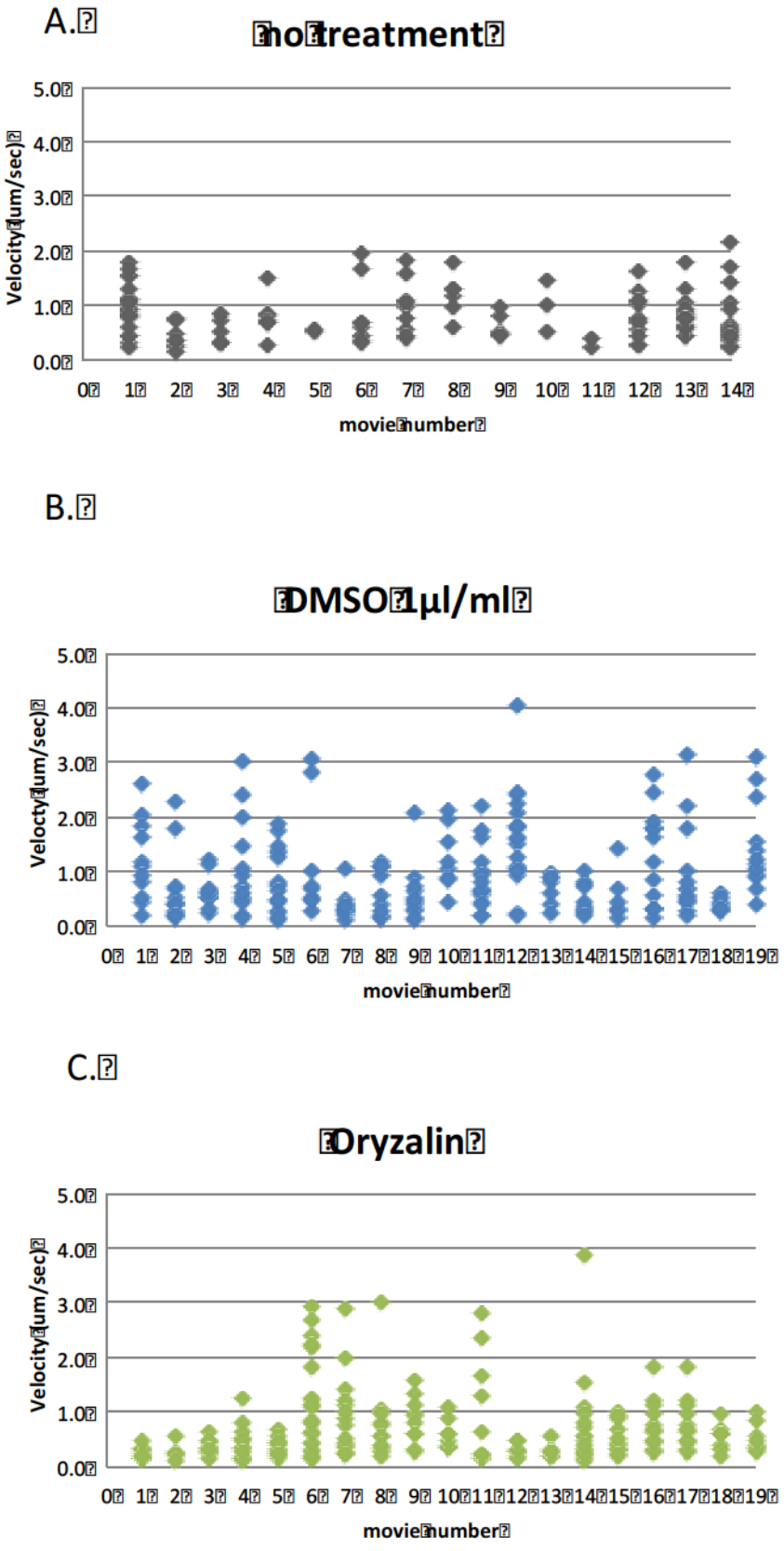
A.
no treatment
Velocity(um/sec)
5.0
4.0
3.0
2.0
1.0
0.0
0 1 2 3 4 5 6 7 8 9 10 11 12 13 14
movie number
B.
DMSO 1µl/ml
Velocty(um/sec)
5.0
4.0
3.0
2.0
1.0
0.0
0 1 2 3 4 5 6 7 8 9 10 11 12 13 14 15 16 17 18 19
movie number
C.
Dryzalin
Velocity(um/sec)
5.0
4.0
3.0
2.0
1.0
0.0
0 1 2 3 4 5 6 7 8 9 10 11 12 13 14 15 16 17 18 19
movie number

**Figure 25.**
**Scatter plot of the velocity values of the untreated sample, DMSO control and treatment with oryzalin. Data pooled altogether.**

The velocity values of each dataset (untreated, DMSO and oryzalin) were plot altogether to detect any trend. Untreated sample (black square), DMSO (blue triangles), oryzalin (green circles).

**Figure 25.**

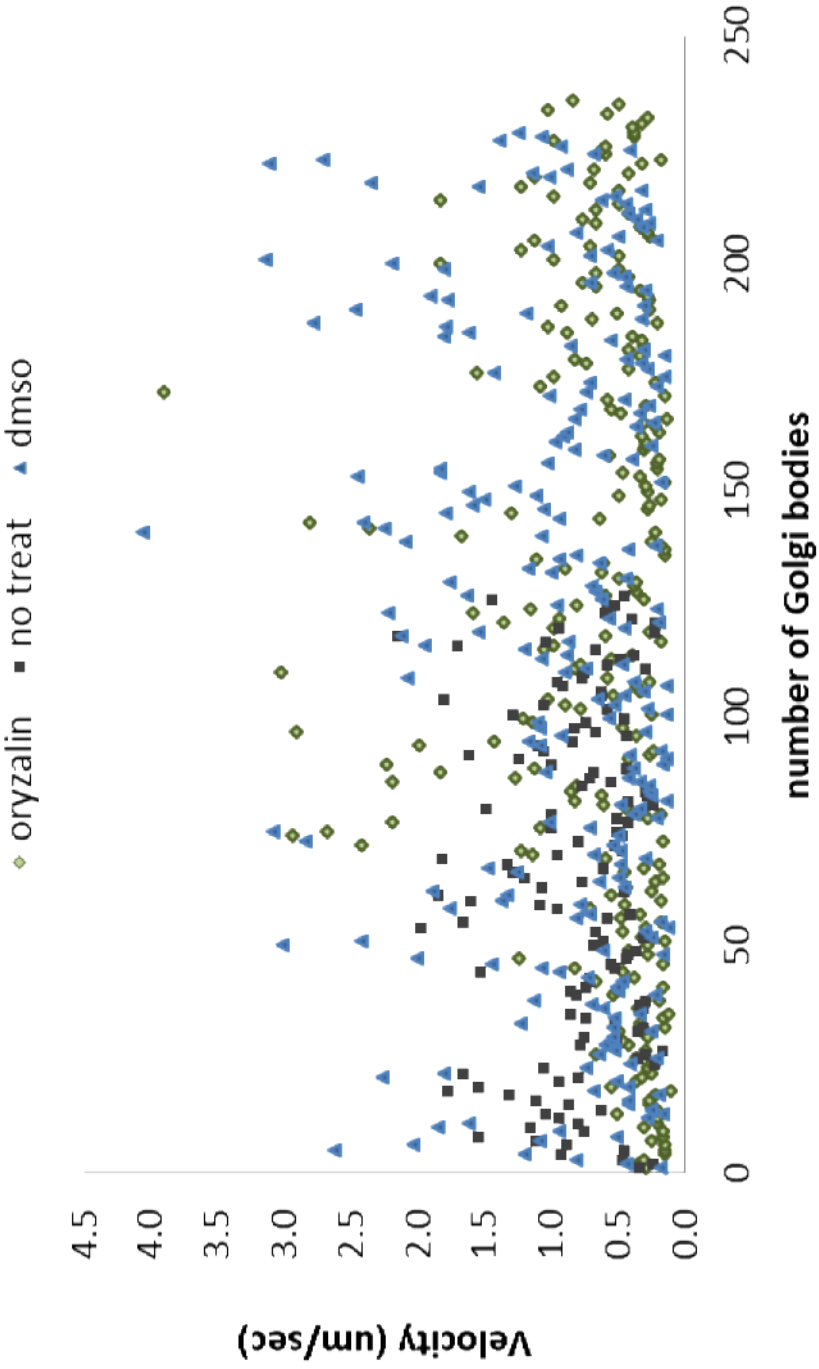
oryzalin
no treat
dmso
Velocity (um/sec)
4.5
4.0
3.5
3.0
2.5
2.0
1.5
1.0
0.5
0.0
0
50
100
150
200
250
number of Golgi bodies

**Figure 26.**
**Snapshot showing the track of a Golgi body and the values of instant velocity.**

The software Volocity can calculate the value of the velocity for each time point.

**Figure 26.**

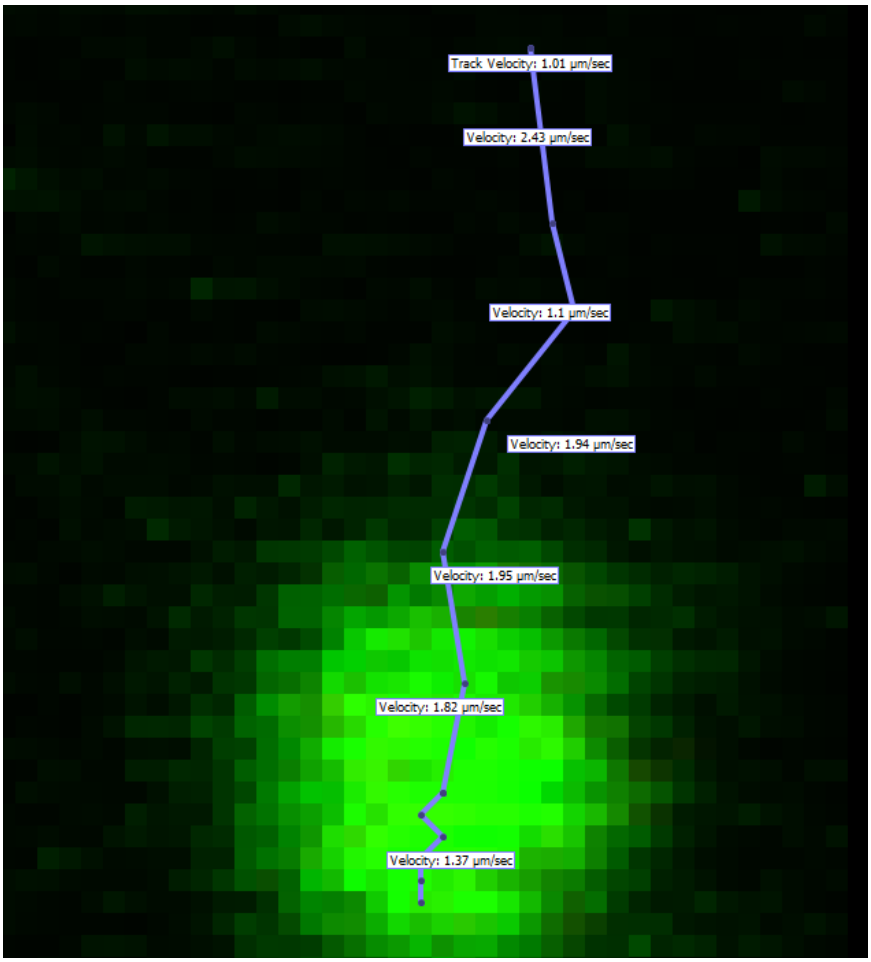
Track Velocity: 1.01 µm/sec
Velocity: 2.43 µm/sec
Velocity: 1.1 µm/sec
Velocity: 1.94 µm/sec
Velocity: 1.95 µm/sec
Velocity: 1.82 µm/sec
Velocity: 1.37 µm/sec

**Figure 27.**
**Histogram representing the meandering index (MI) of the three replicates.**

The meandering indexes are reported for the untreated sample, the DMSO control and treatment with the microtubule depolymerizing drug. The red line indicates significance.
In the first replicate, there are significant difference between the DMSO control and the oryzalin treatment (**A**); in the second replicate the untreated sample is statistically different from the control (**B**) and in the third replicate there are no differences between any of the samples (**C**).

**Figure 27.**

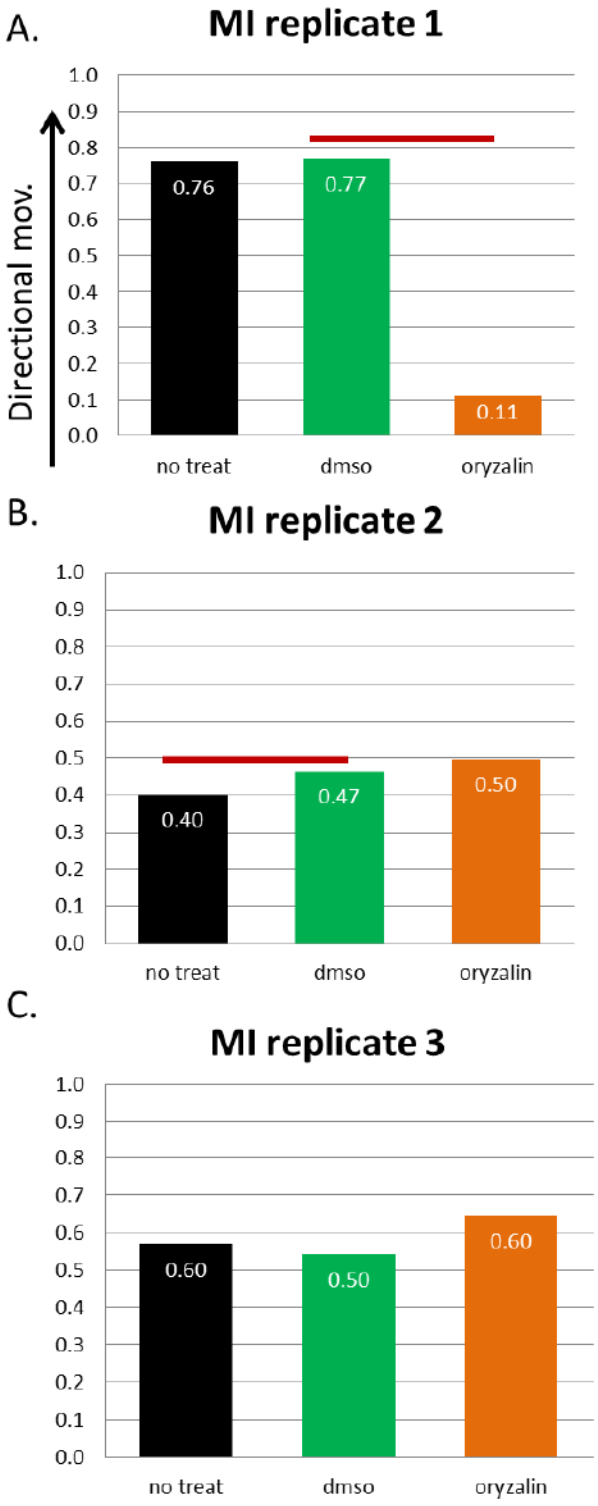
A.
MI replicate 1
Directional mov.
1.0
0.9
0.8
0.7
0.6
0.5
0.4
0.3
0.2
0.1
0.0
0.76
0.77
0.11
no treat
dmso
oryzalin
B.
MI replicate 2
0.40
0.47
0.50
no treat
dmso
oryzalin
C.
MI replicate 3
0.60
0.50
0.60
no treat
dmso
oryzalin

# 4 An alpaca nanobody labels efficiently the plant cytoskeleton *in vivo*

## 4.1 INTRODUCTION

In plant cells, the cytoskeleton is a complex and dynamic filamentous scaffold formed by actin filaments and microtubules, which is present at the cortex of the cell and sustains the cytoplasmic flow of organelles (Avisar *et al.* 2009, Shimmen and Yokota 2004). The actin filaments can form higher order structures known as actin-bundles; fluorescent labeling of the actin network have revealed that actin bundles and fine filaments have different fluorescence intensity, resistance to depolymerizing agents and dynamics. Bundles are brighter, more stationary over time and depolymerize slower whereas fine filaments have faint fluorescence, are more dynamic and depolymerize rapidly (Henty-Ridilla *et al.* 2013).

Different labeling strategies have been developed to study the organization and dynamics of actin filaments in plants both *in vivo* and in fixed tissue. The expression of fluorescent G-actin monomers itself did not prove to be efficient because most of it stays in monomeric form diffused in the cytoplasm, resulting in a strong fluorescent cytoplasmatic background (Lemieux *et al.* 2013). Actin binding proteins (ABPs) however are involved in regulating the organization and assembly of actin filaments and therefore are good marker candidates (Higaki *et al.* 2007). The

actin binding domain of different ABPs have been fused to fluorescent proteins and expressed in plants. Lifeact is a 17 amino acid peptide from the yeast protein Abp140 that decorates filamentous-actin (F-actin) (Riedl *et al.* 2008). In *Arabidopsis thaliana* Lifeact fused to the fluorescent protein Venus reduces the rearrangement of the actin-cytoskeleton and favours the bundling in a concentration-dependent manner (van der Honing *et al*. 2010).

One of the two actin-binding domains of the *A. thaliana* fimbrin1 protein (AtFIM1) was also fused to GFP and labels the fine actin dynamic scaffold in different species and cells, and this is the only fluorescent marker derived from plant ABPs (Sheahan *et al*. 2004). Thus, the visualization of the cytoskeleton with actin binding fluorescent proteins is based on protein-protein interactions. Other staining methods based on chemical binding have often been used such as fluorescent phalloidin (Vandekerckhove *et al*. 1985). Phalloidin is a toxin extracted from death cap *Amanita phalloides* and binds and stabilizes F-actin. Phalloidin conijugated to the fluorescent dye rhodamine, selectively stains actin filaments in permeabilized and fixed plant cells. Phalloidin-rhodamine staining is also effective in unfixed cells but favors the formation of bundles (Sonobe and Shibaoka 1989).

All of the fluorescent reporters available so far depict a very differing organization of the actin network. This may be due to a preferential binding to fine actin filaments rather than bundles or because the marker is derived from an actin-bundling protein, therefore causing the aggregation of actin filaments. Considering that the actin-cytoskeleton is a continuously rearranging scaffold that provides tracks for movement and positioning of diverse organelles such as Golgi bodies (Akkerman *et al*. 2011), a more

reliable and less interfering fluorescent marker is needed for *in vivo* imaging.

Nanobodies have been proven to be advantageous in detecting intracellular structures. They consist of the smallest functional domain of a heavy chain-only antibody isolated from *Camelidae* sera (De Meyer *et al*. 2014) (Figure 3). Because of their small size, solubility and stability it is possible to use them in heterologous systems. In contrast to the flat or concave antigen binding site of conventional antibodies, nanobodies display a convex conformation and preferably bind 3D epitopes (Muyldermans 2001, Panza *et al*. 2015), allowing binding into otherwise inaccessible clefts and pockets (Desmyter *et al*. 1996). They also can be fused to fluorescent proteins to detect and label cell structures *in vivo* (Olichon and Surrey 2007). When the nanobody gene is cloned and conjugated to a fluorescent protein, it is called "chromobody" (Figure 3). The Actin-Chromobody® (ChromoTek, Martinsried, Germany) allows detection of real-time changes in the cytoskeleton of various animal cells lines (Panza *et al*. 2015, Rothbauer *et al*. 2006)

In this study the commercially available Actin-Chromobody® was modified (ChromoTek, Martinsried, Germany) and used for visualizing actin-cytoskeleton in tobacco leaf cells and studying the impact on Golgi bodies and actin filaments.

# 4.2 Results

## *4.2.1 In planta expression of the actin-chromobody and evaluation of the impact on cytoskeleton dynamics.*

*Agrobacterium tumefaciens* was transformed with constructs fusing the antibody sequence with both N- and C-terminus fluorescent protein tags (Figure 5) and *Nicotiana tabacum* leaves were infiltrated with the transformed agrobacteria, either on their own or with the Golgi marker ST-GFP.

In various mammalian cell lines the C-terminal fusion allowed expression and actin targeting of the chromobody (http://www.chromotek.com/products/chromobodies/actin-chromobodyr) whereas in plant cells the nanobody C-terminal fusion remained cytosolic (Figure 28,1A) and localizes in the nucleoplasm (Figure 28,1C), which is common for cytosolic fluorescent proteins (Brandizzi *et al*. 2002). Since the cytoplasmic fluorescent pattern is very similar to that of the endoplasmic reticulum, actin-Cb-YFP was co-expressed with the ER marker GFP-HDEL. The fluorescent nanobody and the ER marker do not co-localize, confirming that the antibody is in the cytoplasm (Figure 28, 1B).

The localization of the N-terminus fusions to different fluorophores (GFP and YFP) was compared. The N-terminal YFP clearly labelled actin filaments (Figure 28, 2A-C) and N-terminal GFP-fusion decorates the actin filaments in a comparable manner (Figure 28, 3A-C). To determine optimal expression conditions that would allow investigation of actin dynamics as well as providing sufficient expression levels for visualization, tobacco leaves were infiltrated with three different concentrations of

*Agrobacterium tumefaciens* for either constructs: OD600 of 0.1, 0.05 and 0.01 with 0.1 being the standard infiltration OD. When YFP-Actin-Cb was expressed at the highest OD of 0.1, it resulted in major bundling of actin filaments (Figure 28, 2A) and the lowest OD of 0.01 mainly bound to thicker actin bundles (Figure 28, 2C and 3C). The OD of 0.05 for YFP N-terminal fusion labelled both thicker filaments as well as finer ones (Figure 28, 2B and 3B) and was therefore chosen for follow-up experimentation. In general at OD 0.05 what appeared to be a more complete overview of the actin cytoskeleton with thick bundles and thinner filaments was obtained compared to that with Lifeact expression (Figure 29). For GFP-Actin-Cb, at OD of 0.1 and 0.05, actin filaments were decorated but cytoplasmic fluorescence was detected (Figure 28, 3B and 3C); the lowest OD 0.01 labels both actin fine strands and thicker cables without any background noise (Figure 28, 3A). This last OD setting was used for further experiments.

In plants, the motility of Golgi bodies is mainly dependent on the actin cytoskeleton: treatment with the actin depolymerizing agent cytochalasin D causes the organelle to stop directional movement (Boevink *et al*. 1998) (See section 3.3.3). Labelling of the actin cytoskeleton might compromise the dynamics of the organelle by changing the organization of the actin network (van der Honing *et al*. 2010).

In order to evaluate the effect of Lifeact-GFP and YFP-Actin-Cb on the movement of Golgi bodies, the cytoskeleton markers were transiently coexpressed with the Golgi marker ST-GFP and compared to the transient expression of ST-GFP alone. Movies were collected for each combination and analyzed with Volocity software (See section 2.8). The expression of either of the cytoskeleton markers significantly slows down the motility of the Golgi bodies compared to the control (Figure 30C). The

displacement rate is not significantly affected by the expression of Lifeact-GFP but is significantly reduced in the presence of YFP-actin-Cb (Figure 30D). Both velocity and displacement rate in the combinations of ST-GFP and YFP-Actin-Cb or Lifeact-GFP, respectively, were normalised to the datasets for expression of ST-GFP alone and presented as a percentage of the latter (Figure 30E). Upon the expression of Lifeact-GFP, the relative mean of the meandering index is significantly increased by 19% compared to ST-GFP indicating that the organelles move more directionally (Figure 30E,F). YFP-Actin-Cb significantly reduces the meandering index by 11% with respect to ST-GFP (Figure 30E,F) indicating that saltatory movement is slightly favored.

### 4.2.2 Depolymerisation of the actin-cytoskeleton labeled with different fluorescent markers

Actin filaments labeled with the chromobody were treated with a depolymerizing agent to investigate if the binding of the probe stabilized the actin filaments and affected the actin dynamics. Leaf segments of plants transiently expressing YFP-actin-Cb were treated with 25 µM latrunculin B, an actin depolymerizing compound (See section 2.7.2). Already after 15 min of latrunculin B treatment the thinner strands were completely absent; after 30 min only the bundled actin strands were visible and after 45 min most of the strands were depolymerized and just a few actin bundles were left (Figure 31A).

With latrunculin B being a relatively small molecule of less than 0.4 kDa and binding transiently to monomeric actin, it is possible to reverse its effects by immersing the leaf cuttings in water and thereby washing out the drug and repolymerising the actin

cytoskeleton. A rapid recovery of filamentous actin within less than one hour of washing was observed with a visible increase in the number of strands in 30 min (Figure 31B).

The effect of latrunculin B in tobacco leaf samples transiently expressing the fluorescent marker GFP-FABD2 (Sheahan *et al*. 2004) was studied. The depolymerization process starts quickly and by 5 min most of the fine filaments have been depolymerized and only parts of the major strands are visible; after 15 min all the thinner filaments are disassembled and most of the actin bundles are trimmed to short chunks. The depolymerization continues over 30 mins, when pieces of actin bundles are still visible; after 45 min the thicker segments of filaments are reduced to thinner strands (Figure 32). Latrunculin B is a largely apolar molecule which dissolves in dimethyl sulfoxide (DMSO), and this is soluble in water allowing the dilution of latrunculin B in a water solution. DMSO solution (10 µl/ml) was used as control. Leaf samples expressing FABD2-GFP were immersed in the DMSO solution and the effect monitored over 45 mins (Figure 33). During the entire treatment, the filamentous actin network remains intact and re-organizing, thus no depolymerization is occurring. A modification of the shape of the stomata is observed after 45 mins from the beginning of the treatment (Figure 33).

Lifeact-GFP is a small fluorescent marker (~30 KDa) that has been used in animal cells to see the cytoskeleton and study the dynamics (Riedl *et al*. 2008), but in plant cells favors the bundling of actin filaments (van der Honing *et al*. 2010). To evaluate the effect of Lifeact-GFP on the cytoskeleton stability, leaf cells expressing the cytoskeleton marker were treated with the actin depolymerizing compound (Figure 34) and DMSO as control (Figure 35). The depolymerization of fine filaments occured between 20 min and 30 min; thick bundles start to be disassembled after 30 mins and at 50 min and 60 min the actin

cytoskeleton is completely depolymerized in most of the cells (Figure 34). Treatment with DMSO shows that both fine filaments and bundles are present throughout the entire treatment (Figure 35).

# 4.3 Discussion

## *6.3.1 Expression of the nanobody and analysis of the dynamics of Golgi bodies.*

The actin-Chromobody was originally developed to be used in animal cells. It efficiently labels the cytoskeleton and does not perturb the actin-cytoskeleton dynamics (Panza *et al*. 2015). Because the structural and binding characteristics of nanobodies are different from the fluorescent probes commonly used in plants, the actin-chromobody is a promising tool to investigate actin dynamics in the plant system. The expression of the fluorescent nanobody in tobacco was optimized and analyzed. The expression in tobacco leaves of actin-Cb-YFP resulted in the fluorescence remaining cytoplasmic, suggesting that the short peptide linker between the nanobody sequence and fluorophore might perturb the folding of chimeric protein, hence misfolding the recognition site of the nanobody for the actin strands. As result, actin-Cb-YFP is not able to bind the target sequence and is dispersed in the cytoplasm and in the nucleus (Figure 28, 1A-C). When the nanobody sequence was inserted at the C-terminus of YFP, the short peptide sequence was not inserted between the nanobody and the fluorescent protein (See Figure 5). This could result in the correct folding of the fluorescent tagged antibody and the preservation of the 3D structure of the recognition site for the cytoskeleton, therefore decoration of actin strands. The same order of sequence was applied when the protein fusion between the nanobody and GFP was made. When GFP-actin-Cb was expressed in tobacco plants, it targeted and decorated both thin and thicker actin strands (Figure 28, 3A-C). For the fluorescent tagged nanobodies, different infiltration ODs were tested to find

the optimal concentration of agrobacterium cells carrying the fluorescent proteins. The optimal conditions were specified as the OD that allowed a labelling of fine actin filaments and thick bundles and low background fluorescent noise in most of the infected cells. YFP-actin-Cb and GFP-actin-Cb have optimal OD of 0.05 (Figure 28, 2B) and 0.01 (Figure 28, 3C) respectively. For a protein fused to different fluorophores at the same sequence ending, and according to same cloning and expression procedure, the identical OD setting could be expected. The different OD settings reported can be explained in the use of multicopy binary vector agrobacterium strains (GV3101), which can host multiple copies of the expression vector and therefore transfer to the plant a variable number of copies of DNA; this would result in the insertion of unpredictable number of copies of the transgene into the host plant and different levels of protein expression (Lee and Gelvin, 2008).

The two fluorescent versions of the nanobody show less bundling (Figure 29A and B) compared to the labelling with Lifeact-GFP (Figure 29C). A different rendering of the cytoskeleton is observed by comparing YFP-actin-Cb and GFP-actin-Cb (Figure 29A and B). As reported by Shaner *et al*. (2007), eYFP can form weak dimers. Since the interaction of eYFP monomers is classified as weak, it can be assumed that eYFP dimers can affect the cytoskeleton organization and the difference observed in the fluorescent pattern of the actin network can be explained by the fact that they bind the filament as dimers, and not due to a reorganization of the filamentous frame as happens upon the expression of Lifeact-GFP. In Cranfill *et al* (2016) it is shown that eGFP fluorophore can form dimers, but the majority (98%) is in the monomeric form.
To further investigate the relationship between the actin filament organization and Golgi bodies, and the differences in the labelling

between YFP-actin-Cb and Lifeact-GFP, the movement of fluorescent Golgi bodies in presence of either Lifeact-GFP or YFP-actin-CB was analysed with the software Volocity. Upon Lifeact-GFP expression, the CDF curve representing the velocity of Golgi bodies is shifted towards smaller values, indicating that the organelles move more slowly (Figure 30C, green line). The mean values for the velocity (Figure 30E, green bar) shows that a significant reduction of ~20% occurred compared to the control, expressing ST-GFP only. To characterize the movement in more detail, the displacement rate is taken into consideration. The curve of the displacement rate (Figure 30D, green line) has the distribution as the control and, confirmed by the mean values analysis (Figure 30E, green bar) and there is no significant difference in the organelle displacement when Lifeact-GFP is expressed. The mean values of the meandering index indicates that there is an increase of the saltatory movement compared to the control (Figure 30E, green bar). The expression of Lifeact-GFP reduces the velocity of Golgi bodies, has no effect on the linear distance travelled by the organelle but decreases the complexity of the movement (Figure 30F). The changes in the dynamics determined by the expression of Lifect-GFP were compared to YFP-actin-Cb. The fluorescent nanobody causes a shift of the velocity CDF curve towards smaller values (Figure 30C, yellow curve), and as quantified by the mean numbers, a reduction of ~80% occurs (Figure 3E, yellow bar). When the cytoskeleton is labelled with the nanobody, the CFD of displacement rate is also shifted towards smaller values (Figure 30D, yellow curve) and the mean reduced by ~90% compared to the control (Figure 30E, yellow bar). The ratio between the velocity and displacement rate, that is the meandering index, is significantly reduced by 10% indicating that the changes in both parameters is of similar extent and proportionality is maintained (Figure 30E, yellow bar). Upon

the expression of YFP-actin-Cb, both velocity and displacement rate are equally affected meaning that the Golgi bodies move slower but conserve their dynamic features (Figure 30F). This can be explained by looking at the nature of the binding of the two fluorescent markers. Lifeact-GFP derives from the cross-bundling factor (van der Honing *et al*. 2010, Riedl *et al*. 2008) and the peptide sequence used to make the fluorescent marker might have induced the cross-bundling properties. The aggregation of thick actin cables following the expression of Lifect-GFP, would slow down organelle and favour a more directional movement (Figure 30F). The nanobody targets a three dimensional non-characterized site of the actin through an epitope- recognition mechanism, and is not involved in a physiological binding, like Lifeact-GFP. My hypothesis is that the expression of the fluorescent nanobody does not induce rearrangement of the cytoskeleton and probably induces steric hindrance that would interfere with the sliding of myosins. This would explain how the general movement of Golgi bodies is slowed down but maintains the same dynamic features as control Golgi bodies (Figure 30F). These characteristics make the antibody a valuable tool to further investigate the actin network and Golgi dynamics (See Chapter 6).

### *4.3.2 Depolymerization of the actin cytoskeleton labeled with actin markers.*

To investigate whether the nanobody affects the ability of actin to polymerize and depolymerize, tobacco leaf cells expressing the YFP-Actin-Cb were treated with the depolymerizing compound latrunculin B and compared to treatment with DMSO. Fine actin filaments are partially disassembled after 15 mins of treatment and at 30 mins, only major bundles are visible. The depolymerizing agent completely disrupts the cytoskeleton after

45 mins (Figure 31A). To assess if the nanobody affects the re-polymerization of the filaments, a washout of the chemical compound was performed. Leaf samples previously treated with latrunculin B were immersed in water and the reassembly of the actin filaments followed over time. The network started to reassemble at 30 min and by 60 min more defined filamentous structures were detected, indicating that YFP-actin-Cb does not interfere with the re-polymerization and organization of the actin cytoskeleton (Figure 31B). The depolymerization data were compared to the depolymerization of Lifeact-GFP and FABD2-GFP labeled actin filaments (Figure 34 and 32, respectively). The depolymerization of the actin filaments decorated by the nanobody was complete at 45 min whereas parts of filaments labeled with FABD2 were still present (Figure 32) and in cells labeled with Lifeact-GFP long strands of actin filaments were detected (Figure 34). This suggests that Lifeact-GFP and FABD2-GFP have a stabilizing effect on the actin filaments, which causes a slower depolymerization process. This may be due to the fact that both of these cytoskeletal markers derive from cross-bundling factor (Riedl *et al*. 2008, Voigt *et al*. 2005). The binding of the nanobody to the actin filaments is not physiological and is not inducing bundling therefore is not stabilizing the filamentous structure.

According to the model of actin strand polymerization, actin monomers (G-actin) constitute a pool in the cytoplasm and are recruited at the growing (+) tip of actin filaments to elongate the strand. At the (-) end, the F-actin depolymerizes (Figure 36A). When treatment with latrunculin B is performed, the agent binds and sequesters actin monomers in the cytoplasm, which are not available anymore for the (+) end to grow (Morton *et al*. 2000). The depolymerization process at the (-) end is then the

predominant process, resulting in the complete depolymerisation of the cytoskeleton frame as observed after 45 min of treatment (Figure 31A; 36B). Since the actin monomers are in the cytoplasm, a fluorescent cytoplasmic signal would be expected upon the treatment with latrunculin B following the release of the fluorescent marker from the filaments. In my experiments a labeling of the cytoplasm has not been detected with any of the cytoskeleton markers used (Figure 31; Figure 32 and 34). A similar situation happens when cytochalasin D is used (Prokhnevsky *et al*. 2005). Two scenarios are possible. The fluorescent marker is not released from the actin monomers and latrunculin B forms a complex with them. The complex actin-marker-latrunculin B is sent for degradation or determines a reversible misfolding of the marker which results in the loss of the fluorescence (Figure 37A). The other possibility is that the marker is released from the actin monomers and binds to latrunculin B. The binding to drug determines a change in the fluorescent marker structure that leads to the degradation or loss of the ability to fluorescence (Figure 37B).

In conclusion the actin nanobody is a useful marker that has lesser effects on actin filaments, compared to routinely used fluorescent cytoskeletal proteins, and can be used to study intracellular dynamics mechanisms such as the motility of organelles in relation to actin filaments.

**Figure 28.**
**Confocal images of *Nicotiana tabacum* leaves transiently expressing the fluorescent nanobody.**

**1.** actin-Cb-YFP (A) co-expressed to endoplasmic reticulum marker GFP-HDEL (B). The nanobody localises in the cytoplasm and no co-localization is found with the ER (C).
**2.** YFP-actin-Cb transiently expressed in *Nicotiana tabacum* leaves at different agrobacterium concentrations: $OD_{600}$=0.1 (A), $OD_{600}$=0.0.5 (B), $OD_{600}$=0.01 (C).
**3.** GFP-actin-Cb expressed in *Nicotiana tabacum* leaves at different Agrobacterium concentrations: $OD_{600}$=0.1 (A), $OD_{600}$=0.0.5 (B), $OD_{600}$=0.01 (C).

**Figure 28.**

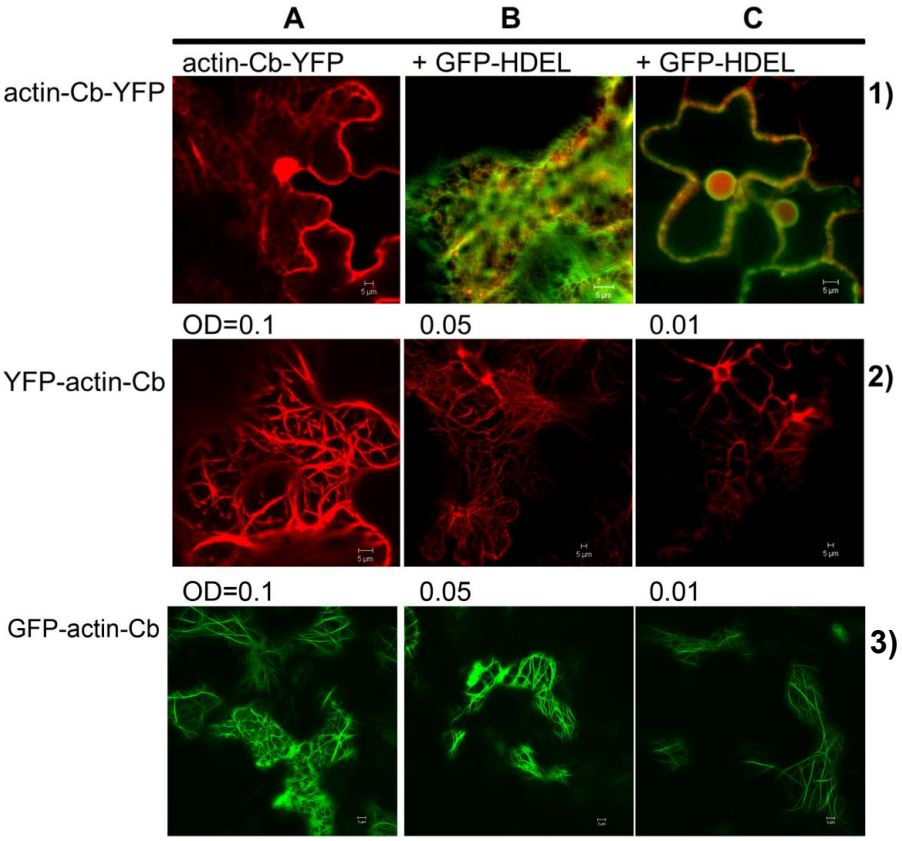
A
B
C
actin-Cb-YFP
+ GFP-HDEL
+ GFP-HDEL
actin-Cb-YFP
1)
OD=0.1
0.05
0.01
YFP-actin-Cb
2)
OD=0.1
0.05
0.01
GFP-actin-Cb
3)

**Figure 29.**
**Comparison of cytoskeletal markers transiently expressed in *N. tabacum* leaves.**

**A.** Transient expression of YFP-actin-Cb;
**B.** Transient expression of GFP-actin-Cb;
**C.** Transient expression of Lifeact-GFP.

**Figure 29.**

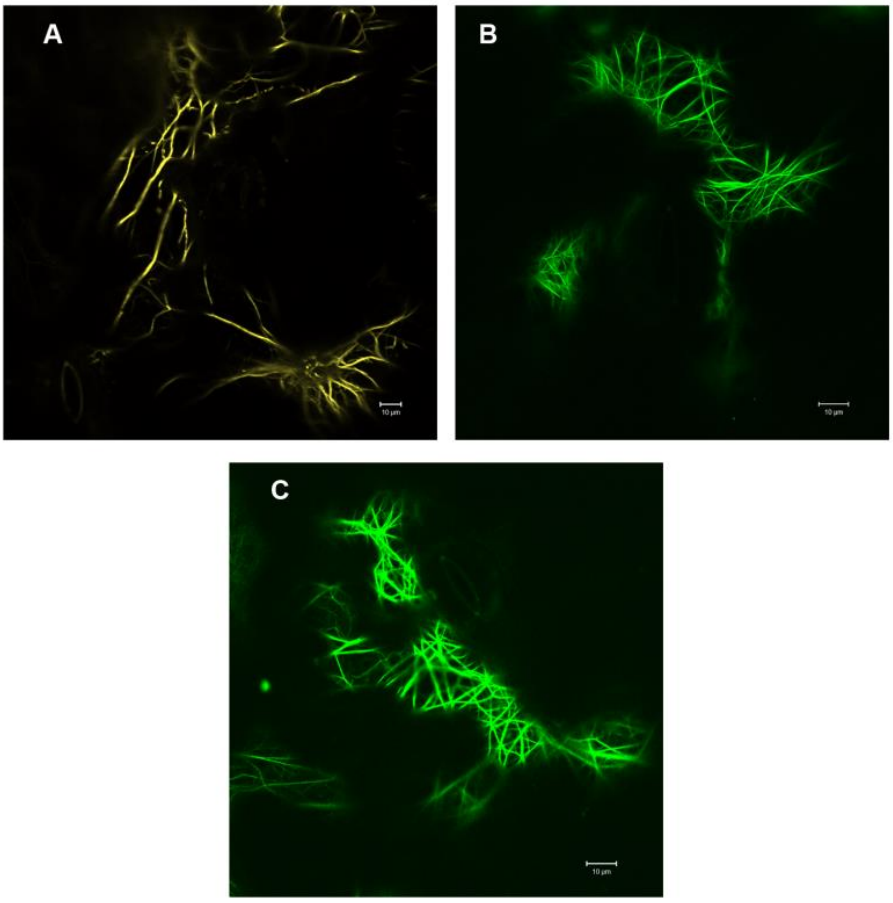

**Figure 30.**
**Analysis of the effect of the fluorescent nanobody expression on Golgi motility compared to Lifeact-GFP.**

**A and B**. tobacco plant cells transiently co-expressing ST-GFP and YFP-actin-Cb and ST-GFP and Lifeact-GFP, respectively. Scale bar 5μm
**C**. Cumulative distribution frequency graph (CDF) of the velocity values of Golgi bodies. ST-GFP (blue line), ST-GFP co-expressed with YFP-actin-Cb (yellow line) and ST-GFP co-expressed with Lifeact-GFP (green line). Curves marked with shapes (*, ♦) indicate a statistically significant difference from the control ST-GFP (KS test, $p < 0.05$).
**D.** CDF curves of the displacement rates values. ST-GFP (blu line), ST-GFP co-expressed with YFP-actin-Cb (yellow line) and ST-GFP co-expressed with Lifeact-GFP (green line). Curves marked with shapes (*, ♦) indicate a statistically significant difference from the control ST-GFP (KS test, $p < 0.05$)
**E.** Boxplot of the relative mean values of velocity, displacement rate and meandering index expressed as percentage of the control ST-GFP (blu), ST-GFP co-expressed with YFP-actin-Cb (yellow) and ST-GFP co-expressed with Lifeact-GFP (green line).
**F.** Representation the movement pattern of Golgi bodies. When ST-GFP is co-expressed with Lifeact-GFP, Golgi bodies move same linear distance as the control but have a less saltatory path. The co-expression of the antibody determines Golgi bodies moving shorter linear distance and slightly more saltatory. The pattern of movement in presence of the nanobody is maintained.

**Figure 30.**

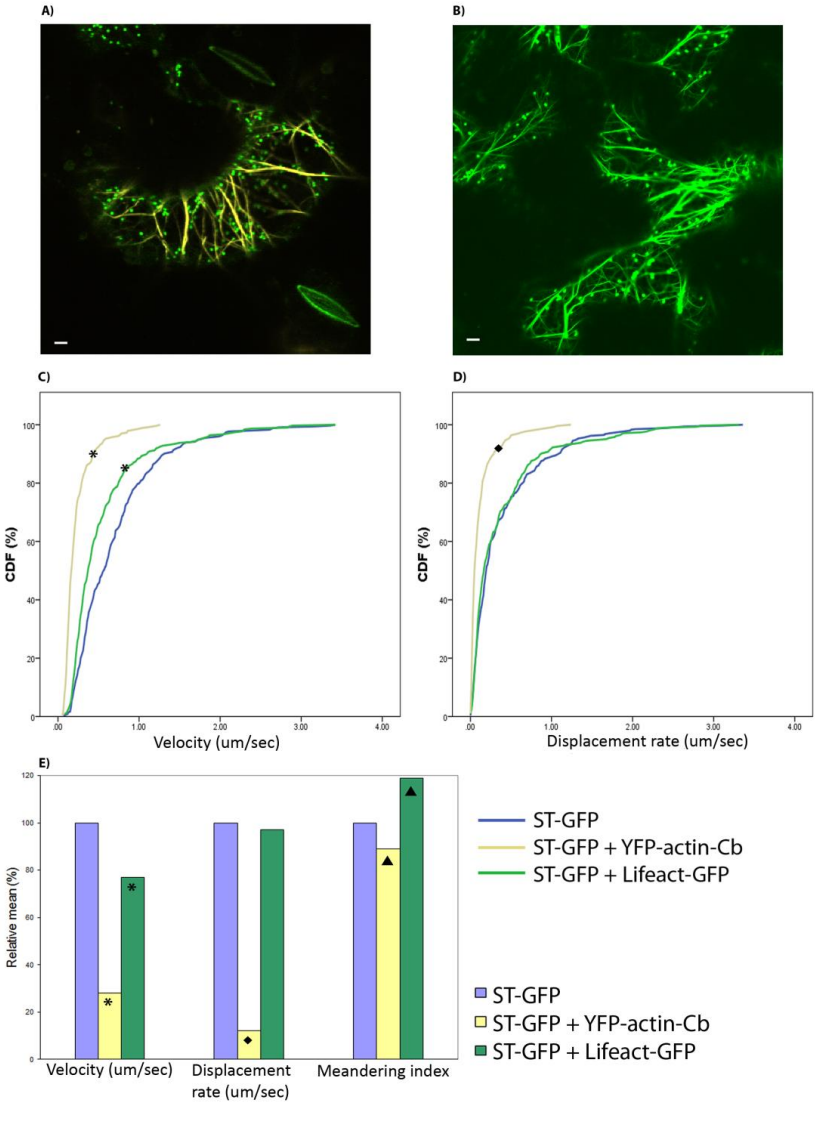
A)
B)
C)
D)
CDF (%)
Velocity (um/sec)
Displacement rate (um/sec)
E)
Relative mean (%)
Velocity (um/sec)
Displacement rate (um/sec)
Meandering index
ST-GFP
ST-GFP + YFP-actin-Cb
ST-GFP + Lifeact-GFP
F)
ST-GFP
ST-GFP + Lifeact-GFP
ST-GFP + YFP-actin-Cb

**Figure 31.**
**Depolymerization and repolymerization of actin filaments labelled with fluorescent nanobody.**

*N.tabacum* leaf epidermal cells transiently expressing YFP-actin-Cb and treated with latrunculin B (25 μM) after 15 min, 30 min, and 45 min (**A**). Repolymerization of the actin filaments by washing out latrunculin B. The recovery of the fluorescence is recorded after 30 min, 45 min and 60 min from the washout (**B**).

**Figure 31.**

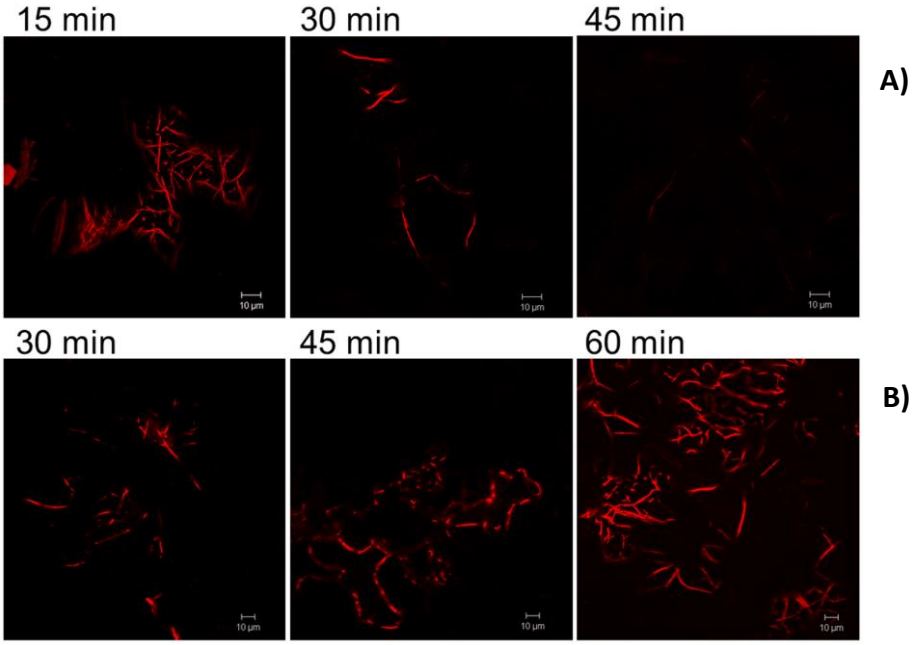

**Figure 32.**
**Depolymerization of actin filaments stably labelled with FABD2-GFP.**

Time series of the effect of the actin-cytoskeleton depolymerizing drug latrunculin B over 45 mins on Arabidopsis epidermal cells stably expressing cytoskeletal marker FABD2-GFP

**Figure 32.**

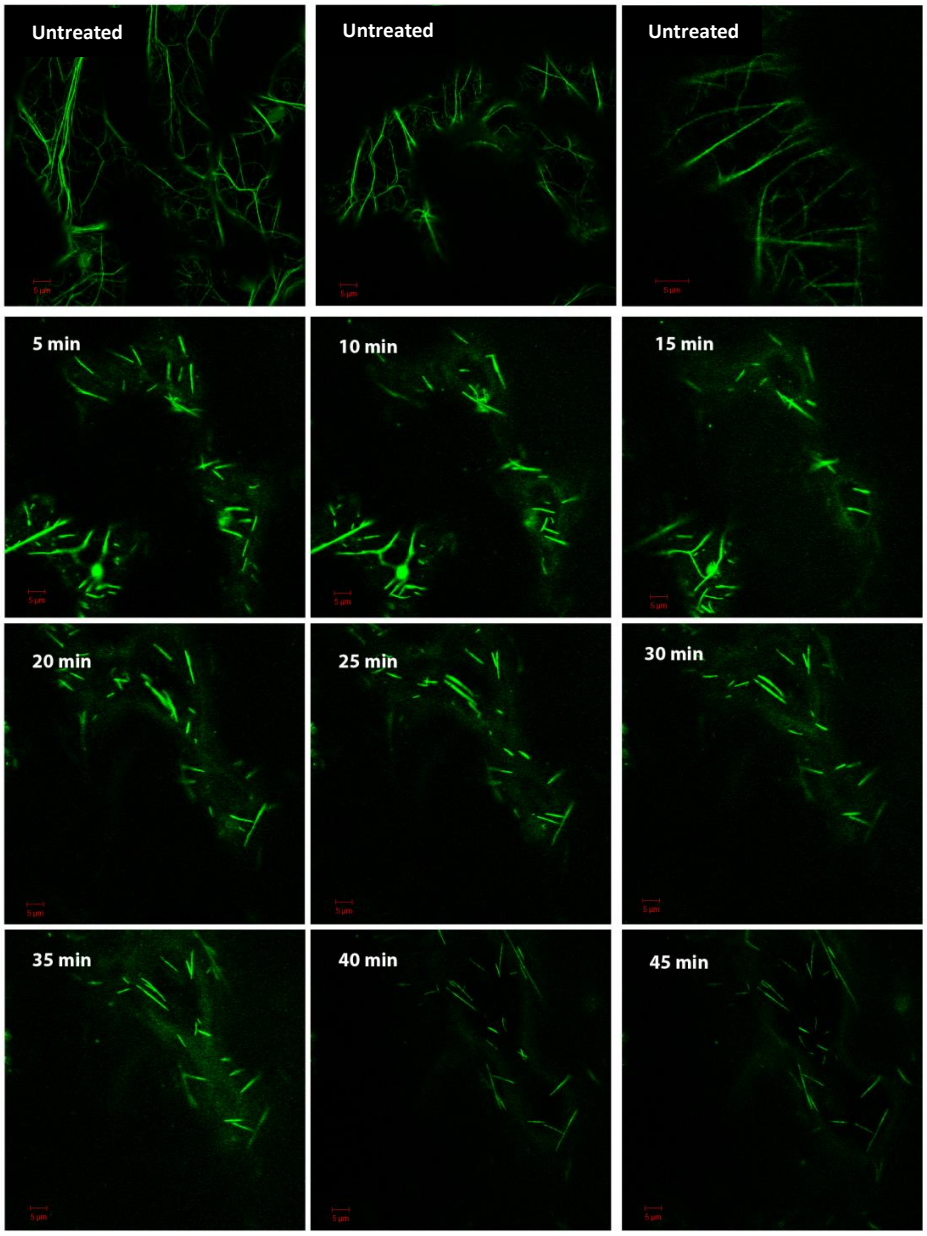
Untreated
Untreated
Untreated
5 min
10 min
15 min
20 min
25 min
30 min
35 min
40 min
45 min

**Figure 33.**
**Treatment of Arabidopsis epidermal cells stably expressing the cytoskeletal marker FABD2-GFP with the control DMSO.**

Time series of the effect of DMSO treatment (10µl/ml) over 45 min. Imags are collected at 5 min, 10 min, 15 min, 20 min, 25 min, 30 min, 35 min, 40 min, 45 min and after 45 min from the start of the treatment.

**Figure 33.**

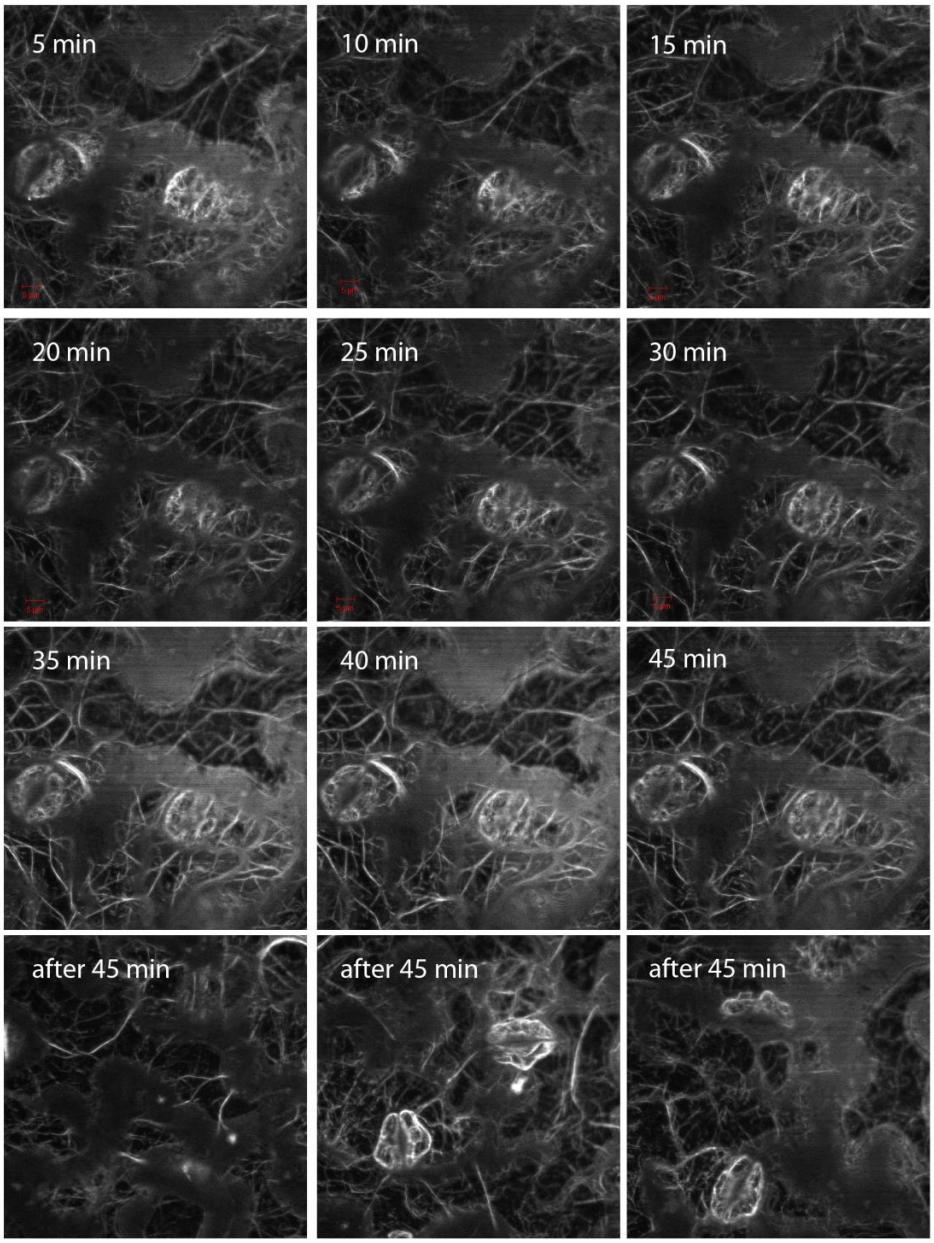
5 min
10 min
15 min
20 min
25 min
30 min
35 min
40 min
45 min
after 45 min
after 45 min
after 45 min

**Figure 34.**
**Depolymerization of actin filaments labelled with Lifeact-GFP.**

Tobacco leaf epidermal cells transiently co-expressing the Golgi marker ST-GFP and Lifect-GFP, and treated with latrunculin B. Images after 10 min, 20 min, 30 min, 40 min, 50 min and 60 min from the start of the treatment are reported. Scale bar 5μm.

**Figure 34.**

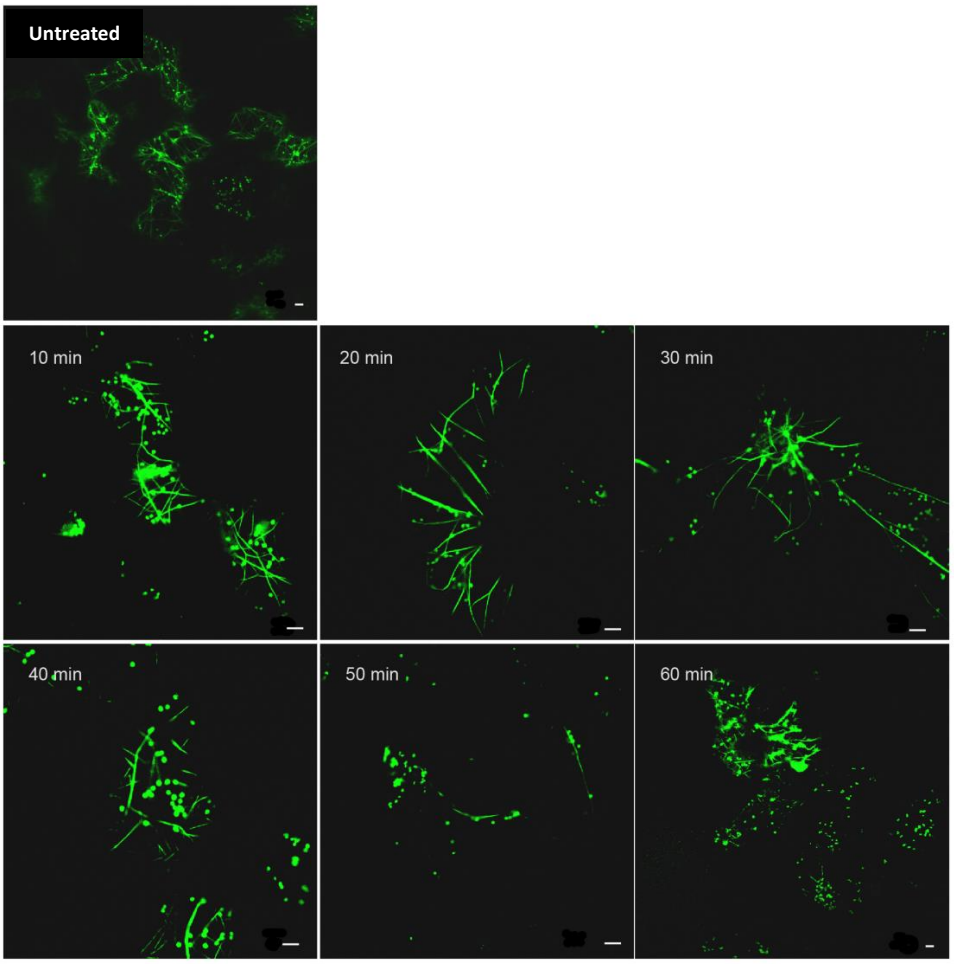

**Figure 35.**
**Treatment of tobacco leaves transiently expressing Lifeact-GFP with DMSO.**

Leaf sections of plants transiently expressing Lifeact-GFP and ST-GFP were immerged in a solution of DMSO (10 µl/ml) and images taken at 10 min, 20 min, 30 min, 40 min and 50 min to monitor the affect of the drug over the time. Scale bar 5µm.

**Figure 35.**

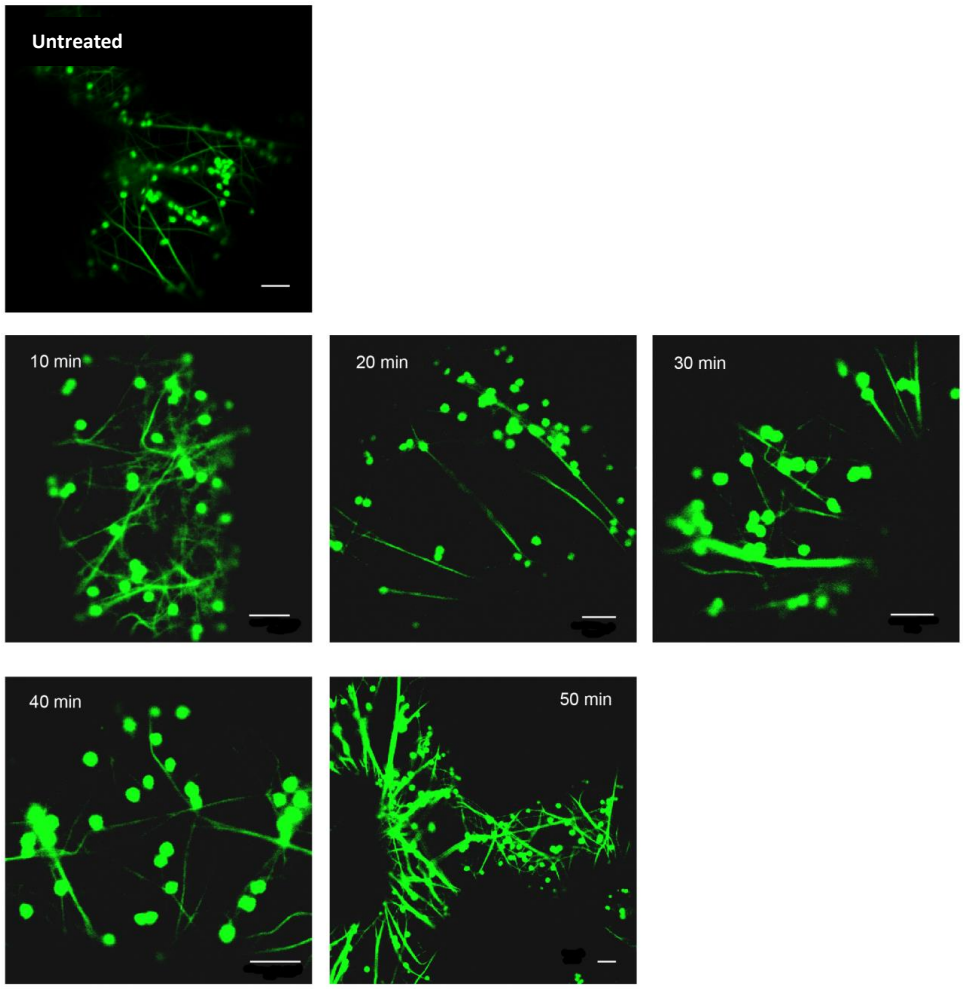

**Figure 36.**
**Representation of latrunculin B effect on actin filaments.**

**A**. Actin filaments have a plus growing end, to which actin monomers (G-actin) are recruited, and depolymerize at the minus end.
**B**. When latrunculin B is present, it binds to G-actin present in the cytoplasm and they are not available anymore for actin polymerization. This results in the depolymerisation of actin filaments.

**Figure 36.**

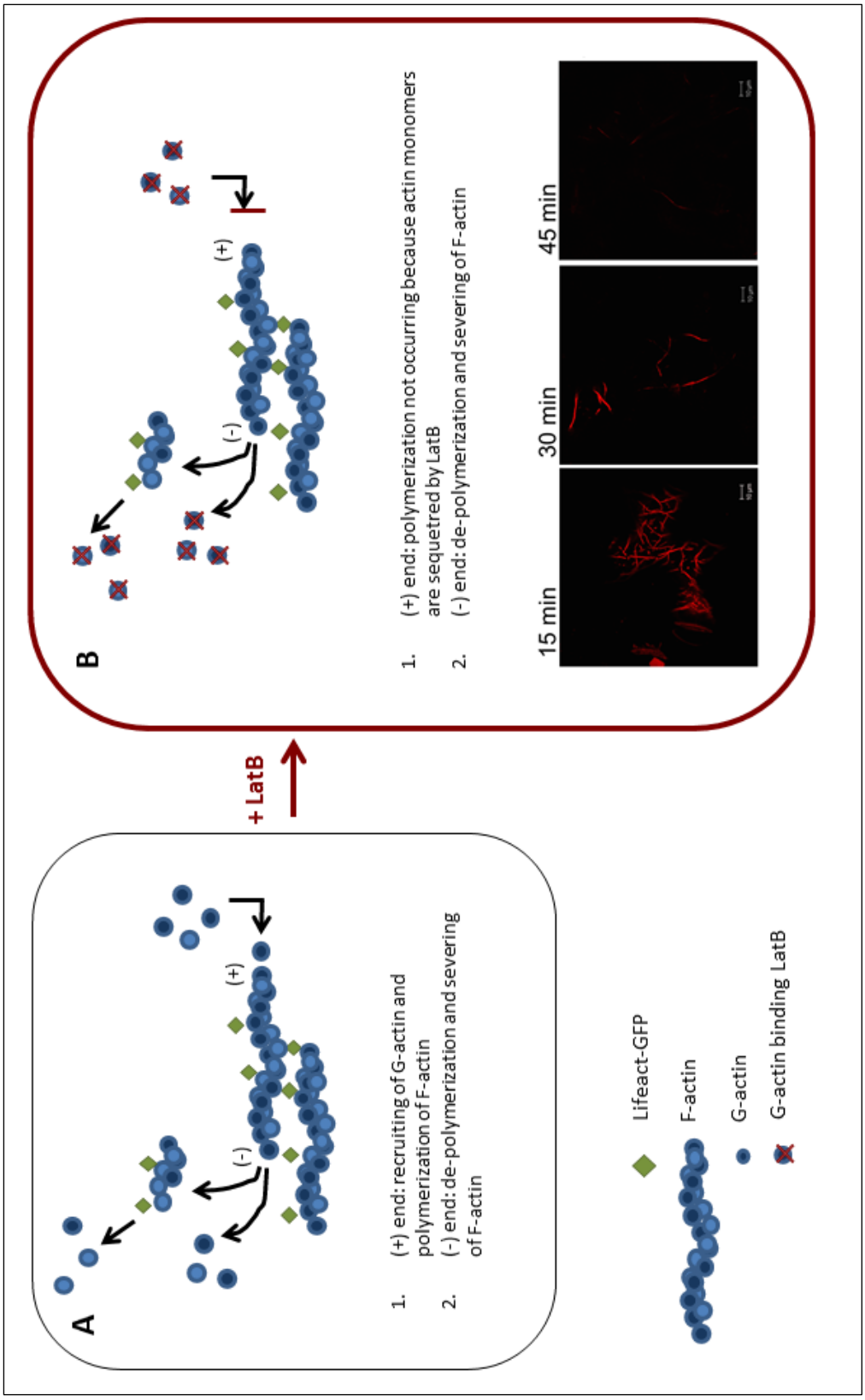
A
(+)
(-)
1. (+) end: recruiting of G-actin and polymerization of F-actin
2. (-) end: de-polymerization and severing of F-actin
+ LatB
B
(+)
(-)
1. (+) end: polymerization not occurring because actin monomers are sequetred by LatB
2. (-) end: de-polymerization and severing of F-actin
15 min
30 min
45 min
Lifeact-GFP
F-actin
G-actin
G-actin binding LatB

**Figure 37.**
**Possible mechanism of interaction between latrunculin B and actin filaments labelled with fluorescent marker.**

Latrunculin B (LatB) could bind to the actin monomers labelled with the fluorescent marker and either inactivates the fluorophore and the complex actin-fluorophore-latB remains in the cytoplasm or it is sent for degradation (**A**). Another option is that latB bind to the fluorescent marker, inactivate it and the complex fluorophone-latB either ramins cytoplasmic or is targeted for degradation (**B**).

**Figure 37.**

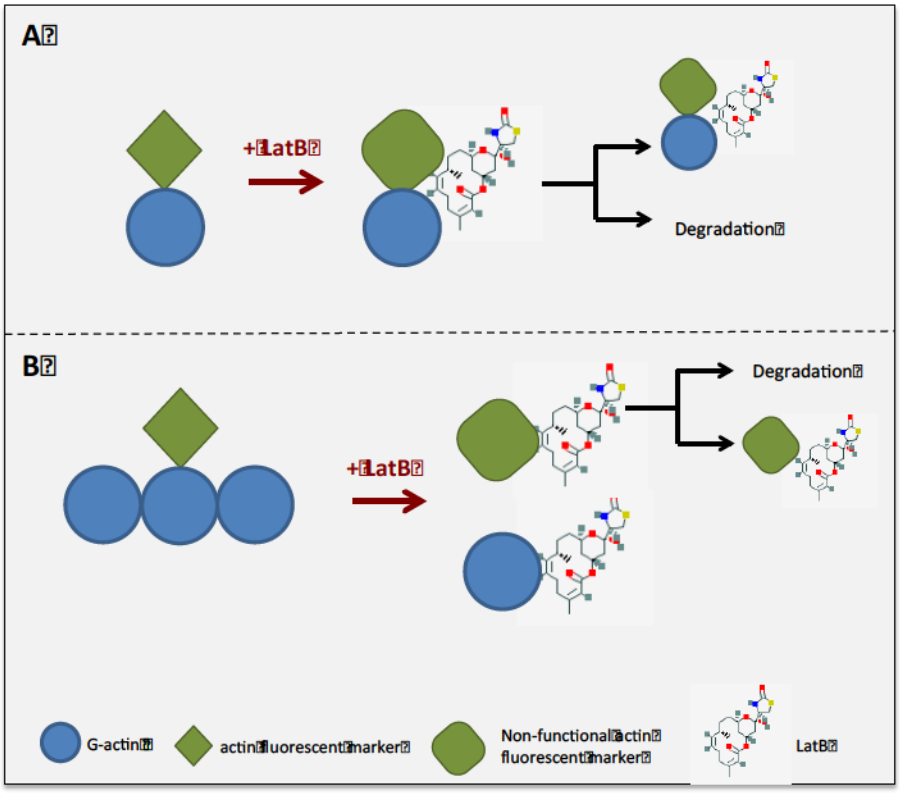
A
+LatB
Degradation
B
+LatB
Degradation
G-actin
actin fluorescent marker
Non-functional actin fluorescent marker
LatB

# 5. Micromanipulation of Golgi bodies with optical tweezers

## 5.1 Introduction

Plant Golgi bodies are dynamic organelles. Labelling of Golgi bodies with appropriate fluorescent marker proteins, revealed that, in plants they are dispersed and moving on the ER/cytoskeleton interface in the cortical cytoplasm (Boevink *et al*. 1998).

The motion of Golgi bodies is dependent on an intact actin-cytoskeleton: treatment with the actin depolymerizing agent cytochalasin D caused the Golgi bodies to stop moving and cluster in groups (See chapter 3) (Akkerman *et al*. 2011, Boevink *et al*. 1998). Further studies demonstrated that the molecular motor myosin is powering the movement and non-functional versions of these proteins arrest the movement of Golgi bodies (Griffing *et al*. 2014, Sparkes 2011a).

Optical tweezers are a promising tool because they permit manipulation and displacement of micron-size particles. Laser-based optical trapping was described for the first time by Ashkin (1970). In his work he used the pressure generated by a continuous and focused laser beam to trap and move micron-size neutral transparent particles in the air and liquid medium. Initially, the laser was used only on particles (Ashkin 1978) but soon was tested on living cells; from this point this technique

started to be referred as optical tweezer (Ashkin 1991). The optical trap used here was built on a TIRF microscope that provided a better resolution than confocal microscopy of subcellular components such as the actin filaments, especially fine and individual filaments (Blanchoin at al 2010). An infrared laser beam was tightly focused through a series of lens and generated a force of pico-Newton order, which can trap biological particles with optical density higher (or refractive index) than the surroundings (Neuman and Block 2004). The trapped object can be displaced in the XY plane in living cells without damaging the cell (Ashkin 1991). Some applications of the optical tweezer on biological samples are micromanipulation of the whole cells such as fungi (Wright *et al*. 2007), to study the dynamic activity of viruses (Arias-Gonzalez 2013) and probing components of the endomembrane system. In Sparkes *et al*. (2009) optical tweezers were used to trap fluorescent Golgi bodies under cytoskeleton depolymerizing conditions and revealed that there is a physical connection between the ER and Golgi bodies. Gao *et al*. (2016) used the optical tweezer to study the relation between chloroplasts and peroxisomes and quantify the tethering mechanism.

In this chapter, the optical trapping technique is used to investigate whether physical forces are acting between Golgi bodies and the cytoskeleton, and estimate the roles of microtubules and actin filaments in the dynamic behaviour of the organelle.

## 5.2 Results

Laser trapping of Golgi bodies was performed on tobacco leaf epidermal cells transiently expressing the Golgi marker ST-GFP, and in *A. thaliana* leaf epidermal cells of plants stably expressing ST-GFP.

At a first stage, fluorescent Golgi bodies were trapped and displaced from fluorescent actin filaments labelled with Lifeact-GFP in order to investigate the validity of the approach (Figure 38; movie 4). A Golgi body moving on an actin filament can be successfully removed from the filament and the actin filament bends and stretches to follow the trapped organelle (Figure 38, 00:003-00:008). Once the Golgi body is released from the trap, it continues to move (Figure 38, 00:15-00:19).

Subsequently, a 100 fluorescent Golgi Body test was performed, where a maximum of 100 Golgi bodies per sample per condition are trapped and classified according to two categories: 'trapped' (if captured and displaced by the laser) or 'not trapped' (if can not be trapped and displaced). For this experiment, cytoskeletal markers were not used because their expression proved to perturb Golgi dynamics (See Chapter 4). Samples were treated with oryzalin or latrunculin B to depolymerize the microtubules or actin filaments respectively. In tobacco leaves transientlu expressing the Golgi marker, the mean numbers of Golgi bodies trapped (expressed as percentage) was 58% in the untreated sample, 58% in the DMSO control, 74% when the leaf plant cells were treated with latrunculin B and 57% when treated with oryzalin (Figure 39A). In Arabidopsis plants, the mean numbers of Golgi bodies trapped in the untreated sample was 58%, in the DMSO control was 64%, in plants treated with the actin-

depolymerizing drug was 72%, and in sample treated with microtubule disrupting drug was 46% (Figure 39B).

The number of trapped Golgi bodies was analysed for the homogeneity of variance (F-test) and, according to this result, the appropriate t-test was performed. The results were plotted as relative mean of the control (either not treated or DMSO treatment) and the differences between the means were assessed with paired t-test equal variance or unequal variance, with the significance level set at 0.05.

In *N. tabacum* plants, the number of trapped Golgi bodies in untreated samples was compared to the treatment with DMSO (Figure 40). The comparison of the variances of the untreated sample and the one treated with DMSO assesses that their variances are unequal (Figure 40A) and the t-test for equal variances resulted that the differences recorded are not statistically different (p: 0.9). It can be therefore concluded that DMSO has no effect on trapping efficiency and can be used as a control to assess the effect of depolymerizing agents. The comparison of variances between the treatment with DMSO and latrunculin B indicated that they are equal and the increase in the number of trapped Golgi bodies (29%) is significant (p:0.039) (Figure 40B). The depolymerisation of microtubules resulted in a slight reduction (2%) in the number of trapped Golgi bodies and the t-test for equal variances proved that is not statistically significant (p: 0.89).

In *A. thaliana* stably expressing ST-GFP, the percentage of trapped Golgi bodies in the untreated sample was compared to the treatment with the DMSO solvent (Figure 41). An increase of 10%, compared to the control, was recorded and is not significantly different as assessed by a t-test with equal variances (p: 0.5)(Figure 41A). The DMSO measurement was used as control to

evaluate the effect of cytoskeleton disrupting drugs. Treatment with latrunculin B resulted in an increase of 16% in the number of trapped Golgi bodies, which is not significant as results from a t-test with equal variances (p: 0.2); when microtubules are absent, the number of trapped Golgi bodies was reduced by 28% compared to DMSO control and t-test with equal variances indicates that this is not significant (p:0.1) (Figure 41B).

## 5.3 Discussion

The manipulation of Golgi bodies in plant cells expressing the cytoskeletal marker Lifeact-GFP showed that a Golgi body can be displaced from an actin filament and when a Golgi body is pulled away from the filament, the strand would bend and stretch to follow the organelle, until it finally detaches (Figure 38, movie 4). This observation suggests that there are physical links between the motile organelle and the cytoskeleton, which keep the Golgi bodies on the actin tracks.

An additional aspect needs to be taken into consideration. Optical tweezers showed that the ER are Golgi bodies are closely associated; when Golgi bodies are displaced by optical tweezer manipulation, the ER remains attached to the Golgi and stretches to follow the organelle (Sparkes *et al*. 2009a). Additionally, the motility of Golgi bodies is dependent on an intact actin network and myosin XIK (Boevink *et al*. 1998, Avisar *et al*. 2008).

In another work, the persistency mapping technique was used and demonstrated that the remodelling of the ER depends on the actin-cytoskeleton: the overexpression of non-functional myosin XIK or treatment with actin-depolymerizing drug increase the presence of more persistent (non-rearranging) ER domains

(Sparkes *et al*. 2009b). This work confirmed previous observations that the endoplasmic reticulum, Golgi bodies and actin filaments are correlated (Boevink *et al*. 1998, Moreau *et al*. 2007); therefore the fact that the actin filaments follow the Golgi bodies could be also explained as a consequence of pulling the ER. When a Golgi body is trapped and displaced, the ER would remain attached and the actin filaments associated to it would follow.

To investigate if there is a link between the actin-cytoskeleton and Golgi bodies, the 100 Golgi bodies test was performed, and the number of trapped Golgi bodies would give information about the strength of the link between the cytoskeleton and the organelle.
Two model plants were tested (*N. tabacum* transiently expressing ST-GFP and *A. thaliana* stably expressing ST-GFP) to check if the variability between samples recorded in tobacco was due to the transient expression.
The comparison between DMSO and untreated samples demonstrated that the solvent had no impact on the number of trapped Golgi bodies. The results were the same across stable and transient lines, indicating that the data were reliable and the type of interaction between actin/microtubules and Golgi bodies was not influenced by the expression system.
As shown from the analysis of the Volocity data (See Chapter 3), the actin filaments play a major role in organelle dynamics, and from the trapping experiments a significant difference upon latrunculin B treatment was expected. The absence of actin filaments resulted in an increase (16-29%) of trapped Golgi bodies both in the stable and transient system (Figure 40), and this result is significant in tobacco and not significant in stable Arabidopsis plants. This difference in the significance level may be due to the different sample size: a total of 16 repetitions were performed for tobacco and 12 in Arabidopsis. The fact that there

is a same trend increase in the number of Golgi bodies trapped when actin filaments are disrupted indicates that actin filaments exert a force on Golgi bodies, which is released when the filaments are not present anymore.

It has to be taken into consideration the fact that, following the pharmacological treatment, Golgi bodies are not moving so it easier to get them in the trap. The experiment could be expanded by adding a control that is trapping non motile Golgi bodies in untreated cells. This would allow a comparison of the trapping rate of not motile Golgi bodies in cells where the actin-cytoskeleton is still intact and in cells where actin filaments are not present; given the same level of accessibility of Golgi bodies, the trapping would measure the role of the actin.

The treatment with oryzalin was expected to affect the trapping, but to a minor extent, given the partial contribution of microtubules to Golgi movement (Figure 41) (Crowell *et al*. 2009). The trapping in the absence of microtubules showed a minor but not significant decrease in the mean of trapped Golgi bodies (2-28%) compared to the DMSO control.

A non-significant result for the oryzalin treatment might reflect the limitation of optical trapping: the order of laser power that was used to trap the organelles could be too high for the interaction between actin/microtubules cytoskeleton and Golgi bodies. Thus that laser power setting cannot be used to collect quantitative data about microtubules and a calibration test should be run to establish the suitable order of power.

Furthermore, the trapping data were analysed using paired t-test at $P<0.05$. The t-test is a very basic statistical test: a more sensible and suitable test for the optical tweezers dataset will be considered to ascertain that the results were not due to an inappropriate statistical test.

From this set of experiments where I used optical tweezer, it can be hypothized that there is a connection between Golgi bodies, ER and actin cytoskeleton and that to estimate the forces actin on the organelle it is necessary to improve the settings of the optical trap.

**Figure 38.**

**Movie sequence showing optical trapping of a Golgi body in tobacco leaf epidermal cell.**

A Golgi body (red circle) is trapped and displaced from the actin filaments, labelled with Lifeact-GFP. The organelle can be displaced from the actin filaments (min 00:01 to 00:04), and in doing so the filaments bends. When the Golgi body separated form the filament (min 00:008), the trap is switched off and the Golgi body is released from the trap. After few seconds of pausing (00:08-00:15, not shown) the organelle starts to move again (00:15-00:19). See movie 4.

**Figure 38.**

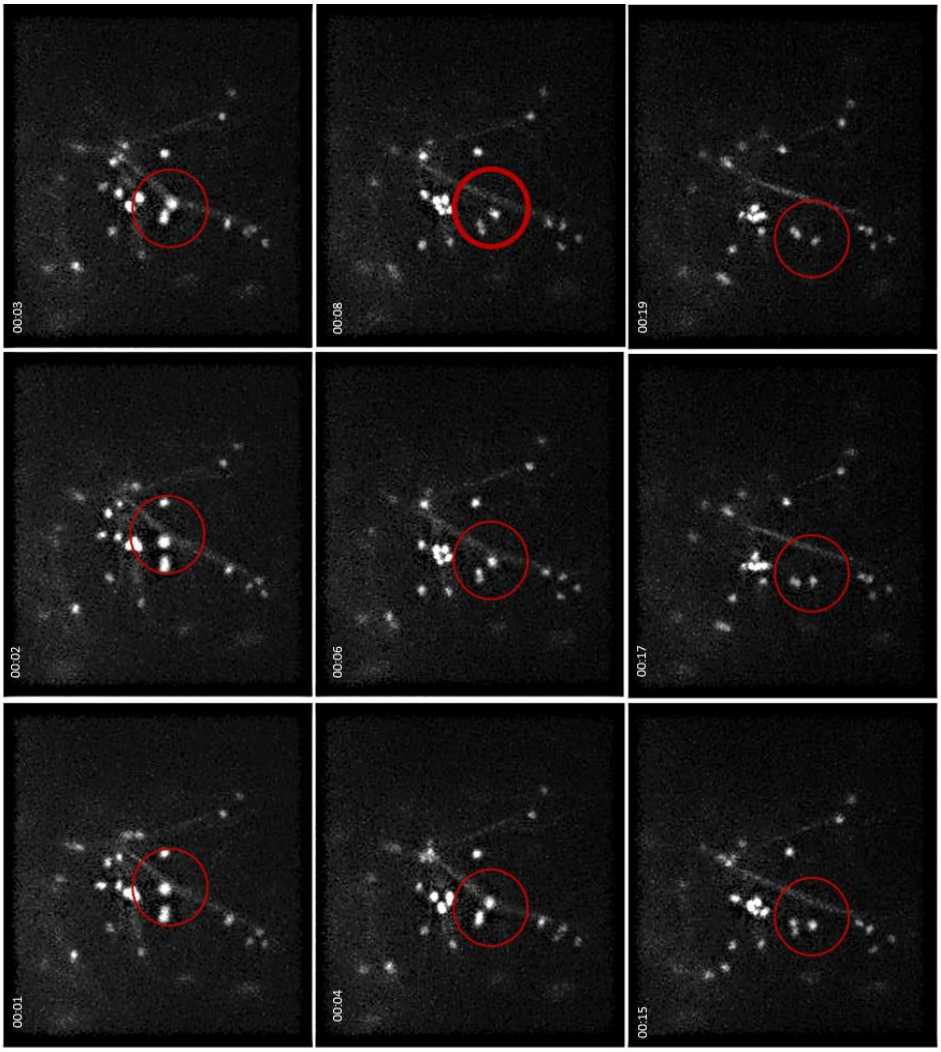

**Figure 39.**
**Percentage of trapped Golgi bodies in *N.tabacum* transiently expressing the Golgi marker and *A. thaliana* stably expressing ST-GFP and.**

**A.** Mean number of trapped Golgi bodies in tobacco expressed as percentage. Untreated sample 58%, DMSO 58%, latrunculin B 74%, oryzalin 57%.
**B**. Mean number of trapped Golgi bodies in Arabidopsis expressed as percentage. Untreated sample 58%, DMSO 64%, latrunculin B 72%, oryzalin 46%.

**Figure 39.**

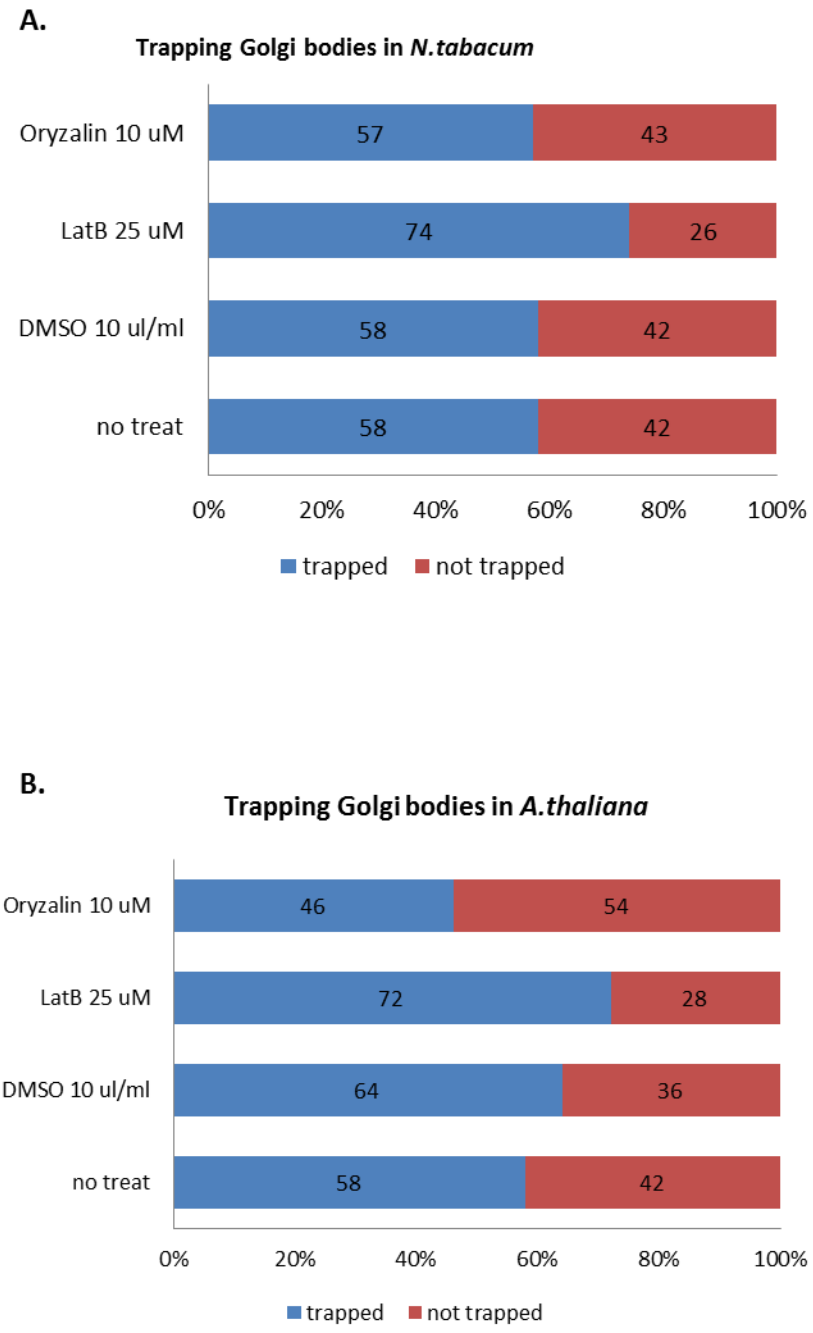
A.
Trapping Golgi bodies in N.tabacum
Oryzalin 10 uM
LatB 25 uM
DMSO 10 ul/ml
no treat
57
43
74
26
58
42
58
42
0%
20%
40%
60%
80%
100%
trapped
not trapped
B.
Trapping Golgi bodies in A.thaliana
Oryzalin 10 uM
LatB 25 uM
DMSO 10 ul/ml
no treat
46
54
72
28
64
36
58
42
0%
20%
40%
60%
80%
100%
trapped
not trapped

**Figure 40.**
**Relative mean (% of the control) of trapped Golgi bodies in *N. tabacum* transiently expressing ST-GFP.**

**A.** Treatment with DMSO resulted in a non-significant increase in respect to the control. The F-test assesses that variances are unequal.
**B.** Trapping values of samples treated with depolymerizing agents compared to DMSO. Depolymerisation of actin filaments (latrunculin B, 25 μM) resulted in a significant increase (29%, indicated as *) of trapped Golgi bodies. Treatment with oryzalin (10 μM) to depolymerize microtubules gave a not significant decrease of 2%. A paired t-test was performed at significance level <0.05. The F-test results that variances are equal.

**Figure 40.**

**A.**

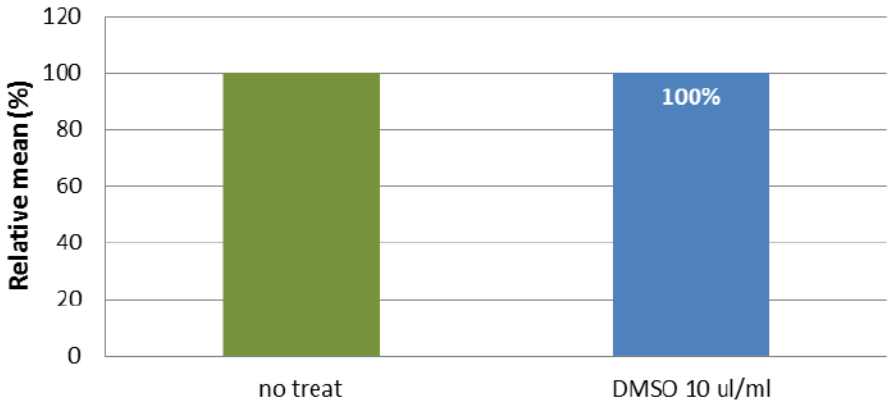


| | no treat | DMSO |
|---|---|---|
| Mean | 57.67 | 58.00 |
| Variance | 463.53 | 601.71 |
| Observations | 18.00 | 15.00 |
| df | 17.00 | 14.00 |
| F | 0.77 | |
| P(F<=f) one-tail | 0.30 | |
| F Critical one-tail | 0.43 | |

**B.**

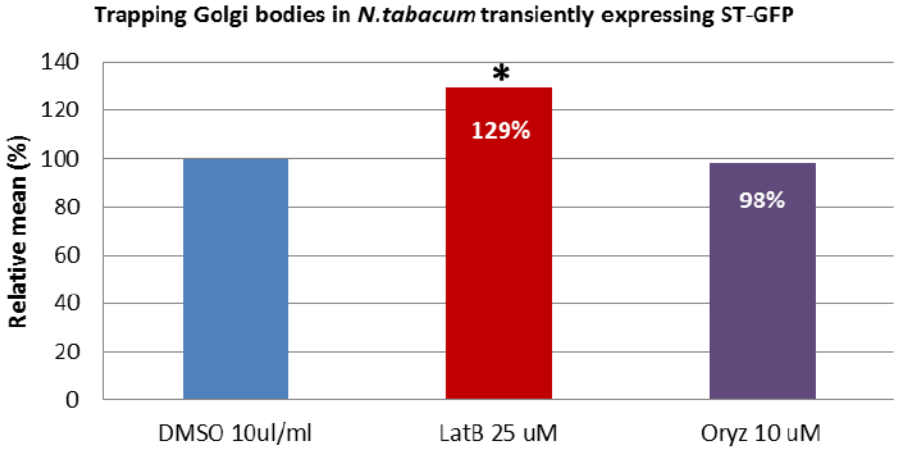


| | DMSO | Latrunculin B |
|---|---|---|
| Mean | 58.00 | 74.56 |
| Variance | 601.71 | 324.53 |
| Observations | 15.00 | 16.00 |
| df | 14.00 | 15.00 |
| F | 1.85 | |
| P(F<=f) one-tail | 0.12 | |
| F Critical one-tail | 2.42 | |

| | DMSO | Oryzalin |
|---|---|---|
| Mean | 58.00 | 56.73 |
| Variance | 601.71 | 518.02 |
| Observations | 15.00 | 11.00 |
| df | 14.00 | 10.00 |
| F | 1.16 | |
| P(F<=f) one-tail | 0.41 | |
| F Critical one-tail | 2.86 | |

**Figure 41.**
**Relative mean (% of the control) of trapped Golgi bodies in *A. thaliana* stably expressing ST-GFP.**

**A**. Treatment with DMSO resulted in a non-significant increase by 10% compared to the control as assessed by t-test unequal variances.
**B**. Percentage of trapped Golgi body in samples treated with depolymerizing agents compared to the control DMSO. The absence of actin filaments (Latrunculin B, 25 μM) determines a not significant increase (16%) of trapped Golgi bodies. Treatment with oryzalin (10 μM) to depolymerize microtubules resulted in a not significant decrease of 28%. Paired t-test equa variances was performed with significance level set at 0.05.

**Figure 41.**

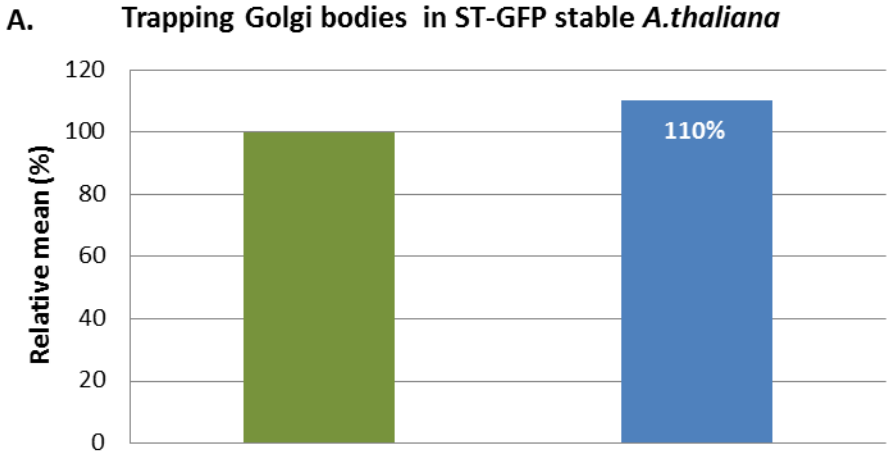


| | no treat | DMSO |
|---|---|---|
| Mean | 28.83 | 31.60 |
| Variance | 190.33 | 133.40 |
| Observations | 23.00 | 15.00 |
| df | 22.00 | 14.00 |
| F | 1.43 | |
| P(F<=f) one-tail | 0.25 | |
| F Critical one-tail | 2.37 | |

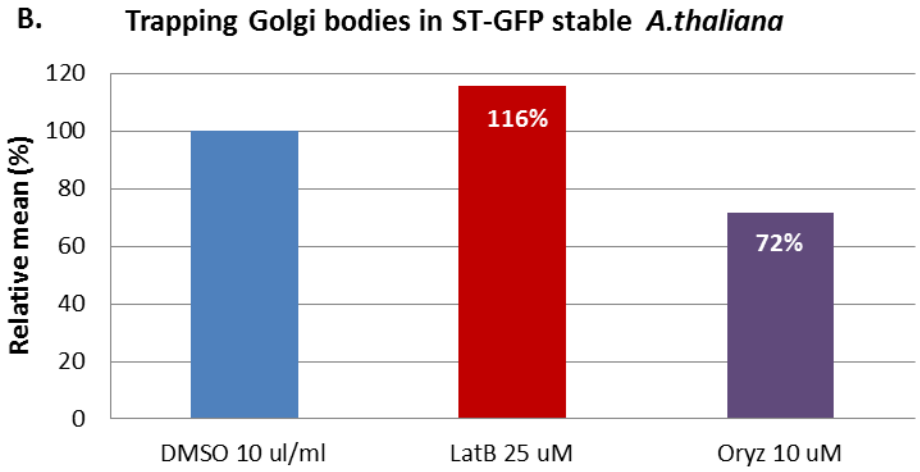


| | DMSO | Latrunculin B |
|---|---|---|
| Mean | 31.60 | 36.50 |
| Variance | 133.40 | 95.00 |
| Observations | 15.00 | 12.00 |
| df | 14.00 | 11.00 |
| F | 1.40 | |
| P(F<=f) one-tail | 0.29 | |
| F Critical one-tail | 2.74 | |

| | DMSO | Oryzalin |
|---|---|---|
| Mean | 31.60 | 23.00 |
| Variance | 133.40 | 40.40 |
| Observations | 15.00 | 6.00 |
| df | 14.00 | 5.00 |
| F | 3.30 | |
| P(F<=f) one-tail | 0.10 | |
| F Critical one-tail | 4.64 | |

# 6 A new model for actin filaments dynamics

## 6.1 Introduction

The visualization of the structure of the cytoskeleton, while maintaining the dynamics unaltered, is challenging both in plant and animal cells. Phalloidin staining is considered the closest to the real representation of the cytoskeleton and is used to compare the labelling efficiency of other *in vivo* fluorescent probes (Belin *et al*. 2014).

In animal cells, phalloidin does not pass readily through lipid bilayers and must be microinjected to image actin filaments in live cells. In addition, phalloidin binding stabilizes actin filaments, perturbing their normal dynamics. *In vivo* labelling with genetically encoded fluorescent markers such as Lifeact does not accurately reflect the structure of the actin-cytoskeleton (Chapter 4). Actin probes show preferential binding to certain classes of actin filaments over others. Lifeact-GFP, for example, is excluded from actin-rich membrane protrusions in the limb mesenchymal cells of chick embryos (Belin *et al*. 2014).

In plants, the phalloidin staining protocol requires fixation (Sonobe and Shibaoka 1989) and in live imaging it has been demonstrated that different probes can depict a very different organization of the actin network (Lemieux *et al*. 2013). It can be proposed that this may be due to a preferential binding to fine actin filaments rather than bundles, or because the marker is

derived from an actin-bundling protein, therefore causing the aggregation of actin filaments. Considering that the actin-cytoskeleton is a continuously arranging scaffold that provides tracks for movement and positioning of diverse organelles such as Golgi bodies and peroxisomes, a more reliable and less interfering fluorescent marker is needed for live imaging.

Studying the kinetics of these probes (in terms of binding and diffusion) can be helpful when choosing a marker for a specific study.

In Chapter 3 the fluorescent nanobody proved to be better than Lifeact-GFP in maintaining the dynamics of Golgi bodies but slowed their overall movement. Studying the kinetics of these two markers would provide further information about their interaction with the actin cytoskeleton and whether they can be used to study actin dynamics such as filament sliding.

FRAP (fluorescent recovery after photobleaching) is a technique that consists of bleaching the fluorophore through the use of a high intensity beam and monitoring the recovery over the time (Lemieux *et al*. 2013) and as such can be used to study actin filament dynamics.

The organelle transport in plants is dependent on the integrity of the actin cytoskeleton (Boevink *et al*. 1998) and is powered by motor proteins, myosins (Avisar *et al*. 2009). All myosins share a structural pattern: a highly conserved N-terminal motor domain, a neck region containing the 'IQ motif' and a C-terminal tail domain. The motor domain marches directionally on the actin arrays while hydrolyzing ATP and the tail domain can bind the cargo (Reddy 2001). The quaternary structure is also conserved: functional myosins assemble in dimers; dimers can be homodimers or heterodimers (Avisar *et al*. 2009, Lowey *et al*. 1991). In higher plants, the myosin class XI and VIII are involved in propelling the

movement of organelles such as Golgi bodies and peroxisomes (Sparkes 2010b). The role of myosins in organelle movement has been studied through the expression of non-functional versions of these proteins. Myosins lacking the head domain have been fused to fluorescent markers and the dimerization with the native myosin generates a non-processive dimer. The truncated myosins have been co-expressed along with organelle markers for Golgi, peroxisomes and mitochondria and the organelle dynamics analysed. Two members of XI class (XI-K and XI-E) reduce the velocity of Golgi bodies and peroxisomes, to a lesser extent compared to the treatment with the actin depolymerizing agent, and without perturbing the organization of actin network (Avisar *et al*. 2008, Sparkes *et al*. 2008).

The gene expression pattern shows that myosin XI-K is expressed throughout the plant while XI-E is tissue specific for pollen and stamen (Peremyslov *et al*. 2011), so XI-K is a good candidate to study the relationship between Golgi bodies and actin arrays in plant leaf tissue. The subcellular localization of myosins has been investigated. The tail domains of both XI class members were fused to a fluorescent reporter and various locations are reported. When transiently expressed in tobacco leaves, XI-K localizes in large or small puncta (Sparkes *et al*. 2008) or is diffuse in the cytosol. No co-localization with Golgi bodies or peroxisomes was found (Avisar *et al*. 2009). However, the expression of the XI-K tail perturbs the motility of Golgi, peroxisomes and mitochondria. It cannot be excluded that XI-K interacts with other myosins and participates in the organization of the cytoskeleton (Sparkes *et al*. 2008). Triple and quadruple mutants of Arabidopsis myosins XI (xi-1, xi-2, xi-i, xi-k) show a different ratio between cytoskeletal bundles and fine actin filaments (Cai *et al*. 2014, Peremyslov *et al*. 2010). In plants, the Golgi bodies and ER are physically connected (Sparkes *et al*. 2009) so the effect of the truncated myosin XI-K on

the ER geometry and remodelling has been studied. The expression of tail mutants increases the persistency of tubules and reduces active remodelling of the ER (Griffing *et al*. 2014).

The fact that myosin tails have not been detected on target organelles and the evidence that they can affect the organization of the cytoskeleton and the ER lead me to hypothise that if actin filaments could slide one on top of the other (and XI-K might mediate this mechanism); Golgi bodies could be anchored to the actin filaments and dragged by the filaments sliding rather than a direct interaction of Golgi with myosins.

The FRAP technique can be used to test this model: the actin cytoskeleton is marked with either the fluorescent nanobody or Lifeact and co-expressed with XIK tail; segments of actin arrays are photobleached and the pattern of recovery is followed and compared to the recovery in presence of the native myosin.

## 6.2 Results

Tobacco leaves transiently expressing Lifeact-GFP or GFP-actin-Cb (See Chapter 4) were used for photobleaching of actin filaments. The fluorescence recovery of bleached areas was then analysed and plotted in figure 42A and 42B, respectively. The recovery of bleached cells expressing Lifeact-GFP (Figure 42A) ranges from ~50% to ~90%, while the recovery of bleached cells labelled with fluorescent nanobody (Figure 42B) was between ~20% and ~90%.

The fitting of FRAP data permits evaluation of the general tendency of the recovery and the profiles of FRAP curves allows a comparison of the fluorescent recovery of the two cytoskeletal markers.

The normalised and fitted curves of the two cytoskeletal markers were compared in Figure 43A and the figures of the normalized fluorescent intensity and the half-time are reported in the table 43B. The recovery of Lifeact-GFP was 72.95% and of GFP-actin-Cb was 53.26%. The recovery half-time was 0.76 sec and 0.34 sec for Lifeact-GFP and the fluorescent nanobody respectively. From the half-times, the recovery rates of fluorescence per second were extrapolated (R); R of Lifeact-GFP was 48% $sec^{-1}$ while the R of GFP-actin-Cb was 73% $sec^{-1}$.

To understand if the differences observed in the maximum recovery of the fluorescence and the half-times were significant, the mean values of both parameters were calculated and unpaired t-test equal variances performed (Figure 43 and 44, respectively). The mean fluorescent intensity recovery (MFIR) of Lifeact-GFP was 73.1 ± 12.7% and the MFIR of GFP-actin-Cb was 53.6 ± 16.6% (Figure 44A and 44B).

The mean half-time recovery of bleached Lifeact-GFP was 0.77 ± 0.25 sec and the mean half-time recovery of the fluorescent nanobody was 0.47 ± 0.2 sec (Figure 45A and 45B). The recovery of the markers and half-times of the cytoskeletal markers were statistically different as shown in the tables of figure 44B and 45B.

The cytoskeletal markers (Lifeact-GFP and GFP-actin-Cb) were transiently co-expressed with the tail domain of the myosin XIK fused to RFP (RFP-XIK tail) according to Sparkes *et al*. (2009) upon the expression of XIK tail, the mutant could either compete or combine with the native protein and form inactive truncated dimers (Sparkes 2010a). Some fluorescent signal is detected in the red channel but it is due to cross-talking between the green channel and red channel; indeed the fluorescence visible in the red channel corresponds to the saturated signal of GFP. The fluorescent signal of RFP-XIK tail was not detected in either of the

combinations with the cytoskeletal probes (Figure 46a and b). To exclude that this is because the labelling of the cytoskeleton interferes with the expression or localization of RFP-XIK tail, the latter was co-expressed with the Golgi bodies marker ST-GFP (Figure 46c) and also in this case, the fluorescent signal of the truncated myosin was not detected.
To assess if the RFP-XIK tail was expressed and exerting the inhibiting function, the dynamics of Golgi bodies were observed when the truncated myosin was co-expressed. The lack of movement of Golgi bodies indicates that the non-functional protein was expressed in the cells; this can be appreciated from the time lapse images plate in figure 47A and from the time lapse color-coded image, where a colour is assigned to each frame and the frames superimposed (Figure 47B). In the control where only the native form of the myosin is present (Figure 48A and 48B), Golgi bodies maintain their characteristic motility in the cell cortex as described in Nebenführ *et al*. (1999).

Segments of actin filaments transiently labelled with either Lifeact-GFP or GFP-actin-Cb were quenched and the time-lapse images of the fluorescence recovery were inspected in order to evaluate if there was any change in the localization of the bleached areas (Figure 49 and 51, respectively). The quenched segment remains in the same position where the bleaching event occurred. The same observation was made when the RFP-XIK tail was expressed. The presence of the non-processive myosin did not change the position of the bleached areas when co-expressed to either Lifect-GFP (Figure 50) or GFP-actin-Cb (Figure 52).

A further analysis of the bleached ROI was carried out to evaluate the pattern of the recovery of the fluorescence. From the inspection of the bleached areas (Figure 53) no differences in the

pattern of the probe recovery when were co-expressed with the truncated myosin or the cytoskeletal markers solely was observed.

The numerical figures of the fluorescence recovery after photobleaching were recorded in presence of RFP-XIK tail and were normalized, fitted and compared to assess if the truncated myosin had any effect on the marker fluorescence recovery (See section 2.10.1).

When Lifeact-GFP solely was expressed, the FRAP range was 50-90% while when the RFP-XIK tail was co-expressed, the recovery values range between 20% and 95% (Figure 54A and 54B, respectively).

When the fitted curves were compared, the maximum recovery of Lifeact-GFP could be seen to be 72.95% with half-time of 0.76 sec; the recovery rate per second was extrapolated and was 48%$sec^{-1}$.

When co-expressed with the non-functional motor protein, the maximum recovery was 64.43%, t ½ 0.53 sec and the recovery of the fluorescence was 61% $sec^{-1}$ (Figure 55A and 55B).

The mean of the Lifeact-GFP fluorescence recovery was 73±13% (Figure 56A) and when the mutated truncated motor protein was expressed, the mean fluorescence intensity recovery (MFIR) was 65±19%; unpaired t-test unequal variances results show that the differences between MFIR were not significant (Figure 56B). The mean half-time of Lifeact-GFP was 0.77±0.2 sec and, when the non-functional myosin was co-expressed, the half-time was 0.6±0.2 sec; the unpaired t-test equal variances assess that the mean values of the half-time recovery are statistically different (Figure 57A and 57B).

The same analysis was performed for the fluorescent nanobody. When only GFP-actin-Cb was expressed, the range of FRAP

recovery is 20-90%, and with the co-expression of the mutated motor protein the range become wider (20-98%) (Figure 58A and 58B, respectively).

When the fitted data are compared (Figure 59A), the maximum recovery of GFP-actin-Cb was 53.26%, with half-time of 0.34 sec and recovery rate was 73% $sec^{-1}$. When the truncated myosin was expressed with GFP-actin-Cb, the maximum recovery was 52%, $t^{1/2}$ 0.42 sec, and R was 62% $sec^{-1}$. The fluorescent recovery percentage and the half-time were then compared to assess if the differences are statistically different (59B).

The mean fluorescence recovery of GFP-actin-Cb was 53.6±16.6% and upon the co-expression with RFP-XIK tail was 61±24.2% (Figure 60A). The unpaired t-test unequal variances showed that the presence of the non-functional myosin had no effect on the recovery of the quenched fluorescent protein (Figure 60B). The mean half-times of recovery were compared and tested. The mean half-time of GFP-actin-Cb solely was 0.47±0.25 sec and when co-expressed with the tail domain of XIK was 0.74±0.4 sec (Figure 61A); from an unpaired with t-test unequal variances it could be concluded that the mutated myosin has a significant impact on the half-time recovery of the nanobody (Figure 61B).

## 6.3 Discussion

The normalised fluorescence recovery curves represent the fraction of mobile molecules that move into the bleached area, thus provide information about the mobility of the fluorescent probes. In this study, the molecules investigated were two markers binding to the actin cytoskeleton. From the tracking analysis (See Chapter 3) the two cytoskeletal labels demonstrated

to affect the motility of Golgi bodies to different extents; the profiles of the recovery gave additional detail about the mechanism of interaction between the fluorescent markers and the actin cytoskeleton.
Additionally, a new model was proposed and tested, where the myosin XIK anchors Golgi bodies to actin filaments sliding one on top of the other. The sliding of actin filaments would drag the Golgi bodies along. When the non-functional myosin was expressed, the movement of the Golgi stack would cease because actin filaments are not able to slide anymore.
A combination of FRAP and image analysis techniques were used to evaluate this model.

In Figure 42A and 42B all the experimental FRAP curves of Lifeact-GFP and GFP-actin-Cb are reported.
The range of the recovery curves of the fluorescent nanobody was larger than that of Lifeact-GFP (20-90% vs 50-90%, respectively), and this could reflect that the nanobody had a higher variability in mobility compared to Lifeact-GFP. The mobility could depend on several factors: the freedom of diffusion, the strength of interaction between the fluorescent marker and the target region (Matsuda and Nagai 2014) or the sliding of actin filaments. For Lifeact-GFP and GFP-actin-Cb it is assumed that the probes are diffusing freely in the cytoplasm and subject only to cytoplasmic streaming, the interaction between the fluorescent proteins and the actin (filaments or monomers) represents the major limitation to their movement.
The target binding site (antigenic site) of the nanobody on the actin filaments is not known; it can be speculated that the nanobody binds either to a specific target recurring in a constant amino acid region but the accessibility depends on the polymerization of the actin, or that a same target occurs multiple

times in the sequence and is found in different protein domains (Figure 62). If the latter option were considered, a different amino acid surrounding and domain folding would make the target site more or less accessible. In both cases, more accessible sites would interact stronger and more stably with the nanobody, while less accessible site would interact weakly and less stably with the cytoskeletal marker. This scenario would result in a population of molecules with variable apparent mobility properties (Figure 62).
Lifeact is a short peptide sequence deriving from the actin-binding peptide of an actin crossbundling factor (Riedl *et al*. 2008). It can be proposed that the binding between Lifeact and actin filaments is specific and physiological and therefore it is subject to constant binding conditions that would explain a smaller variability in the fluorescence recovery compared to GFP-actin-Cb (Figure 42).

The values of the maximum fluorescent recovery, which correspond to the plateau segment of the FRAP curves provide information about the mobility of the fluorescent molecules.
The fact that the signal of Lifeact-GFP recovers more than the nanobody (Figure 43) may indicate that a larger number of fluorescent Lifeact molecules release/bind to actin filaments; this can be also interpreted as Lifeact-GFP is more motile than the nanobody. The lower recovery of GFP-actin-Cb indicates that nanobody interacts longer with the actin target. It can be assumed that the cytoskeletal markers diffuse in the cytoplasm without any constriction, therefore the binding to actin filaments would represent the limiting step in the recovery of the fluorescence.
The recovery rate (R) would then represent how quickly the fluorescent proteins bind to the target as well as potential sliding of actin filaments. Lifeact-GFP interacts more slowly with the actin fibers while GFP-actin-Cb more quickly (48% $sec^{-1}$ vs 73% $sec^{-1}$, Figure 43); these results suggest that the former fluorescent

proteins take more time to release/bind the actin target respect to the latter.

Lifeact is the actin binding domain of the yeast protein ABP140, a methyltransferase that acts on tRNA (Noma *et al*. 2011). The actin binding domain of ABP140 maintains cross-bundling activity of actin fibers (Asakura *et al*. 1998). In animal cells, Lifeact-GFP is used to study actin dynamics (Riedl *et al*. 2008) and does not interfere with cellular processes. The expression of Lifeact-GFP in plants was shown to affect the dynamics of the cytoskeleton and induced the formation of bundles (van der Honing *et al*. 2010).

This observation is corroborated by the tracking data of Golgi stacks; the movement of Golgi bodies mainly relies on actin filament integrity (See Chaper 3, Figure 15, Figure 18, Figure 21) and the expression of Lifeact-GFP determines a change in the dynamic pattern of the organelles (See Chaper 4, Figure 29). It can be speculated the expression of such cytoskeletal marker induces rearrangement and aggregations of the actin fibers, which affect the movement of Golgi bodies. When the probe is expressed, Golgi bodies assume a more directional and slower dynamic, and this observation correlates to the prevalence of bundled actin.

The combination of tracking data and FRAP of Lifeact-GFP permits a better understanding of the kinetics of this probe. The high percentage of fluorescent recovery indicates that Lifeact-GFP molecules associated with the actin filaments are mobile but the association/dissociation rate is slow because of the cross-bundling activity; Lifeact-GFP would bind to multiple sites and this process would require a longer time (Figure 63). The result of the cross-bundling properties is that Golgi bodies assume a more directional movement.

In the literature, the characterization of the nanobody target is not available, however from the general mechanism of antibody binding, they are highly specific and have high affinity for the

target sequence (Arevalo *et al*. 1993) and are not expected to rapidly turn over on the actin filaments. As shown by the results of the recovery rate per second, the interaction between the nanobody and target is quicker and it can be proposed that this is because of a one-to-one interaction.

The findings from FRAP and the tracking analysis of Golgi bodies when the nanobody is expressed, allow us to generate a model describing the interaction of the antibody with actin filaments and the effect on the organelle dynamics. GFP-actin-Cb quickly recognizes the sequence on actin filaments and binds stably to them. The presence of the nanobody on actin filaments would not interfere with the actin organization, and act as steric hindrance to the fast displacement of Golgi bodies. The nanobody would reduce the overall movement of Golgi bodies whilst maintaining the features of the dynamics (See Chapter 4, Figure 29).

In Arabidopsis, myosin XIK is involved in maintaining the movement of Golgi bodies but fluorescent versions of this motor protein do not locate on the stacks. The sliding of actin filaments over other filaments is part of the buckling process (Staiger *et al*. 2009) and it has not yet been defined if the process is mediated by proteins or not.

The transient co-expression of the actin probes and the RFP-XIK tail showed that the signal of the lattter is not detected (Figure 46). This is in accordance with what is already published, that the fluorescent signal of the truncated myosin is dispersed in the cytoplasm or shows as blobs or in few cases is not detected (Sparkes 2010b).

The fluorescent tail domain of XIK was co-infiltrated with the Golgi body marker ST-GFP in order to test if the truncated myosin is present and exerting the inhibiting effect in the transformed cells. Time-frame images shows that the truncated myosin

perturbs the dynamics of Golgi bodies in all the cells of the examined area (Figure 47B). In the controls (ST-GFP alone) the native form of the myosin triggers the movement of the organelles so the lack of motility observed in the co-expression conditions is related to the expression of XIK-tail and not to the physiological state of the plant (Figure 48B). From the high transformation rate observed, it can be assumed that RFP-XIK tail is equally and efficiently co-expressed as the cytoskeletal markers Lifeact-GFP and GFP-actin-Cb. A more reliable approach could be using KO lines for XI myosins to ensure that all the cells of the plant will not express the myosin and stop the motility of Golgi bodies (Peremyslov *et al*. 2010, Ojangu *et al*. 2012).

To test the hypothesis that if XIK has a role in maintain the sliding of actin filaments and the Golgi bodies are dragged along with these, a close observation of time-lapse images following the photo-bleaching of actin arrays was performed. Indeed, if this model is valid, bleached areas are expected to shift in the control and to remain in the same localization when the tail of XIK is expressed. When the native XIK is present, the bleached areas of either cytoskeletal probes do not shift but maintain the same position (Figure 49 and 51); the same is observed when the tail domain of XIK is overexpressed (Figure 50 and 52) indicating that there is no sliding of actin filaments.

A closer observation of the bleached area was carried out in order to evaluate if there was a pattern of the recovery of the probes. If the filaments are sliding over one another, the recovery of the probe would be expected to appear from the periphery of the bleached area towards the center. When the truncated myosin is expressed, the fluorescence is expected to appear homogeneous because the filaments are not able to slide anymore. Unfortunately the analysis of enlarged time-series images (Figure 53) did not provide any additional information about the recovery pattern.

A higher image resolution, faster imaging acquisition and bigger ROI followed by image analysis, such as a kymograph or measurement of the fluorescence recovery localization over the time, could provide further details on this result. Also better resolution of the single actin filaments may be achieved with TIRF microscopy (total internal refraction fluorescence) (Blanchoin *et al*. 2010). Another option could be using photo-switchable markers, such as EOS (Mathur *et al*. 2010), which would allow following the activated dynamics of the ROI for a longer time.

It can be concluded that from this settings of the experiment, XIK does not seem to be involved in the sliding of actin filaments. Further investigations were carried to evaluate if the truncated myosin has an effect on the recovery pattern of the fluorescent cytoskeletal markers.

The combination of RFP-XIK tail with Lifeact-GFP shows recovery values below 50%, suggesting that the fluorescent marker has reduced motility (Figure 54). GFP-actin-Cb has a high variability in the recovery values and, upon the expression of the truncated motor protein the range is slightly higher indicating that part of the fluorescent nanobody is more mobile (Figure 58).

XIK has an effect on each marker, which is difficult to define from these data. The overall effect of the co-expression of RFP-XIK tail to either cytoskeletal markers is widening the range of the fluorescence recovery values, indicating that the dynamics of fluorescent probes become more variable (Figure 54 and 58). Transient expression techniques do not ensure that all the cells have the same expression level of the truncated protein; Arabidopsis knock-out lines in XIK could be used instead to avoid cell-to-cell protein expression variation (Peremyslov *et al*. 2008). It can therefore be proposed that XIK is participating to the organization of the actin filaments, and the expression of the mutant would loosen the actin fibers and make them less dynamic

so that the probes are more free to bind and release their targets. Higher magnification microscopy can be used to obtain a higher resolution of actin filaments and study the pattern of recovery in the bleached areas.

This could be also because the expression of RFP-XIK is variable from cell to cell, therefore its effect.

The global values of the FRAP fitted curves provide information about the trend in the fluorescence and the recovery half-time. The expression of RFP-XIK tail determines a reduction of the fluorescence recovery of Lifeact-GFP and GFP-actin-Cb, but in both cases this is not significant. This means that the cytoskeletal probes can access to the binding sites to the same extent as in the control where the native form of the myosin is present. A significant difference is instead recorded in the half-times of recovery and R values of both markers compared to the relative control. Presence of RFP-XIK tail results in a quicker recovery of Lifeact-GFP (Figure 57 and 59), while the recovery of the nanobody is slower (Figure 60 and 61). This would be in accordance with what was observed for the recovery rate of Lifeact-GFP, which XIK would loosen the cross-bundling of actin filaments and the biding of the probe is weaker and the binding/release is quicker. Such a model is also supported by Cai *et al*. (2014) and Peremyslov *et al*. (2010), where it is observed that triple and quadruple mutants of Arabidopsis myosins XI (xi-1, xi-2, xi-i, xi-k) determines rearrangement of the cytoskeleton.

If the filament-filament sliding model is valid, no significant differences in the half-time recovery of the nanobody should be recorded. Indeed, according to the results obtained in Chapter 4 and Figure 30**,** the nanobody does not have cross-bundling properties therefore it is not expected to alter the actin-cytoskeleton organization and at the same time, the binding

properties of the nanobody shouldn't be affected by the bundling level of actin filaments.

The half-time value of GFP-actin-Cb shows a significant increase of the recovery time indicating that the expression of XIK tail has a stabilizing effect on binding/release of the nano-probe from the actin target. These last results do not support the model of filaments sliding, but further experiments could be carried to test this hypothesis. Improvements to the experimental settings can be implemented in order to assess wheter the obtained results are not due to experimental limitations. Transient expression techniques do not ensure that all the cells have the same expression level of the truncated protein; Arabidopsis knock-out lines in XIK could be used instead to avoid cell-to-cell protein expression variation (Peremyslov *et al*. 2008). Super resolution microscopy would allow obtaining a higher resolution of the single filaments and the bleaching of larger areas would allow analysing the pattern of the fluorescent recovery of several filaments at the same time.

**Figure 42.**

**Normalised curves of the fluorescence recovery after photobleaching of Lifeact-GFP and GFP-actin-Cb.**

Diagrams showing the fluorescence recovery after photobleaching of Lifeact-GFP (**A**) and GFP-actin-Cb (**B**) up to 20 seconds after photobleaching. The profile of 27 photobleached areas are reported and the range of the fluorescence recovery is between 50 and 90% for Lifeact-GFP, while 26 photobleached areas are used for GFP-actin-Cb and the recovery range is 20-90%.

**Figure 42.**

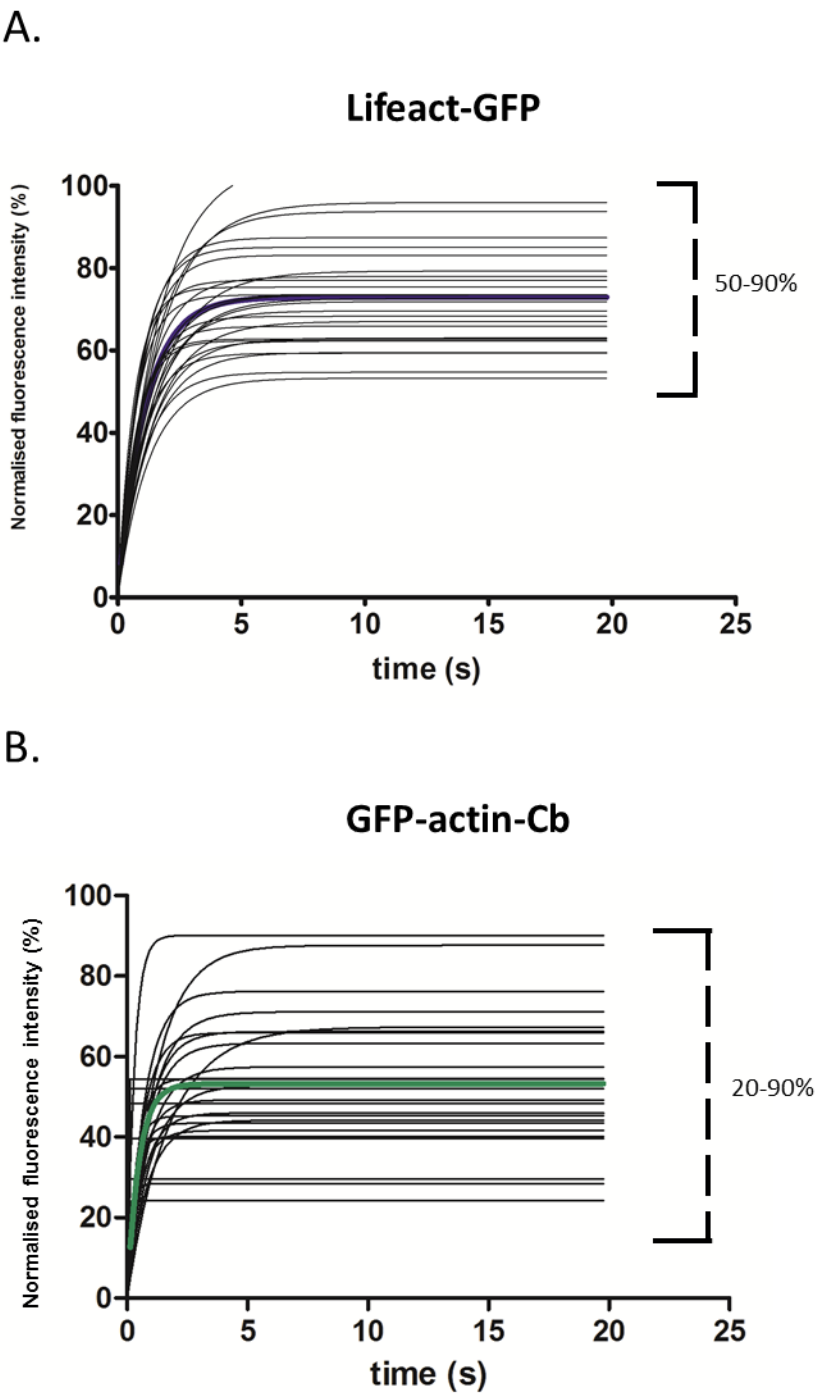
A.
Lifeact-GFP
Normalised fluorescence intensity (%)
100
80
60
40
20
0
0
5
10
15
20
25
time (s)
50-90%
B.
GFP-actin-Cb
Normalised fluorescence intensity (%)
100
80
60
40
20
0
0
5
10
15
20
25
time (s)
20-90%

**Figure 43**.
**Profiles of fitted FRAP curves Lifeact-GFP and GFP-actin-Cb.**

The fitted FRAP curves of Lifeact-GFP (blue line) and GFP-actin-Cb (green line) are compared (**A**). The % of the max fluorescence recovery, half-times (t ½) and recovery rate (R) are reported in the table **B**.
Lifeact-GFP max recovery percentage is 72.95%, half-time is 0.76 sec and R is 48% $sec^{-1.}$ GFP-actin-Cb max recovery percentage is 53.26%, t ½ is 0.34 and R is 73% $sec^{-1}$.

**Figure 43.**

A.

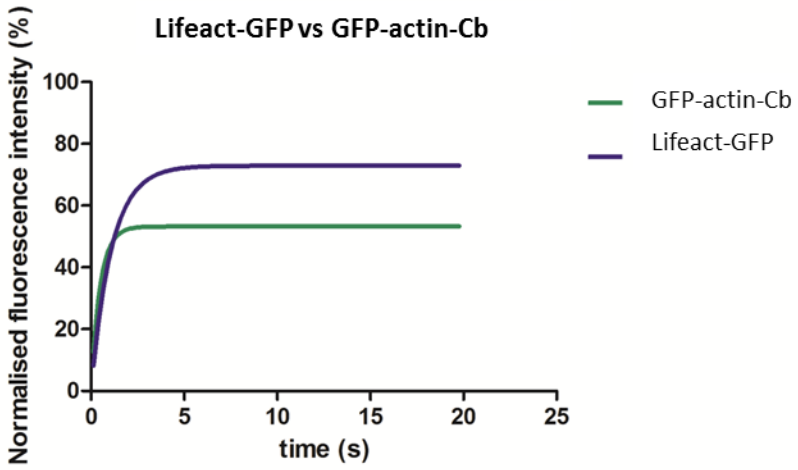


B.

| | Fluor. Recovery | t ½ | R |
|---|---|---|---|
| Lifeact-GFP | 72.95 % | 0.76 sec | 48% $sec^{-1}$ |
| GFP-actin-Cb | 53.26 % | 0.34 sec | 73% $sec^{-1}$ |

**Figure 44.**
**Bar-chart of the mean fluorescence intensity recovery of Lifeact-GFP and GFP-actin-Cb.**

**A**: the mean fluorescence intensity recovery (MFIR) after photobleaching of Lifeact-GFP (blue bar) and GFP-actin-Cb (green bar) are plotted; the bar lines represent the standard deviation (SD).
**B**: The figures of mean and SD are reported. The differences in the mean are statistically significant (p: 0.00005, indicated as ****) as assessed by the unpaired t-test equal variances (significance level < 0.05).

**Figure 44.**

A.

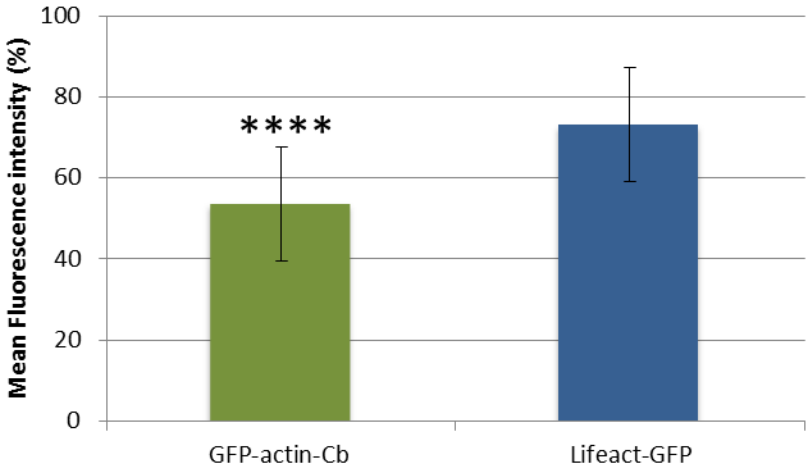


B.

| | MFIR (%) | SD |
|---|---|---|
| Lifeact-GFP | 73.1 | ± 12.7 |
| GFP-actin-Cb | 53.6 | ± 16.6 |
| Significance (p<0.005) | 0.00005 | |

**Figure 45.**
**Bar-chart of the mean half-time recovery of Lifeact-GFP and GFP-actin-Cb fluorescence after photobleaching.**

Half-times mean values of Lifeact-GFP (blue bar) and GFP-actin-Cb (green bar) are plotted; the bar lines represent the standard deviation (SD)(**3A**).
The figures of means and SD are reported in the table **3B**. The differences observed in the means are statistically significant (p: 0.00001, indicated as ****) as assessed by the unpaired t-test equal variances (significance level < 0.05).

**Figure 45.**

A.

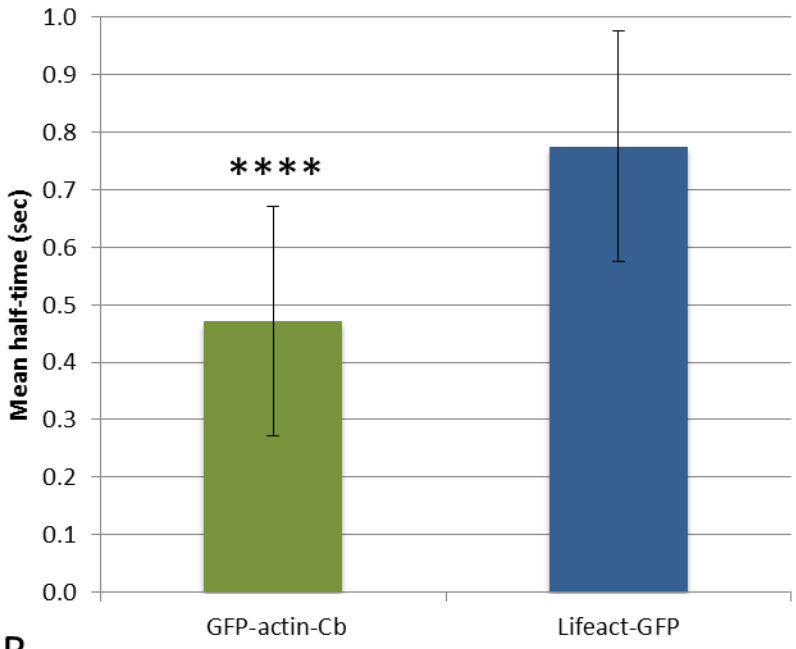


B.

| | Mean $t^{½}$ (sec) | SD |
|---|---|---|
| Lifeact-GFP | 0.77 | ± 0.25 sec |
| GFP-actin-Cb | 0.47 | ± 0.2 sec |
| Significance ($p<0.005$) | 0.00001 | |

**Figure 46.**
**Transient co-expression Lifeact-GFP, GFP-actin-Cb, ST-GFP to RFP-XIK tail in tobacco leaves.**

**a)** Lifeact-GFP decorates actin filaments. The signal detected in the red channel (middle column) is due to a channel cross-talking and not RFP-XIK tail; scale bar 5 μm.

**b)** GFP-actin-Cb binds actin filaments, The signal detected in the red channel (middle column) is due to a channel cross-talking and not RFP-XIK tail; scale bar 5 μm.

**c)** Golgi bodies labelled with ST-GFP. The signal detected in the red channel (middle column) is due to a channel cross-talking and not RFP-XIK tail; scale bar 20 μm.
The expression of RFP-XIK was not detected in any experiment and pictures were not taken because there was no signal.
The signal detected in the red channel, that is the RFP-XIK column, is GFP fluorescence leaking into the RFP detection channel.

**Figure 46.**

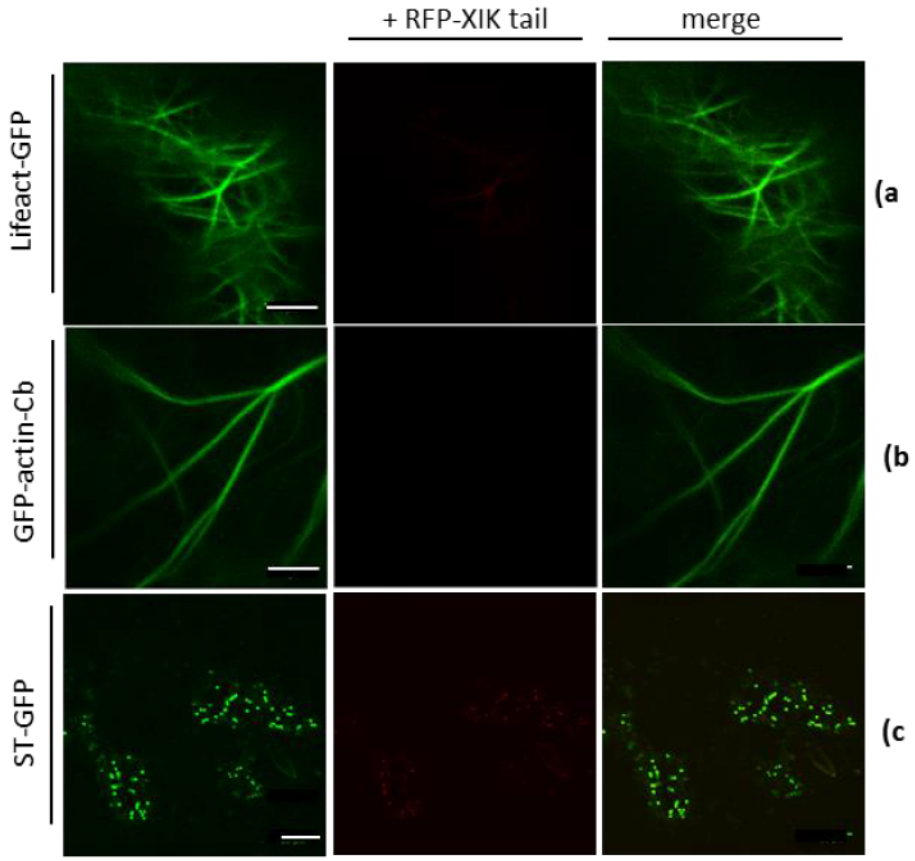

**Figure 47.**
**Time-frame images of tobacco leaf cells co-expressing ST-GFP and RFP-XIK tail.**

**A**: Representative time-lapse images of Golgi bodies movement, inhibited by the expression of the non-functional myosin. The arrow indicates the localization of a Golgi body over the time; time interval 5 sec.
**B**: Time-lapse colour coder image; a colour assigned to each frame of the movie the frames merged. Scale bar 10 μm.

**Figure 47.**

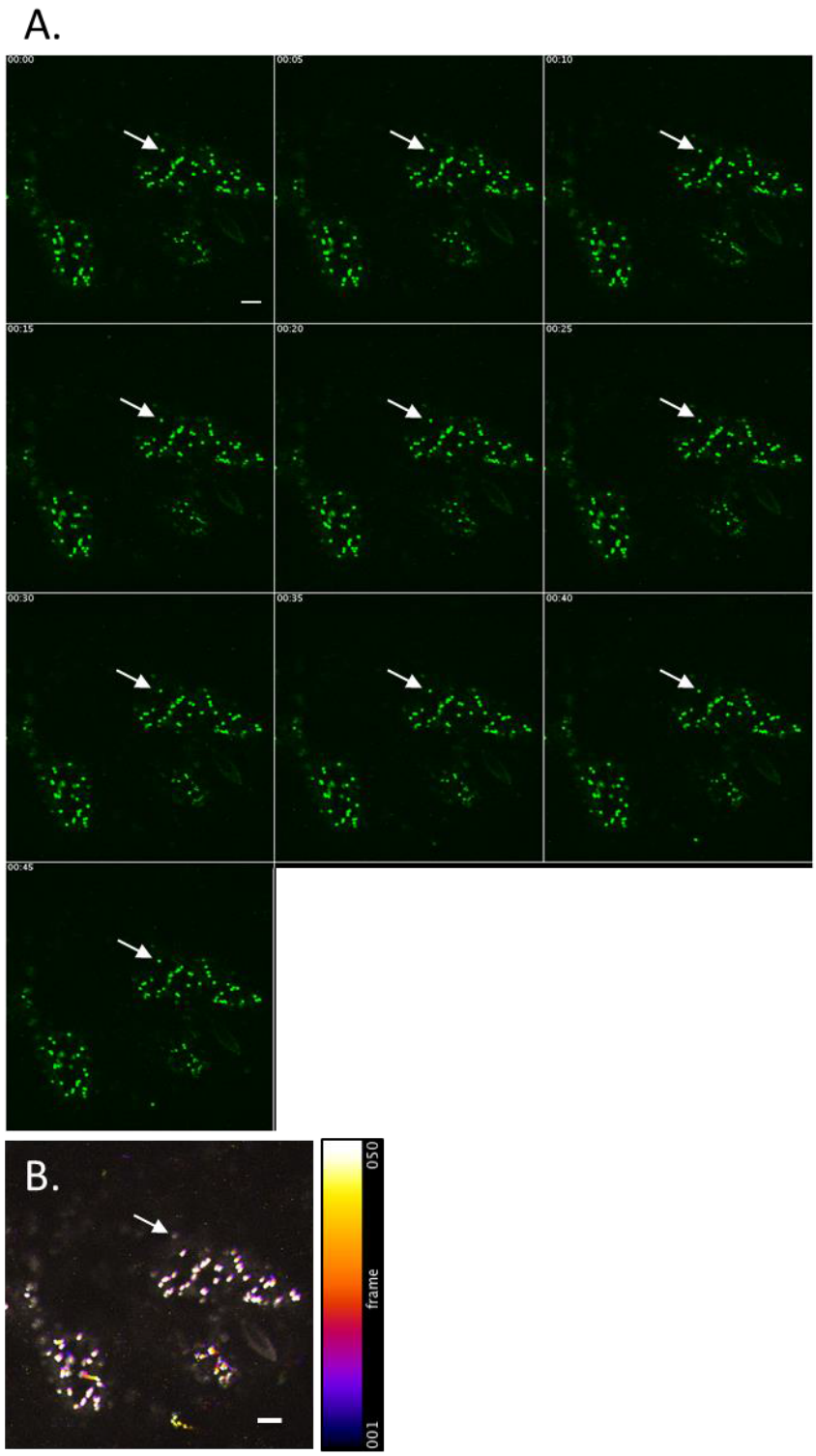
A.
00:00
00:05
00:10
00:15
00:20
00:25
00:30
00:35
00:40
00:45
B.
050
frame
001

**Figure 48.**
**Time-series images of Golgi bodies labelled with ST-GFP moving in the cytoplasm.**

**A**: Representative time-series of Golgi bodies; the arrow is highlighting one Golgi body moving over the time; time interval 5 sec.
**B**: Time-lapse colour coder image; a colour assigned to each frame of the movie the frames merged. Scale bar 5 μm.

**Figure 48.**

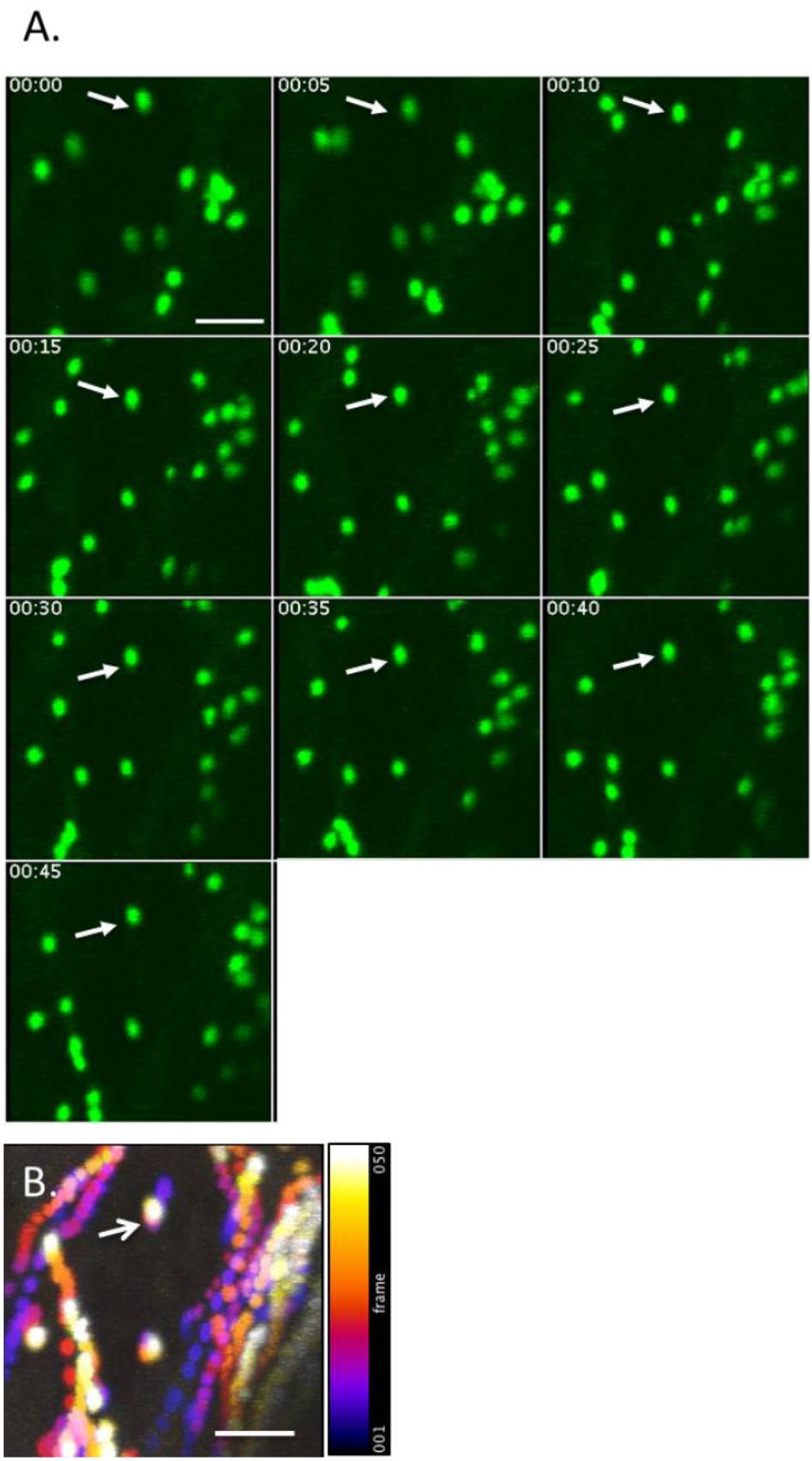
A.
00:00
00:05
00:10
00:15
00:20
00:25
00:30
00:35
00:40
00:45
B.
050
frame
001

**Figure 49.**
**Time-lapse images of FRAP of actin filaments labelled with Lifeact-GFP.**

Time-lapse images showing bleaching (at 0.05 sec, in the circle area) and recovery of Lifeact-GFP. Interval between frames 0.01 sec. Scale bar 5μm.

**Figure 49.**

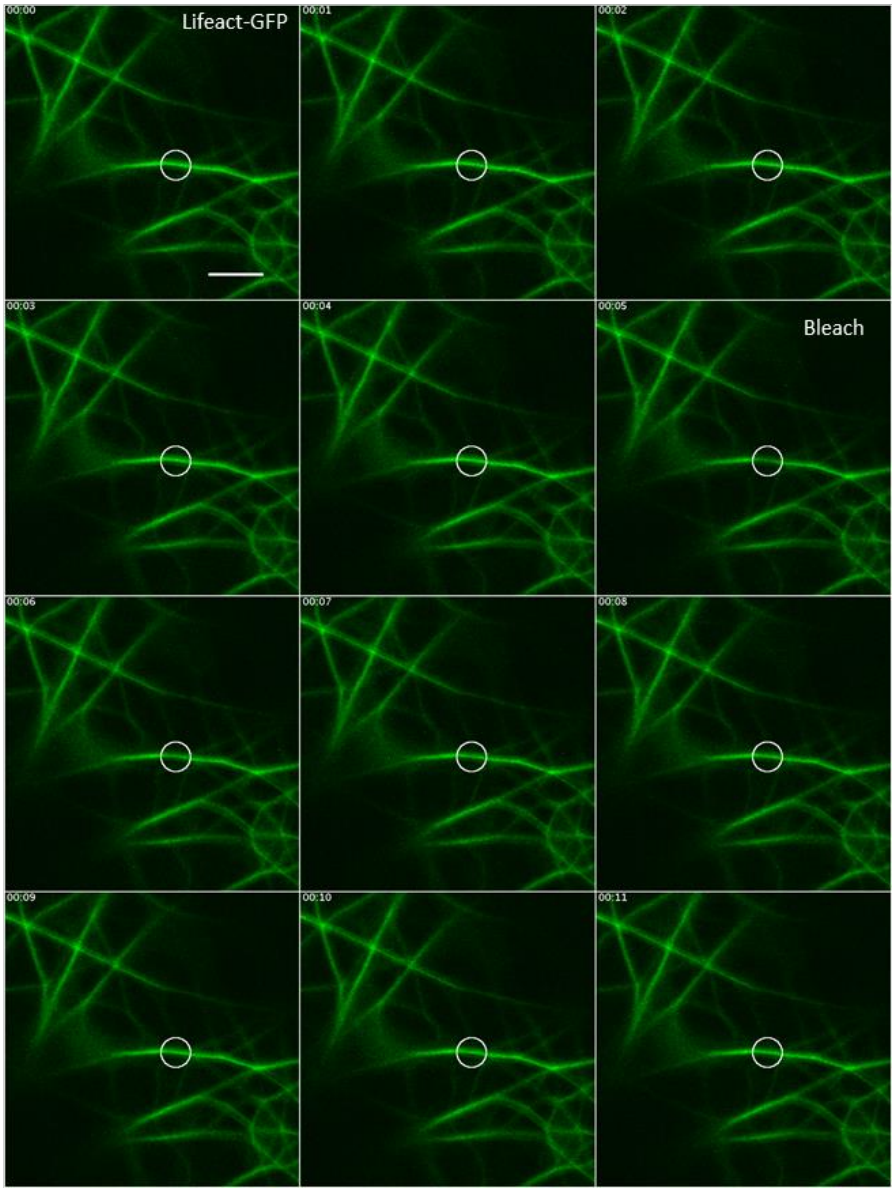
00:00
Lifeact-GFP
00:01
00:02
00:03
00:04
00:05
Bleach
00:06
00:07
00:08
00:09
00:10
00:11

**Figure 50.**
**FRAP time-series images of Lifeact-GFP coexpressed to RFP-XIK tail.**

Time-lapse images showing quenching (at 0.05 sec, in the circle area) and recovery of Lifeact-GFP co-expressed to RFP-XIK tail. Interval between frames 0.01 sec. Scale bar 5μm.

**Figure 50.**

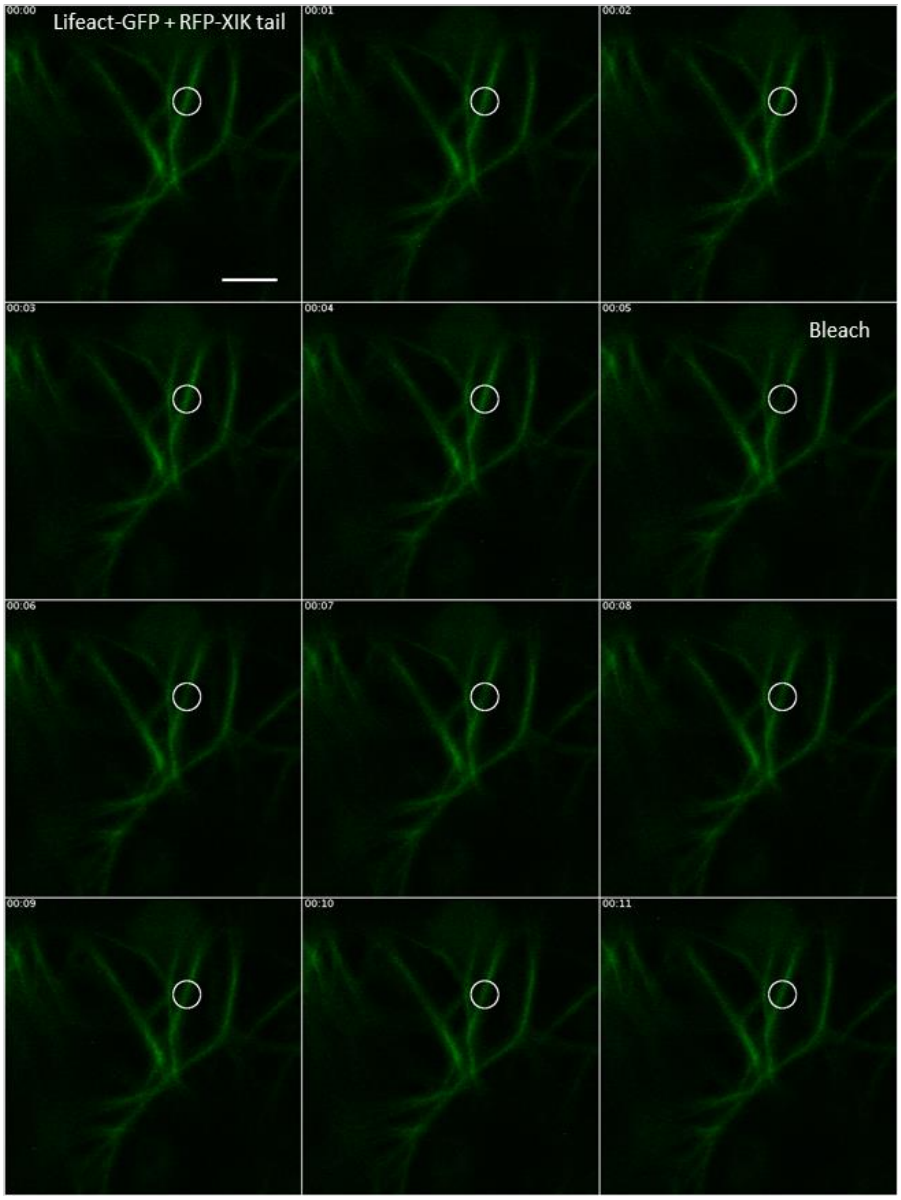
00:00
Lifeact-GFP + RFP-XIK tail
00:01
00:02
00:03
00:04
00:05
Bleach
00:06
00:07
00:08
00:09
00:10
00:11

**Figure 51.**
**Time-lapse images showing bleaching and recovery of GFP-actin-Cb.**

Time-series images showing quenching (at 0.05 sec, in the circle area) and recovery of GFP-actin-Cb. Interval between frames 0.01 sec. Scale bar 5μm.

**Figure 51.**

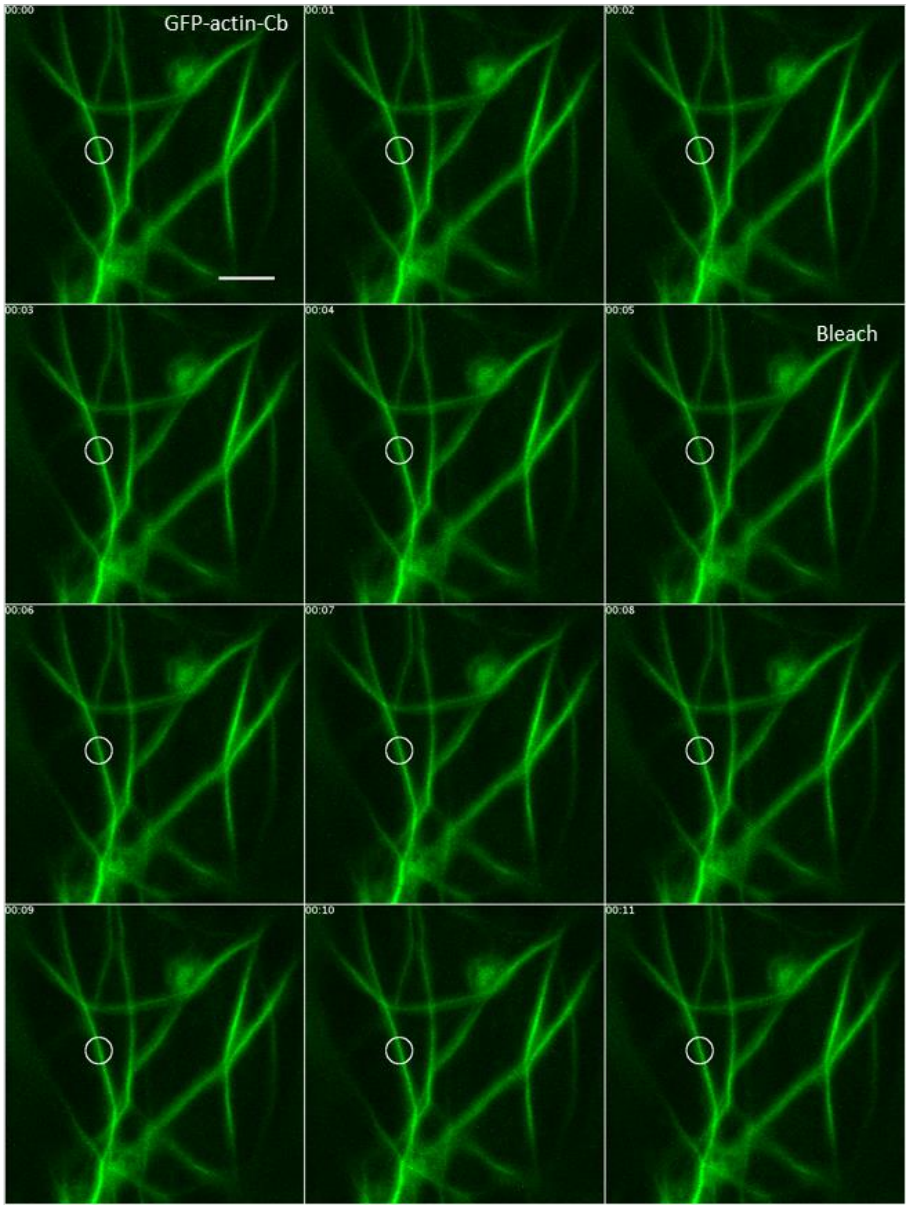
00:00
GFP-actin-Cb
00:01
00:02
00:03
00:04
00:05
Bleach
00:06
00:07
00:08
00:09
00:10
00:11

**Figure 52.**
**FRAP time-series images of GFP-actin-Cb coexpressed to RFP-XIK tail.**

Time-lapse images showing quenching (at 0.05 sec, in the circle area) and recovery of GFP-actin-Cb co-expressed to RFP-XIK tail. Interval between frames 0.01 sec. Scale bar 5μm.

**Figure 52.**

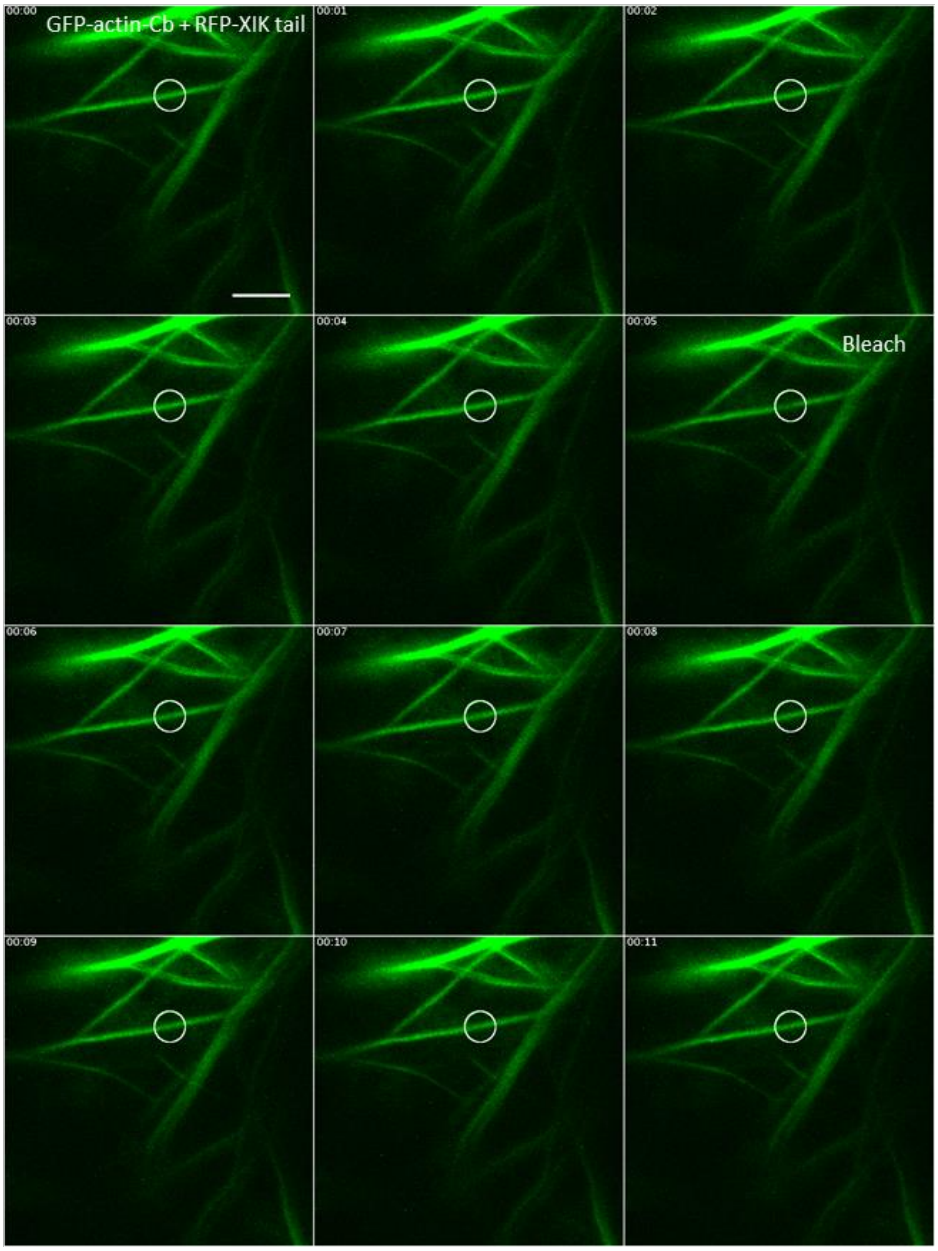
00:00
GFP-actin-Cb + RFP-XIK tail
00:01
00:02
00:03
00:04
00:05
Bleach
00:06
00:07
00:08
00:09
00:10
00:11

**Figure 53.**
**Enlarged time-lapse images of the fluorescence recovery after photobleaching of the cytoskeletal probes Lifeact-GFP and GFP-actin-Cb.**

Zoom-in images of the fluorescence recovery are inspected in order to assess the pattern of the probes recovery.
The circle indicates ROI area and the bleaching event occurs at time 0.05 sec. The bleached areas have all the same size and the different size here are due to the zooming factor.
a) Lifeact-GFP
b) Lifeact-GFP and RFP-XIK tail
c) GFP-actin-Cb
d) GFP-actin-Cb and RFP-XIK tail
Time interval between frames 1 sec. Scale bar 1 μm.

**Figure 53.**

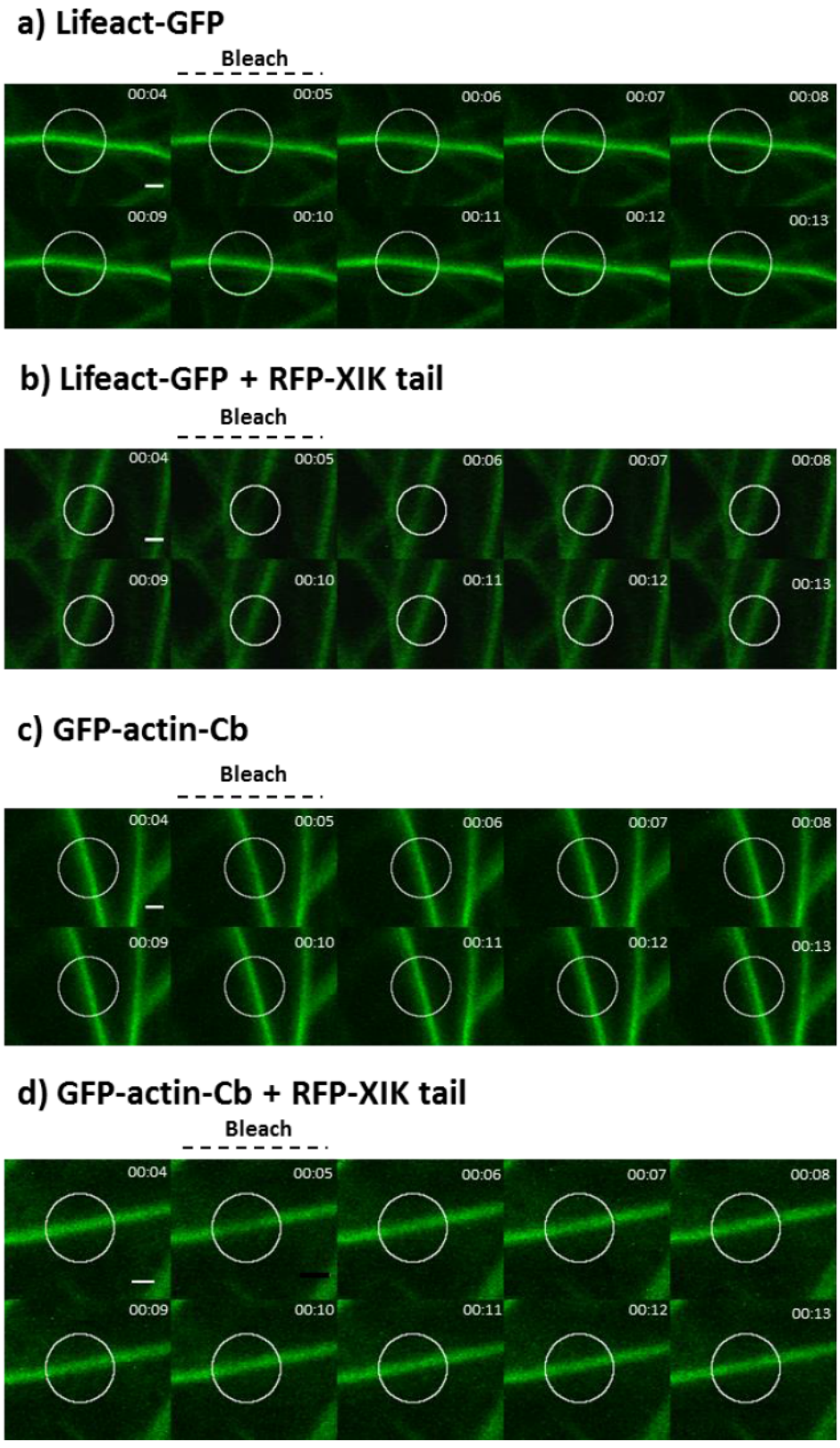
a) Lifeact-GFP
Bleach
00:04
00:05
00:06
00:07
00:08
00:09
00:10
00:11
00:12
00:13
b) Lifeact-GFP + RFP-XIK tail
Bleach
00:04
00:05
00:06
00:07
00:08
00:09
00:10
00:11
00:12
00:13
c) GFP-actin-Cb
Bleach
00:04
00:05
00:06
00:07
00:08
00:09
00:10
00:11
00:12
00:13
d) GFP-actin-Cb + RFP-XIK tail
Bleach
00:04
00:05
00:06
00:07
00:08
00:09
00:10
00:11
00:12
00:13

**Figure 54.**
**Normalised curves of the fluorescence recovery after photobleaching of Lifeact-GFP and Lifeact-GFP co-expressed to RFP-XIK tail.**

The fluorescence recovery after photobleaching of (**A**) Lifeact-GFP only (20 bleached areas) or (**B**) co-expressed to RFP-XIK tail ( 22 photobleached area) is reported up to 20 seconds; the range of the fluorescence recovery is between 50 and 90% for Lifeact-GFP, while the co-expression of the truncated myosin has a range of 25-90%.

**Figure 54.**

A.

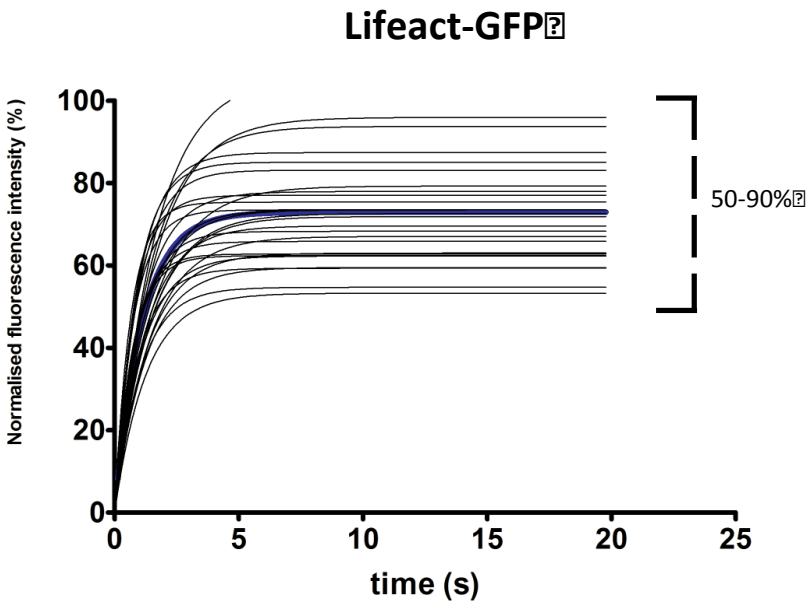
Lifeact-GFP
Normalised fluorescence intensity (%)
100
80
60
40
20
0
0
5
10
15
20
25
time (s)
50-90%

B.

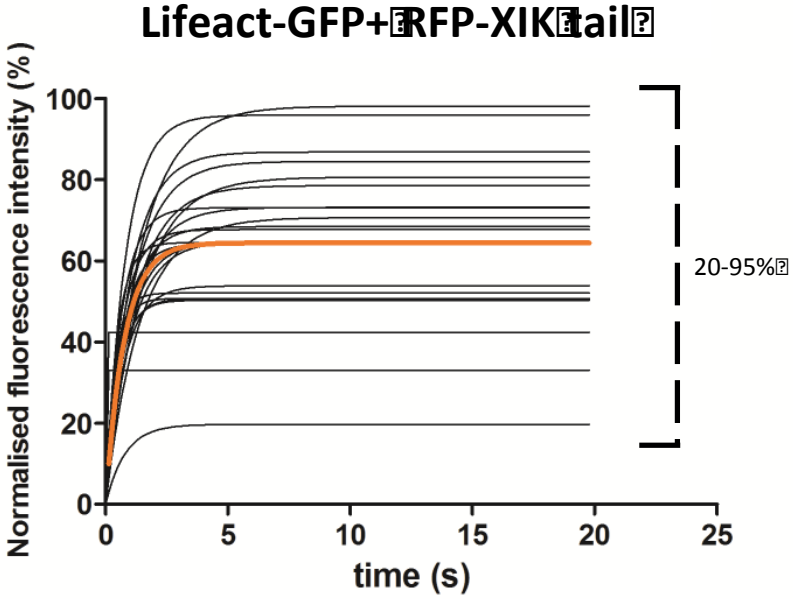
Lifeact-GFP+ RFP-XIK tail
Normalised fluorescence intensity (%)
100
80
60
40
20
0
0
5
10
15
20
25
time (s)
20-95%

**Figure 55.**
**Profiles of fitted FRAP curves of Lifeact-GFP and Lifeact-GFP co-expressed to RFP-XIK tail.**

Fitted FRAP curves of Lifeact-GFP solely (blue line) and co-expressed to RFP-XIK tail (orange line) are compared (**A**). The % of the max fluorescence recovery, half-times (t ½) and recovery rate (R) are reported in the table **B**.
Lifeact-GFP has max recovery percentage of 72.95%, half-time 0.76 sec and R 48% $sec^{-1}$.Lifeact-GFP and RFP-XIK tail has recovery percentage 64.43 %, t ½ is 0.53 and R is 61% $sec^{-1}$.

**Figure 55.**

A.

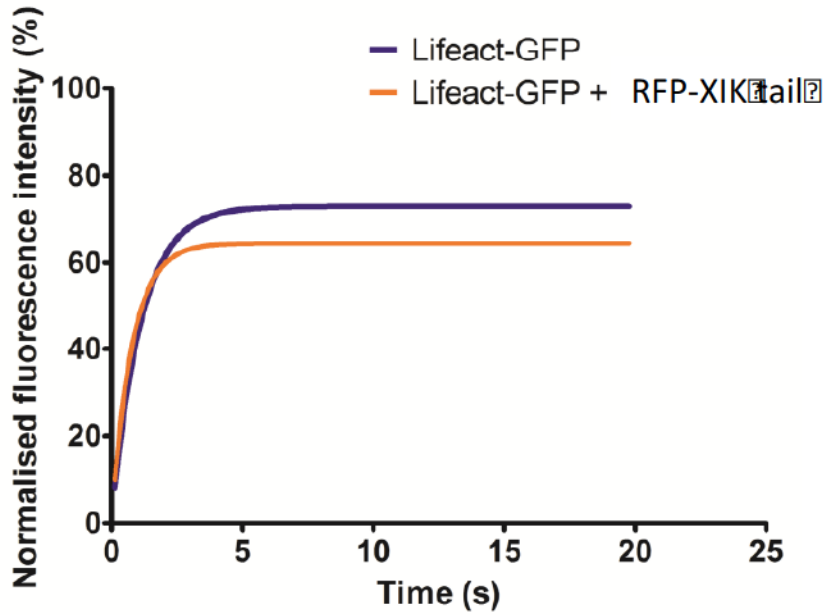


B.

| | Fluor. Recovery | t½ | R |
|---|---|---|---|
| Lifeact-GFP | 72.95% | 0.76 sec | 48% $sec^{-1}$ |
| Lifeact-GFP + RFP-XIK tail | 64.43% | 0.53 sec | 61% $sec^{-1}$ |

**Figure 56.**
**Bar-chart of the mean fluorescence recovery of Lifeact-GFP and Lifeact-GFP co-expressed to RFP-XIK tail.**

Mean intensity fluorescence recovery (MFIR) after photobleaching of Lifeact-GFP solely (blue bar) and expressed along with RFP-XIK tail (orange bar) are plotted; the bar lines represent the standard deviation (SD) (**A**).
The figures of mean and SD reported in the table **B**. The differences in the mean are not statistically different as assessed by the unpaired t-test equal variances (significance level < 0.05).

**Figure 56.**

A.

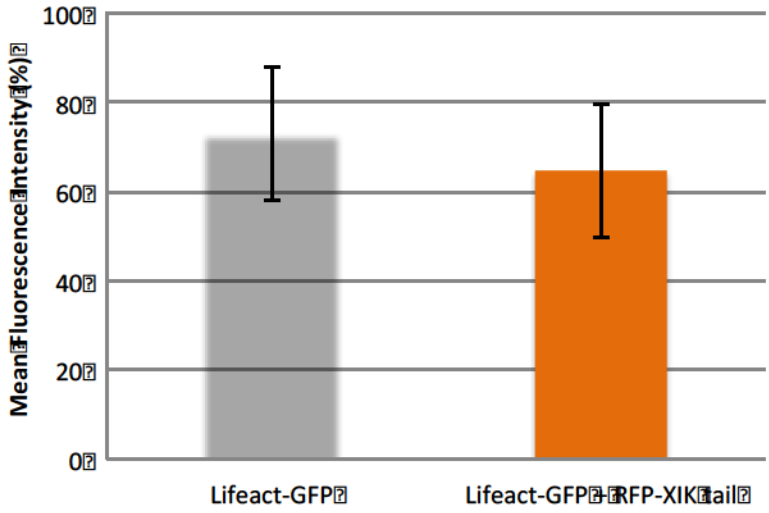


B.

| | MFIR (%) | SD |
|---|---|---|
| Lifeact-GFP | 73.1 | ± 12.7 |
| Lifeact-GFP + RFP-XIK tail | 65 | ± 19 |
| Significance (p<0.005) | 0.08 | |

**Figure 57.**
**Bar-chart of the mean fluorescence half-time recovery of Lifeact-GFP solely and co-expressed to the tail domain of XIK.**

Half-times mean values of Lifeact-GFP (blue bar) and the cytoskeletal marker co-expressed to RFP-XIK tail (orange bar) are plotted (**A**). The bar lines represent the standard deviation (SD).
The figures of means and SD are reported in the table below the plot. The figures of mean and SD reported in the table below the plot. The differences in the mean are statistically different (p: 0.004, indicated as *) as assessed by the unpaired t-test equal variances (significance level < 0.05) (**B**).

**Figure 57.**

A.

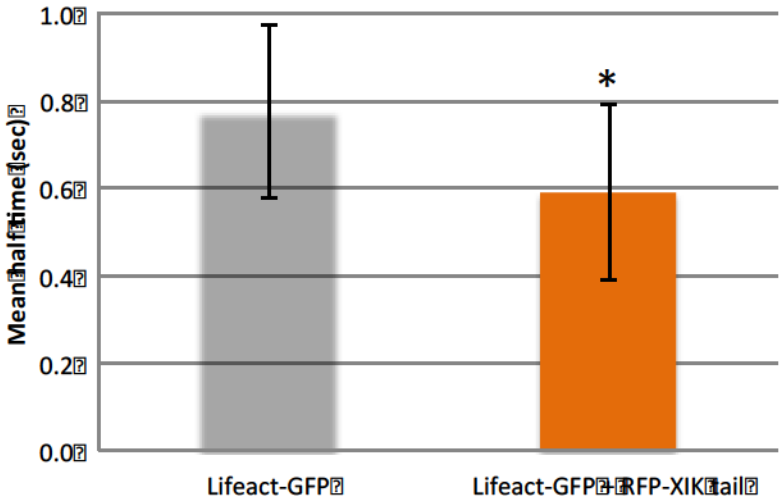


B.

| | Mean (sec) | SD |
|---|---|---|
| Lifeact-GFP | 0.77 | ± 0.25 sec |
| Lifeact-GFP + RFP-XIK tail | 0.6 | ± 0.2 sec |
| Significance (p<0.005) | 0.004 | |

**Figure 58.**
**Normalised curves of the fluorescence recovery after photobleaching of GFP-actin-Cb and GFP-actin-Cb co-expressed to RFP-XIK tail.**

The fluorescence recovery after photobleaching of GFP-actin-Cb (**A**) or co-expressed to RFP-XIK tail (**B**) is reported up to 20 seconds; the range of the fluorescence recovery is between 20 and 90% for GFP-actin-Cb, and the co-expression of the truncated myosin determines a range of 20-98%.

**Figure 58.**

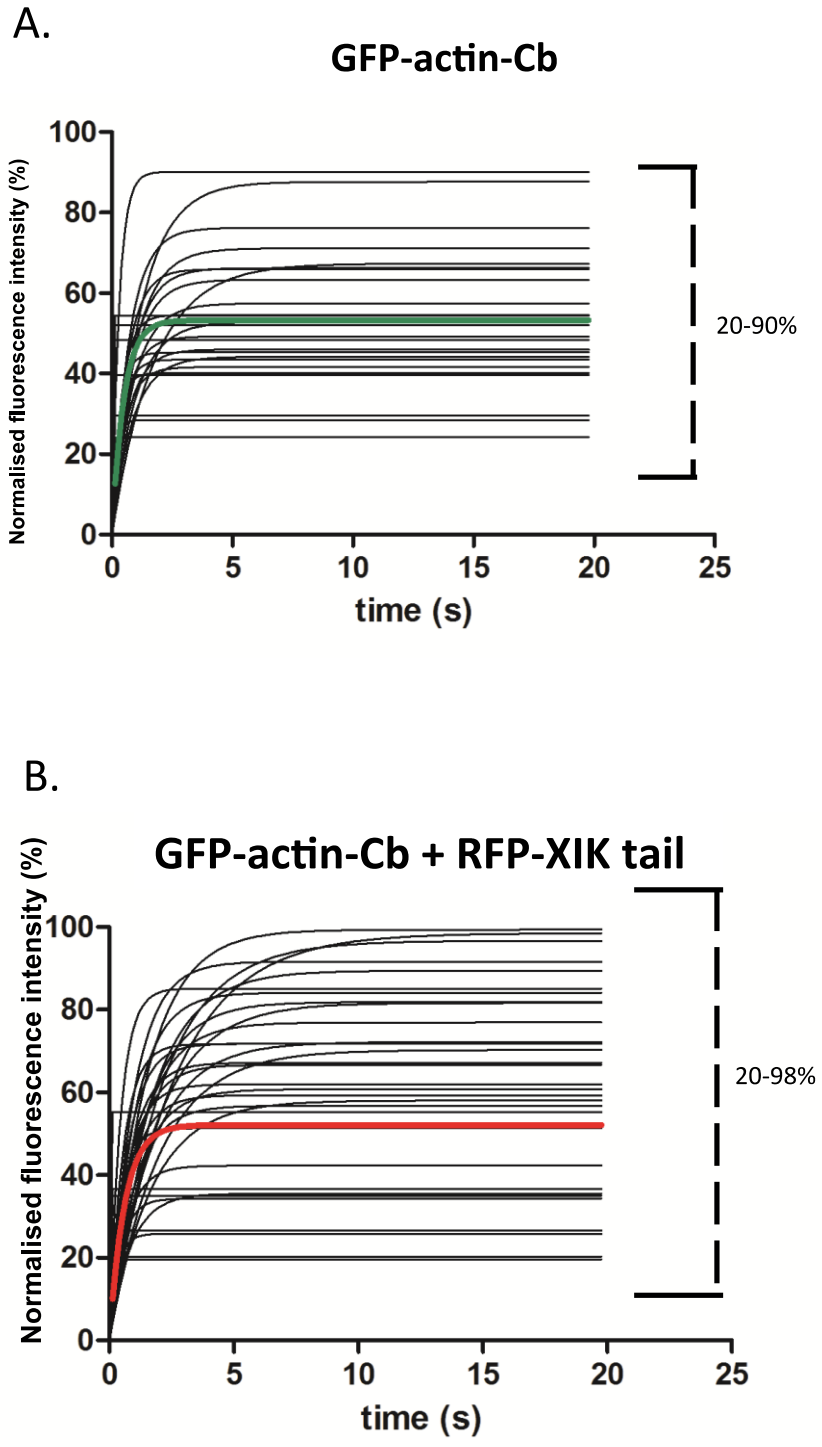
A.
GFP-actin-Cb
Normalised fluorescence intensity (%)
100
80
60
40
20
0
0
5
10
15
20
25
time (s)
20-90%
B.
GFP-actin-Cb + RFP-XIK tail
Normalised fluorescence intensity (%)
100
80
60
40
20
0
0
5
10
15
20
25
time (s)
20-98%

**Figure 59.**
**Profiles of fitted FRAP curves of GFP-actin-Cb and GFP-actin-Cb co-expressed to RFP-XIK tail.**

Fitted FRAP curves of GFP-actin-Cb solely (green line) and co-expressed to RFP-XIK tail (red line) are compared (**A**). The % of the max fluorescence recovery, half-times (t ½) and recovery rate (R) are reported in the table **B**.
GFP-actin-Cb has max recovery percentage of 53.26%, half-time 0.34 sec and R 73% $sec^{-1}$. GFP-actin-Cb and RFP-XIK tail has recovery percentage 52 %, t ½ is 0.42 and R is 62% $sec^{-1}$.

**Figure 59.**

A.

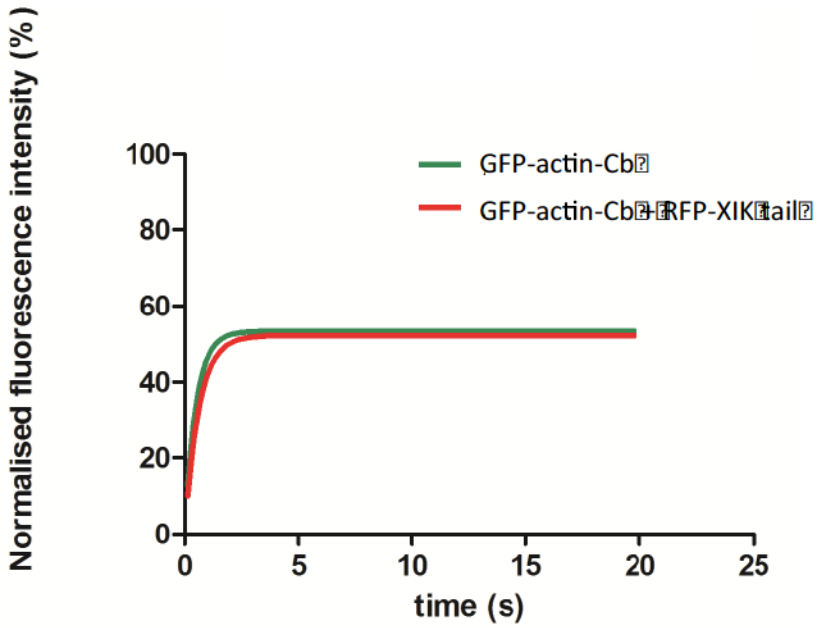


B.

| | Fluor. Recovery | t½ | R |
|---|---|---|---|
| GFP-actin-Cb | 53.26% | 0.34 sec | 73% sec$^{-1}$ |
| GFP-actin-Cb + RFP-XIK tail | 52% | 0.42 sec | 62% sec$^{-1}$ |

**Figure 60.**
**Bar-chart of the mean fluorescence recovery of GFP-actin-Cb and GFP-actin-Cb co-expressed to RFP-XIK tail.**

Mean fluorescence intensity recovery (MFIR) after photobleaching of GFP-actin-Cb (green bar) and GFP-actin-Cb co-expressed to RFP-XIK tail (magenta bar) are plotted (**A**); the bar lines represent the standard deviation (SD).
The figures of mean and SD reported in the table below the plot (**B**). The differences in the mean are not statistically different as assessed by the unpaired t-test equal variances (significance level < 0.05).

**Figure 60.**

A.

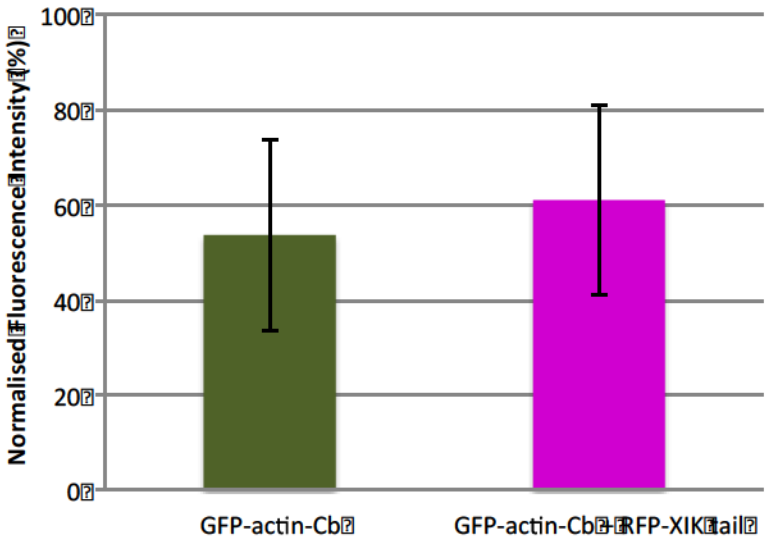


B.

| | MFIR (%) | SD |
|---|---|---|
| GFP-actin-Cb | 53.6 | ± 16.6 |
| GFP-actin-Cb + RFP-XIK tail | 61 | ± 24.2 |
| Significance (p<0.005) | 0.17 | |

**Figure 61.**
**Bar-chart of the mean fluorescence half-time recovery of the fluorescent nanobody solely and co-expressed to the tail domain of XIK.**

Half-times mean values of GFP-actin-Cb (green bar) and the cytoskeletal marker co-expressed to RFP-XIK tail (magenta bar) are plotted. The bar lines represent the standard deviation (SD) (**A**).
The figures of means and SD are reported in the table (**B**). The differences observed in the means are statistically different (p: 0.004, indicated as *) as assessed by the unpaired t-test equal variances (significance level < 0.05).

**Figure 61.**

A.

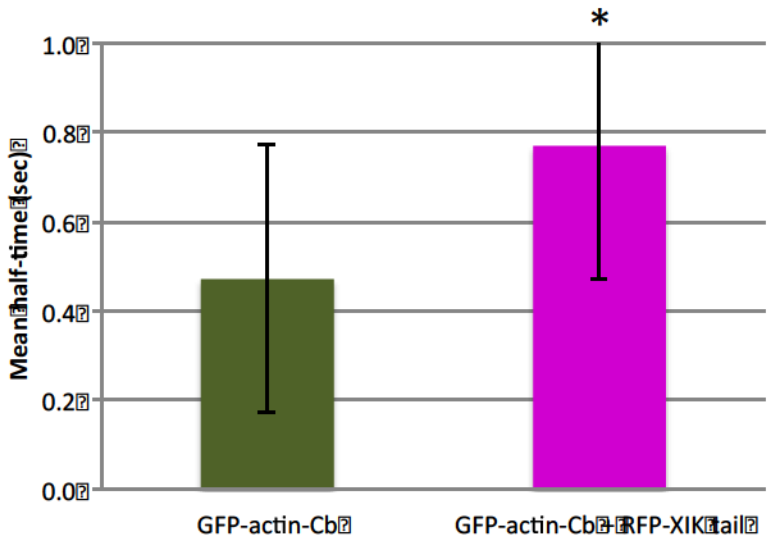


B.

| | Mean (sec) | SD |
|---|---|---|
| GFP-actin-Cb | 0.47 | ±0.25 sec |
| GFP-actin-Cb + RFP-XIK tail | 0.76 | ±0.4 sec |
| Significance (p<0.005) | 0.004 | |

**Figure 62.**
**Mechanisms of interaction between the fluorescent nanobody and actin strands.**

According to outcomes of FRAP data, two scenarios are hypothised. The nanobody has a single target on actin subunits and accessibility to it can vary when the actin is polymerized (top panel). The other option is that the target sequence of the antibody is present in multiple domains, which are more or less accessible (panel below). The grade of accessibility to the target sequence, would determine a different stabilization and strength of the interaction, therefore a wide variability in the recovery of the fluorescence.
The possible interactions are:

**1**- target partially accessible to the antibody - no stable binding
**2**- target not accessible to the nanoboby - no binding
**3**- target is accessible to the nanobody - stable binding

**Figure 62.**

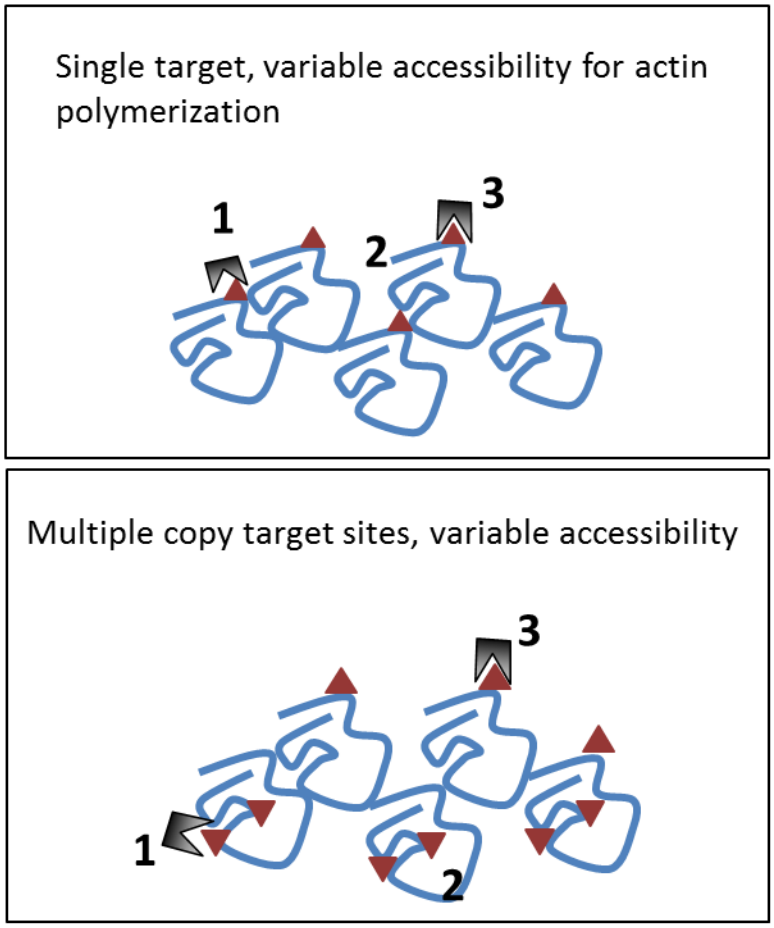
Single target, variable accessibility for actin polymerization
1
2
3
Multiple copy target sites, variable accessibility
3
1
2
GFP-actin-Cb
Nanobody target
Actin monomer

**Figure 63.**
**Model showing the interaction between Lifeact-GFP and actin filaments.**

The results from the fluorescence recovery after photobleaching of Lifect-GFP, lead us to elaborate the following model. Lifeact peptide maintains the cross-bundling properties and for this reason interacts with the actin target slower and more stably.

**Figure 63.**

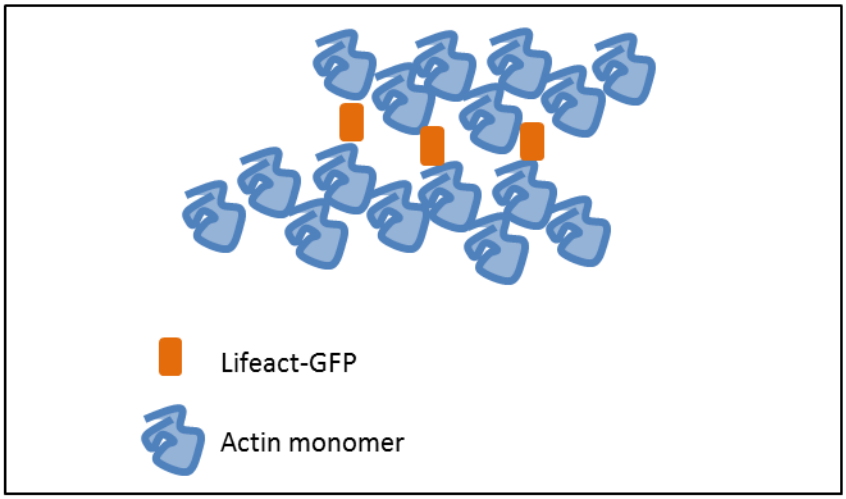

# 7. Localization study of Kinesin-13a

## 7.1 Introduction

For a long time, actin and microtubule networks have been viewed as separate and with different functions. Recent results demonstrate that instead these two components can cross-talk and a physical dynamic interaction exists (Collings and Nick 2008). Several classes of proteins are involved in connecting the actin filaments to the microtubules (Petrasek and Schwarzerova 2009) and both types of filaments are involved in moving and positioning organelles, such as plastids, mitochondria and Golgi bodies (Brandizzi and Wasteneys 2013).

In plants, the largely accepted model is that F-actin provides the main tracks for Golgi body movement and the myosins are the driving forces (Akkerman *et al*. 2011, Brandizzi and Wasteneys 2013, Sparkes *et al*. 2008)(See section 1.3.2). The role of microtubules, in relation to Golgi body kinetics, is not very clear and it is suggested that they assist the positioning of organelles. Work by Crowell *et al*. (2009) demonstrates that in Arabidopsis the insertion of the cellulose synthase complex (CSC) in the plasma membrane is concomitant to Golgi pausing on microtubules.

The movement of cargo on animal microtubules is mediated by two classes of motor proteins: the kinesins and dynein. The first group

drives a plus-end directed movement, while dynein determines the movement towards the minus-end (Horgan and McCaffrey 2011). The analysis of plant genomes showed that plants lack dynein and compensated the loss of these motor proteins by developing the functional homologous minus-end kinesins (Wickstead and Gull 2007). In Arabidopsis, 61 genes encode kinesin proteins and they are grouped into 14 families (Lee and Liu 2004, Reddy and Day 2001). Among them, immunochemistry has shown that kinesin-13a localizes on Golgi bodies in Arabidopsis cells (Lu *et al*. 2005). Kinesin-13a is has an internal motor domain (Figure 64) and is not able to move along microtubules, but does have a microtubule depolymerizing activity (Wei *et al*. 2009). A knock-out mutant of Kinesin-13a in Arabidopsis shows a different morphology of Golgi stacks in root-cap peripheral cells with aggregation of Golgi bodies (Lu *et al*. 2005, Wei *et al*. 2009), four branched thrichomes and smaller secondary cell wall pits (Oda and Fokuda 2013). The overexpression of kinesin-13a causes the disruption of cortical microtubules in root epidermal cells and the formation of large secondary cell wall pits in root metaxylem vessel (Oda and Fokuda 2013). A mutant of kinesin-13a lacking the motor domain but maintaining the coiled-coil domain localizes to the cytoplasm and the microtubule depolymerizing activity is lost (Oda and Fokuda 2013).

The localization studies published so far used immunolabeling techniques in an inducible system in Arabidopsis.

In this chapter, the localization of kinesin-13a full length and a mutated version fused to a fluorescent marker at either termini is studied after transient expression in tobacco to understand if this protein is involved in anchoring the Golgi bodies to microtubules.

## 7.2 Results

Initially a bioinformatics analysis was performed to gain information about the domain organization of Atkinesin-13a. The protein sequence is 794 aa long and the putative motor domain is comprised between the amino acid 185 and 533, followed by a predicted coiled-coiled domain (Figure 64). This confirmed the work by Lu *et al*. (2005). The mutated version of the protein was obtained by removing the motor domain (aa 1-607) while the coiled-coil domain was maintained (Figure 65). The truncated protein was 188 amino acids long and was fused to fluorescent tags at either end (Figure 66).
Kinesin-13a is coded by the At3g16630 gene, the cDNA sequence was obtained from Genebank (accession number AY056129) (Figure 67) and the DNA sequence was cloned via PCR (See section 2.6.2). Primers were designed to pair at the start codon and at the stop codon of the At3g16630 gene to generate the full length or in position 1601 and at the stop codon to produce the motor truncated version (See section 2.5). The products of the PCR reactions were checked on agarose gels that confirmed the expected base pair length for the full length (2500 bp approximately) and for the truncated version (approximately 900bp) (Figure 68).
After gel extraction, the PCR products were sent for sequencing and the sequence alignment was performed for both the full length and the mutant (Appendix IV). PCR products were cloned into the appropriate expression vector that allowed the N or C terminal fusions to a fluorescent tag and expression in tobacco plants via agrobacterium infiltration.

The plasmids containing the gene sequence for fusion proteins were sent for sequencing and successively aligned to the CDS sequence to verify if the kinesin sequence was in frame with the fluorescent marker (only the alignment of GFP-kinesin-13a is reported, Appendix IV). The plasmids were then used to transform agrobacterium which was infiltrated into tobacco plants (See section 2.4). Different infiltration OD were tested (0.1, 0.03 and 0.05) and the optimal expression settings were found as in Table 11.

**Table 11. List of kinesin fusion proteins and relative transient expression conditions.**

| Construct | $OD_{600}$ | Days from infiltration |
|---|---|---|
| Kinesin-13aD-GFP | 0.05 | 2 or 3 |
| Kinesin-13aD-RFP | 0.05 | 2 or 3 |
| GFP- Kinesin-13aD | 0.05 | 2 |
| RFP- Kinesin-13aD | 0.05 | 2 |
| Kinesin-13a-GFP | 0.03 | 2 |
| Kinesin-13a-RFP | 0.03 | 2 |
| GFP- Kinesin-13a | No expression | - |
| RFP- Kinesin-13a | No expression | - |

Kinesin-13a with the truncated motor domain and to GFP or RFP at either ends localized in the cytoplasm (Figure 69 C, D, E, and F). The full-length sequence tagged with the fluorescent marker at the C-terminus was also found in the cytoplasm (Figure 69 A and B) but the full length fused to GFP or RFP at the N-terminus is not expressed in plants (fluorescence not detected, data not shown). Unfortunately no Golgi labelling was found in any of the experiments.

## 7.3 Discussion

The localizations of kinesin-13a and its mutant lacking the motor domain were studied *in vivo* in tobacco leaves.

As shown in Chapter 4 (Figure 28), the position and the type of fluorescent tag in the fusion protein can affect the localization and the cytoskeleton organization. This last aspect has to be taken into consideration when investigating the dynamics of organelles in relation to the cytoskeleton. Therefore, different combinations of fluorophores and kinesin motor protein (RFP or GFP at N-terminus or C-terminus) were generated to evaluate if there is any difference in the intracellular localization of the fusion protein. When the full-length protein fused to GFP or RFP at N-terminal, no fluorescent signal was detected (images not shown). Two further strategies could be attempted to make sure that it was not due to a technical error. The infiltration ODs were tested to a maximum of 0.05; an higher optical density (0.1) could be used to exclude that the lack of fluorescent signal is not due to a low level of fluorescent protein. Furthermore, the expression was monitored to a maximum of 2 days from the infiltration event, and a prolonged expression time can be tested for instance, as observed with GFP-TUA (See section 2.4) microtubules markers can take up to 3 day to be visible. However, it cannot be excluded that the tag at the N-terminus could interfere with the protein folding and generate an aberrant fusion protein that is degraded. This could have been tested performing western blot technique with either an antibody detecting the kinesin or the GFP tag.

Immunochemical studies (Lu *et al*. 2005, Wei *et al*. 2009) localised Atkinesin-13a on Golgi stacks and *in vivo* studies showed inconsistent results. The construct GFP-kinesin-13a, under its native promoter, is expressed in differentiating xylem Arabidopsis cultured cells and localises along microtubules in secondary wall pits and in the cytoplasm. In non-xylem cultured cells RFP-kinesin-13a expressed under LexA inducible system, labels microtubule segments (Oda and Fukuda 2013).

In differentiating cultured Arabidopsis cells, the mutant RFP-kinesin-13aD localizes on microtubule pits whereas GFP-kinesin-13aD mainly locates in the cytoplasm and only small fraction of microtubule pits were labelled; the differences in the localization of the two fluorescent version of the same truncated construct was not investigated further.

The over-expressed kinensin-13a-GFP/RFP in tobacco leaf cells, was not detected either on Golgi bodies (Lu *et al*. 2005) or on microtubule pits (Oda and Fukuda 2013); both the fluorescent constructs labelled the cytoplasm (Figure 69A and B); the localization of kinesin-13a deprived of the motor domain fused to fluorescent reporter (GFP/RFP at N or C terminal) resulted in a cytoplasmic localization (Figure 69 C,D,E,F) indicating the position of the fluorophore does not affect the intracellular localization and partially confirming the work by Oda *et al*. (2010) in Arabidopsis suspension cells.

A more attentive analysis of the nucleotidic sequences of the fusion protein Kinesin-13a revealed that the sequencing covered only a small part of the construct and was not possible to understand if the nucleotide sequence of kinesin-13a is aligned to that of the GFP. The differences in the localization of Kinesin-13a between the results presented in this chapter and previous works may be due to a

technical error in the cloning that led to an aberrant fusion protein. Further experiments are required to assess if such errors occurred.

If the technical error will be excluded, and the differeing localization it is confirmed, it can be suggested that it is due to differences in the cell types and developmental stage used, Arabidopsis culture cells and leaf tobacco non-dividing cells respectively.

In the work by Oda and Fukuda (2013) it is hypothized that kinesin-13a is involved in pausing the movement of Golgi bodies on microtubules; this together with the evidence that Golgi bodies pause on microtubules to insert CasA into the plasma membrane to synthetize cellulose fibrils (Crowell *et al.* 2009) led me to postulate that there is a correlation between kinesin-13a and the deposit of cellulose, therefore it can be argued that function and localization of kinesin-13a depends on the developmental stage of the cell and cell types. For example, dividing cells cellulose is rapidly laid down at the cell plate, while in fully developed cells the deposit of cellulose is reduced (Boron and Vissenberg 2014, Miart *et al.* 2014). In Oka and Fukuda (2013) it is also hypothised that the localization of kinesin-13a is regulated by MDD1 (Microtubule depletion domain 1); this argument is used to explain the discrepancy in the localization of the kinesins (Lu *et al*. 2005, Wei *et al*. 2009). Both the full-length and mutated fusion could be used for further experiments. The constructs could be co-expressed to MDD1; MDD1 would recruit the kinesin from the cytoplasm to the microtubules where it exerts its depolymerizing function. Additionally, the movement of Golgi bodies could be tracked when both kinesin-13a and MDD1 are expressed. The instant velocities of Golgi bodies in correspondence of microtubules could be compared when the full-length motor protein

or the mutant are over-expressed to evaluate the role of kinesin-13a in the microtubule/Golgi bodies interaction.

In conclusion it is unclear as to the real function of the putative plant Golgi kinesin and further experimentation is required.

**Figure 64.**
**Representation of the domain organisation of *At*Kinesin-13a.**

**A.** Primary protein sequence of *At*Kinesin 13a. The protein length is 794 aa. The internal motor domain is 185-533 aa (highlighted in yellow), coiled-coil domain predicted 703-742aa (highlighted in green).
**B.** Diagram representing the domain organization. In yellow the internal motor domain and in green the coiled-coil domain
**C.** Table summarizing the functions of the kinesin single domains.

## Figure 64.

### *At*kinesin-13a

**A.**

```
MGGQMQQNNA AAATALYDGA LPTNDAGDAV MARWLQSAGL QHLASPVAST
        60         70         80         90        100
GNDQRHLPNL LMQGYGAQTA EEKQRLFQLM RNLNFNGEST SESYTPTAHT
       110        120        130        140        150
SAAMPSSEGF FSPEFRGDFG AGLLDLHAMD DTELLSEHVI TEPFEPSPFM
       160        170        180        190        200
PSVNKEFEED YNLAANRQQR QQTEAEPLGL LPKSDKENNS VAKIKVVVRK
       210        220        230        240        250
RPLNKKETAK KEEDVVTVSD NSLTVHEPRV KVDLTAYVEK HEFCFDAVLD
       260        270        280        290        300
EDVSNDEVYR ATIEPIIPII FQRTKATCFA YGQTGSGKTF TMKPLPIRAV
       310        320        330        340        350
EDLMRLLRQP VYSNQRFKLW LSYFEIYGGK LFDLLSERKK LCMREDGRQQ
       360        370        380        390        400
VCIVGLQEYE VSDVQIVKDF IEKGNAERST GSTGANEESS RSHAILQLVV
       410        420        430        440        450
KKHVEVKDTR RRNNDSNELP GKVVGKISFI DLAGSERGAD TTDNDRQTRI
       460        470        480        490        500
EGAEINKSLL ALKECIRALD NDQLHIPFRG SKLTEVLRDS FVGNSRTVMI
       510        520        530        540        550
SCISPNAGSC EHTLNTLRYA DRVKSLSKSG NSKKDQTANS MPPVNKDPLL
       560        570        580        590        600
GPNDVEDVFE PPQEVNVPET RRRVVEKDSN SSTSGIDFRQ PTNYREESGI
       610        620        630        640        650
PSFSMDKGRS EPNSSFAGST SQRNNISSYP QETSDREEKV KKVSPPRGKG
       660        670        680        690        700
LREEKPDRPQ NWSKRDVSSS DIPTLTNFRQ NASETASRQY ETASRQYETD
       710        720        730        740        750
PSLDENLDAL LEEEEALIAA HRKEIEDTME IVREEMKLLA EVDQPGSMIE
       760        770        780        790
NYVTQLSFVL SRKAAGLVSL QARLARFQHR LKEQEILSRK RVPR
```

**B.**

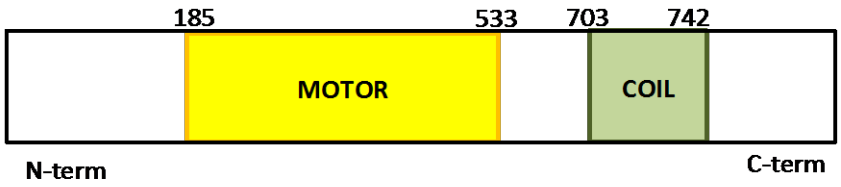


**C.**

| Domain | Function |
|---|---|
| Internal motor | Depolymerisation of microtubules<br>ATP hydrolysis<br>(Ovechkina 2003) |
| Coiled-coil | Homo-dimerization?<br>(Ovechkina 2003)<br>Interaction with MDD1<br>(Oda and Fokuda, 2013) |

**Figure 65.**
**Representation of the domain organisation of the truncated version of *At*Kinesin-13a.**

**A:** Primary protein sequence of *At*Kinesin-13a deleted of the motor domain. To generate *At*Kinesin-13aD The internal motor and flanking sequences (highlighted in grey) are deleted while the coiled-coil domain is maintained resulting in a protein of approximately 150 aa and unable to dimerize.
**B:** Diagram representing the domain organization of *At*Kinesin-13aD . In yellow the internal motor domain and in grey the sequence deleted.

**Figure 66.**
**Representation of the microtubule motors fusion proteins.**

**1 and 2**: Full length sequence of kinesin-13a fused to GFP/RFP either N or C terminal end
**3 and 4**: kinesin-13a truncated of the motor domain domain and fused to RFP/GFP at either ends

## Figure 65.

***At*kinesin-13a-D**

**A.**

```
MGGQMQQNNA AAATALYDGA LPTNDAGDAV MARWLQSAGL QHLASPVAST
        60         70         80         90        100
GNDQRHLPNL LMQGYGAQTA EEKQRLFQLM RNLNFNGEST SESYTPTAHT
       110        120        130        140        150
SAAMPSSEGF FSPEFRGDFG AGLLDLHAMD DTELLSEHVI TEPFEPSPFM
       160        170        180        190        200
PSVNKEFEED YNLAANRQQR QQTEAEPLGL LPKSDKENNS VAKIKVVVRK
       210        220        230        240        250
RPLNKKETAK KEEDVVTVSD NSLTVHEPRV KVDLTAYVEK HEFCFDAVLD
       260        270        280        290        300
EDVSNDEVYR ATIEPIIPII FQRTKATCFA YGQTGSGKTF TMKPLPIRAV
       310        320        330        340        350
EDLMRLLRQP VYSNQRFKLW LSYFEIYGGK LFDLLSERKK LCMREDGRQQ
       360        370        380        390        400
VCIVGLQEYE VSDVQIVKDF IEKGNAERST GSTGANEESS RSHAILQLVV
       410        420        430        440        450
KKHVEVKDTR RRNNDSNELP GKVVGKISFI DLAGSERGAD TTDNDRQTRI
       460        470        480        490        500
EGAEINKSLL ALKECIRALD NDQLHIPFRG SKLTEVLRDS FVGNSRTVMI
       510        520        530        540        550
SCISPNAGSC EHTLNTLRYA DRVKSLSKSG NSKKDQTANS MPPVNKDPLL
       560        570        580        590        600
GPNDVEDVFE PPQEVNVPET RRRVVEKDSN SSTSGIDFRQ PTNYREESGI
       610        620        630        640        650
PSFSMDKGRS EPNSSFAGST SQRNNISSYP QETSDREEKV KKVSPPRGKG
       660        670        680        690        700
LREEKPDRPQ NWSKRDVSSS DIPTLTNFRQ NASETASRQY ETASRQYETD
       710        720        730        740        750
PSLDENLDAL LEEEEALIAA HRKEIEDTME IVREEMKLLA EVDQPGSMIE
       760        770        780        790
NYVTQLSFVL SRKAAGLVSL QARLARFQHR LKEQEILSRK RVPR
```

**B.**

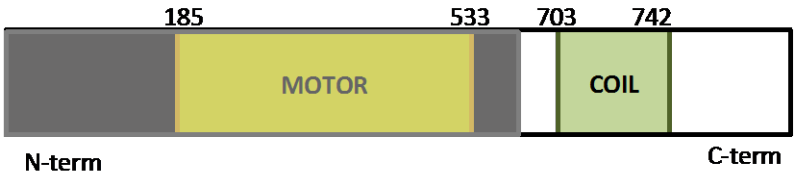


## Figure 66.

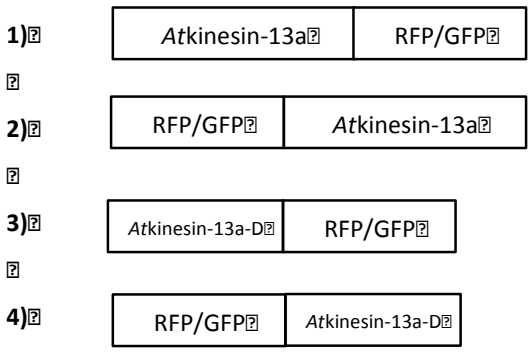

**Figure 67.**
**cDNA sequence of *At*3g16630 coding for *At*kinesin-13a.**

The cDNA sequence of kinesin-13a gene is obtained from Genebank. In bold, the nucleotide sequence where the forward primer pair to obtain the truncated version *At*kinesin-13D

**Figure 68.**
**Agarose gel of PCR cloning products kinesin-13a and kinesin13a-D.**

*At*kinesin-13a and *A*tkinesin-13D cDNA sequence are amplified with PCR and the PCR products loaded on 1% agarose gel. The molecular weights are as expected: full-length 2.500 bp and the mutant 700 bp. A 1kb DNA ladder is loaded as well to estimate the PCR products length.

## Figure 67.

```
1 ATGGGCGGCC AAATGCAGCA AAACAATGCT GCGGCTGCGA CGGCGCTTTA
51 CGATGGGGCT TTACCCACTA ATGACGCAGG AGATGCAGTC ATGGCACGGT
101 GGCTTCAATC CGCTGGTTTG CAGCATTTGG CGTCTCCTGT TGCTTCTACA
151 GGCAATGATC AGCGTCACCT CCCAAACCTT CTCATGCAGG GTTATGGAGC
201 TCAGACTGCT GAAGAGAAAC AAAGACTGTT CCAACTAATG AGAAATCTCA
251 ATTTTAATGG GGAGTCGACT TCTGAATCAT ATACACCAAC TGCTCACACA
301 TCAGCAGCTA TGCCCTCTTC GGAAGGATTT TTTTCACCTG AGTTCAGAGG
351 TGATTTTGGA GCAGGATTAT TGGATCTTCA TGCAATGGAT GATACAGAGC
401 TTCTATCTGA GCATGTGATT ACCGAACCCT TTGAGCCGTC ACCTTTCATG
451 CCTAGTGTAA ATAAAGAATT TGAAGAAGAC TATAATTTGG CAGCTAATCG
501 TCAACAGCGG CAACAGACAG AAGCTGAACC TTTGGGTTTA TTGCCTAAAA
551 GTGATAAAGA AAATAACAGT GTAGCCAAGA TTAAAGTAGT GGTAAGGAAA
601 AGACCCCTAA ACAAGAAAGA AACAGCTAAA AAGGAGGAGG ATGTCGTGAC
651 GGTATCTGAT AATTCTTTGA CTGTCCATGA GCCCAGAGTG AAGGTTGATT
701 TGACTGCTTA TGTGGAAAAG CATGAGTTCT GCTTTGATGC TGTTCTAGAT
751 GAGGATGTTT CAAATGACGA GGTGTATCGG GCCACAATTG AGCCAATAAT
801 TCCCATTATT TTCCAGAGAA CTAAAGCTAC ATGCTTTGCA TATGGCCAAA
851 CAGGTAGTGG TAAGACATTT ACAATGAAAC CATTACCTAT ACGAGCAGTT
901 GAAGATCTTA TGAGGTTGTT GCGTCAACCA GTATACAGCA ATCAGAGGTT
951 TAAATTGTGG CTCAGCTATT TTGAGATATA TGGTGGAAAG CTGTTCGATC
1001 TTCTCAGTGA GAGAAAGAAA CTTTGCATGC GAGAAGATGG TAGACAGCAA
1051 GTTTGCATTG TTGGCCTGCA AGAATATGAA GTTTCAGATG TACAAATTGT
1101 AAAGGATTTT ATCGAGAAAG GAAATGCCGA AAGGAGCACA GGTTCAACTG
1151 GAGCAAATGA GGAATCTTCT AGATCGCATG CCATCCTACA GCTTGTTGTA
1201 AAAAAGCATG TTGAGGTAAA AGACACTAGA CGGAGGAATA ATGATAGTAA
1251 TGAATTGCCT GGGGAAAGTTG TGGGAAAGAT TTCTTTCATT GACCTTGCTG
1301 GCAGTGAAAG AGGTGCAGAC ACCACAGACA ATGATCGCCA GACAAGGATT
1351 GAAGGCGCAG AAATCAACAA GAGTCTCTTG GCTCTTAAGG AATGTATACG
1401 TGCACTGGAC AATGACCAGC TACATATACC ATTTCGTGGA AGCAAACTAA
1451 CGGAAGTGCT CCGTGACTCA TTTGTTGGAA ACTCAAGAAC GGTGATGATT
1501 TCCTGCATCT CTCCAAATGC AGGATCGTGT GAACATACCC TCAATACTCT
1551 AAGATATGCT GATCGAGTCA AAAGTCTATC TAAAAGTGGA AATAGCAAGA
1601 AAGATCAAAC TGCGAATTCA ATGCCTCCGG TTAAT AAGGA TCCTTTGTTG
1651 GGCCCAAATG ATGTAGAAGA TGTCTTTGAG CCTCCACAGG AAGTGAATGT
1701 ACCAGAAACC AGGAGGAGGG TGGTCGAGAA GGACAGCAAC AGCAGTACGT
1751 CGGGTATTGA CTTCAGACAG CCTACAAATT ATCGAGAGGA AAGTGGAATC
1801 CCATCATTCT CAATGGACAA GGGAAGATCA GAGCCGAACA GTTCTTTTGC
1851 TGGCTCCACT AGTCAGAGAA ACAACATTTC TTCATATCCC CAAGAAACTT
1901 CAGACCGTGA AGAGAAAGTA AAGAAAGTGT CACCACCTCG TGGGAAAGGG
1951 TTGCGGGAAG AAAAACCAGA CAGACCACAA AATTGGTCTA AAAGAGATGT
2001 CAGTTCGTCG GATATCCCTA CCTTGACAAA TTTTAGACAG AACGCAAGTG
2051 AAACTGCTTC AAGGCAATAT GAAACCGCTT CAAGGCAATA TGAAACCGAC
2101 CCTTCGCTTG ATGAAAACCT CGATGCACTG CTTGAGGAAG AAGAAGCTCT
2151 GATTGCAGCG CACAGAAAAG AAATTGAGGA TACAATGGAG ATTGTTCGCG
2201 AGGAAATGAA ACTTCTAGCG GAGGTGGACC AACCGGGAAG CATGATAGAA
2251 AACTATGTGA CGCAACTGAG CTTTGTGTTG TCCCGGAAAG CAGCAGGGCT
2301 AGTCAGTCTT CAAGCCAGGC TTGCTCGGTT CCAACACCGT CTCAAGGAAC
2351 AAGAAATACT GAGCCGTAAG AGAGTTCCTC GGTAG
```

## Figure 68.

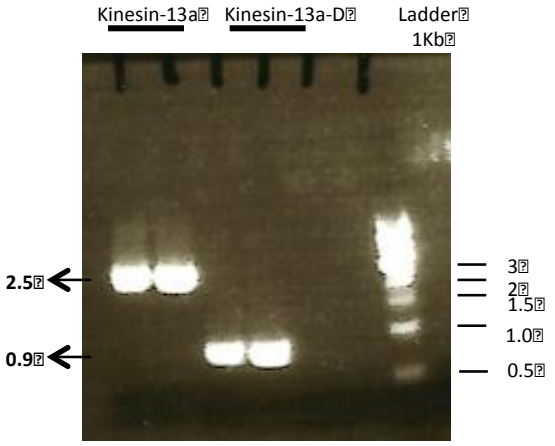

**Figure 69.**
**Transient expression of kinesin-13a and kinesin-13aD fused to fluorescent tags to with ends in *N.tabacum*.**

**A and B**: Kinesin-13A-GFP and kinesin-13a-RFP localize in the cytoplasm. Pictures of RFP/GFP N-terminal fusions are not reported because no fluorescent signal was detected.
**C and F**: Kinesin-13A-GFP/RFP localize in the cytoplasm.
**D and E**: GFP/RFP-Kinesin-13A localize in the cytoplasm.

**Figure 69.**

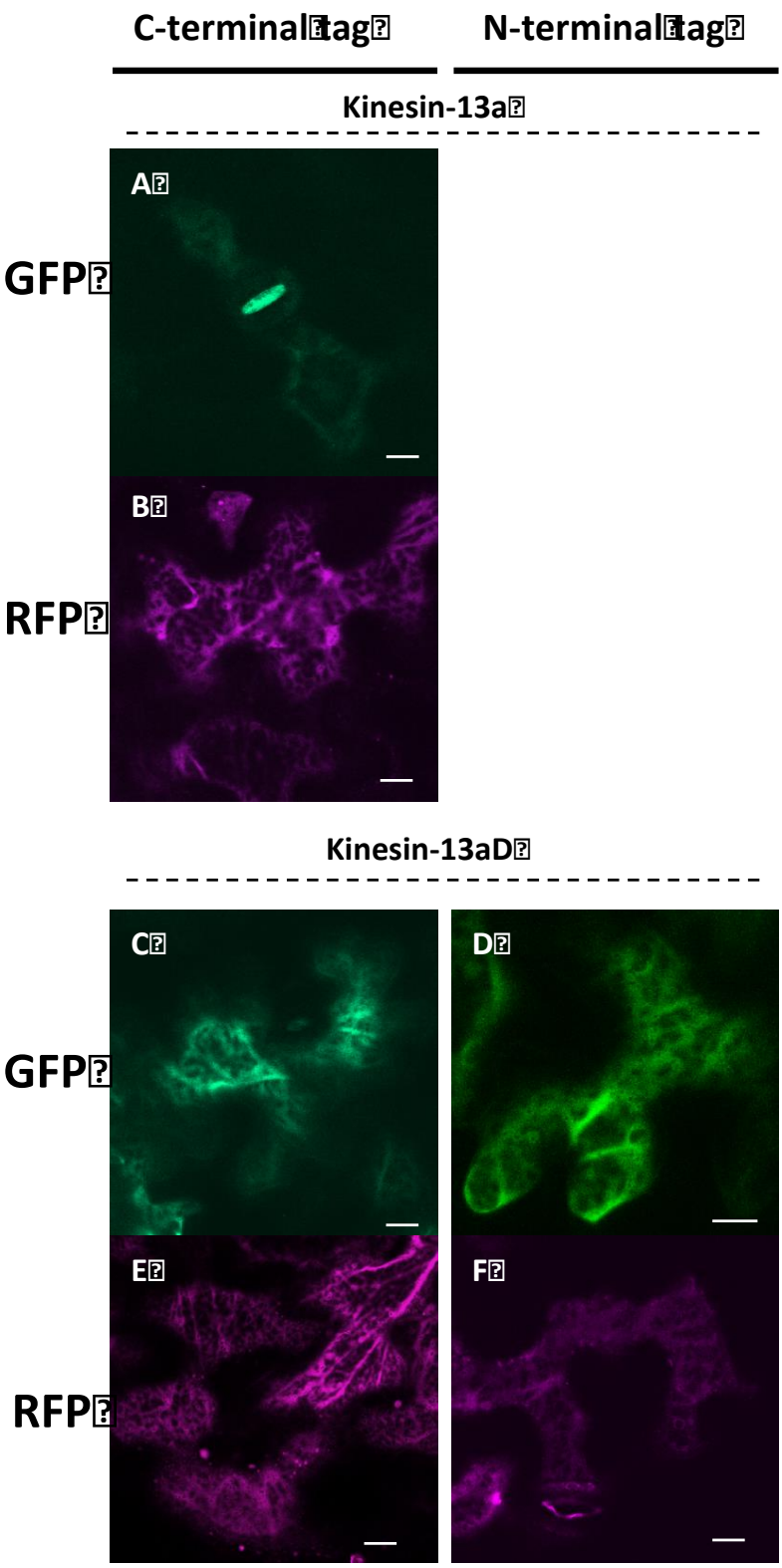
C-terminal tag
N-terminal tag
Kinesin-13a
A
GFP
B
RFP
Kinesin-13aD
C
D
GFP
E
F
RFP

# General discussion and future work

In this thesis, Golgi body dynamics are studied in relation to the components of the cytoskeleton. The movement of Golgi bodies mainly depends on the actin-cytoskeleton, and the depolymerisation of actin filaments stops the movement of the organelles (Boevink *et al* 1998, Akkermann *et al*. 2011). Fluorescent Golgi bodies were tracked to understand and quantify the contribution of actin filaments and microtubules to the organelle dynamics. A more accurate statistical approach is described and validated to generate an accurate analysis of the tracking data. Tracking results showed that the movement of Golgi bodies is very variable and disruption of actin filaments reduces the velocity, displacement rate and meandering index indicating that they have a major role in their motility. Several works in literature demonstrate that the rearranging of actin is highly regulated. For example, chloroplasts move in response to environmental light conditions and their relocation is mainly depending on actin filaments. Indeed, the exposure to the light triggers a signalling cascade that regulates the organization of actin filaments (Kong and Wada 2014). The plant actin cytoskeleton plays a role in signalling defence triggered by pathogen infection (Porter and Day, 2016). Three actin-binding protein formins, profilins and ADF (actin depolymerization factors) demonstrated to be involved in mediating between the cell wall and the actin-cytoskeleton (Cvrčková, 2013). In Takemoto *et al* 2003, it was observed that actin filaments form bundles, the ER membrane aggregates and and Golgi bodies cluster together at the pathogen infection site suggesting that the production and

secretion of plant materials were activated around the penetration site.

It was also demonstrated that Golgi bodies and ER are physically connected (Sparkes *et al.* 2009) and that actin filaments are also involved in rearranging the ER and in controlling cell growth (Griffin *et al.* 2016).

The motility of Golgi bodies is depending on intact actin filaments, as demonstrated in this thesis, and myosins (Avisar *et al*, 2008). Only recently, a SNARE-type protein anchoring the ER to the actin has been characterised (Cao *et al*, 2016). The disruption of the cytoskeleton has no obvious effect on the ER-Golgi trafficking in plants (Brandizzi *et al* 2002, Saint-Jore *et al* 2002) but it inhibits the trafficking of two vacuolar reporters (Kim *et al*, 2005) and of the cellulose synthase complexes (Wightman and Turner, 2010). On the basis of the observations that both ER and Golgi bodies are linked to the actin filaments and that they are physically connected, together with the work presented in this thesis, it can be hypothesised that the actin-cytoskeleton coordinates the dynamics of Golgi bodies and ER, probably to increase the efficiency of the protein trafficking between these two compartments and from the Golgi bodies to the final destination.

The cytoskeleton also represents the link between the extracellular events and intracellular processes such as the defence response to pathogen invasion. While the actin filaments bundle on the site of penetration, the disruption of actin either by actin depolymerizing drugs eases penetration of pathogens into plant tissue. In addition, for cell wall deposition, the vesicular trafficking is an indispensable process in which actin cytoskeleton plays an important role (Porter and Day, 2016).

The tracking was also performed when microtubules were depolymerised but the movement analysis conducted was not sensitive enough to quantify the role of microtubules and no

conclusion could be drawn. A further analysis is proposed: the study of instant velocities, that is the velocity value in each frame, could provide this information and, together with the data obtained from the disruption of actin filaments, how the motility of these organelles is modulated. The evidence that Golgi bodies pause on microtubules to deposit the cellulose synthase complex (Crowell *et al.* 2009) indicates that the movement of Golgi bodies is not random but finely regulated to deliver the cargo of Golgi bodies to specific locations. Proteins bridging between microtubules and actin filaments (Collings 2008) support such a model, and the cross-talk between the components of the cytoskeleton may be involved in the positioning of the organelles.

The organisation of the actin cytoskeleton is not known and different fluorescent fusions markers have been developed to label it (Riedl *et al*. 2008, Katelaar *et al*. 2004, Sheahan *et al*. 2004, Lemieux *et al.* 2013). All the fluorescent reporters available depict a different organisation of the actin network and it is not known if they preferentially bind fine filaments rather than cables (and *vice versa*) or if they change the aggregation state of actin filaments. The study of Golgi dynamics using tracking techniques can provide information about the effect of the actin-markers on the filament organization and dynamics. Different actin-cytoskeletal markers were tested for their suitability for Golgi body dynamics studies and compared to a novel cytoskeletal probe, a fluorescent actin nanobody. Lifeact-GFP is commonly used to label the actin filaments but proved to affect the organization of actin and favours the formation of stable actin bundles (Van der Honing *et al.* 2011). An alpaca nanobody fused to a fluorescent protein, was optimised for decorating the actin cytoskeleton in plant *in vivo*. The nanobody did not favour the aggregation of actin filaments and had less effect on their stability compared to Lifect-GFP. To further investigate the effect of the markers on the organelle

motility, Golgi bodies were tracked in presence of either Lifeact-GFP or the fluorescent nanobody (YFP-actin-Cb). The data demonstrated that Lifeact-GFP changed the behaviour of Golgi bodies whereas the nanobody did not affect the pattern of the movement. The FRAP technique (fluorescent recovery after photo-bleaching) can provide information about the binding dynamics of the probes (Sprague and McNally, 2005) and such a technique was used to compare the binding dynamics of YFP-actin-Cb and Lifeact-GFP. The fluorescent nanobody stably binds to the actin and did not perturb actin filament organization, proving it to be a valuable tool to study the movement of organelles in relation to actin filaments; Lifeact-GFP has cross-bundling properties and this leads to the formation of actin bundles which changes the pattern of the organelle dynamics and favours the directional movement. Therefore is not a good probe to study the actin-dependent motility of organelles. Although expression of the nanobody construct slows organelle movement, I recommend its use for the study of the pattern of actin and organelle dynamics. Subsequent to the work carried out in this thesis, a stable actin nanobody stable arabidopsis line has been generated in our laboratory. This should be used to repeat the Golgi movement studies and to carry them out using higher resolution confocal microscopy. In animal, fluorescent actin monomers are used to study the dynamic behaviour of actin (Ladt *et al* 2016). In plants, the expression of fluorescent G-actin monomers itself did not prove to be efficient because most of it stays in monomeric form diffused in the cytoplasm, resulting in a strong fluorescent cytoplasmatic background (Lemieux *et al.* 2013). The optimisation of fluorescent actin monomers in plants could represent the solution to actin labelling without compromising the dynamics.

Optical tweezers permit the manipulation and displacement of micro-size particles and were used to trap Golgi bodies and investigate any physical links between the organelles and actin filaments (Sparkes and Brandizzi, 2012). Optical trapping showed that when a Golgi body is pulled away from a filament, the filament would follow until the organelle separated; considering the evidence that actin is involved in maintaining the organization of the endoplasmic reticulum and that Golgi bodies are linked to the ER, it cannot be excluded that, when a Golgi body is displaced by the optical trap, the actin filaments would follow because it is associated to the ER and this would support the hypothesis that actin is coordinating the dynamics of these two compartments. The trapping was also performed under depolymerizing conditions: when the actin filaments were disrupted there was an increase in the number of the Golgi bodies that could be trapped, which may indicate that the Golgi bodies and actin filaments are connected. Trapping results were not significant when the microtubules were absent and this could reflect the fact that microtubules only partially contribute to Golgi dynamics and a limitation of the system in detecting weak interactions. Higher resolution confocal microscopy could in future be used to achieve a better resolution of single actin filaments and, in combination with optical tweezers, could reveal if there is any physical connection between the actin filaments and Golgi bodies. Additionally, I would recommend performing a calibration test of the laser power to establish the suitable settings to detect minor interations, such as the relation between Golgi bodies and microtubules.

The model in which organelles move on actin filaments (Boevink *et al*. 1998) and their movement is powered by the actin motor proteins myosin (Akkerman *et al*. 2011) was challenged. The fact that myosin XIK, that is specifically involved in the regulation of

Golgi body movement and does not decorate Golgi bodies *in vivo* (Avisar *et al.* 2011), led to the hypothesis that actin filaments may slide one on top of one another and pull Golgi bodies along with the ER rather than Golgi bodies moving on actin filaments (Sparkes 2010). This hypothesis was tested using the FRAP technique: fluorescent labelled actin filaments were bleached when the native myosin or the non-functional version was over expressed, and the recovery of the fluorescence followed; the results did not totally support this model but suggested that myosin XIK may have a role in the organization of the actin-cytoskeleton. In future, bleaching protocols using the new generation of super resolution confocal microscopes with more sensitive detectors should be used to repeat these experiments with much higher sensitivity and over larger areas of cells.

I also investigated the role of the microtubule motor protein kinesin-13a. This kinesin is the only microtubule protein localised on Golgi bodies (Lu *et al.* 2005) and may represent the link between Golgi and microtubules; its localisation was studied with immunochemical techniques (Lu *et al.* 2005, Oda and Fukuda, 2013) but the evidence was not clear. A fluorescent version of kinesin-13a and a mutant lacking the motor domain were produced and overexpressed in tobacco plants to study the localization *in vivo*. Additional experiments could be conducted with these constructs, like for example, tracking and trapping in the presence of the full-length kinesin and truncations to check if there is any change in the fine regulation of Golgi bodies by microtubules.

Tracking, trapping and FRAP techniques combined with the expression of motor protein mutants are promising tools to reveal how actin and microtubule regulate the movement of Golgi bodies. Further adjustments to these techniques are needed to increase their ability to detect the fine- tuning of the organelle dynamics

regulated by microtubules. Finally, an *in vitro* system could be designed where fluorescent Golgi bodies are added to actin and microtubule network gown on glass slides. Motility could be induced by the addition of cytosol and/or ATP and depolymerising agents and inhibitors could subsequently be tested. Movement data and trapping data could be collected under these more controlled conditions. Likewise proteins bridging the components of the cytoskeleton could be also tested to evaluate how they co-regulate the movement of the organelles.

Golgi bodies are main stations in the secretory pathway and are involved in protein processing and sorting to different destinations (Drakakaki and Dandekar, 2013; Foresti and Denecke, 2008) and their movement is essential to the correct trafficking of proteins to the final destination (Kim *et al*, 2005; Wightman and Turner, 2010). This work aimed at analysing how the cytoskeleton regulates Golgi bodies dynamics and what is the contribution of each component of the cytoskeleton to the movement. Understanding the relation between actin/microtubules and Golgi bodies has biotechnological application such as directing the trafficking of proteins to a certain compartment. Golgi bodies also regulate the localization cell wall components, so the dissection of their movement mechanism potentially could increase the cellulose yield in plants. Golgi bodies have also a role in pathogen response and resistance (Porter and Day, 2016); therefore can be considerated good candidates to improve plant resistance to pathogens.

# References

Akhshi TK, Wernike D and Piekny A (2014) Microtubules and actin crosstalk in cell migration and division. *Cytoskeleton* 71(1): 1–23.

Akkerman M, Overdijk EJR, Schel JHN, Emons AMC and Ketelaar T (2011) Golgi body motility in the plant cell cortex correlates with actin cytoskeleton organization. *Plant & Cell Physiology* 52(10): 1844–1855.

Amari K, Di Donato M, Dolja VV and Heinlein M (2014) Myosins VIII and XI play distinct roles in reproduction and transport of tobacco mosaic virus. *PLoS pathogens* 10(10): e1004448.

Ambrose JC and Wasteneys GO (2008) CLASP modulates microtubule-cortex interaction during self-organization of acentrosomal microtubules. *Molecular Biology of the Cell* 19(11): 4730–4737.

Andreeva A, Kutuzov M, Evans D and Hawes C (1998) The structure and function of the Golgi apparatus: a hundred years of questions. *Journal of Experimental Botany* 49 (325): 1281–1291.

Anon (2016) *SPSS Statistics Tutorials and Statistical Guides | Laerd Statistics*. Available at: https://statistics.laerd.com/.

Arevalo JH, Taussig MJ and Wilson IA (1993) Molecular basis of cross reactivity and the limits of antibody-antigen complementarity. *Nature* 365(6449): 859–863.

Arias-Gonzalez JR (2013) Optical tweezers to study viruses. *Sub-Cellular Biochemistry* 68: 273–304.

Asakura T, Sasaki T, Nagano F, Satoh A, Obaishi H, Nishioka H, Imamura H, Hotta K, Tanaka K, Nakanishi H and Takai Y (1998) Isolation and characterization of a novel actin filament-binding protein from

*Saccharomyces cerevisiae*. *Oncogene* 16(1): 121–30.

Ashkin A (1970) Acceleration and trapping of particles by radiation pressure. *Physical Review Letters* 24(4): 156–159.

Ashkin A (1978) Trapping of atoms by resonance radiation pressure. *Physical Review Letters* 40(12): 729–732.

Ashkin A (1991) The study of cells by optical trapping and manipulation of living cells using infrared laser beams. *ASGSB bulletin: publication of the American Society for Gravitational and Space Biology* 4(2): 133–146.

Avisar D, Abu-Abied M, Belausov E and Sadot E (2011). Myosin XIK is a major player in cytoplasm dynamics and is regulated by two amino acids in its tail. *Journal of Experimental Botany* 63 (1): 241-249.

Avisar D, Abu-Abied M, Belausov E, Sadot E, Hawes C and Sparkes IA (2009) A comparative study of the involvement of 17 Arabidopsis myosin family members on the motility of Golgi and other organelles. *Plant Physiology* 150: (2): 700–709.

Avisar D, Prokhnevsky AI, Makarova KS, Koonin EV and Dolja VV (2008) Myosin XI-K is required for rapid trafficking of Golgi stacks, peroxisomes, and mitochondria in leaf cells of *Nicotiana benthamiana*. *Plant Physiology* 146(3): 1098–1108.

Barlowe CK and Miller EA (2013) Secretory protein biogenesis and traffic in the early secretory pathway. *Genetics* 193(2): 383–410.

Batoko H, Zheng HQ, Hawes C and Moore I (2000) A rab1 GTPase is required for transport between the endoplasmic reticulum and Golgi apparatus and for normal Golgi movement in plants. *Plant Cell* 12(11): 2201–2218.

Baur P (1997) Lognormal distribution of water permeability and organic solute mobility in plant cuticles. *Plant, Cell & Environment* 20(2): 167–177.

Beach JR and Hammer JA (2015) Myosin II isoform co-assembly and differential regulation in mammalian systems. *Experimental Cell Research* 334(1): 2–9.

Belin BJ, Goins LM and Mullins RD (2014) Comparative analysis of tools for live cell imaging of actin network architecture. *BioArchitecture* 4(6): 189–202.

Betapudi V (2014) Life without double-headed non-muscle myosin II motor proteins. *Frontiers in Cellular Biochemistry* 2: 45.

Blanchoin L, Boujemaa-Paterski R, Henty JL, Khurana P and Staiger CJ (2010) Actin dynamics in plant cells: a team effort from multiple proteins orchestrates this very fast-paced game. *Current Opinion in Plant Biology* 13(6): 714–23.

Boevink P, Oparka K, Santa Cruz S, Martin B, Betteridge A and Hawes C (1998) Stacks on tracks: the plant Golgi apparatus traffics on an actin/ER network. The *Plant Journal* 15(3): 441–447.

Bonifacino JS and Glick BS (2004) The mechanisms of vesicle budding and Fusion. *Cell* 116(2): 153–166.

Boron AK, Vissenberg K (2014) The Arabidopsis thaliana hypocotyl, a model to identify and study control mechanisms of cellular expansion. Plant cell report 33(5):697-706

Brandizzi F, Snapp EL, Roberts AG, Lippincott-Schwartz J and Hawes C (2002) Membrane protein transport between the endoplasmic reticulum and the Golgi in tobacco leaves is energy dependent but cytoskeleton independent: evidence from selective photobleaching. *The*

*Plant Cell* 14(6): 1293–1309.

Brandizzi F and Wasteneys GO (2013) Cytoskeleton-dependent endomembrane organization in plant cells: an emerging role for microtubules. *The Plant Journal* 75(2): 339–349.

Buchnik L, Abu-Abied M and Sadot E (2015) Role of plant myosins in motile organelles: is a direct interaction required? *Journal of Integrative Plant Biology* 57(1): 23–30.

Burkhard P, Stetefeld J and Strelkov SV (2001) Coiled coils: a highly versatile protein folding motif. *Trends in Cell Biology* 11(2): 82–88.

Cai C, Henty-Ridilla JL, Szymanski DB and Staiger CJ (2014) Arabidopsis myosin XI: a motor rules the tracks. *Plant Physiology* 166(3): 1359–1370.

Cai G and Cresti M (2012) Are kinesins required for organelle trafficking in plant cells? *Frontiers in Plant Science* 3: 170.

Chang L and Goldman RD (2004) Intermediate filaments mediate cytoskeletal crosstalk. *Nature Reviews. Molecular Cell Biology* 5(8): 601–613.

Chen J, Doyle C, Qi X and Zheng H (2012) The endoplasmic reticulum: a social network in plant cells. *Journal of Integrative Plant Biology* 54(11): 840–850.

Chen S, Novick P and Ferro-Novick S (2013) ER structure and function. *Current Opinion in Cell Biology* 25(4): 428–433.

Chen T, Wang X, von Wangenheim D, Zheng M, Šamaj J, Ji W and Lin J (2012) Probing and tracking organelles in living plant cells. *Protoplasma* 249 Suppl 2: 157-167.

Collings D (2008) Crossed-wires: interactions and cross-talk between the microtubule and microfilament networks in plants microtubules. In: Nick P *Plant microtubules* (2nd edition). Springer 11: 47–79.

Cranfill PJ, Sell BR, Baird MA, Allen JR, Lavagnino Z, de Gruiter HM, Kremers GJ, Davidson MW, Ustione A, Piston DW (2016) Quantitative assessment of fluorescent proteins. *Nature Methods* 13(7):557-62.

Crowell EF, Bischoff V, Desprez T, Rolland A, Stierhof YD, Schumacher K, Gonneau M, Hofte H and Vernhettes S (2009) Pausing of Golgi bodies on microtubules regulates secretion of cellulose synthase complexes in Arabidopsis. *Plant Cell* 21(4): 1141–54.

Cvrčková F (2013) Formins and membranes: anchoring cortical actin to the cell wall and beyond. *Frontiers in Plant Science* 4: 436

Day KJ, Staehelin LA and Glick BS (2013) A three-stage model of Golgi structure and function. *Histochemistry and cell biology* 140(3): 239–249.

daSilva LLP, Snapp EL, Denecke J, Lippincott-Schwartz J, Hawes C and Brandizzi F (2004) Endoplasmic reticulum export sites and Golgi bodies behave as single mobile secretory units in plant cells. *The Plant cell* 16(7): 1753–1771.

De Meyer T, Muyldermans S and Depicker A (2014) Nanobody-based products as research and diagnostic tools. *Trends in biotechnology* 32(5):263-270

Deeks MJ, Fendrych M, Smertenko A, Bell KS, Oparka K, Cvrckova F, Zarsky V and Hussey PJ (2010) The plant formin AtFH4 interacts with both actin and microtubules, and contains a newly identified

microtubule-binding domain. *J Cell Sci* 123(Pt 8): 1209–1215.

Desai A and Mitchison TJ (1997) Microtubule polymerization dynamics. *Annual Review of Cell Developmental Biology* 13: 83–117.

Desmyter A, Transue TR, Ghahroudi MA, Thi MH, Poortmans F, Hamers R, Muyldermans S and Wyns L (1996) Crystal structure of a camel single-domain VH antibody fragment in complex with lysozyme. *Nature Structural Biology* 3(9): 803–811.

Desnos C, Huet S and Darchen F (2007) 'Should I stay or should I go? Myosin V function in organelle trafficking. *Biology of the Cell* 99(8): 411–423.

Dixit R (2012) Putting a bifunctional motor to work: insights into the role of plant KCH kinesins. *New Phytologist* 193(3): 543–545.

Dominguez R and Holmes KC (2011) Actin structure and function. *Annual Review of Biophysics* 40: 169–186.

Donaldson JG, Finazzi D and Klausner RD (1992) Brefeldin A inhibits Golgi membrane-catalysed exchange of guanine nucleotide onto ARF protein. *Nature* 360(6402): 350–352.

Donohoe BS, Kang B-H and Staehelin LA (2007) Identification and characterization of COPIa- and COPIb-type vesicle classes associated with plant and algal Golgi. *Proceedings of the National Academy of Sciences of the United States of America* 104(1): 163–168.

Drakakaki G and Dandekar A (2013) Protein secretion: how many secretory routes does a plant cell have? *Plant science* 203–204: 74–78.

Dröscher A (1998) Camillo Golgi and the discovery of the Golgi apparatus. *Histochemistry and Cell Biology* 109(5-6): 425–430.

Ems-McClung SC and Walczak CE (2010) Kinesin 13s in mitosis: key players in the spatial and temporal organization of spindle microtubules. *Seminars in cell & developmental biology* 21(3): 276–282.

Erhardt M, Stoppin-Mellet V, Campagne S, Canaday J, Mutterer J, Fabian T, Sauter M, Muller T, Peter C, Lambert AM and Schmit AC (2002) The plant Spc98p homologue colocalizes with gamma-tubulin at microtubule nucleation sites and is required for microtubule nucleation. *Journal of Cell Science* 115(Pt 11): 2423–31.

Fletcher DA and Mullins RD (2010) Cell mechanics and the cytoskeleton. *Nature* 463(7280): 485–92.

Foresti O and Denecke J (2008) Intermediate organelles of the plant secretory pathway: identity and function. *Traffic* 9(10): 1599–1612.

de Forges H, Bouissou A and Perez F (2011) Interplay between microtubule dynamics and intracellular organization. *International Journal of Biochemisty & Cell Biology* 44(2): 266–74.

Foth BJ, Goedecke MC and Soldati D (2006) New insights into myosin evolution and classification. *Proceedings of the National Academy of Sciences of the United States of America* 103(10): 3681–3686.

Frey N, Klotz J and Nick P (2009) Dynamic bridges—a calponin-domain kinesin from rice links actin filaments and microtubules in both cycling and non-cycling cells. *Plant and Cell Physiology* 50(8): 1493–1506.

Freund R and Wilson W (2003) *Statistical methods* (2nd edition). Academy Press.

Fujikura U, Elsaesser L, Breuninger H, Sánchez-Rodríguez C,

Ivakov A, Laux T, Findlay K, Persson S and Lenhard M (2014) Atkinesin-13A Modulates Cell-Wall Synthesis and Cell Expansion in *Arabidopsis thaliana* via the THESEUS1 Pathway. *PLoS Genetics* 10(9): e1004627.

Galili G, Sengupta-Gopalan C and Ceriotti A (1998) The endoplasmic reticulum of plant cells and its role in protein maturation and biogenesis of oil bodies. *Plant Molecular Biology* 38(1–2): 1–29.

Gao H, Metz J, Teanby NA, Ward AD, Botchway SW, Coles B, Pollard MR and Sparkes I (2016) *In vivo* quantification of peroxisome tethering to chloroplasts in tobacco epidermal cells using optical tweezers. *Plant Physiology* 170(1): 263–272.

Golomb L, Abu-Abied M, Belausov E and Sadot E (2008) Different subcellular localizations and functions of Arabidopsis myosin VIII. *BMC plant biology* 8: 3.

Grefen C and Blatt MR (2008) SNAREs-molecular governors in signalling and development. *Current Opinion in Plant Biology* 11(6): 600–609.

Griffing LR, Gao HT and Sparkes I (2014) ER network dynamics are differentially controlled by myosins XI-K, XI-C, XI-E, XI-I, XI-1, and XI-2. *Frontiers in Plant Science* 5:218

Gurtovenko AA and Anwar J (2007) Modulating the structure and properties of cell membranes: the molecular mechanism of action of dimethyl sulfoxide. *The journal of physical chemistry. B* 111(35): 10453–10460.

Haigler CH and Jr RMB (1986) Transport of rosettes from the Golgi apparatus to the plasma membrane in isolated mesophyll cells of *Zinnia elegans* during differentiation to tracheary elements in suspension culture. *Protoplasma* 134(2–3): 111–120.

Hamada T, Tominaga M, Fukaya T, Nakamura M, Nakano A, Watanabe Y, Hashimoto T and Baskin TI (2012) RNA processing bodies, peroxisomes, Golgi bodies, mitochondria, and endoplasmic reticulum tubule junctions frequently pause at cortical microtubules. *Plant Cell Physiology* 53(4): 699–708.

Hamada T, Ueda H, Kawase T and Hara-Nishimura I (2014) Microtubules contribute to tubule elongation and anchoring of endoplasmic reticulum, resulting in high network complexity in Arabidopsis. *Plant Physiology* 166(4): 1869–1876.

Hanton SL, Matheson LA, Chatre L and Brandizzi F (2009) Dynamic organization of COPII coat proteins at endoplasmic reticulum export sites in plant cells. *The Plant Journal* 57(6): 963–974.

Harries PA, Park J-W, Sasaki N, Ballard KD, Maule AJ and Nelson RS (2009) Differing requirements for actin and myosin by plant viruses for sustained intercellular movement. *Proceedings of the National Academy of Sciences of the United States of America* 106(41): 17594–17599.

Hashimoto T (2015) Microtubules in Plants. *The Arabidopsis Book* 13:e0179.

Hawes C (2012) The ER/Golgi interface: is there anything inbetween? *Frontiers in Plant Science* 3: 73.

Henty-Ridilla JL, Li J, Blanchoin L and Staiger CJ (2013) Actin dynamics in the cortical array of plant cells. *Current opinion in Plant Biology* 16(6): 678–687.

Higaki T, Sano T and Hasezawa S (2007) Actin microfilament dynamics and actin side-binding proteins in plants. *Current opinion in Plant Biology* 10(6): 549–556.

Hirokawa N and Noda Y (2008) Intracellular transport and kinesin superfamily proteins, KIFs: structure, function, and dynamics. *Physiological Reviews* 88(3): 1089–1118.

van der Honing HS, van Bezouwen LS, Emons AMC and Ketelaar T (2010) High expression of Lifeact in *Arabidopsis thaliana* reduces dynamic reorganization of actin filaments but does not affect plant development. *Cytoskeleton* 68(10): 578–587.

Horgan CP and McCaffrey MW (2011) Rab GTPases and microtubule motors. *Biochemical Society Transactions* 39(5): 1202–6.

Hughes ZE, Mark AE and Mancera RL (2012) Molecular dynamics simulations of the interactions of DMSO with DPPC and DOPC phospholipid membranes. *The Journal of Physical Chemistry. B* 116(39): 11911–11923.

Hwang I and Robinson DG (2009) Transport vesicle formation in plant cells. *Current Opinion in Plant Biology* 12(6): 660–669.

Kang B-H and Staehelin LA (2008) ER-to-Golgi transport by COPII vesicles in Arabidopsis involves a ribosome-excluding scaffold that is transferred with the vesicles to the Golgi matrix. *Protoplasma* 234(1–4): 51–64.

Ketelaar T, Allwood EG, Anthony R, Voigt B, Menzel D and Hussey PJ (2004) The actin-interacting protein AIP1 is essential for actin organization and plant development. *Current Biology* 14(2): 145–149.

King SM (2000) The dynein microtubule motor. *Biochimica et Biophysica Acta* 1496(1): 60–75.

Kitchen CMR (2009) Nonparametric versus parametric tests of location in biomedical research. *American Journal of Ophthalmology*

147(4): 571–572.

Klausner RD, Donaldson JG and Lippincott-Schwartz J (1992) Brefeldin A: insights into the control of membrane traffic and organelle structure. *The Journal of Cell Biology* 116(5): 1071–1080.

Klumperman J (2011) Architecture of the mammalian Golgi. *Cold Spring Harbor Perspectives in Biology* 3(7):a005181.

Kollman JM, Merdes A, Mourey L and Agard DA (2011) Microtubule nucleation by gamma-tubulin complexes. *Nature Review in Molecular Cell Biol*ogy 12(11): 709–721.

Kong S-G and Wada M (2014) Recent advances in understanding the molecular mechanism of chloroplast photorelocation movement. *Biochimica et Biophysica Acta* 1837(4): 522–530.

Koretz JF (1979) Structural studies of synthetic filaments prepared from column-purified myosin. *Biophysical Journal* 27(3): 423–432.

Kriechbaumer V, Botchway SW, Slade SE, Knox K, Frigerio L, Oparka K and Hawes C (2015) Reticulomics: protein-protein interaction studies with two plasmodesmata-localized reticulon family proteins identify binding partners enriched at plasmodesmata, endoplasmic reticulum, and the plasma membrane. *Plant Physiology* 169(3): 1933–1945.

Ladt K, Ganguly A, Roy S (2016) Axonal actin in action: imaging actin dynamics in neurons. *Methods Cell Biology* 131:91-106

Landau S and Everitt B (2004) *A handbook of statistical analyses using SPSS*. Boca Raton: Chapman & Hall/CRC.

Langhans M, Hawes C, Hillmer S, Hummel E and Robinson DG (2007) Golgi regeneration after Brefeldin A treatment in BY-2 cells entails stack enlargement and cisternal growth followed by division. *Plant Physiology* 145(2): 527–538.

Langhans M, Niemes S, Pimpl P and Robinson DG (2009) Oryzalin bodies: in addition to its anti-microtubule properties, the dinitroaniline herbicide oryzalin causes nodulation of the endoplasmic reticulum. *Protoplasma* 236(1–4): 73–84.

Langhans M, Meckel T, Kress A, Lerich A and Robinson DG (2012) ERES (ER exit sites) and the 'secretory unit concept'. *Journal of Microscopy* 247(1): 48–59.

Lawrence CJ, Dawe RK, Christie KR, Cleveland DW, Dawson SC, Endow SA, Goldstein LSB, Goodson HV, Hirokawa N, Howard J, Malmberg RL, McIntosh JR, Miki H, Mitchison TJ, Okada Y, Reddy ASN, Saxton WM, Schliwa M, Scholey JM, Vale RD, Walczak CE and Wordeman L (2004) A standardized kinesin nomenclature. *The Journal of Cell Biology* 167(1): 19–22.

Ledbetter MC and Porter KR (1964) Morphology of microtubules of plant cell. *Science* 144(3620): 872–874.

Lee YR and Liu B (2004) Cytoskeletal motors in Arabidopsis. Sixty-one kinesins and seventeen myosins. *Plant Physiology* 136(4): 3877–83.

Lee Y-RJ, Giang HM and Liu B (2001) A novel plant kinesin-related protein specifically associates with the phragmoplast organelles. *The Plant Cell* 13(11): 2427–2440.

Lee L-Y and Gelvin SB (2008) T-DNA binary vectors and systems. *Plant Physiology* 146(2): 325–332.

Lemieux MG, Janzen D, Hwang R, Roldan J, Jarchum I and Knecht DA (2013) Visualization of the actin cytoskeleton: different F-actin-binding probes tell different stories. *Cytoskeleton* 71 (3): 157-169.

Lerich A, Hillmer S, Langhans M, Scheuring D, van Bentum P and Robinson DG (2012) ER import sites and their relationship to ER exit sites: a new model for bidirectional ER-Golgi transport in higher plants. *Frontiers in plant science* 3: 143.

Li J-F and Nebenführ A (2008) The tail that wags the dog: the globular tail domain defines the function of myosin V/XI. *Traffic* 9(3): 290–298.

Limpert E, Stahel WA and Abbt M (2001) Log-normal distributions across the sciences: keys and clues. *BioScience* 51(5): 341–352.

Lloyd C (2011) Dynamic microtubules and the texture of plant cell walls. *Intrnational Review of Cell and Molecular Biology* 287: 287–329.

Lowey S, Waller GS and Bandman E (1991) Neonatal and adult myosin heavy chains form homodimers during avian skeletal muscle development. *The Journal of Cell Biology* 113(2): 303–310.

Lu L, Lee YR, Pan R, Maloof JN and Liu B (2005) An internal motor kinesin is associated with the Golgi apparatus and plays a role in trichome morphogenesis in Arabidopsis. *Molecular Biology of the Cell* 16(2): 811–23.

MacGregor WS (1967) The chemical and physical properties of DMSO. *Annals of the New York Academy of Sciences* 141(1 Biological Ac): 3–12.

Madison SL, Buchanan ML, Glass JD, McClain TF, Park E and

Nebenführ A (2015) Class XI myosins move specific organelles in pollen tubes and are required for normal fertility and pollen tube growth in Arabidopsis. *Plant Physiology* 169(3): 1946–1960.

Martinière A, Gayral P, Hawes C and Runions J (2011) Building bridges: formin1 of Arabidopsis forms a connection between the cell wall and the actin cytoskeleton. *The Plant Journal* 66(2): 354–365.

Matsuda T and Nagai T (2014) Quantitative measurement of intracellular protein dynamics using photobleaching or photoactivation of fluorescent proteins. *Microscopy* 63(6): 403–408.

Mathur J, Radhamony R, Sinclair AM, Donoso A, Dunn N, Roach E, Radford D, Mohaghegh PS, Logan DC, Kokolic K and Mathur N (2010) mEosFP-based green-to-red photoconvertible subcellular probes for plants. *Plant Physiol*ogy 154(4): 1573–87.

Mattila PK, Batista FD and Treanor B (2016) Dynamics of the actin cytoskeleton mediates receptor cross talk: an emerging concept in tuning receptor signaling. *The Journal of Cell Biology* 212(3): 267–280.

Mazzarello P, Garbarino C and Calligaro A (2009) How Camillo Golgi became 'the Golgi'. *FEBS Letters* 583(23): 3732–3737.

Mimori-Kiyosue Y (2011) Shaping microtubules into diverse patterns: molecular connections for setting up both ends. *Cytoskeleton* 68(11): 603–18.

Miart F, Desprez T, Biot E, Morin H, Belcram K, Höfte H, Gonneau M, Vernhettes S (2014) Spatio-temporal analysis of cellulose synthesis during cell plate formation in Arabidopsis. Plant Journal 77(1):71-84

Mitchison TJ, Nguyen P, Coughlin M and Groen AC (2013) Self-organization of stabilized microtubules by both spindle and midzone mechanisms in Xenopus egg cytosol. *Molecular biology of the cell* 24(10):

1559–1573.

Mizuno K (1985) *In vitro* assembly of microtubules from tubulins of several higher plants. *Cell biology international reports* 9(1): 13–21.

Moreau P, Brandizzi F, Hanton S, Chatre L, Melser S, Hawes C and Satiat-Jeunemaitre B (2007) The plant ER-Golgi interface: a highly structured and dynamic membrane complex. *Journal of Experimental Botany* 58(1): 49–64.

Morton WM, Ayscough KR and McLaughlin PJ (2000) Latrunculin alters the actin-monomer subunit interface to prevent polymerization. *Nature Cell Biology* 2(6): 376–378.

Munro S (2011) The golgin coiled-coil proteins of the Golgi apparatus. *Cold Spring Harb Perspect Biol* 3(6): a005256.

Murata T and Hasebe M (2007) Microtubule-dependent microtubule nucleation in plant cells. *Journal Plant Research* 120(1): 73–8.

Muyldermans S (2001) Single domain camel antibodies: current status. *Journal of Biotechnology* 74(4): 277–302.

Nebenführ A, Gallagher LA, Dunahay TG, Frohlick JA, Mazurkiewicz AM, Meehl JB and Staehelin LA (1999) Stop-and-go movements of plant Golgi stacks are mediated by the acto-myosin system. *Plant Physiology* 121(4): 1127–42.

Nebenführ A and Staehelin LA (2001) Mobile factories: Golgi dynamics in plant cells. *Trends in Plant Science* 6(4): 160–7.

Neto H, Collins LL and Gould GW (2011) Vesicle trafficking and membrane remodelling in cytokinesis. *Biochemical Journal* 437(1): 13–

24.

Neuman KC and Block SM (2004) Optical trapping. *The Review of scientific instruments* 75(9): 2787–2809.

Nogales E, Whittaker M, Milligan RA and Downing KH (1999) High-resolution model of the microtubule. *The Cell* 96(1): 79–88.

Noma A, Yi S, Katoh T, Takai Y, Suzuki T and Suzuki T (2011) Actin-binding protein ABP140 is a methyltransferase for 3-methylcytidine at position 32 of tRNAs in Saccharomyces cerevisiae. *RNA* 17(6): 1111–1119.

Oda Y and Fukuda H (2013) Rho of plant GTPase signaling regulates the behavior of Arabidopsis kinesin-13A to establish secondary cell wall patterns. *The Plant Cell* 25(11): 4439–4450.

Ohta K, Seo N, Yoshida T, Hiraga K and Tuboi S (1987) Tubulin and high molecular weight microtubule-associated proteins as endogenous substrates for protein carboxymethyltransferase in brain. *Biochimie* 69(11–12): 1227–1234.

Ojangu E-L, Tanner K, Pata P, Järve K, Holweg CL, Truve E and Paves H (2012) Myosins XI-K, XI-1, and XI-2 are required for development of pavement cells, trichomes, and stigmatic papillae in Arabidopsis. *BMC Plant Biology* 12: 81.

Olek AT, Rayon C, Makowski L, Kim HR, Ciesielski P, Badger J, Paul LN, Ghosh S, Kihara D, Crowley M, Himmel ME, Bolin JT and Carpita NC (2014) The structure of the catalytic domain of a plant cellulose synthase and its assembly into dimers. *The Plant Cell* 26(7): 2996–3009.

Olichon A and Surrey T (2007) Selection of genetically encoded fluorescent single domain antibodies engineered for efficient expression in *Escherichia coli*. *The Journal of Biological Chemistry* 282(50): 36314–

36320.

Olmsted JB and Borisy GG (1973) Microtubules. *Annual Review of Biochemistry* 42: 507–540.

O'Rourke BP, Gomez-Ferreria MA, Berk RH, Hackl AMU, Nicholas MP, O'Rourke SC, Pelletier L and Sharp DJ (2014) Cep192 controls the balance of centrosome and non-centrosomal microtubules during interphase. *PloS One* 9(6): e101001.

Osterrieder A (2012) Tales of tethers and tentacles: golgins in plants. *Journal of Microscopy* 247(1): 68–77.

Panteris E, Adamakis I-DS, Daras G, Hatzopoulos P and Rigas S (2013) Differential responsiveness of cortical microtubule orientation to suppression of cell expansion among the developmental zones of *Arabidopsis thaliana* root apex. *PloS One* 8(12): e82442.

Panza P, Maier J, Schmees C, Rothbauer U and Söllner C (2015) Live imaging of endogenous protein dynamics in zebrafish using chromobodies. *Development* 142(10): 1879–1884.

Park E and Nebenführ A (2013) Myosin XIK of *Arabidopsis thaliana* accumulates at the Root Hair Tip and Is Required for Fast Root Hair Growth. *PLOS ONE* 8(10): e76745.

Parr AJ, Robins RJ and Rhodes MJ (1984) Permeabilization of *Cinchona ledgeriana* cells by dimethylsulphoxide. Effects on alkaloid release and long-term membrane integrity. *Plant cell reports* 3(6): 262–265.

Pavin N and Tolić IM (2016) Self-organization and forces in the mitotic spindle. *Annual Review of Biophysics* 45: 279-298.

Peremyslov VV, Klocko AL, Fowler JE and Dolja VV (2012)

Arabidopsis myosin XI-K localizes to the motile endomembrane vesicles associated with F-actin. *Plant Cell Biology* 3: 184.

Peremyslov VV, Mockler TC, Filichkin SA, Fox SE, Jaiswal P, Makarova KS, Koonin EV and Dolja VV (2011) Expression, splicing, and evolution of the myosin gene family in plants. *Plant Physiology* 155(3): 1191–1204.

Peremyslov VV, Prokhnevsky AI and Dolija VV (2010) Class XI myosins are required for development, cell expansion, and F-actin organization in Arabidopsis. *The Plant Cell* 22(6): 1883-1897

Peremyslov VV, Prokhnevsky AI, Avisar D and Dolja VV (2008) Two class XI myosins function in organelle trafficking and root hair development in Arabidopsis. *Plant Physiology* 146(3): 1109–1116.

Petrasek J and Schwarzerova K (2009) Actin and microtubule cytoskeleton interactions. *Current Opinion in Plant Biol*ogy 12(6): 728–34.

Pimpl P, Movafeghi A, Coughlan S, Denecke J, Hillmer S and Robinson DG (2000) *In situ* localization and *in vitro* induction of plant COPI-coated vesicles. *The Plant Cell* 12(11): 2219–2236.

Porter K and Day B (2016) From filaments to function: the role of the plant actin cytoskeleton in pathogen perception, signaling and immunity.
Jo*urnal of Integrative Plant Biology* 58(4):299-311.

Prokhnevsky AI, Peremyslov VV and Dolja VV (2005) Actin cytoskeleton is involved in targeting of a viral Hsp70 homolog to the cell periphery. *Journal of Virology* 79(22): 14421–14428.

Prokhnevsky AI, Peremyslov VV and Dolja VV (2008) Overlapping functions of the four class XI myosins in Arabidopsis

growth, root hair elongation, and organelle motility. *Proceedings of the National Academy of Sciences* 105(50): 19744–19749.

Puhka M, Vihinen H, Joensuu M and Jokitalo E (2007) Endoplasmic reticulum remains continuous and undergoes sheet-to-tubule transformation during cell division in mammalian cells. *The Journal of Cell Biology* 179(5): 895–909.

Quader H, Hofmann A and Schnepf E (1989) Reorganization of the endoplasmic reticulum in epidermal cells of onion bulb scales after cold stress: involvement of cytoskeletal elements. *Planta* 177(2): 273–280.

Rammler DH and Zaffaroni A (1967) Biological implications of DMSO based on a review of its chemical properties. *Annals of the New York Academy of Sciences* 141(1 Biological Ac): 13–23.

Reddy AS (2001) Molecular motors and their functions in plants. *International Review of Cytology* 204: 97–178.

Reddy AS and Day IS (2001) Kinesins in the Arabidopsis genome: a comparative analysis among eukaryotes. *BMC Genomics* 2: 2.

Riedl J, Crevenna AH, Kessenbrock K, Yu JH, Neukirchen D, Bista M, Bradke F, Jenne D, Holak TA, Werb Z, Sixt M and Wedlich-Soldner R (2008) Lifeact: a versatile marker to see F-actin. *Nature Methods* 5(7): 605–607.

Robinson DG, Brandizzi F, Hawes C and Nakano A (2015) Vesicles versus tubes: is endoplasmic reticulum-Golgi transport in plants fundamentally different from other eukaryotes? *Plant Physiology* 168(2): 393–406.

Robinson DG, Herranz M-C, Bubeck J, Pepperkok R and Ritzenthaler C (2007) Membrane dynamics in the early secretory

pathway. *Critical Reviews in Plant Sciences* 26(4): 199–225.

Rocchetti A, Hawes C and Kriechbaumer V (2014) Fluorescent labelling of the actin cytoskeleton in plants using a cameloid antibody. *Plant Methods* 10:12.

Romagnoli S, Cai G and Cresti M (2003) *In vitro* assays demonstrate that pollen tube organelles use kinesin-related motor proteins to move along microtubules. *The Plant Cell* 15(1): 251–269.

Rothbauer U, Zolghadr K, Tillib S, Nowak D, Schermelleh L, Gahl A, Backmann N, Conrath K, Muyldermans S, Cardoso MC and Leonhardt H (2006) Targeting and tracing antigens in live cells with fluorescent nanobodies. *Nature methods* 3(11): 887–889.

Rothman JE (1996) The protein machinery of vesicle budding and fusion. *Protein Science : A Publication of the Protein Society* 5(2): 185–194.

Sackmann E (2015) How actin/myosin crosstalks guide the adhesion, locomotion and polarization of cells. *Biochimica et Biophysica Acta* 1853(11 Pt B): 3132–3142.

Saint Jore CM (2001) Green fluorescent protein to study Golgi apparatus dynamics. PhD. Oxford Brookes.

Saint-Jore CM, Evins J, Batoko H, Brandizzi F, Moore I and Hawes C (2002) Redistribution of membrane proteins between the Golgi apparatus and endoplasmic reticulum in plants is reversible and not dependent on cytoskeletal networks. *The Plant Journal* 29(5): 661–678.

Sampathkumar A, Lindeboom JJ, Debolt S, Gutierrez R, Ehrhardt DW, Ketelaar T and Persson S (2011) Live cell imaging reveals structural associations between the actin and microtubule cytoskeleton in Arabidopsis. *Plant Cell* 23(6): 2302–13.

Sanders AAWM and Kaverina I (2015) Nucleation and dynamics of Golgi-derived microtubules. *Frontiers in Neuroscience* 9: 431.

Sato Y, Wada M and Kadota A (2001) Choice of tracks, microtubules and/or actin filaments for chloroplast photo-movement is differentially controlled by phytochrome and a blue light receptor. *Journal of Cell Science* 114(2): 269–279.

Schneider R and Persson S (2015) Connecting two arrays: the emerging role of actin-microtubule cross-linking motor proteins. *Frontiers in Plant Science* 6:415

Sciuchetti LA (1967) The effects of DMSO alone and when combined with various growth regulators on the growth regulators in the growth and metabolic products of *Datura* spp. *Annals of the New York Academy of Sciences* 141(1 Biological Ac): 139–147.

Seabra MC and Coudrier E (2004) Rab GTPases and myosin motors in organelle motility. *Traffic* 5(6): 393–399.

Sellers JR (2000) Myosins: a diverse superfamily. *Biochimica et Biophysica Acta* 1496(1): 3–22.

Sellers JR and Knight PJ (2007) Folding and regulation in myosins II and V. *Journal of Muscle Research and Cell Motility* 28(7–8): 363–370.

Sens P and Plastino J (2015) Membrane tension and cytoskeleton organization in cell motility. *Journal of Physics* 27(27): 273103.

Seog D-H, Lee D-H and Lee S-K (2004) Molecular motor proteins of the kinesin superfamily proteins (KIFs): structure, cargo and disease. *Journal of Korean Medical Science* 19(1): 1–7.

Sheahan MB, Staiger CJ, Rose RJ and McCurdy DW (2004) A green fluorescent protein fusion to actin-binding domain 2 of Arabidopsis fimbrin highlights new features of a dynamic actin cytoskeleton in live plant cells. *Plant Physiology* 136(4): 3968–3978.

Shimmen T and Yokota E (2004) Cytoplasmic streaming in plants. *Current Opinion in Cell Biology* 16(1): 68–72.

Short B, Haas A and Barr FA (2005) Golgins and GTPases, giving identity and structure to the Golgi apparatus. *Biochimica et Biophysica Acta (BBA) - Molecular Cell Research* 1744(3): 383–395.

Sinka R, Gillingham AK, Kondylis V and Munro S (2008) Golgi coiled-coil proteins contain multiple binding sites for Rab family G proteins. *The Journal of Cell Biology* 183(4): 607–615.

Sonobe S and Shibaoka H (1989) Cortical fine actin filaments in higher plant cells visualized by rhodamine-phalloidin after pretreatment with m-maleimidobenzoyl N-hydroxysuccinimide ester. *Protoplasma* 148(2–3): 80–86.

Sparkes IA, Runions J, Kearns A and Hawes C (2006) Rapid, transient expression of fluorescent fusion proteins in tobacco plants and generation of stably transformed plants. *Nature Protocol* 1(4): 2019–25.

Sparkes IA and Brandizzi F (2012) Fluorescent protein-based technologies: shedding new light on the plant endomembrane system. *Plant Journal* 70(1): 96–107.

Sparkes IA (2011a) Recent advances in understanding plant myosin function: life in the fast lane. *Molecular Plant* 4(5): 805–12.

Sparkes IA, Hawes C and Frigerio L (2011b) FrontiERs: movers and shapers of the higher plant cortical endoplasmic reticulum. *Current*

*Opinion in Plant Biology* 14(6): 658–65.

Sparkes I, Tolley N, Aller I, Svozil J, Osterrieder A, Botchway S, Mueller C, Frigerio L and Hawes C (2010a) Five Arabidopsis reticulon isoforms share endoplasmic reticulum location, topology, and membrane-shaping properties. *The Plant Cell* 22(4): 1333–1343.

Sparkes IA (2010b) Motoring around the plant cell: insights from plant myosins. *Biochemical Society Transactions* 38(3): 833–8.

Sparkes IA, Runions J, Hawes C and Griffing L (2009a) Movement and remodeling of the endoplasmic reticulum in nondividing cells of tobacco leaves. *The Plant Cell* 21(12): 3937–3949.

Sparkes IA, Ketelaar T, de Ruijter NC and Hawes C (2009b) Grab a Golgi: laser trapping of Golgi bodies reveals in vivo interactions with the endoplasmic reticulum. *Traffic* 10(5): 567–71.

Sparkes IA, Teanby NA and Hawes C (2008) Truncated myosin XI tail fusions inhibit peroxisome, Golgi, and mitochondrial movement in tobacco leaf epidermal cells: a genetic tool for the next generation. *Journal of Experimental Botany* 59(9): 2499–2512.

Staehelin LA (1997) The plant ER: a dynamic organelle composed of a large number of discrete functional domains. *The Plant Journal* 11(6): 1151–1165.

Staehelin LA and Moore and I (1995) The plant Golgi apparatus: structure, functional organization and trafficking mechanisms. *Annual Review of Plant Physiology and Plant Molecular Biology* 46(1): 261–288.

Staiger CJ, Sheahan MB, Khurana P, Wang X, McCurdy DW and Blanchoin L (2009) Actin filament dynamics are dominated by rapid growth and severing activity in the Arabidopsis cortical array. *Journal of*

*Cell Biology* 184(2): 269–280.

Stanley P (2011) Golgi glycosylation. *Cold Spring Harbor Perspectives in Biology* 3(4): a005199

Stefano G, Renna L, Chatre L, Hanton SL, Moreau P, Hawes C and Brandizzi F (2006) In tobacco leaf epidermal cells, the integrity of protein export from the endoplasmic reticulum and of ER export sites depends on active COPI machinery. *The Plant Journal* 46(1): 95–110.

Stefano G, Hawes C and Brandizzi F (2014) ER - the key to the highway. *Current Opinion in Plant Biology* 22: 30–38.

Sztul E and Lupashin V (2006) Role of tethering factors in secretory membrane traffic. *American Journal of Physiology. Cell Physiology* 290(1): 11-26.

Takemoto D, Jones DA and Hardham AR (2003) GFP-tagging of cell components reveals the dynamics of subcellular re-organization in response to infection of Arabidopsis by oomycete pathogens. *The Plant Journal* 33(4): 775–792.

Tamura K, Fukao Y, Kondo M, Okamoto K, Ueda H, Nishimura M, Hara-Nishimura I (2013) Myosin XI-I linkes the nuclear membrane to the cytoskeleton to control nuclear movement and shape in Arabidopsis. *Current Biology* 23(18):1776-81.

Tian J, Han L, Feng Z, Wang G, Liu W, Ma Y, Yu Y and Kong Z (2015) Orchestration of microtubules and the actin cytoskeleton in trichome cell shape determination by a plant-unique kinesin. *eLife* 4: e09351.

Tolley N, Sparkes I, Craddock CP, Eastmond PJ, Runions J, Hawes C and Frigerio L (2010) Transmembrane domain length is responsible for the ability of a plant reticulon to shape endoplasmic reticulum tubules *in vivo*. *The Plant Journal* 64(3): 411–418.

Tominaga M and Ito K (2015) The molecular mechanism and physiological role of cytoplasmic streaming. *Current Opinion in Plant Biology* 27: 104–110.

Ueda H, Yokota E, Kutsuna N, Shimada T, Tamura K, Shimmen T, Hasezawa S, Dolja VV and Hara-Nishimura I (2010) Myosin-dependent endoplasmic reticulum motility and F-actin organization in plant cells. *Proceedings of the National Academy of Sciences of the United States of America* 107(15): 6894–6899.

Upton G and Cook I (2002) *A dictionary of statistics*. Oxford: Oxford University Press.

Van Gestel K, Köhler RH and Verbelen J-P (2002) Plant mitochondria move on F-actin, but their positioning in the cortical cytoplasm depends on both F-actin and microtubules. *Journal of Experimental Botany* 53(369): 659–667.

Vandekerckhove J, Deboben A, Nassal M and Wieland T (1985) The phalloidin binding site of F-actin. *The EMBO journal* 4(11): 2815–2818.

Vassileva VN, Kouchi H and Ridge RW (2005) Microtubule dynamics in living root hairs: transient slowing by lipochitin oligosaccharide nodulation signals. *The Plant Cell* 17(6): 1777–1787.

Voigt B, Timmers ACJ, Samaj J, Müller J, Baluska F and Menzel D (2005) GFP-FABD2 fusion construct allows in vivo visualization of the dynamic actin cytoskeleton in all cells of Arabidopsis seedlings. *European Journal of Cell Biology* 84(6): 595–608.

Vugrek O, Sawitzky H and Menzel D (2003) Class XIII myosins from the green alga Acetabularia: driving force in organelle transport and tip growth? *Journal of Muscle Research and Cell Motility* 24(1): 87–

97.

Wakatsuki T, Schwab B, Thompson NC and Elson EL (2001) Effects of cytochalasin D and latrunculin B on mechanical properties of cells. *Journal of Cell Science* 114(Pt 5): 1025–1036.

Walczak CE, Gayek S and Ohi R (2013) Microtubule-depolymerizing kinesins. *Annual Review of Cell and Developmental Biology* 29(1): 417–441.

Wang P, Hawkins TJ, Richardson C, Cummins I, Deeks MJ, Sparkes I, Hawes C and Hussey PJ (2014) The plant cytoskeleton, NET3C, and VAP27 mediate the link between the plasma membrane and endoplasmic reticulum. *Current biology* 24(12): 1397–1405.

Wang P and Hussey PJ (2015) Interactions between plant endomembrane systems and the actin cytoskeleton. *Frontiers in Plant Science* 6: 422

Ward TH, Polishchuk RS, Caplan S, Hirschberg K and Lippincott-Schwartz J (2001) Maintenance of Golgi structure and function depends on the integrity of ER export. *The Journal of Cell Biology* 155(4): 557–570.

Wei J-H and Seemann J (2010) Unraveling the Golgi ribbon. *Traffic* 11(11): 1391–1400.

Wei L, Zhang W, Liu Z and Li Y (2009) *At*Kinesin-13A is located on Golgi-associated vesicle and involved in vesicle formation/budding in Arabidopsis root-cap peripheral cells. *BMC plant biology* 9: 138.

Wickstead B and Gull K (2007) Dyneins across eukaryotes: a comparative genomic analysis. *Traffic* 8(12): 1708–1721.

Wood DC and Wood J (1975) Pharmacologic and biochemical

considerations of dimethyl solfoxide. *Annals of the New York Academy of Sciences* 243(1 Biological Ac): 7–19.

Woollard AAD and Moore I (2008) The functions of Rab GTPases in plant membrane traffic. *Current Opinion in Plant Biology* 11(6): 610–619.

Wright GD, Arlt J, Poon WCK and Read ND (2007) Optical tweezer micromanipulation of filamentous fungi. *Fungal genetics and biology* 44(1): 1–13.

Wu S-Z and Bezanilla M (2014) Myosin VIII associates with microtubule ends and together with actin plays a role in guiding plant cell division. *eLife* 3: 03498.

Xu Y, Takeda S, Nakata T, Noda Y, Tanaka Y and Hirokawa N (2002) Role of KIFC3 motor protein in Golgi positioning and integration. *The Journal of Cell Biology* 158(2): 293–303.

Yang X-Y, Chen Z-W, Xu T, Qu Z, Pan X-D, Qin X-H, Ren D-T and Liu G-Q (2011) Arabidopsis kinesin KP1 specifically interacts with VDAC3, a mitochondrial protein, and regulates Respiration during seed germination at low temperature. *The Plant Cell* 23(3): 1093–1106.

Yubuki N and Leander BS (2013) Evolution of microtubule organizing centers across the tree of eukaryotes. *Plant Journal* 75(2): 230–244.

Zhu C, Ganguly A, Baskin TI, McClosky DD, Anderson CT, Foster C, Meunier KA, Okamoto R, Berg H and Dixit R (2015) The fragile fiber1 kinesin contributes to cortical microtubule-mediated trafficking of cell wall components. *Plant Physiology* 167(3): 780–792.

# Appendix I

## Example of SPSS original output

**Case Processing Summary**

| | | Cases | | | | | |
|---|---|---|---|---|---|---|---|
| | | Valid | | Missing | | Total | |
| | Vel.48h.notreat.dmso.rep1.code | N | Percent | N | Percent | N | Percent |
| Vel.48h.notreat.dmso.rep1 | no treat | 129 | 100.0% | 0 | 0.0% | 129 | 100.0% |
| | dmso 10 ul/ml | 198 | 100.0% | 0 | 0.0% | 198 | 100.0% |

**Descriptives**

| | Vel.48h.notreat.dmso.rep1.code | | | Statistic | Std. Error |
|---|---|---|---|---|---|
| Vel.48h.notreat.dmso.rep1 | no treat | Mean | | .6093 | .04331 |
| | | 95% Confidence Interval for Mean | Lower Bound | .5236 | |
| | | | Upper Bound | .6950 | |
| | | 5% Trimmed Mean | | .5485 | |
| | | Median | | .4400 | |
| | | Variance | | .242 | |
| | | Std. Deviation | | .49186 | |
| | | Minimum | | .12 | |
| | | Maximum | | 3.17 | |
| | | Range | | 3.05 | |
| | | Interquartile Range | | .53 | |
| | | Skewness | | 2.330 | .213 |
| | | Kurtosis | | 7.483 | .423 |
| | dmso 10 ul/ml | Mean | | .5296 | .03372 |
| | | 95% Confidence Interval for Mean | Lower Bound | .4631 | |
| | | | Upper Bound | .5961 | |
| | | 5% Trimmed Mean | | .4615 | |
| | | Median | | .3750 | |
| | | Variance | | .225 | |
| | | Std. Deviation | | .47442 | |
| | | Minimum | | .07 | |
| | | Maximum | | 3.65 | |
| | | Range | | 3.58 | |
| | | Interquartile Range | | .37 | |
| | | Skewness | | 3.133 | .173 |
| | | Kurtosis | | 13.185 | .344 |

**Tests of Normality**

| | | Kolmogorov-Smirnov[a] | | | Shapiro-Wilk | | |
|---|---|---|---|---|---|---|---|
| | Vel.48h.notreat.dmso.rep1.code | Statistic | df | Sig. | Statistic | df | Sig. |
| Vel.48h.notreat.dmso.rep1 | no treat | .177 | 129 | .000 | .775 | 129 | .000 |
| | dmso 10 ul/ml | .193 | 198 | .000 | .681 | 198 | .000 |

a. Lilliefors Significance Correction

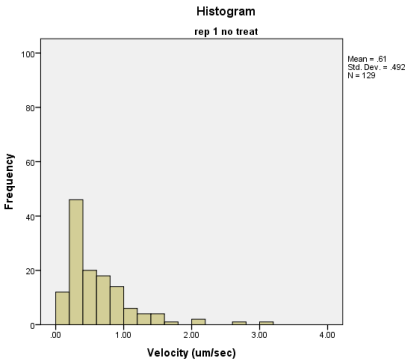


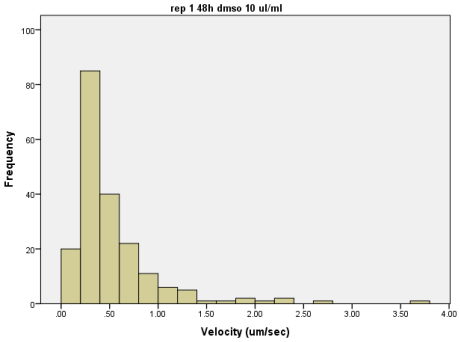


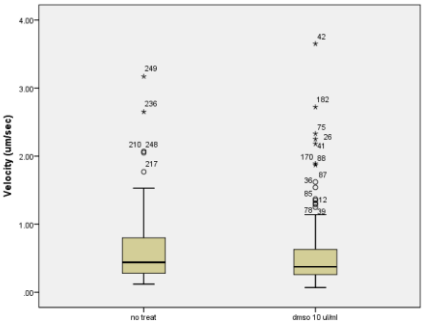


**Hypothesis Test Summary**

| | Null Hypothesis | Test | Sig. | Decision |
|---|---|---|---|---|
| 1 | The distribution of Vel.48h.notreat.dmso.rep1 is the same across categories of Vel.48h.notreat.dmso.rep1.code. | Independent-Samples Mann-Whitney U Test | .058 | Retain the null hypothesis. |
| 2 | The distribution of Vel.48h.notreat.dmso.rep1 is the same across categories of Vel.48h.notreat.dmso.rep1.code. | Independent-Samples Kolmogorov-Smirnov Test | .070 | Retain the null hypothesis. |

Asymptotic significances are displayed. The significance level is .05.

**Hypothesis Test Summary**

| | Null Hypothesis | Test | Sig. | Decision |
|---|---|---|---|---|
| 1 | The distribution of Vel.48h.dmso.LatB is the same across categories of Vel.48h.dmso.LatB.code. | Independent-Samples Mann-Whitney U Test | .000 | Reject the null hypothesis. |
| 2 | The distribution of Vel.48h.dmso.LatB is the same across categories of Vel.48h.dmso.LatB.code. | Independent-Samples Kolmogorov-Smirnov Test | .001 | Reject the null hypothesis. |

Asymptotic significances are displayed. The significance level is .05.

# Appendix II

**Example of frequency tables to generate CDF plots.**

**Statistics**

| | | Vel.48h.LatB | Vel.48h.rep1.dmso |
|---|---|---|---|
| N | Valid | 88 | 198 |
| | Missing | 303 | 193 |
| Mode | | .27 | .25 |

**Vel.48h.LatB**

| | | Frequency | Percent | Valid Percent | Cumulative Percent |
|---|---|---|---|---|---|
| Valid | .13 | 3 | .8 | 3.4 | 3.4 |
| | .14 | 2 | .5 | 2.3 | 5.7 |
| | .15 | 4 | 1.0 | 4.5 | 10.2 |
| | .16 | 1 | .3 | 1.1 | 11.4 |
| | .17 | 2 | .5 | 2.3 | 13.6 |
| | .18 | 3 | .8 | 3.4 | 17.0 |
| | .19 | 4 | 1.0 | 4.5 | 21.6 |
| | .20 | 1 | .3 | 1.1 | 22.7 |
| | .21 | 3 | .8 | 3.4 | 26.1 |
| | .22 | 5 | 1.3 | 5.7 | 31.8 |
| | .23 | 2 | .5 | 2.3 | 34.1 |
| | .24 | 2 | .5 | 2.3 | 36.4 |
| | .25 | 3 | .8 | 3.4 | 39.8 |
| | .26 | 1 | .3 | 1.1 | 40.9 |
| | .27 | 7 | 1.8 | 8.0 | 48.9 |
| | .28 | 2 | .5 | 2.3 | 51.1 |
| | .29 | 4 | 1.0 | 4.5 | 55.7 |
| | .30 | 3 | .8 | 3.4 | 59.1 |
| | .31 | 3 | .8 | 3.4 | 62.5 |
| | .32 | 2 | .5 | 2.3 | 64.8 |
| | .33 | 1 | .3 | 1.1 | 65.9 |
| | .34 | 2 | .5 | 2.3 | 68.2 |
| | .36 | 1 | .3 | 1.1 | 69.3 |
| | .37 | 1 | .3 | 1.1 | 70.5 |
| | .39 | 1 | .3 | 1.1 | 71.6 |
| | .44 | 1 | .3 | 1.1 | 72.7 |
| | .45 | 1 | .3 | 1.1 | 73.9 |
| | .46 | 1 | .3 | 1.1 | 75.0 |
| | .47 | 1 | .3 | 1.1 | 76.1 |
| | .48 | 3 | .8 | 3.4 | 79.5 |
| | .50 | 2 | .5 | 2.3 | 81.8 |
| | .52 | 2 | .5 | 2.3 | 84.1 |
| | .55 | 2 | .5 | 2.3 | 86.4 |
| | .56 | 1 | .3 | 1.1 | 87.5 |
| | .57 | 1 | .3 | 1.1 | 88.6 |
| | .59 | 2 | .5 | 2.3 | 90.9 |
| | .61 | 2 | .5 | 2.3 | 93.2 |
| | .68 | 1 | .3 | 1.1 | 94.3 |
| | .80 | 1 | .3 | 1.1 | 95.5 |
| | .82 | 1 | .3 | 1.1 | 96.6 |
| | .98 | 1 | .3 | 1.1 | 97.7 |
| | 1.02 | 1 | .3 | 1.1 | 98.9 |
| | 1.89 | 1 | .3 | 1.1 | 100.0 |
| | Total | 88 | 22.5 | 100.0 | |
| Missing | System | 303 | 77.5 | | |
| Total | | 391 | 100.0 | | |

**Vel.48h.rep1.dmso**

| | | Frequency | Percent | Valid Percent | Cumulative Percent |
|---|---|---|---|---|---|
| Valid | .07 | 1 | .3 | .5 | .5 |
| | .11 | 1 | .3 | .5 | 1.0 |
| | .12 | 2 | .5 | 1.0 | 2.0 |
| | .13 | 1 | .3 | .5 | 2.5 |
| | .16 | 4 | 1.0 | 2.0 | 4.5 |
| | .17 | 2 | .5 | 1.0 | 5.6 |
| | .18 | 5 | 1.3 | 2.5 | 8.1 |
| | .19 | 4 | 1.0 | 2.0 | 10.1 |
| | .20 | 5 | 1.3 | 2.5 | 12.6 |
| | .21 | 5 | 1.3 | 2.5 | 15.2 |
| | .22 | 5 | 1.3 | 2.5 | 17.7 |
| | .23 | 2 | .5 | 1.0 | 18.7 |
| | .24 | 2 | .5 | 1.0 | 19.7 |
| | .25 | 8 | 2.0 | 4.0 | 23.7 |
| | .26 | 5 | 1.3 | 2.5 | 26.3 |
| | .27 | 7 | 1.8 | 3.5 | 29.8 |
| | .28 | 5 | 1.3 | 2.5 | 32.3 |
| | .29 | 1 | .3 | .5 | 32.8 |
| | .30 | 4 | 1.0 | 2.0 | 34.8 |
| | .31 | 5 | 1.3 | 2.5 | 37.4 |
| | .32 | 6 | 1.5 | 3.0 | 40.4 |
| | .33 | 3 | .8 | 1.5 | 41.9 |
| | .34 | 6 | 1.5 | 3.0 | 44.9 |
| | .35 | 4 | 1.0 | 2.0 | 47.0 |
| | .36 | 3 | .8 | 1.5 | 48.5 |
| | .37 | 3 | .8 | 1.5 | 50.0 |
| | .38 | 5 | 1.3 | 2.5 | 52.5 |
| | .39 | 1 | .3 | .5 | 53.0 |
| | .40 | 3 | .8 | 1.5 | 54.5 |
| | .41 | 2 | .5 | 1.0 | 55.6 |
| | .42 | 1 | .3 | .5 | 56.1 |
| | .43 | 7 | 1.8 | 3.5 | 59.6 |
| | .44 | 2 | .5 | 1.0 | 60.6 |
| | .45 | 1 | .3 | .5 | 61.1 |
| | .46 | 1 | .3 | .5 | 61.6 |
| | .47 | 1 | .3 | .5 | 62.1 |
| | .48 | 1 | .3 | .5 | 62.6 |
| | .49 | 2 | .5 | 1.0 | 63.6 |
| | .50 | 4 | 1.0 | 2.0 | 65.7 |
| | .51 | 1 | .3 | .5 | 66.2 |
| | .53 | 3 | .8 | 1.5 | 67.7 |
| | .54 | 2 | .5 | 1.0 | 68.7 |
| | .55 | 3 | .8 | 1.5 | 70.2 |
| | .56 | 1 | .3 | .5 | 70.7 |
| | .57 | 1 | .3 | .5 | 71.2 |
| | .58 | 2 | .5 | 1.0 | 72.2 |
| | .59 | 2 | .5 | 1.0 | 73.2 |
| | .61 | 1 | .3 | .5 | 73.7 |
| | .62 | 2 | .5 | 1.0 | 74.7 |
| | .63 | 3 | .8 | 1.5 | 76.3 |
| | .64 | 1 | .3 | .5 | 76.8 |
| | .65 | 2 | .5 | 1.0 | 77.8 |
| | .66 | 3 | .8 | 1.5 | 79.3 |
| | .67 | 3 | .8 | 1.5 | 80.8 |
| | .68 | 1 | .3 | .5 | 81.3 |
| | .71 | 1 | .3 | .5 | 81.8 |
| | .72 | 2 | .5 | 1.0 | 82.8 |
| | .74 | 1 | .3 | .5 | 83.3 |
| | .76 | 1 | .3 | .5 | 83.8 |
| | .77 | 1 | .3 | .5 | 84.3 |
| | .80 | 1 | .3 | .5 | 84.8 |
| | .82 | 1 | .3 | .5 | 85.4 |
| | .86 | 2 | .5 | 1.0 | 86.4 |
| | .87 | 1 | .3 | .5 | 86.9 |
| | .89 | 2 | .5 | 1.0 | 87.9 |
| | .92 | 1 | .3 | .5 | 88.4 |
| | .93 | 1 | .3 | .5 | 88.9 |
| | .94 | 1 | .3 | .5 | 89.4 |
| | .95 | 1 | .3 | .5 | 89.9 |
| | 1.03 | 1 | .3 | .5 | 90.4 |
| | 1.07 | 1 | .3 | .5 | 90.9 |
| | 1.09 | 1 | .3 | .5 | 91.4 |
| | 1.10 | 2 | .5 | 1.0 | 92.4 |
| | 1.14 | 1 | .3 | .5 | 92.9 |
| | 1.25 | 1 | .3 | .5 | 93.4 |
| | 1.29 | 1 | .3 | .5 | 93.9 |
| | 1.31 | 1 | .3 | .5 | 94.4 |
| | 1.35 | 1 | .3 | .5 | 94.9 |
| | 1.37 | 1 | .3 | .5 | 95.5 |
| | 1.54 | 1 | .3 | .5 | 96.0 |
| | 1.62 | 1 | .3 | .5 | 96.5 |
| | 1.87 | 1 | .3 | .5 | 97.0 |
| | 1.89 | 1 | .3 | .5 | 97.5 |
| | 2.18 | 1 | .3 | .5 | 98.0 |
| | 2.25 | 1 | .3 | .5 | 98.5 |
| | 2.33 | 1 | .3 | .5 | 99.0 |
| | 2.72 | 1 | .3 | .5 | 99.5 |
| | 3.65 | 1 | .3 | .5 | 100.0 |
| | Total | 198 | 50.6 | 100.0 | |
| Missing | System | 193 | 49.4 | | |
| Total | | 391 | 100.0 | | |

# Appendix III

## Results of Mann-Whitney and Kolmogorov-Smirnov test

| Results of Mann-Whitney (MW) and Kolmogorov-Smirnov (KS) | | | |
|---|---|---|---|
| | **MW** | **KS** | **Sign. (p< 0.05)** |
| Vel 48h untreated rep1 vs rep2 | 0.006 | 0.004 | |
| Vel 72h untreated rep1 vs rep2 | 0.000 | 0.000 | * |
| Vel 72h untreated rep2 vs rep3 | 0.000 | 0.000 | * |
| Vel 72h untreated rep1 vs rep3 | 0.000 | 0.000 | * |
| Vel 48h untreated vs DMSO | 0.058 | 0.07 | |
| Vel 48h DMSO vs latb | 0.000 | 0.001 | * |
| Dr 48h untreated vs DMSO | 0.733 | 0.98 | |
| Dr 48h DMSO vs latb | 0.000 | 0.000 | * |
| Vel 72h rep1 untreated vs DMSO | 0.763 | 0.229 | |
| Vel 72h rep2 untreated vs DMSO | 0.000 | 0.000 | |
| Vel 72h rep1 DMSO vs latb | 0.000 | 0.000 | * |
| Vel 72h rep2 DMSO vs latb | 0.146 | 0.193 | |
| Vel 72h rep3 untreated vs DMSO | 0.455 | 0.309 | |
| Vel 72h rep3 DMSO vs oryzalin | 0.389 | 0.195 | |

# Appendix IV

## Alignment of the sequenced PCR product *At*kinesin-13a to the CDS sequence of the kinesin gene

The Kinesin-13a gene sequence was amplified with PCR and sequenced. The sequenced gene (query) was successively aligned to the *At*kinesin-13a annotated sequence (subject) to verify the cloning.

```
Query  92    CAGGGCTTCATGGGCGGCCAAATGCAGCAAAACAATGCTGCGGCTGCGACGGCGCTTTAC  150
             ||| || ||||||||||||||||||||||||||||||||||||||||||||||||||||||
Sbjct  350   CAGCGCCTCATGGGCGGCCAAATGCAGCAAAACAATGCTGCGGCTGCGACGGCGCTTTAC  409

Query  151   GATGGGGCTTTACCCACTAATGACGCAGGAGATGCAGTCATGGCACGGTGGCTTCAATCC  210
             ||||||||||||||||||||||||||||||||||||||||||||||||||||||||||||
Sbjct  410   GATGGGGCTTTACCCACTAATGACGCAGGAGATGCAGTCATGGCACGGTGGCTTCAATCC  469

Query  211   GCTGGTTTGCAGCATTTGGCGTCTCCTGTTGCTTCTACAGGCAATGATCAGCGTCACCTC  270
             ||||||||||||||||||||||||||||||||||||||||||||||||||||||||||||
Sbjct  470   GCTGGTTTGCAGCATTTGGCGTCTCCTGTTGCTTCTACAGGCAATGATCAGCGTCACCTC  529

Query  271   CCAAACCTTCTCATGCAGGGTTATGGAGCTCAGACTGCTGAAGAGAAACAAAGACTGTTC  330
             ||||||||||||||||||||||||||||||||||||||||||||||||||||||||||||
Sbjct  530   CCAAACCTTCTCATGCAGGGTTATGGAGCTCAGACTGCTGAAGAGAAACAAAGACTGTTC  589

Query  331   CAACTAATGAGAAATCTCAATTTTAATGGGGAGTCGACTTCTGAATCATATACACCAACT  390
             ||||||||||||||||||||||||||||||||||||||||||||||||||||||||||||
Sbjct  590   CAACTAATGAGAAATCTCAATTTTAATGGGGAGTCGACTTCTGAATCATATACACCAACT  649

Query  391   GCTCACACATCAGCAGCTATGCCCTCTTCGGAAGGATTTTTTTCACCTGAGTTCAGAGGT  450
             ||||||||||||||||||||||||||||||||||||||||||||||||||||||||||||
Sbjct  650   GCTCACACATCAGCAGCTATGCCCTCTTCGGAAGGATTTTTTTCACCTGAGTTCAGAGGT  709

Query  451   GATTTTGGAGCAGGATTATTGGATCTTCATGCAATGGATGATACAGAGCTTCTATCTGAG  510
             ||||||||||||||||||||||||||||||||||||||||||||||||||||||||||||
Sbjct  710   GATTTTGGAGCAGGATTATTGGATCTTCATGCAATGGATGATACAGAGCTTCTATCTGAG  769

Query  511   CATGTGATTACCGAACCCTTTGAGCCGTCACCTTTCATGCCTAGTGTAAATAAAGAATTT  570
             ||||||||||||||||||||||||||||||||||||||||||||||||||||||||||||
Sbjct  770   CATGTGATTACCGAACCCTTTGAGCCGTCACCTTTCATGCCTAGTGTAAATAAAGAATTT  829

Query  571   GAAGAAGACTATAATTTGGCAGCTAATCGTCAACAGCGGCAACAGACAGAAGCTGAACCT  630
             ||||||||||||||||||||||||||||||||||||||||||||||||||||||||||||
Sbjct  830   GAAGAAGACTATAATTTGGCAGCTAATCGTCAACAGCGGCAACAGACAGAAGCTGAACCT  889

Query  631   TTGGGTTTATTGCCTAAAAGTGATAAAGAAAATAACAGTGTAGCCAAGATTAAAGTAGTG  690
             ||||||||||||||||||||||||||||||||||||||||||||||||||||||||||||
Sbjct  890   TTGGGTTTATTGCCTAAAAGTGATAAAGAAAATAACAGTGTAGCCAAGATTAAAGTAGTG  949

Query  691   GTAAGGAAAAGACCCCTAAACAAGAAAGAAACAGCTAAAAAGGAGGAGGATGTCGTGACG  750
             ||||||||||||||||||||||||||||||||||||||||||||||||||||||||||||
Sbjct  950   GTAAGGAAAAGACCCCTAAACAAGAAAGAAACAGCTAAAAAGGAGGAGGATGTCGTGACG  1009

Query  751   GTATCTGATAATTCTTTGACTGTCCATGAGCCCAGAGTGAAGGTTGATTTGACTGCTTAT  810
             ||||||||||||||||||||||||||||||||||||||||||||||||||||||||||||
Sbjct  1010  GTATCTGATAATTCTTTGACTGTCCATGAGCCCAGAGTGAAGGTTGATTTGACTGCTTAT  1069

Query  811   GTGGAAAAGCATGAGTTCTGCTTTGATGCTGTTCTAGATGAGGATGTTTCAAATGACGAG  870
             ||||||||||||||||||||||||||||||||||||||||||||||||||||||||||||
Sbjct  1070  GTGGAAAAGCATGAGTTCTGCTTTGATGCTGTTCTAGATGAGGATGTTTCAAATGACGAG  1129

Query  871   GTGTATCGGGCCACAATTGAGCCAATAATTCCCATTATTTTCCAGAGAACTAAAGCTACA  930
             ||||||||||||||||||||||||||||||||||||||||||||||||||||||||||||
Sbjct  1130  GTGTATCGGGCCACAATTGAGCCAATAATTCCCATTATTTTCCAGAGAACTAAAGCTACA  1189
```

## Alignment of the sequenced PCR product *At*kinesin-13aD to the CDS sequence of the kinesin gene.

The identity of the alignment of the sequenced kinesin-13aD clone (query) to the cDNA annotated sequence (subject)

```
Query  105   AAGGATCCTTTGTTGGGCCCAAATGATGTAGAAGATGTCTTTGAGCCTCCACAGGAAGTG  164
              ||||||||||||||||||||||||||||||||||||||||||||||||||||||||||||
Sbjct  1994  AAGGATCCTTTGTTGGGCCCAAATGATGTAGAAGATGTCTTTGAGCCTCCACAGGAAGTG  2053

Query  165   AATGTACCAGAAACCAGGAGGAGGGTGGTCGAGAAGGACAGCAACAGCAGTACGTCGGGT  224
              ||||||||||||||||||||||||||||||||||||||||||||||||||||||||||||
Sbjct  2054  AATGTACCAGAAACCAGGAGGAGGGTGGTCGAGAAGGACAGCAACAGCAGTACGTCGGGT  2113

Query  225   ATTGACTTCAGACAGCCTACAAATTATCGAGAGGAAAGTGGAATCCCATCATTCTCAATG  284
              ||||||||||||||||||||||||||||||||||||||||||||||||||||||||||||
Sbjct  2114  ATTGACTTCAGACAGCCTACAAATTATCGAGAGGAAAGTGGAATCCCATCATTCTCAATG  2173

Query  285   GACAAGGGAAGATCAGAGCCGAACAGTTCTTTTGCTGGCTCCACTAGTCAGAGAAACAAC  344
              ||||||||||||||||||||||||||||||||||||||||||||||||||||||||||||
Sbjct  2174  GACAAGGGAAGATCAGAGCCGAACAGTTCTTTTGCTGGCTCCACTAGTCAGAGAAACAAC  2233

Query  345   ATTTCTTCATATCCCCAAGAAACTTCAGACCGTGAAGAGAAAGTAAAGAAAGTGTCACCA  404
              ||||||||||||||||||||||||||||||||||||||||||||||||||||||||||||
Sbjct  2234  ATTTCTTCATATCCCCAAGAAACTTCAGACCGTGAAGAGAAAGTAAAGAAAGTGTCACCA  2293

Query  405   CCTCGTGGGAAAGGGTTGCGGGAAGAAAAACCAGACAGACCACAAAATTGGTCTAAAAGA  464
              ||||||||||||||||||||||||||||||||||||||||||||||||||||||||||||
Sbjct  2294  CCTCGTGGGAAAGGGTTGCGGGAAGAAAAACCAGACAGACCACAAAATTGGTCTAAAAGA  2353

Query  465   GATGTCAGTTCGTCGGATATCCCTACCTTGACAAATTTTAGACAGAACGCAAGTGAAACT  524
              ||||||||||||||||||||||||||||||||||||||||||||||||||||||||||||
Sbjct  2354  GATGTCAGTTCGTCGGATATCCCTACCTTGACAAATTTTAGACAGAACGCAAGTGAAACT  2413

Query  525   GCTTCAAGGCAATATGAAACCGCTTCAAGGCAATATGAAACCGACCCTTCGCTTGATGAA  584
              ||||||||||||||||||||||||||||||||||||||||||||||||||||||||||||
Sbjct  2414  GCTTCAAGGCAATATGAAACCGCTTCAAGGCAATATGAAACCGACCCTTCGCTTGATGAA  2473

Query  585   AACCTCGATGCACTGCTTGAGGAAGAAGAAGCTCTGATTGCAGCGCACAGAAAAGAAATT  643
              ||||||||||||||||||||||||||||||||||||||||||||||||||||||||||||
Sbjct  2474  AACCTCGATGCACTGCTTGAGGAAGAAGAAGCTCTGATTGCAGCGCACAGAAAAGAAATT  2533

Query  644   GAGGATACAATGGAGATTGTTCGCGAGGAAATGAAACTTCTAGCGGAGGTGGGACCAACCG  702
              ||||||||||||||||||||||||||||||||||||||||||||||||||||||||||||
Sbjct  2534  GAGGATACAATGGAGATTGTTCGCGAGGAAATGAAACTTCTAGCGGAGGTGGACCAACCGG 2593

Query  703   GGAAGCATGATAGAAAACTATGTGACGC
              ||||||||||||||||||||||||||||
Sbjct  2594  GGAAGCATGATAGAAAACTATGTGACGC
```

## Alignment of the sequenced GFP-kinesin-13a (product of the BP reaction) to *At*3g16630.

The nucleotide sequence of kinesin-13a fused to GFP via Gateway cloning was sequenced and aligned to the cDNA sequence of kinesin gene to verify the cloning and that the kinesin gene was in frame with the fluorophore sequence.

```
Query  44    TCCTTGAGACGGCGTTGGAACCGAGCAATCCTGGCTTGAAGACTGACTAGCCCTGCTGCT  101
             |||||||||||| ||||||||||||||| ||||||||||||||||||||||||||||||||
Sbjct  2706  TCCTTGAGACGGTGTTGGAACCGAGCAAGCCTGGCTTGAAGACTGACTAGCCCTGCTGCT  2647

Query  102   TTCCGGGACAACACAAAGCTCAGTTGCGTCACATAGTTTTCTATCATGCTTCCCGGTTGG  161
             ||||||||||||||||||||||||||||||||||||||||||||||||||||||||||||
Sbjct  2646  TTCCGGGACAACACAAAGCTCAGTTGCGTCACATAGTTTTCTATCATGCTTCCCGGTTGG  2587

Query  162   TCCACCTCCGCTAGAAGTTTCATTTCCTCGCGAACAATCTCCATTGTATCCTCAATTTCT  221
             ||||||||||||||||||||||||||||||||||||||||||||||||||||||||||||
Sbjct  2586  TCCACCTCCGCTAGAAGTTTCATTTCCTCGCGAACAATCTCCATTGTATCCTCAATTTCT  2527

Query  222   TTTCTGTGCGCTGCAATCAGAGCTTCTTCTTCCTCAAGCAGTGCATCGAGGTTTTCATCA  281
             ||||||||||||||||||||||||||||||||||||||||||||||||||||||||||||
Sbjct  2526  TTTCTGTGCGCTGCAATCAGAGCTTCTTCTTCCTCAAGCAGTGCATCGAGGTTTTCATCA  2467

Query  282   AGCGAAGGGTCGGTTTCATATTGCCATGAAGCGGTTTCATATTGCCTTGAAGCAGTTTCA  341
             |||||||||||||||||||||||| ||||||||||||||||||||||||||||||||||
Sbjct  2466  AGCGAAGGGTCGGTTTCATATTGCCTTGAAGCGGTTTCATATTGCCTTGAAGCAGTTTCA  2407

Query  342   CTTGCGTTCTGTCTAAAATTTGTCAAGGTAGGGATATCCGACGAACTGACATCTCTTTTA  401
             ||||||||||||||||||||||||||||||||||||||||||||||||||||||||||||
Sbjct  2406  CTTGCGTTCTGTCTAAAATTTGTCAAGGTAGGGATATCCGACGAACTGACATCTCTTTTA  2347

Query  402   GACCAATTTTGTGGTCTGTCTGGTTTTTCTTCCCGCAACCCTTTCCCACGAGGTGGTGAC  461
             ||||||||||||||||||||||||||||||||||||||||||||||||||||||||||||
Sbjct  2346  GACCAATTTTGTGGTCTGTCTGGTTTTTCTTCCCGCAACCCTTTCCCACGAGGTGGTGAC  2287

Query  462   ACTTTCTTTACTTTCTCTTCACGGTCTGAAGTTTCTTGGGGATATGAAGAAATGTTGTTT  521
             ||||||||||||||||||||||||||||||||||||||||||||||||||||||||||||
Sbjct  2286  ACTTTCTTTACTTTCTCTTCACGGTCTGAAGTTTCTTGGGGATATGAAGAAATGTTGTTT  2227

Query  522   CTCTGACTATTGGAGCCAGCAAAAGAACTGTTCGGCTCTGATCTTCCCTTGTCCATTGAG  581
             |||||||| ||||||||||||||||||||||||||||||||||||||||||||||||||||
Sbjct  2226  CTCTGACTAGTGGAGCCAGCAAAAGAACTGTTCGGCTCTGATCTTCCCTTGTCCATTGAG  2167

Query  582   AATGATGGGATTCCACTTTCCTCTCGATAATTTGTAGGCTGTCTGAAGTCAATACCCTAC  641
             |||||||||||||||||||||||||||||||||||||||||||||||||||||||||| ||
Sbjct  2166  AATGATGGGATTCCACTTTCCTCTCGATAATTTGTAGGCTGTCTGAAGTCAATACCCGAC  2107

Query  642   GTACTGCTTGTTGCTGTCCTTCTCGAC
             |||||||||||||||||||||||||||
Sbjct  2106  GTACTGCTTGTTGCTGTCCTTCTCGAC
```

# Appendix V

Movies:

Movie 1: ST-GFP Velocity

Movie 2: ST-GFP LatB

Movie 3: ST-GFP oryzalyn

Movie 4: Trapping

# Appendix VI

**Poster, prentations and publications**

**Oral presentations:**

Seminar series, Oxford Brookes University (UK)- 2015

Young scientists symposium, Bristol (UK)- 2013

ENPER meeting, Lecce (Italy)- 2014
Chair of the session.

Annual postgraduate symposium, Oxford Brookes Univeristy (UK)- 2013

**Publications:**

Rocchetti A, Hawes C and Kriechbaumer V (2014) Fluorescent labelling of the actin cytoskeleton in plants using a cameloid antibody. *Plant Methods* 10: 12.

Rodríguez-Serrano M, Pazmiño DM, Sparkes I, Rochetti A, Hawes C, Romero-Puertas MC and Sandalio LM (2014) 2,4-Dichlorophenoxyacetic acid promotes S-nitrosylation and oxidation of actin affecting cytoskeleton and peroxisomal dynamics. *Journal of Experimental Botany* 65(17): 4783–4793.

**Posters:**

Finalist at L'Orel-Unesco For Woman in science, London (UK)- 2015

Postgraduate symposium, Oxford Brookes University (UK) - 2014

Golgi apparatus symposium, Bad Ischl (Austria)- 2013

Novel Biophysical Approaches in the Investigation of the Cytoskeleton,

The 27th European Cytoskeletal Forum Meeting, Pécs (Hungary)- 2012